An Investigation into the Influence of the Contact Pressure Distribution at the Friction Pair Interface on Disc Brake Squeal

NAVEED ASHRAF

A Thesis Submitted to the University of Huddersfield in Partial Fulfilment of the Requirements for the Degree of Doctor of Philosophy

July 2013

TABLE OF CONTENTS

Chapter **Page**

Chapter **Page**

Chapter **Page**

Chapter **Page**

Chapter **Page**

LIST OF FIGURES

LIST OF TABLES

LIST OF ABBREVIATIONS AND NOTATIONS

BASIC TERMS AND DIMENSIONS

μ	Coefficient of friction at disc/pad interface
∂	Cantilever length
F_L	Friction Force
F_N	Normal Force
μ_s	Sliding friction coefficient at the velocity v_0
v_0	Relative velocity
$\dot{x}$	Velocity
θ_1	Angle of pin orientation to disc surface
a	Pad abutment to centre of piston
b	Pad abutment to centre of disc/pad reaction force, “R”
N	Caliper piston force
R	Reaction force at the disc/pad interface
μ_2	Pad abutment interface friction coefficient
t	Pad thickness (mm)
a	Distance of caliper piston force (N) from pad abutment face
b	Distance of reaction force (R) from pad abutment face
c	Distance from abutment to centre of pad
d	Piston offset
h	Distance from disc surface to caliper mounting plane.
$\mu\,\mu_2$ R	Vertical abutment force
δ	Offset
rpm	rev/min
T_B	Torque generated by the caliper on the rotor
F_c	Clamp Force
R_E	Effective radius of the brake pads from the centre of the disc
P_H	Hydraulic pressure of brake system
A_P	Total area of pistons in one half of caliper

E	Modulus of Elasticity
t_s	Tangential traction
t_n	Normal traction
$\{\phi\}$	Complex eigenvector
σ_i	Real part of the ith eigenvalue
ω_i	Imaginary part of the ith eigenvalue
γ	Complex eigenvalue

Matrices and vectors

$\{x\}$	Global displacement vector
$\{F^a\}$	Vector of applied loads
$[M]$	System mass matrix
$\{\ddot{x}\}$	Global acceleration vector
$[K]$	System stiffness matrix
$\{\phi\}$	Complex eigenvector
$[K_f]$	Friction stiffness matrix
$\{F_f\}$	Interfacial force vector

Standard Abbreviations

PTZ	Piezoelectric beams
ESPI	Electronic Speckle Pattern interferometry
I-Scan	Industrial scan
CoP	Centre of Pressure
FE	Finite Element
x,y,z	Cartesian coordinate for the disc
CPU	Central Processing Unit
CEA	Complex Eigenvalue Analysis
P	Brake hydraulic pressure

ABSTRACT

The main purpose of this thesis is to investigate the dynamic centre of pressure during a noisy brake application. A novel technique is employed to measure the centre of pressure and contact pressure distribution between the disc/pad interfaces during braking events.

The test rig was developed to study the contact pressure distribution between disc/pad interfaces. The caliper and set of pads were modified to measure both static and dynamic centre of pressure during braking events. The brake uses a 12 piston opposed caliper arranged to allow a number of the pistons to be controlled independently using 4 master cylinders. This allows the interface centre of pressure to be adjusted both along the length of the pad and radially. The tests included static pressure measurements with the sensor film between the pad friction face and the disc, the centre of pressure being adjusted using the master cylinders to provide a "system benchmark". Once the static characteristic behaviour of the modified pad is established, the centre of pressure variation is measured under dynamic conditions. This allows the movement of the centre of pressure to be plotted against brake pressure and rotor speed.

Furthermore, a detailed finite element model of a disc brake assembly is developed. Contact analysis was performed to determine the pressure distribution, interfacial contact area and normal contact forces under both frictionless (μ=0) and frictional braking conditions. The effect of varying friction coefficients and the brake hydraulic pressure is also examined. Preliminary finite element results of contact pressure distribution between the disc/pad interfaces were compared with the experimental results, followed by a detailed modal analysis of disc brake to predict the natural frequencies and the mode shapes of disc brake. In addition, a stability analysis of brake assembly is carried out to distinguish the unstable frequencies. Structure modification of disc brake assembly was also investigated to understand the characteristics behaviour of brake system in terms of squeal noise performance.

It is established from the results that there is a strong relationship between the interface pressure distribution, the effective centre of pressure and the propensity of the brake to generate noise. It is noticed that the centre of pressure may vary both along the pad and radially during braking which adds to the complex analysis of instability.

The finite element results compared well with the experimental results. It is observed that the contact pressure distribution and the magnitude of normal contact forces are much higher towards the leading edge of the pads comparing to the trailing edge. It is also established yet again that with a leading centre of pressure the brake is more prone to noise whereas with a trailing centre of pressure the system is more likely to be stable.

DECLARATION

No portion of the work referred to in this thesis has been submitted in support of an application for another degree or qualification of this at any other university or institute of learning.

COPYRIGHT STATEMENT

1. The author of this thesis (including any appendices and/or schedules to this thesis) owns any copyright in it (the "Copyright") and s/he has given The University of Huddersfield the right to use such Copyright for any administrative, promotional, educational and/or teaching purposes.

2. Copies of this thesis, either in full or in extracts, may be made only in accordance with the regulations of the University Library. Details of these regulations may be obtained from the Librarian. This page must form part of any such copies made.

3. The ownership of any patents, designs, trademarks and any and all other intellectual property rights except for the Copyright (the "Intellectual Property Rights") and any reproductions of copyright works, for example graphs and tables ("Reproductions"), which may be described in this thesis, may not be owned by the author and may be owned by third parties. Such Intellectual Property Rights and Reproductions cannot and must not be made available for use without the prior written permission of the owner(s) of the relevant Intellectual Property Rights and/or Reproductions.

ACKNOWLEDGEMENTS

There are many individuals to whom I would like to offer my thanks, the most importantly my supervisors; Professor John Fieldhouse and Dr Chris Talbot. I deeply appreciate their invaluable academic guidance throughout the course of my doctoral studies. Their encouragement to be innovative with this project has resulted in a study that is far more extraordinary than I could ever have envisaged.

My appreciation extends to the many professional colleagues who consistently provided encouragement and support, in particular Dr David Bryant and Dr Andrew Crampton. I would also like to thank Mr. Peter Norman and Mr. Geoff Skenfield, for their technical expertise and guidance, without their generous contribution this study would not have been possible.

I am grateful to Alcon Components Limited for their financial support throughout this study. I would also like to thank all my peers who have constantly supported and encouraged me to work towards the completion of this project.

Finally, completion of this study would certainly not have been possible without the exceptional support I received from Professor John Fieldhouse. Thank you.

Chapter 1

Introduction

1.1 Brake Instabilities

Disc brake noise remains a fugitive problem in the automotive industry. In order to manufacture high quality automobiles, the occurrence of disc brake noise and vibration must be minimised. Brake noise is an annoyance to consumers who may assume that the brake is not functioning properly and files a warranty claim, even though the brake is in excellent working condition [1]. Therefore noise generation and suppression has become an important consideration in brake component design and manufacture. Warranty costs associated to brake squeal has been estimated to 100 million Euros annually, in Europe alone [2].

There are several types of disc brake instabilities associated with disc brake systems. However they are usually classified into two main categories.

Judder - A low frequency mechanical instability with a frequency related to wheel speed. The frequency is typically less than 200 Hz and is caused by a variation of the geometry along the disc rubbing path. The variation may be caused by corrosion, uneven surface film transfer, disc thickness variation or thermoelastic/plastic deformation where the disc adopts a wavelike shape. The vibration generally results in brake torque variation leading to brake load variation which causes vibration of the wheel and brake assembly about the suspension [3]. Although of major concern, it does not form part of the studies described herein.

Squeal - The other instability issue is a dynamic instability between 500 Hz to 20 kHz with frequencies in the region of 4 kHz being the most annoying because it relates to most sensitive frequency of human ear. Such noises are generally referred to as brake squeal with higher frequencies referred to as squeak [3]. Brake squeal is a phenomenon of dynamic instability that occurs at one or more of the natural frequencies of the brake system. There are many theories to explain brake squeal but

the excitation comes from the friction couple at the disc/pad interface and the rotor acts like an amplifier with sound waves radiating from the rotor surfaces. Pad and rotor coupling has a major impact on mid to high frequency (4 to 16 kHz) squeal. Low frequency (1 to 3 kHz) squeal typically involves caliper, anchor bracket, knuckle and suspension, in addition to the pads and rotor.

1.2 Historical Overview

Disc brake noise is accepted to be a complex subject as indicated through the vast range of literature already published on the subject. The comprehensive review by Kinkaid et al [1] in their review of brake squeal provides an excellent insight into the numerous approaches up to 2003.

With very few exceptions it is accepted that the principal vibration characteristic of the disc is a diametrical mode and it has been shown by Fieldhouse and Newcomb [4] that in all cases of disc brake noise, whether the system is a sliding fist or rigid opposed piston type caliper, the dynamic noise frequency may be related directly to the free mode vibration characteristic of the disc.

In an attempt to explain the mechanisms involved a variety of mathematical models have been proposed, each of which go some way to explain the phenomenon over a specific frequency range. The overview of research fields and activities of friction induced vibration in brakes, as detailed by Hoffman and Gaul [5], provides another insight into the work up to the present day and clearly demonstrates the vast range of work in the areas of brake noise. No single mathematical model is currently capable of expressing the differing mechanisms involved over the frequency ranges of 300 Hz to 20 kHz, as this range is too broad, for a dynamically unstable system. Regardless of how the mathematical models are limited they do allow the designer to introduce basic parameter and criteria at the design stage in an attempt to reduce the propensity of a brake to generate noise. It is generally accepted that the higher the coefficient of friction at the pad/disc interface the greater the tendency will be for the brake to promote noise (a detailed finite element analysis was performed in Chapter 6 to confirm the latter statement). This increase in friction coefficient increases the disc/pad in-plane interface force for a given pressure which in turn results in a

greater braking torque. What it does not show is why there is a greater tendency for the disc to be excited in an out-of-plane mode, the movement of a disc vibrating in a diametrical mode order. It is some time ago that work by Spurr [6] had shown that a spragging effect could cause instability resulting in a variable normal force if the sprag angle equated to the interface friction coefficient. When the inclination angle was set at the "sprag angle" of $\tan^{-1}\mu$ or greater the strut would "dig-in". The normal force to the rubbing surface would then increase until flexure of the system allowed a secondary strut arrangement to be established whereby the sprag angle was reduced, the normal force would reduce and the strut would then continue to slide. The mechanism was shown by a semi-rigid strut (PO') which was inclined to a rubbing surface and pushed horizontal to the surface as shown in Figure 1.1.

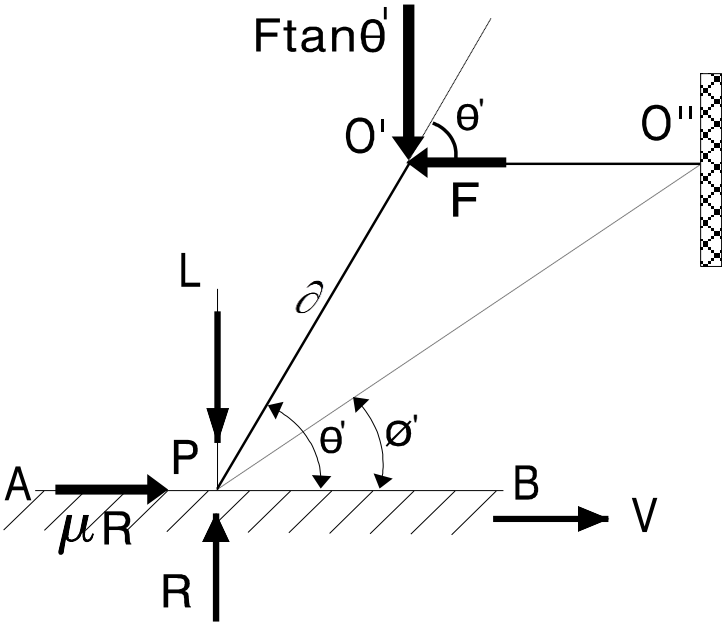

Figure 1.1 Sprag Model as proposed by Spurr [4]

The lever PO' is considered to be rigid and pivoted at O'. Flexibility within the system is provided by a second cantilever O'O" which allows pivot O' to move under load. The lever PO', of length, ∂, is loaded against a moving surface AB with a normal force L.

Resolving vertically gives:

$$R = L + F\tan\theta' \qquad (1.1)$$

and taking moments about O' gives:

$$L\partial\cos\theta' + \mu R\partial\sin\theta' - R\partial\cos\theta' = 0 \quad (1.2)$$

which reduces to:

$$L + \mu R\tan\theta' - R = 0 \quad (1.3)$$

substituting R from equation (1.1) in the above gives:

$$L + \mu(L + F\tan\theta')\tan\theta' - (L + F\tan\theta') = 0 \quad (1.4)$$

resulting in:

$$\mu L + \mu F\tan\theta' - F = 0 \quad (1.5)$$

and rearranging gives:

$$\mu L = F(1 - \mu\tan\theta') \quad (1.6)$$

so that:

$$F = \frac{\mu L}{(1 - \mu\tan\theta')} \quad (1.7)$$

with F approaching infinity as μ tends towards $\cot\theta'$, when spragging will occur. This work was continued on discs with Jarvis and Mills [7] and Earles et al [8-12]. A detail review of these theories and models is discussed in the literature review.

Clearly because of the construction of the test rigs, and the in-built flexibility of the members, the system was able to establish more than one sprag angle for it to work. The caliper is a similar system with a multiple of "sprag angles" and it is this mechanism, in relation to the coefficient of friction at the pad/disc interface, which this thesis examines.

For a caliper to be capable of spragging it is a requirement that the centre of pressure which provides the force normal to the disc surface, as generated by the caliper pistons, would need to be offset from the centreline of the caliper mounting arrangement [13]. This normal force combined with the in-plane frictional force would provide the resultant spragging force and thus an out-of-plane excitation force. This thesis will consider a theoretical approach as a means to explain how this may

occur and then an empirical approach to examine the effects of an imposed offset centre of pressure.

However prior to a detailed study, it was essential to explore a number of techniques available to measure the contact pressure distribution and the centre of pressure (CoP) movements effectively. The subject of interface pressure distributions in disc brakes has been studied by a number of researchers. Dubensky [14] used pressure-sensitive paper and Tumbrink [15] employed a ball pressure method. Samie and Sheridan [16] used a commercial pressure-sensitive film to measure the static pressure distribution between the disc/pad interfaces. Fieldhouse [18] inserted a thin steel wire between the piston face and the pad back plate to offset the pressure distribution towards the trailing side. A common observation found that the contact pressure distributions shifted towards the leading side. This correlated well with the observation made by Limpert [19] that more wear appears on the leading side than the trailing side.

Although the static pressure distribution may be calculated, and measured using pressure sensitive films, there was little information regarding its calculated or measured position during a dynamic braking event. While collaborating with Bosch prior to the PhD research work, Bosch Braking Systems were experiencing a squeal noise at around 2 kHz on one of their braking systems. Extensive experimental work was considered using laser techniques and modal analysis but a firm solution was not identified or secured. This promoted an investigation of the friction pair interface with regard to possible geometric relationships and then an examination of the caliper mounting position and possibility of "spragging" due to position of pad centre of pressure in relation to the caliper/carrier bracket mounting plane. It was proposed by a research team [20] to make use of pressure sensitive films to understand the characteristic behaviour of pads centre of pressure under static and dynamic conditions. The technique was to use an embedded pressure sensitive film within the pad. This method allowed the dynamic centre of pressure to be measured during a normal noisy brake application. A pad was prepared to receive the laminate by machining a recess and "plug". The film laminate was then inserted into the recess and the "plug" used to form a sandwich of the film laminate. The pad was then

machined to give a level rubbing surface and the assembly used to measure the dynamic centre of pressure on a test rig. It was established by the research team [20] that the centre of pressure (CoP) varied most at low pressures but tended to be less erratic as pressure increased. It was observed that at low brake pressure there was greater leading centre of pressure and greater instability. The centre of pressure hardly ever shifted towards the trailing side of the piston centre. This is generally what is experienced on a vehicle; noise is most prevalent as brake pressure is reduced. It was also determined that the position of the mounting plane for the caliper carrier bracket was important because of its influence over the spragging angle. It needs to be as close to the plane of the disc-rubbing surface as possible. A detailed case study of this work can be found in Appendix A.

Clearly the preceding research work demonstrated that the centre of pressure would move during a braking event but the exploratory work gave no indication as to how much it would move due to a varying radial and tangential pressure distribution. The purpose of the research carried out as part of this thesis was to extend the knowledge and understanding by deliberately inducing a variety of braking conditions and pressure distributions.

The research carried out in this thesis determines the basic mechanisms involved in instability generation resulting in brake squeal via the use of experimental and finite element models. From previous studies [18, 42], it can be perceived that the co-planar forces acting on the pad/caliper contact regions and its influence on the position of the disc/pad centre of pressure plays critical roles in the generation of brake squeal. Thus, the scope of this thesis was to analyse the contact pressure distribution between disc/pad interfaces and then examine the movement of the CoP during braking.

1.3 Aims and Objectives of Current Research

The overall aim of this thesis is to gain insight into the influence of the friction pair, contact pressure distribution on disc brake squeal to provide a basic understanding of the contributing mechanisms which cause the brake instability.

The objectives of the current research are:

1. The design and development of test rig equipment to measure the static and dynamic pressure distribution during braking events.

2. To investigate the methods to measure the contact pressure distribution between the disc/pad interfaces under both static and dynamic conditions and then examine the movement of centre of pressure during braking events.

3. The development of a detailed finite element model and then comparing the FE results of contact pressure distribution and normal contact forces with the experimental results. Executing a modal analysis at components level and then correlate it with the real brake components. Examine the effects of varying friction coefficients and the brake hydraulic pressure on disc brake squeal.

4. To conduct a comprehensive FE modal analysis using complex eigenvalue method to establish the natural frequencies and the mode shapes of brake assembly. Furthermore a stability analysis of brake assembly is executed to distinguish the unstable frequencies to validate it with the experimental results.

5. To perform a number of parametric studies on disc brake assembly to understand the characteristics behaviour of disc brake in terms of squeal noise performance.

1.4 Outline of Thesis

This thesis consists of eight chapters outlined as follows:

Chapter 2: Literature Review

The literature review covers a number of background theories and models relating to brake noise. This chapter also comprises a detailed literature review on experimental and finite element methods relating to brake squeal noise.

Chapter 3: Development of Test Rig for Dynamic Pressure Distribution Measurements

Chapter 3 presents detailed information on the development of a test rig for both static and dynamic pressure distribution measurements.

Chapter 4: Experimental Studies

Chapter 4 concentrates on the results of the experimental studies. A number of tests are carried out to measure the contact pressure distribution between the friction pair of disc/pad under various conditions. It also presents a detailed study on the behaviour of the centre of pressure along the length of the pad and radially during squeal events.

Chapter 5: Finite Element method

Chapter 5 outlines a detailed procedure on the development of a finite element model of a disc brake assembly. A finite element model is developed to accommodate both contact pressure distribution analysis as well as complex eigenvalue analysis. Various types of contact methods are considered and compared. Furthermore a number of extraction methods were examined to solve the eigenvalue and eigenvector problems.

Chapter 6: Finite Element Results

Chapter 6 concentrates on finite element results. This chapter discusses the effect of coefficient of friction and hydraulic brake pressures on the contact pressure distribution and on the normal contact force. Finite element results are compared

with the experimental data to verify the accuracy of the finite element method. Furthermore, a detailed FE modal analysis is performed using the complex eigenvalue method to ascertain the instability measurement, natural frequencies and modes of vibration of the disc brake assembly.

Chapter 7: Parametric Studies

This chapter presents a number of parametric studies to determine a set of controlling parameters which can be employed to suppress or eliminate the brake squeal noise.

Chapter 8: Conclusions

Chapter 8 provides the main conclusions, contributions to knowledge and novel outcomes of the present study. This thesis concludes with the recommendations for future work.

Chapter 2

Literature Review

2.1 Automotive Disc Brake System

The main purpose of a disc brake is to generate the friction between the pads and rotor to dissipate the kinetic energy of the vehicle [1]. The foundation brake consists of the disc, a caliper and set of brake pads. The disc is securely mounted on the axle hub and the caliper body is attached with the mounting bracket to the vehicle as shown in Figure 2.1. The brake pad consists of a steel backplate with the friction material bound to the surface of the backplate. The caliper body houses the hydraulic pistons which actuate the pad assemblies causing them to be pushed against the disc, in order to generate a frictional torque to slow the vehicle.

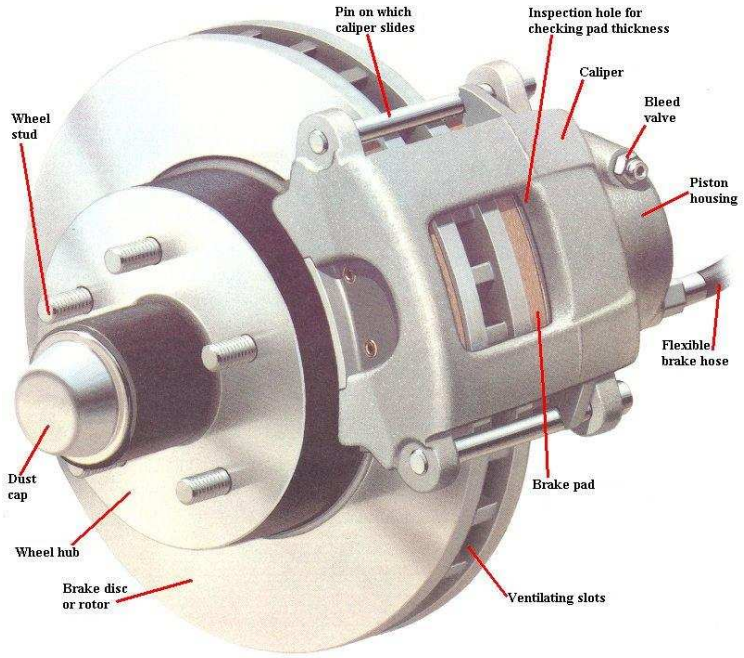

Figure 2.1 Solid model of a disc brake assembly

It is well known phenomenon that the tangential force (friction force) between the disc/pad interfaces is an important factor related to a brake system. It is evident from

Coulomb's friction law that tangential force is directly proportional to hydraulic pressure. The relationship between the normal force, F_N, and the friction force, F_L, can be formulated as:

$$\mu = F_L / F_N \tag{2.1}$$

where μ is the coefficient of friction

It was also found by Eriksson [21] that no squeal occurs when the coefficient of friction (μ) is below the squeal threshold (a typical value of this threshold found to be $\mu = 0.4$). However the level of the threshold depends on the design of the brake system, the material parameters and the friction characteristics [21].

2.2 Brake Instability

A large number of theories and models relating to brake noise, squeal in particular, have been developed to achieve an understanding of the problem of brake noise and then discover a feasible solution ensuring quiet brakes. A detail review of these theories and models is discussed below.

2.2.1 Stick-Slip Theory

Stick-slip motion accompanies oscillatory vibration of friction force and is responsible for squeal, creep-groan and jerking of brakes. Stick-slip vibration generally occurs because the static friction coefficient is greater than the sliding friction coefficient [23]. The relationship between the sliding friction coefficient, μ_s, and the relative velocity v_0 is:

$$\frac{\partial \mu_s}{\partial v_0} < 0 \tag{2.2}$$

Figure 2.2 exhibits a diagram of stick-slip motion. The velocity of the belt is called the relative velocity, v_0. The surface between the blocks and the belt is rough so that the belt exerts a dry friction force on block that sticks on it.

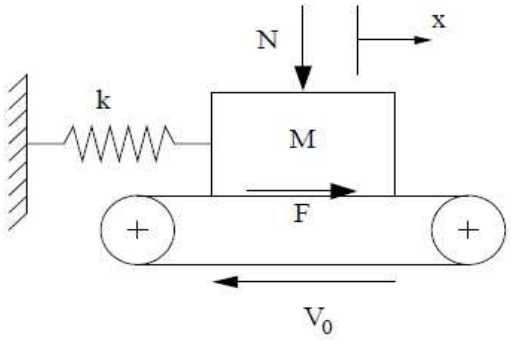

Figure 2.2 A simple elastic rubbing system [23]

For diminishing relative velocity, (sticking phase with $v_0 = 0$) the magnitude of the friction force depends on the relative force governed by the equation of motion and its direction depends on the tendency of the motion. To calculate the responses of the system, it is necessary to separate the motion into two phases "slipping phase" and "sticking phase". The criteria for slip-to-stick transition are:

Slipping phase: $$F = \mu_s N \quad (2.3)$$

Sticking phase: $$\dot{x} = v_0 \quad (2.4)$$

If both criteria are met, the mass will stick to the belt. However, if only the first criterion is met the mass will not stick to the belt but will accelerate beyond the speed of the belt. At this point the friction force will reverse its direction so as to oppose further motion of the mass and, eventually, the velocity of the mass will be reduced to the belt velocity and stick-slip transition will occur. Stick-slip motion occurs when the friction force reaches its maximum allowable value $\mu_s N$. The mass then slips backward relative to the belt and finally oscillates repeatedly and the system enters the limit-cycle vibration [23].

2.2.2 Sprag-Slip Theory

In 1962, Spurr [24] established a novel theory of brake squeal called sprag-slip, by which the unstable oscillation in the system could occur even with constant friction coefficient. This sprag-slip phenomenon occurs due to locking action of the slider

into the sliding surface. Spurr [24] demonstrated this by rubbing a flexible spring against various grades of emery paper and went on to confirm it with more practical examples using a railway brake shoe with an adjustable pin bearing on the wheel. To relate spragging to disc brake squeal, a modified brake disc also showed this to be the case [24]. In this example the pad was restricted from moving by studs in the rear of the pads and the pads then ground in such a manner as to allow only a small radial strip to be in contact with the disc. The line of action was then from the contact strip to the restraining studs with θ being measured from the studs to the normal to the disc face as shown in Figure 2.3. Spurr [24] found that squeal was only generated when this contact strip was sufficiently close to the leading edge of the pad. It was also found that brake squeal depends upon the magnitude of the coefficient of friction and also on the position of the contact areas between the friction material and surface of the disc. He concluded that squeal is therefore fugitive and occurs only at certain pressures and is very dependent upon how the friction material is bedded-in. A detailed review of this theory has been presented in Chapter 1.

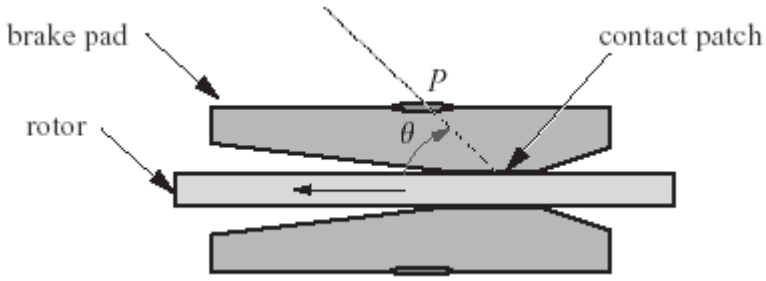

Figure 2.3 Brake pads contacting a rotor to exhibit Spurr's sprag-slip theory [1]

2.2.3 Jarvis and Mills Model

Jarvis and Mills [7] developed the sprag-slip theory with their "cantilever-disc" model, as shown in Figure 2.4, and although the apparatus was not on a brake system itself, it was readily amenable to mathematical analysis and the experimental work was the first to be accompanied by significant mathematical analysis. In their study of system behaviour they concluded that the amplitude of vibration of the disc remained stationary in space, being located by the action of the cantilever on the disc surface. They also observed that there were no true node positions and by scanning the surface of the disc determined that the amplitude was seen to vary about a mean

level with the phase changing continuously. It was explained that this behaviour was due to the existence of at least two vibrations of the same mode order but with different phases in time and space. The analysis considered two situations; one with a varying coefficient of friction with speed and the other with constant friction. In both cases it was assumed that the complex motion of the disc involved two simultaneous modes and that this situation accounted for a number of phenomena. It was possible that either mode could exist or that the amplitude around the periphery could vary about a mean level with a steadily changing phase. The relative amplitudes determined which possibility actually occurred.

It was shown by calculation that the practical variation of coefficient of friction with velocity was not enough to maintain oscillation. The theoretical analysis showed that instability could arise and this was generally confirmed by experimental investigation where the variables considered were the cantilever length, the cantilever slope, the radius of contact on the disc and the applied load. It was found that the difference between the predicted and actual results could be due to the predicted results making use of constants, such as damping factors, which were obtained from forced vibration tests.

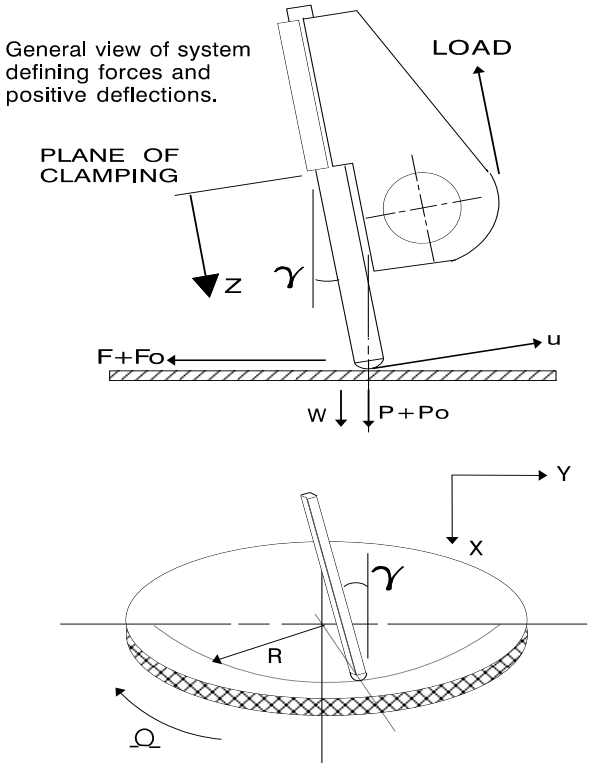

Figure 2.4 Cantilever-Disc Model [7]

It was concluded by Jarvis and Mills that the cause of vibration was due to the nature of coupling between the two components of the system and it was shown that there was a limiting minimum radius at which point the system became stable, this radius being dependent upon the length of the cantilever. It was suggested that it should be possible to prevent undesirable vibrations by a suitable choice of parameters in the initial design stage of the system but the application of the general theory of coupling depends on the ability to analyse the vibration modes of the individual components, an approach favoured by Spurr [24].

2.2.4 Pin-Disc Models by Earles

The work was extended further extended by Earles et al [8-12] with the "pin-disc" model. The single head test rig, shown in Figure 2.5a, comprises a "rigid" pin held in a pivoted arm which is loaded onto the face of a rotating disc. The mechanism is modelled as shown in Figure 2.6 with four degrees of freedom. The disc is assumed to vibrate in a single dominant mode and therefore has only one axial degree of freedom whereas the pin has three, two translational and one rotational. Without exception it was observed that squeal was developed when the pin was in torsional mode with the condition of pin angle $\tan^{-1}\mu > \theta_1 > 0$, where θ_1 is the angle of pin orientation to disc surface. It was concluded that noise was generated as a result of geometrically induced instability, the region of instability being dependent upon the coefficient of friction and the physical parameters of the system. It is argued that the model contains the essential squeal noise producing characteristics the model being developed to be more representative of a braking system but it is difficult to relate the findings to that of a real brake system. The situation has been recognised by Earles and in the later papers the criticism has been addressed, to some degree, with the consideration of an opposed two pin system, one either side of the disc as shown in Figure 2.5b yet even with this model the disc still had only one degree of freedom. In this case it was concluded that for instability to be possible it was necessary for at least one of the pin mechanisms to fall within the instability boundary although this in itself was not sufficient to cause noise. Sufficient conditions were again dependent upon the magnitudes of the system parameters and in particular the ratio of the

corresponding pin support parameters with certain ratios giving stable motion. The general finding was that unstable motion was again as a result of geometrically induced instability and that this was essentially the mechanism by which squeal noise is generated in a disc brake.

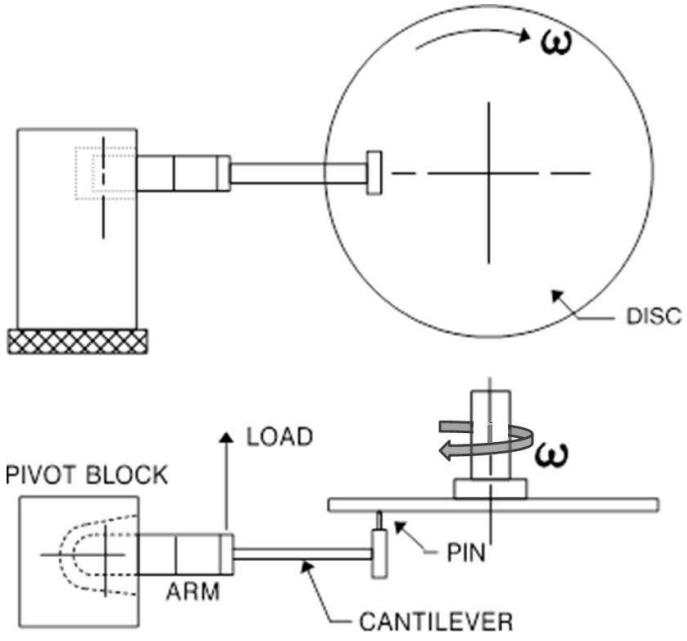

Figure 2.5a Pin - Disc model (Single head)

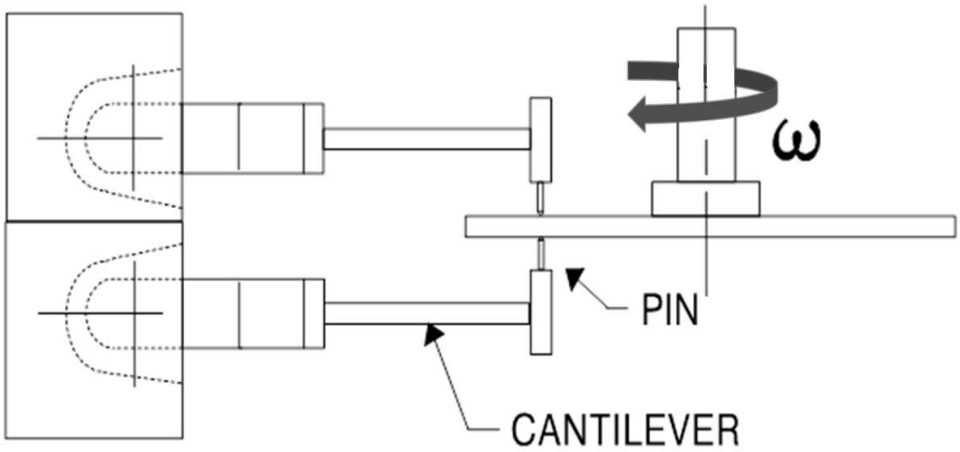

Figure 2.5b Pin - Disc model (Double head)

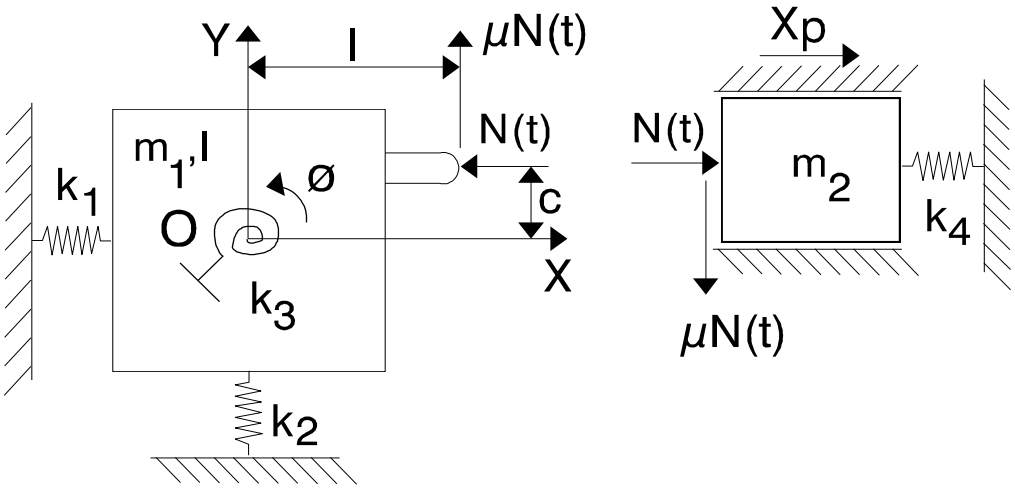

Figure 2.6 Four degree-of-freedom model for a pin-on-disc system

2.2.5 North's Binary Flutter Model

North [25] proposed a mathematical model which was designed to represent a disc brake system as shown in Figure 2.7. His proposal was an eight degree of freedom model which treated the disc in the vicinity of the pads as a solid beam. He modelled the disc, pads and the caliper as lumped masses and inertias, each with two degrees of freedom, transverse and rotational, giving a total of eight degrees of freedom. The principal feature of this approach was the recognition of the need to give the disc two degrees of freedom, these being necessary to represent the generalised motion of the disc in the vicinity of the pads as described by Jarvis [7]. In this sense the disc is considered to hold two independent modes of vibration, these being a sine mode and a cosine mode about the mid-point of the pads. If a pad sized portion of disc is considered the cosine mode provides a mainly translational displacement in a direction parallel to the axis of the disc whereas the sine mode results in a largely rotational displacement. The disc was therefore represented as a lumped parameter with an equivalent mass and equivalent physical characteristics which adequately represented the complex distributed nature of the disc. A simplified two degree of freedom model by North [26] considered the disc sandwiched between the pads which are in turn bounded by immovable planes. The predominant motion considered is that of the disc where it is related to the instability experienced by aircraft wings and is referred to as binary flutter. To achieve good agreement

between measured results and calculated results, with the eight degree of freedom model, it was necessary to make slight adjustments to the measured stiffnesses. Agreement was also close for the measured mode shapes and for the phases of the pad with the largest amplitudes.

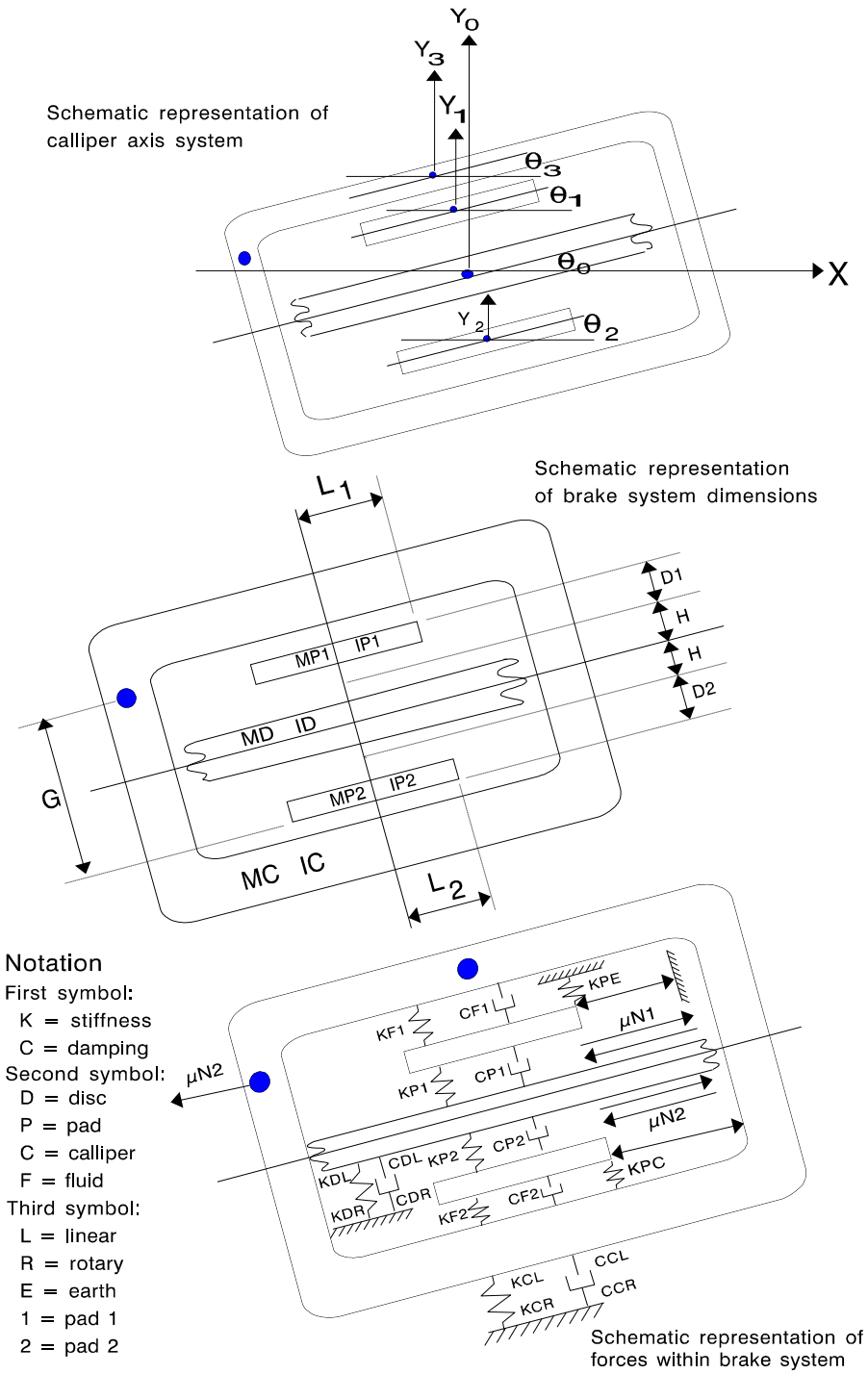

Figure 2.7 Eight degree-of-freedom model [25]

2.3 Experimental Work

In the past, all research on brake noise and vibration were carried out using experimental methods. It is still the most popular and effective way to measure brake vibration frequencies and identifying noise sources and still the most important method for verifying solutions. An experimental approach can directly expose the nature of vibration and subsequently can reveal the precise noise sources within the brake system. According to Yang [27], experimental methods are the only means to judge or verify any possible solutions or designs to make quiet or powerful brakes. This section explores a number of experimental techniques available to investigate the brake instabilities in a brake system.

2.3.1 Experiments using Holographic Interferometry Techniques

The most important earlier work using holography technique was performed by Felske et al [28]. Their analysis of self-excited brake system using "yoke" and "fist" type calipers clearly demonstrates the versatility and usefulness of this technique when both time average and double pulsed techniques were employed. Contrary to the findings of other workers the conclusions of this work are that the caliper and pads transmit the main part of the noise energy and in particular that the frequency of squeal is a function of the yoke-type or fist-type caliper resonant frequency. With regard to the disc it is commented that frequently the noise level transmitted by the disc is of little consequence. This latter belief is based on an assumption that there is acoustic short circuiting in front of the disc as a result of the sound waves being emitted from adjacent antinodes which are 180° out of phase with each other. The majority of the investigation was based on the yoke-type caliper where the pad is of square format but in essence the technique is used solely as a modal analysis technique [29].

Nishiwaki et al [30] also made use of holographic interferometry with their finite element modelling for their analysis of a pin slider "fist" type caliper. A high coefficient of friction material was specifically produced for the trials and the same

noise frequencies which were found on the vehicle were able to be recreated on the test rig, a detail which led to the belief that brake squeal was not influenced by the suspension parts. This is an important consideration when endeavouring to simulate the brake system mounting as on the vehicle. Early tests revealed that the frequency components of the pads and caliper were not necessarily close to the brake squeal frequencies whereas their findings revealed that the vibration modes of the disc during brake squeal generation were strongly influenced by the natural frequency and mode of the disc component. The holographic analysis concluded that the pads vibrated in a bending mode but more importantly that the disc vibrated in a diametral mode which remained static with respect to the ground despite the fact that the disc was rotating. Furthermore, it was observed that when the disc was excited artificially the point of maximum excitation occurred at the point of excitation. It was this combination of events which prompted their belief that the introduction of asymmetry into the rotor may reduce the formation of symmetrical diametral modes of vibration and propensity to generate squeal noise. In effect if the point of excitation can be decoupled from the mode of vibration then squeal will not be possible. It was because of this hypothesis that the work tends to concentrate on the analysis and modification of the disc. Both the analysis and experimental work consider either added masses to or from the disc in an attempt to fix the mode of vibration relative to the disc. Finite element analysis showed that for low disc stiffness the mode was fixed to the disc but at high stiffness the mode remained stationary. Pad pressure was also found to affect the situation. Modified vented discs were tested and it was found that the vibration mode rotated with the disc and that there was an improvement in noise generation. The authors concluded that brake squeal was strongly influenced by the natural frequency of the disc and that a cure could possibly be achieved by a modification in the mass distribution of the disc. This infers that there is a need to build asymmetry into the disc in order to disrupt the symmetrical modes of vibration.

A combination of experimental modal analysis measurements and finite element modelling was also used by Lang and Newcomb [31] in their study of drum brake squeal. They found the drum modes to be stationary in space and hence rotating

relative to the drum. They established the presence of two identical normal modes, superimposed but phase shifted spatially and temporally to each other. They also proposed and concluded that if asymmetry can be introduced into the drum by added masses then the normal modes can be split and the mode ceased to adopt a preferred position on the drum, and would therefore rotate with the drum. Their work continued [32] with the analysis of a wide drum brake with a predominant frequency of 580 Hz having a complex squeal mode comprising two modes displaced by 90°. The investigation considered coincidences of component natural frequencies but concluded that brake component modal analysis was not a reliable indicator of squeal frequency or potential but did support the proposals that the binary flutter mechanism as proposed by North [25] was consistent with measured squeal modal characteristics. The theoretical considerations for decoupling the two drum modes indicated that to decouple all potential squeal modes two diametrically opposed masses were required. Two dimensional finite element analysis examined the limit of effectiveness of a distributed mass over the circumference.

Fieldhouse and Newcomb [4] made excellent use of holographic interferometry technique. They found that squealing frequency was near the individual natural frequencies of the components, concluding that noise propensity might be influenced by the coupling of these natural frequencies when they are close together. They demonstrated that the pad excitation plays a vital contribution in the generation of noise. It was also confirmed that the disc mode is always diametral but sometimes mode travel around the disc and the instability in the system is probably driven by the pad vibration.

Fieldhouse et al [33] also investigated a twin caliper brake system using holographic interferometry technique. They presented a holographic study of a sliding type rear disc brake to predict the possible noise frequency based on disc/pad interface geometry. They noted that when the caliper setting of 170º has been applied to brake system, the squeal noise reduced drastically. It was also observed that twin calipers may behave differently, one holding an antinode below the pad and the other a node, however they may also behave in a similar manner with either both holding an antinode or node below the pad.

Steel et al [34] examined the measurement and analysis of both out-of-plane and in-plane vibration of a twin caliper disc rotor during squeal generation. They once again made excellent use of the non-contact technique of holographic interferometry to record a set of three interferograms viewed from different viewing perspectives. Additionally, they developed a Matlab algorithm from holographic theory to separate in-plane and out-of-plane motion and developed 3D displacement models of the real disc rotor. They recommended that considerable attention should be given not only to out-of-plane but also to the in-plane contribution of displacement.

2.3.2 Experiments Using Accelerometers

For years, accelerometers have been used to measure the vibration of a brake and its components such as the disc, caliper and pads. Once an accelerometer is mounted on the test component, its vibration amplitude, frequency, phase angle and even mode shape can be measured with respect to a reference point [27].

In 1993, Ichiba and Nagasawa [35] considered the problem of brake noise from a purely experimental approach in an attempt to determine the mechanisms involved. The proposal was to record discrete excitation, using small accelerometers, at several points along the backplate of the pad including one mounted into the vented disc. In doing so it was possible to construct the mode of vibration of the pair and establish their phase relationship. It is interesting to note that they had selected this method of study simply because holographic interferometry could not provide phase information. Modal analysis of the disc, by hammer tests, suggested that the disc mode was comprised of two waveforms, a sine and cosine which resulting in a compound stationary wave. It would appear that the disc waveform was stationary with respect to the disc although an accelerometer inset into the disc would not be able to detect a moving wave which travelled at a speed relating to the disc mode order, it would see it as a stationary wave excitation. It was concluded that instability was as a result of the changes in the friction force and not the μ-velocity characteristic and that noise was as a result of fluctuations in surface pressure.

In 1996, Ishihara et al [36] used accelerometers to measure the vibrating motion of the caliper. The rotor was rotated at 30 rev/min while hydraulic pressure was applied. Random oscillation waves were applied to the caliper by an electromagnetic shaker in the normal and circumferential direction of the rotor. It was found that the caliper's diagonal deformation and the linear stiffness of the lining material had a great effect on the generation of squeal. It is also confirmed that when the coefficient of friction is constant, low frequency brake squeal was generated due to geometric dynamic instabilities. It was also revealed that brake squeal can be reduced by decreasing the pad/disc coefficient of friction, changing the linear stiffness of the pad material and by minimising the vibration characteristics of the caliper and rotor. Since rotor frequency can be controlled relatively easily by changing rotor material and structural shape, the propensity of squeal instability could be reduced by shifting rotor frequency which had most influence on squeal to a higher region. Theoretical analysis based on the experimental results also showed that low frequency brake squeal is a dynamic unstable phenomenon caused by kinetic energy influencing the system vibration when a pressure fluctuation between rotor and pads is coupled with relative displacement in the rotor-rotating direction.

In 2003, James [37] used non-contact displacement transducers to measure the vibration at the disc surface. He investigated three different brake systems a Rover solid disc, Mercedes solid and vented discs. Non-contact displacement transducers were used to measure the normal displacement of the disc during a squeal event and located at 11 equi-spaced positions near the outer disc radius. He clarified that the displacement signals produced by a squealing disc could be processed to determine the mode shapes of the disc and the behaviour of the waves that produce the squeal noise in brake system. The least-squares approach was used successfully to produce detailed analysis of the behaviour of the wave motion in the disc from the available data. Squeal frequencies up to 8 kHz were analysed. He established that the Rover disc brake experienced four main squeal diametrical modes while both Mercedes brakes experienced five squeal diametrical modes. These diametral modes were then compared with the hammer test results. It was also shown that a squeal mode in the discs could produce either a stationary wave or travelling waves (backward or

forward). In general it was recognised that the squeal modes most commonly consisted of stationary waves and squeal would occur at temperature above 100°C.

In 2004, Kumamoto et al [38] studied the correlation between the contact and squeal generation. They measured pressure, noise level and contact load between pad and the caliper. A Piezoelectric accelerometer was mounted on the caliper to measure the vibration waveform and contact pressure distribution was measured by using pressure sensors between pad and caliper. It was found that squeal was generated at two different frequencies of 2 kHz and 2.5 kHz respectively and squeals generation was due to the disturbance of the movement of the pad in the tangential direction causing instability in the pads because of the soft connection between the pad and caliper. The results clearly demonstrated that squeal performance could be improved with a rigid and stable connection between the pad abutment and the caliper [38]. Lubrication on the abutment can also preserve noise as the friction dependent variable abutment oscillating force goes to zero and the resulting offset does not give a spragging angle. Their investigation was restricted to contact pressure of pad/caliper interfaces however in this thesis; more focus is given on measurements of CoP between the disc/pad interfaces to perceive its effect on squeal instability.

2.3.3 Experiments Using Piezoelectric Beams (PTZ)

Fieldhouse [39] used a number of piezoelectric (PTZ) beams (a description of the piezoelectric (PTZ) beams is given in Appendix B) to investigate the frequency and phase relationship of different components of a brake assembly. A number of piezoelectric (PTZ) beams were mounted at relevant points on the principal component parts of a brake assembly to measure their frequency and phase relationships. An Alfred Teves (AT) brake assembly was investigated as shown in Figure 2.8 which indicates the position of PTZ beams.

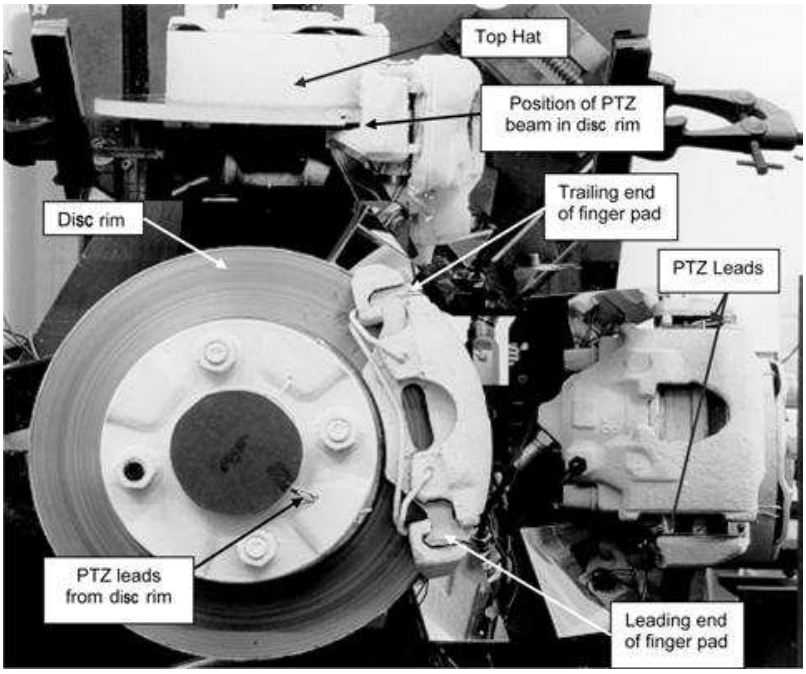

Figure 2.8 The AT brake system as used by Fieldhouse [39]

The brake generated an intermittent noise with an audible frequency of 8.5 kHz with an additional harmonic frequency of 31.4 kHz. In order to capture full sequence of the results, four excitation waveform traces were detected simultaneously. It was found that the piston pad trailing end appeared to start modulation to a lower frequency. During this progression of frequency shift, the trailing end of the piston pad played an important part in the development of the audible noise frequency. It was explained by Fieldhouse [39] that perhaps the onset of noise was always preceded by a very high frequency vibration which develops by convenient mechanical coupling of components until all are excited at a lower, audible, frequency.

It was suggested that due to this effect the piston pad may be the "trigger" in most brake system generating noise. The other possible reasons might be the damping or frictional forces at the abutment face that causes such a major frequency change. This may also answer the question as to why noise propensity increases as the brake force is reduced or noise is most pronounced during light braking. If this is the case there may be a relationship between the braking force and the pad abutment force leading to some form of spragging as proposed by Spurr [6].

2.3.4 Experiments Using High Speed Electronic Speckle Pattern Interferometry

Recently new developments in ESPI techniques allow three dimensional measurements for complete 3D analysis of complex structures. In 1997, Wang & Ettemeyer [40] demonstrated that the pulsed ESPI technique can be employed successfully to investigate the noise and vibration in a brake system. The brake was excited at 2 kHz by light braking at rotational speed of 18 rev/min. It was explained that there was no influence of rotation on the measurements up to 40 rev/min and precise results can be measured without any special optical alignment. It was explained further that the phase map due to rotation can be compensated numerically after evaluation. It was concluded that the pulsed ESPI technique is a distinctive tool for brake noise analysis and that this technique can be used for three dimensional measurements to measure the in-plane and out-of-plane components of the vibration.

In 2000, Reeves et al [41] also used high speed electronic speckle pattern interferometry (ESPI) technique to measure the out-of-plane vibration of a brake disc during naturally excited squeal. The complex mode was generated by the superposition of two diametral modes of the same order that had a spatial and chronological phase difference. It was concluded that the high-speed ESPI provided a real-time visualisation of surface deformation equivalent to double-pulsed holographic interferometry, with the benefit of giving a true time series of the surface deformation during a single vibration cycle.

2.3.5 Experimental Study of Abutment Effects on Noise Propensity

During noise generation it is generally observed that the trailing end of the pad will vibrate even though it is abutting against the caliper carrier finger. Clearly the abutment force will be related to the braking force. If it is accepted that the pad is vibrating, and the abutment force is varying with brake load, then the pad/caliper interface, abutment, force will vary with brake load [42].

It was demonstrated by Fieldhouse et al [42] through co-planar analysis that the centre of pressure of a brake pad varied along the pad axis due to the

backplate/caliper finger friction variation during pad vibration and this subsequently leads to a dynamic situation where the caliper may "sprag" causing out-of-plane vibration of the disc initiating noise. However in a practical situation there will be an interaction between frictional effects at the pad abutment and the various dimensions of the brake pad when it is in equilibrium. This equilibrium can vary with different pad abutment arrangements as shown in Figure 2.9. It was established by Fieldhouse [42] that with such abutment arrangements, it was possible to analyse the co-planar geometry with a trailing, leading or combined abutment arrangement. Their work correlated well with the results from Liles [43] who also observed that noise propensity reduced as the pad wears. In practice, the various abutment conditions can be achieved by using a combined abutment pad and appropriate shimming of the abutments. The summary of the analysis is shown in Appendix C.

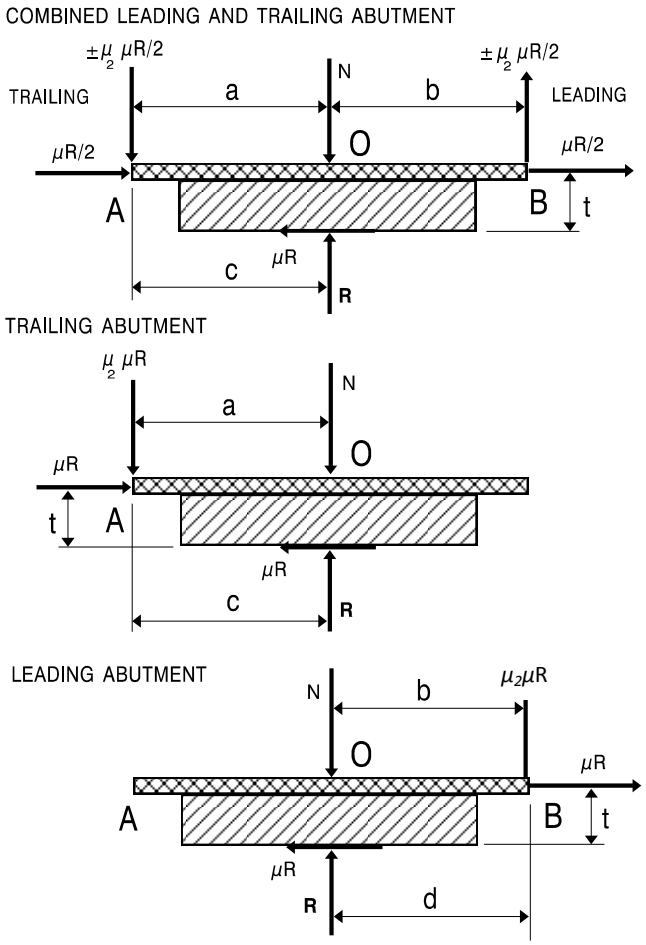

Figure 2.9 Free body diagram of brake pad assuming co-planar frictional forces and differing abutment arrangements [42]

2.3.6 Experimental Investigation of Imposed Offset Centre of Pressure

In his research work, Fieldhouse [18] employed a simple method to examine the noise propensity of the brake by varying the centre of pressure between the piston and piston pad. The centre of pressure was varied by using a 0.75mm diameter silver steel wire inserted between the piston face and pad backplate as shown in Figure 2.10. The offset of the wire was varied 18mm either side of the piston centre, generally in increments of 6mm but in increments of 3mm at critical points. The wire was supported by a backing plate to prevent local indentation of the wire as a result of the piston wall [18]. The method of testing was, at each wire setting, to increase the disc surface temperature to over 150^{o}C and then to vary the system pressure from 1MPa, in increments of 0.136MPa (20psi) down to zero and then back up to 1MPa. The temperature was then allowed to fall 10^{o}C and the process repeated. During this cycle of events the noise frequency, duration and amplitude was noted over several revolutions of the disc to ensure a steady situation was being recorded.

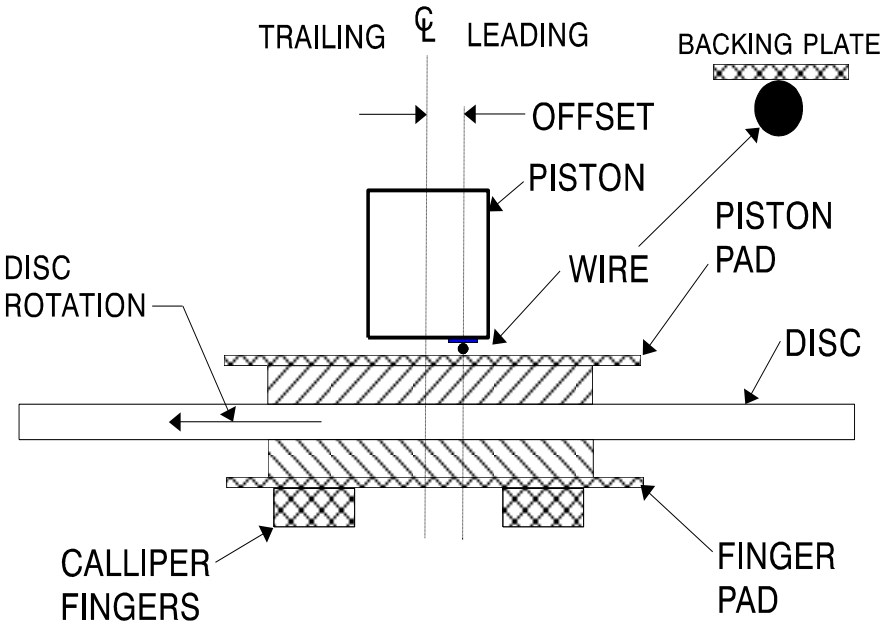

Figure 2.10 Diagram showing position of wire between piston and pad [18]

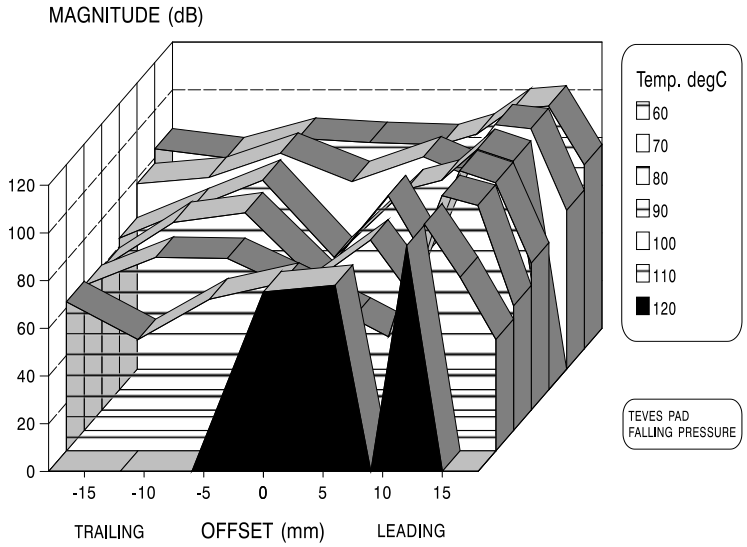

Figure 2.11 Offset and noise magnitude ($L_{eq(tot)}$) for a range of temperatures [18]

It was established by Fieldhouse [18], as shown in Figure 2.11, that with a leading offset of between 12mm and 15mm the system generally generated noise regardless of temperature, the more stable situations being obtained with a zero or trailing offset arrangement. It was further evident that as the temperature reduced, with a resulting increase in coefficient of friction (μ), the critical offset changed from 12mm at 120°C (μ = 0.5 to 0.6) towards 15mm at 60°C (μ = 0.6 to 0.7). A detailed case study of this work can be found in Appendix D.

2.4 Finite Element Models

A number of analyses have been performed on disc brake systems using the finite element method to understand the problem of noise and therefore develop a predictive design tool. The most commonly used technique is the complex eigenvalue analysis. Complex eigenvalues usually result from the frictional coupling of brake components due to the off-diagonal terms that arise in the stiffness matrix of the system causing it to be unsymmetrical. Complex eigenvalues with positive real parts are labelled as unstable modes, which always appear in complex conjugate pairs. Such unstable modes are more prone to squeal noise. Traditionally, pads and rotors have been connected by so-called friction springs. In recent years, researchers have suggested an alternative method associated with the direct connection of stator

and rotor and the elimination of these "imaginary" springs. Other studies have combined the above method with investigations related to pressure distribution and non-uniform contact between the brake components. The major disadvantage of performing a complex eigenvalue analysis through finite element analysis is that it is time consuming and consequently requires considerable computing power [44].

Liles [43] was one of the earliest researchers to present a paper associated with a complex eigenvalue analysis of a finite element disc brake assembly. The finite element model of brake components was generated using solid elements and the brake components were then coupled together in a system model, including friction coupling terms between the rotor and linings. A complex eigenvalue formulation was derived to provide the frequency and damping for each vibration mode. The finite element models were verified using vehicle test results on the same brake system. It was found by Liles [43] that shorter and stiffer brake lining assemblies reduced the tendency to squeal. It was also established that the likelihood of squeal can be decreased using a slightly softer rotor and higher coefficients of friction could increase the likelihood of squeal. These explanations suggested that the flexure of the pad plays an important role in the generation of brake noise and needs to be accounted for in future brake analyses.

Tirovic and Day [17] also studied the influence of various parameters such as friction material compressibility, coefficient of friction and disc stiffness on the interface pressure distribution. It was established from their results that the pad/disc coefficient of friction plays a vital role in the interface pressure distribution and the leading part of the pad maintains contact while the trailing part loses contact with higher coefficient of friction resulting in squeal in the brake system.

Contact pressure distribution followed by complex eigenvalue analysis has been investigated by Lee et al [45, 46]. A non-linear contact analysis was performed to study the interfacial contact behaviour of a disc brake assembly. Furthermore, the modal analysis was performed, using complex eigenvalue analysis, to extract the natural frequencies and the mode shapes of a disc brake system. They emphasised

that the key to the linearisation process lies in replacing only the non-linear elements, which are closed (in-contact) as a result of the applied force with equivalent linear interface elements. The propensity of the system to squeal was represented by a single number as against a set of eigenvalues. The number was derived from the standard deviation of all positive instability measures of those eigenvalues within a pre-determined frequency range from the mean value of zero. It was established that the instability standard deviation was directly related to the magnitude of rubbing interface friction coefficient but independent of the brake hydraulic pressure. It was also found from the finite element model that squeal propensity was reduced if the interface contact between the pad and disc was engineered to be uniform.

Nack [47] constructed a large-scale finite element model under steady sliding conditions with constant coefficient of friction. A finite element model was developed with solid elements containing approximately 120000 degrees of freedom. The model consisted of rotor, pad, caliper and mounting bracket. A non-linear contact analysis was performed followed by a complex eigenvalue analysis to investigate the instability in a brake system. Linearised stability method and a friction stiffness matrix were considered to model the contact between the pad and rotor using a geometric nonlinear solution. It was established that the dynamic instabilities can occur due to coupled motions due to friction which need to decouple to stabilise the system. It was shown that the complex mode analysis was sensitive to the variation in pressure and velocity. The degree of nonlinearity during brake squeal was observed from experimental results. The coupled modes were verified experimentally with a laser vibrometer.

AbuBakar [48] proposed a new method of predicting squeal using the finite element method. A finite element model of a disc brake was constructed and validated through contact analysis where static contact pressure distribution and its contact area correlated well with the experimental results. In the FE analysis he considered a real surface topography of which measurements were carried out in order to obtain a realistic contact interface model. Complex eigenvalue analysis was also performed to predict squeal generation. It was shown that the real contact interface model

predicted squeal occurrences much better than the perfect contact interface model by considering the effect of negative μ-ν slope and friction damping. The results showed that with the inclusion of wear, squeal events were predicted to appear and disappear as wear progressed even though similar boundary conditions and operating conditions were imposed to apparently the same disc brake model. This phenomenon explains the fugitive nature of squeal behaviour adding complexities to a brake system.

2.5 Summary

It was established from the literature review that the stick-slip phenomenon can generate vibration and cause instability in brakes but it cannot function at higher speeds where squeal is also observed. Therefore this theory is limited to low frequency noise less than 200Hz (such as creep groan noise) and can be used to explain low frequency noises.

It is evident from a number of studies [18, 24] that the spragging does occur on both test rigs and vehicle trials. It was obvious from the previous research [18] that a mechanical instability that is not influenced by temperature or pressure fluctuations is possible within a brake system. Such a mechanical instability is caused by "spragging" of the system, which would encourage low frequency noise generation (squeal). It is also obvious that the position of the mounting plane for the caliper carrier bracket is important because of its influence over the spragging angle [18].

It was evident from the literature review that squeal is considered to arise from geometrically induced or kinematic constraint instability of the system. It was noted that the conditions for instability were dependent upon the coefficient of friction, the mass and stiffness parameters of the assembly and the contact configuration of the pad and piston.

The finite element method has become an important tool to predict instability in a brake system. Most of the researchers favour complex eigenvalue analysis because it is a much faster and more cost efficient solution compared to experimental

techniques. The finite element method can effectively predict mode shapes of the disc brake components which are similar to a real disc brake. Reasonably accurate predictions against experimental squeal results can be obtained. Nonetheless the finite element method is only a predictive tool rather than a diagnostic tool.

A binary flutter model plays a significant role in the generation of brake squeal. Most of the mathematical models such as North's binary flutter models [25, 26], Lee's FE model [45] and AbuBakar's FE models [48] are associated with the complex eigenvalues analysis. It is discovered that even when the friction coefficient is constant, the model can be unstable if the friction force couples two degrees-of-freedom together. A large-scale finite element analysis of the stability of a linearised brake system [1] also confirmed that instability arises when two modes merge under the influence of friction.

A number of techniques and equipment are available to capture squeal behaviour through experiments. Accelerometers, piezoelectric (PTZ) beams and non-contact transducers can be employed to identify the mode shapes of brake components but laser holography and EPSI have the edge over accelerometers and non-contact transducers. Laser holography and EPSI have the ability to visualise both out-plane and in-plane modes of vibration of moving components which makes them an excellent tool to identify the mode shapes of the brake components under dynamic conditions; however one must consider the costs associated with these expensive systems.

It was found from the literature review that the movement of the CoP is a very important factor to control the noise in disc brakes and a leading centre of pressure (CoP) tended to have a high propensity to generate noise in brakes. A number of researchers [20, 18, 43, 46] have conducted detailed studies to measure the static and dynamic contact pressure distribution between the disc/pad interfaces. However these studies did not fully identify the influence on brake noise of the position of the dynamic centre of pressure. Some studies considered manipulation of the static CoP in the tangential direction only [18], whilst others considered the dynamic CoP [20],

but were only able to conclude that large variations in position led to more instability (noise). Therefore, there remains a clear knowledge gap that the work contained in this thesis intends to fill. The next chapter details the design and development of a test rig and associated equipment to study the contact pressure distribution and CoP movements under both static and dynamic conditions.

Chapter 3

Development of Test Rig for Dynamic Pressure Distribution Measurements

3.1 Introduction

There are many theories attributed to brake noise but at the higher frequencies the mechanism is generally related to the friction pair of disc/pad and its associated interface geometry. The interface pressure distribution is considered to be important since the dynamic friction force at the disc/pads interface normally depends on the local pressure. Contact between the friction material pad and the rotor is generally considered to occur across the full length of the pad however in practice irregular contact may be observed during brake operation. The variation of brake contact pressure or contact area distribution between rotor and pad may have significant influence on squeal generation. It is now universally established that there is a strong relationship between the interface pressure distribution, the effective centre of pressure and the propensity of the brake to generate noise [17, 20, 46]. It is also known that the centre of pressure may vary both along the length of pad and radially during braking which adds to the complex analysis of instability. The matter is further complicated by the relative sliding between the disc and the pads, leading to an interface pressure offset to the leading edge.

A number of researchers have previously measured static pressure distribution between friction pair of disc/pad in disc brakes but there were limited experimental methods available for the direct measurement of dynamic interface pressure distribution during a braking event. Measurement of the dynamic centre of pressure during braking remains difficult until now. In this study, a distinctive experimental method is employed to determine the movement of dynamic centre of pressure as well as contact pressure distribution between friction pairs of disc/pad during braking events.

The test rig was developed to study the contact pressure distribution and centre of pressure (CoP) movement during both static and braking events. The caliper and set of pads were modified to measure both static and dynamic centre of pressure during braking events. The brake used a 12 piston opposed caliper arranged to allow a number of the pistons to be controlled independently using 4 master cylinders. This allowed the interface centre of pressure to be adjusted both along the length of the pad and radially. The tests included static pressure measurements with the sensor film between the pad friction face and the disc, the centre of pressure being adjusted using the master cylinders to provide a "system benchmark". Once the static characteristic behaviour of the modified pad was established, the centre of pressure variation was measured under dynamic conditions. This allowed the movement of the centre of pressure to be plotted against brake pressure and rotor speed.

3.2 Brake Components

The Alcon brake assembly was selected for this particular investigation. The brake system consists of a caliper, a vented disc and set of pads.

3.2.1 Caliper

The caliper used in this experimental work was a Brabus/Alcon caliper, part number CAR88118, as shown in Figure 3.1 (see Appendix I for detailed drawing). The Alcon caliper is a fixed type caliper consists of 6 pistons at each side of the caliper which provides loading on each brake pad. Under normal use this arrangement allows the pressure to be distributed uniformly on both sides of the caliper allowing greater control of the clamping forces on the rotor and thus wear.

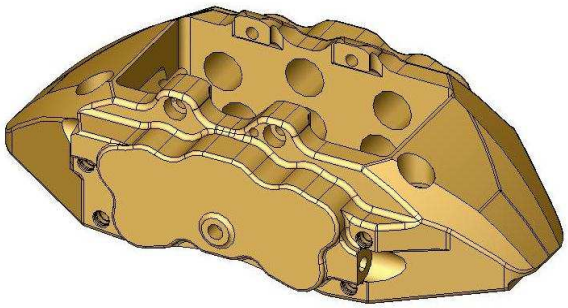

Figure 3.1 Alcon/Brabus caliper

The pistons are normally interconnected by small cross drillings and cast voids within the caliper body. To allow individual pressure at each piston the fluid passages between each piston were sealed by inserting tapered cylindrical plug smeared with epoxy resin on both ends of the passages to prevent the leakage of brake fluid from inter-cylindrical passages. The aim was to control all 6 pistons independently however the fluid passages between two pairs (leading and trailing pistons) could not be sealed because of the large cast voids within the caliper as shown in Figure 3.2. A number of attempts were made to isolate all pistons in the caliper however the fluid channels between two pairs (leading and trailing pistons) could not be sealed and inserted plugs failed to prevent the leakage between these two channels. Another alternative method was to machine a new caliper with all pistons isolated within the caliper but it was not feasible at that time because of the financial and time constraints. It was therefore decided to control four different sets of pistons as shown in Figure 3.2. In the present study the opposing pistons on each half of the caliper were controlled by the same master cylinders.

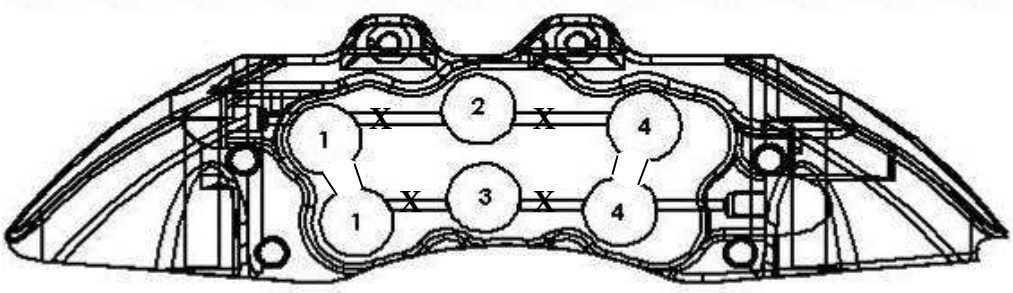

Figure 3.2 Arrangement of pistons ("X" shows where cross drillings were blocked off)

3.2.2 Pads

In order to measure the dynamic pressure distribution during braking, a set of standard pads were carefully prepared by machining a recess and "plug" as shown in Figure 3.3. The sensor was then embedded to the recess and the "plug" used to form a sandwich of the sensor film as shown in Figure 3.4. A thin metal plate was glued to recess pad to provide a smooth and even surface for the sensor film. This eliminates the possibilities of uneven pressure distribution due to irregular contact surface between the sensor and the pad. The pad was then machined to give a level rubbing

surface and the assembly used to measure the dynamic centre of pressure on a test rig.

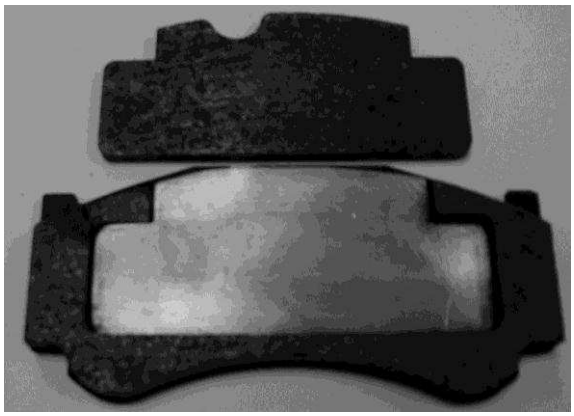

Figure 3.3 Recessed pad and associated "plug"

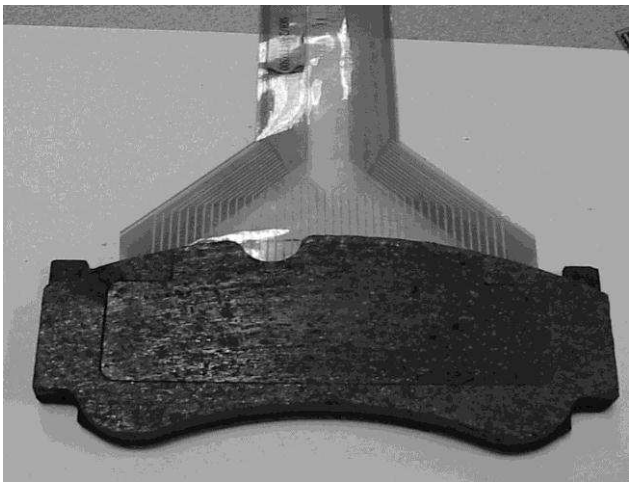

Figure 3.4 Pad assembly with embedded pressure sensor

3.3 Overview of Test Rig Design

A dedicated test rig was developed specifically to perform these tests. The disc was mounted on a solid shaft of Ø100mm that was held in taper roller bearings, loaded to give zero axial float, and held in a bearing housing. The housing had two end flanges. One flange allowed the housing to be aligned to the driveshaft and bolted to the rig frame and the second front flange allowed mounting and circumferential adjustment of the calipers using slotted holes. The brake disc was driven through partial flexible couplings direct from a 45 kW, 2440 rev/min 3-phase a.c. motor through a 30:1 worm gear speed reducer. The couplings were used to accommodate

the radial and angular misalignment between the shaft, flange and the gearbox. Disc brake speed was controlled by using a vector controller that provided variable speed down to 1.0 rev/min. The maximum speed of 80 rev/min was achieved by driving the motor to its maximum output power whilst the shaft could be rotated in both the clockwise and anti-clockwise directions. The test rig was mounted on a rigid base plate fixed securely to a bedplate as indicated in Figures 3.5.

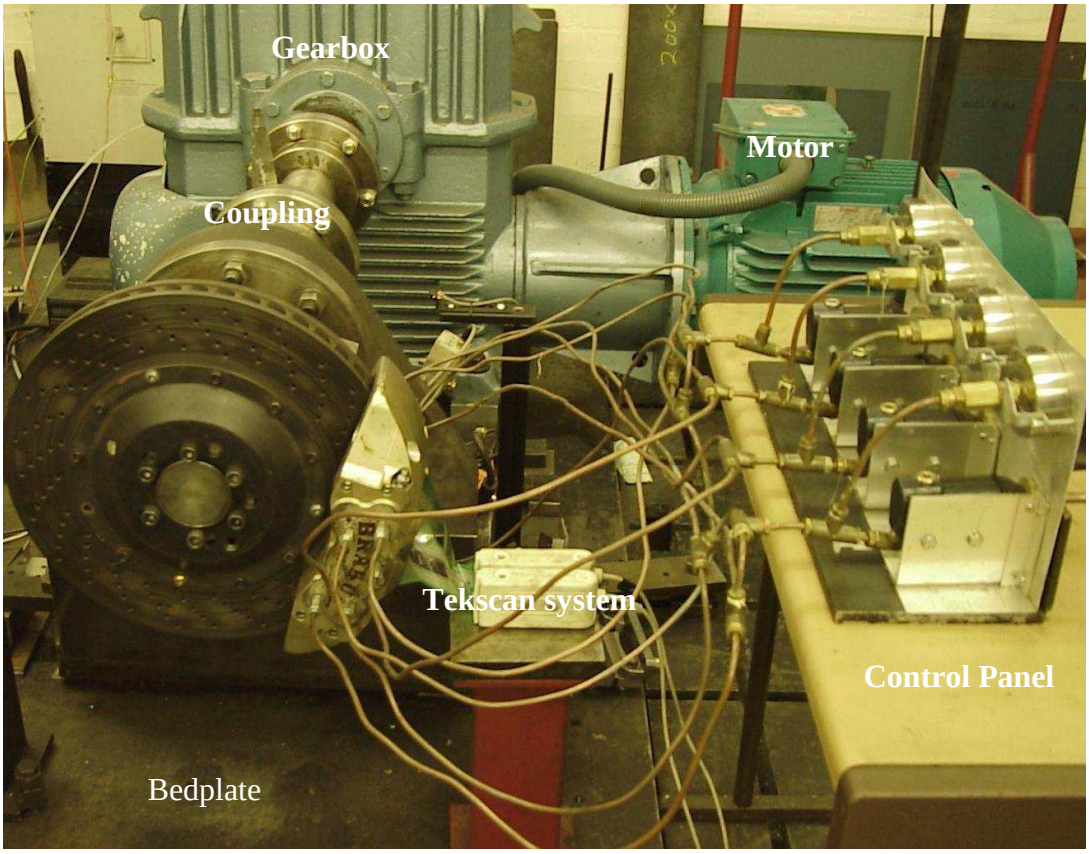

Figure 3.5 General view of test rig

The brake used a 12 piston opposed caliper modified to allow the centre of pressure to be controlled manually. Pressure was limited to a number of the pistons giving 4 sets of pistons, controlled independently using 4 master cylinders which were applied manually using screwed adjusters (see section 3.4). This allowed the interface centre of pressure to be adjusted both along the length of the pad and radially. The caliper was bolted to a bracket and bracket itself was mounted to the flange as shown in Figure 3.6. The line pressure was observed on four different pressure gauges. The maximum hydraulic pressure of 4MPa (40 bar) could be recorded on each of the

pressure gauges; however brake squeal rarely occurred at such high pressures. It is known by experience that the majority of squeal instability occurs at brake pressures less than 2MPa (20 bar).

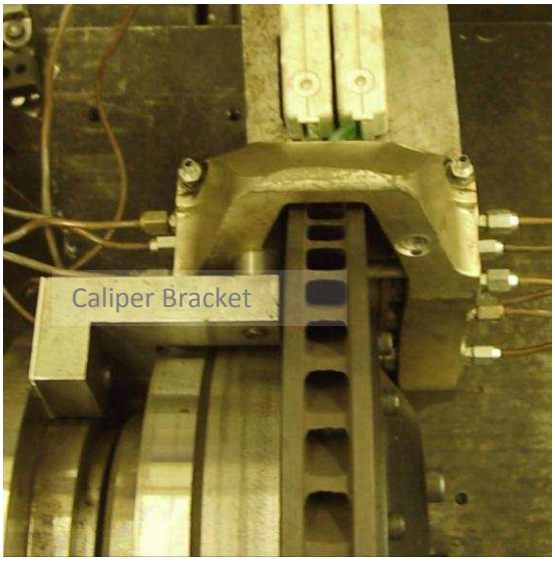

Figure 3.6 Caliper mounting arrangements

3.4 Development of Control Panel

A control panel was developed to control four different sets of pistons (Leading and trailing pair and two middle individual pistons). The control panel consisted of four master cylinders with screwed knobs and pressure gauges. The outlet from the master cylinder connected to individual pressure gauges and then branched out to the caliper at the centre of each cylinder piston as shown in Figure 3.7. This ensured that each master cylinder was capable of providing independent pressure to each connected pistons. It was also ensured that each master cylinder distributed equal line pressure to both inboard and outboard pads. A standard hydraulic brake fluid, Ferodo DOT 4, was used in the current investigation.

Figure 3.8 shows a detailed layout of the modified caliper. As shown in Figure 3.8, the pistons pairs at the leading edge **(1)** are connected together by cast voids and are supplied with a common pressure and controlled by a single master cylinder. The same principal applied for piston pairs at the trailing edge and its opposite pair **(4)**, which was controlled by another master cylinder. The central pistons outer (piston 2)

and inner (piston 3) are pressurised independently using two master cylinders so giving control over the radial pressure distribution.

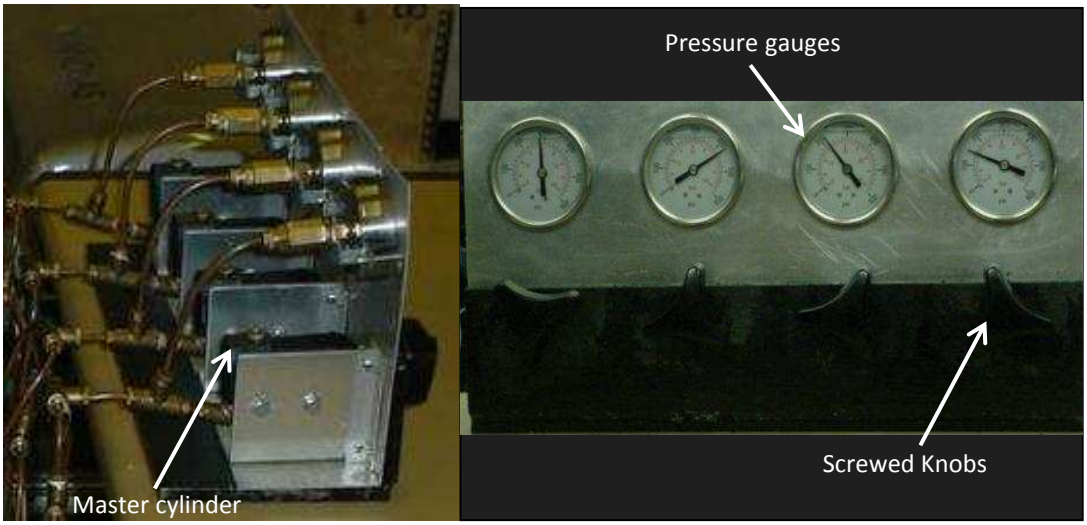

Figure 3.7 Showing various view of control panel with tubes configuration

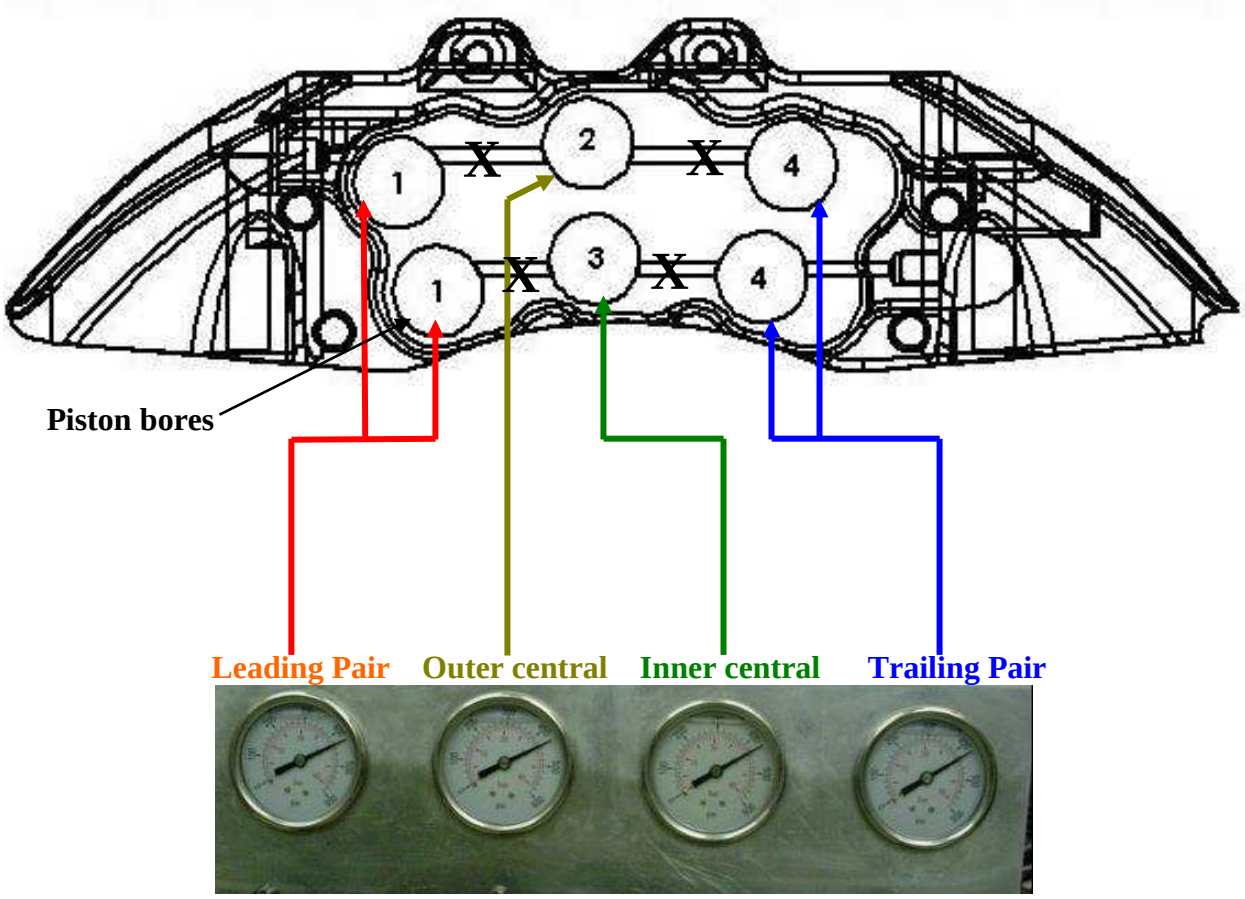

Figure 3.8 Pistons arrangement at each cylinder position.
"X" indicates where brake fluid (DOT 4) passages were blocked.

3.5 Instruments

3.5.1 Pressure Distribution Measurement System

3.5.1.1 Introduction

The Tekscan pressure mapping system (model no; I-Scan®) was used to measure the contact area, contact force distribution and the movement of centre of pressure during braking events.

I-Scan® is an inclusive system which converts a Microsoft PC into an advanced pressure distribution measurement system. It is comprised of both hardware and software components. The hardware components collect pressure information from the system and make the data available to the system software to view the collected pressure data [49]. PC Interface Board is a data acquisition card installed in the computer expansion slot and the Parallel Interface consists of a parallel interface module, a parallel extension cable and a sensor handle as shown in Figure 3.9.

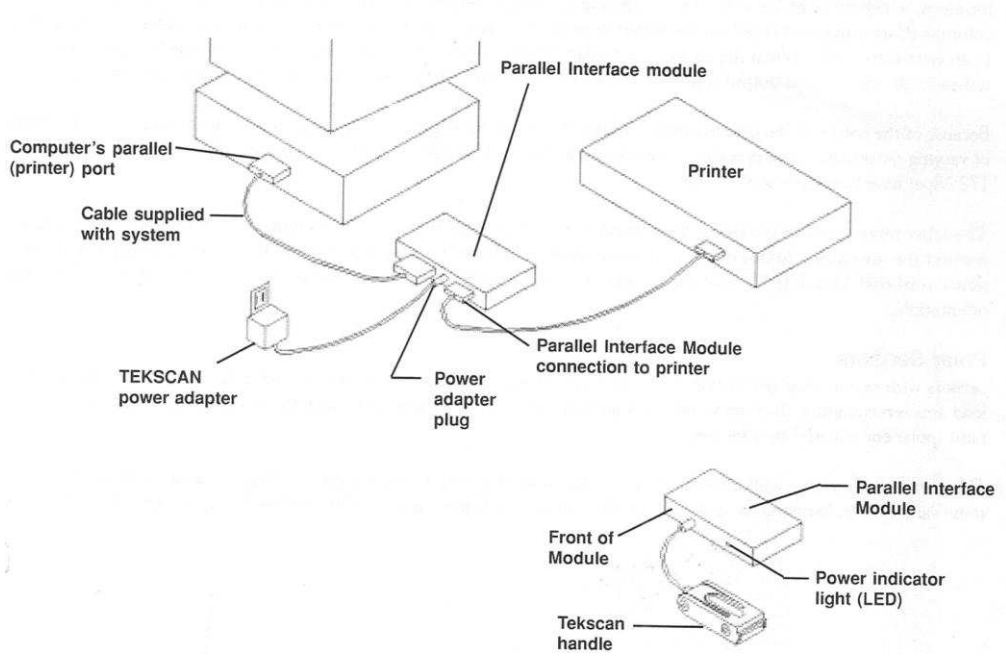

Figure 3.9 Schematic layout of Tekscan system [49]

3.5.1.2 Tekscan Pressure Sensors

Tekscan sensors consist of two thin, flexible polyester sheets which have electrically conductive electrodes placed in varying patterns. They also contain a thin semi-conductive ink coating as an intermediate layer between the electrical contacts. The ink provides the electrical resistance at each of the intersection points (called sensels) and this resistance changes as the stress across the cell changes. By measuring the changes in current flow at each intersecting point, the applied force distribution pattern can be measured and recorded by the Tekscan system. The lattice of the mat allows the software to determine the location of the load. The sensor tab is placed into the sensor handle which connects directly to the interface board to parallel interface module and gathers the data from the sensor and processes it so that it can send it to the computer [49].

A sensor type 5105 was used in this investigation to measure the pressure distribution between disc/pad interfaces (see data sheet in Appendix E.1). The sensing area of this particular sensor was 111.8mm x 111.8mm; number of sensing elements was 1936 with the spatial resolution of 15.7 sensels per cm^2 and the operational pressure range was from 0 to 3.4MPa (34bar). The sensor was trimmed to fit into the pad recess. An explanation of the cutting process of the sensors is given in Appendix E.2.

3.5.1.3 Conditioning the Sensor

It is important that the sensors were properly ‘conditioned’ prior to use and calibrated. This process helped to lessen the effect of drift and hysteresis (hysteresis is the difference in the sensor output response during loading and unloading, at the same applied force). All Sensors were conditioned at a brake pressure of 2.4MPa (120% of the maximum pressure) for 3 seconds and then the pressure was removed and the entire process was repeated four times to ensure accurate results.

3.5.1.4 Calibrating the Sensor

Prior to using sensors, it was important to show that the results they provided were accurate under the required test conditions. It was therefore necessary to calibrate the

sensors to reduce uncertainties in the results. Calibration also helped to compare the same sensor in various environments and allowed comparison of outputs of various sensors. For calibration the software calculated an average applied pressure based on the area of loaded intersection points (sensels) and the entered force value. This meant care had to be taken to ensure the loaded area of sensors remained constant for all calibration points. The sensors were calibrated using the Tekscan guidelines from the Tekscan manual [49]. Tekscan provides two methods of calibrating sensors, a one point calibration or a two-point calibration. A one point calibration assumes a linear output from the sensor with zero force (pressure) applied resulting in zero total raw sum of output. In this case the Tekscan system uses two points to calculate the calibration relationship. This type of calibration is attractive for applications where similar loads are applied in the tests. The other type of calibration is a two-point calibration, which takes into account the non-linearity of the intersection points (sensels). It determines a power logarithmic curve using two other calibration points. This is the preferred method when the applied load varies during testing. A two-point calibration method was employed in this work, as the brake line pressure varied substantially during tests. Rose and Stith [50] also found that the two point calibration provided much better results compared to a one point calibration and this method also gave more accurate mean and total contact forces.

In order to evaluate the sensor calibration, a number of uniform pressures of 0.5, 1.0, 1.5 and 2MPa were applied. The contact forces were calculated and compared to the applied loads (pressures). Force measurement error (%) was calculated by taking the difference between calibrated Tekscan output and applied forces to each sensor. The calibration results indicated (Appendix F.1) that the overall sensel pressures, obtained by Tekscan sensors, were found to be in good correlation with the pressure applied to the sensor. The calibration results showed an overall error varying between ±4%. It should be noted that at the higher pressure of 2MPa, the measured force error was much higher in the range of 8-11%. This could be because at the high pressure settings the pressure sensor was subject to high deformation and shear stresses which can adversely affect the accuracy of the pressure distribution results. A study into the sensitivity of the pressure to change in brake temperature was also undertaken. These tests included static pressure measurements at various brake

temperatures with the sensor film placed between the disc/pad interfaces. Again, force measurement error (%) was calculated by taking the difference between the calibrated Tekscan output and applied forces to each sensor. It was found from the results, as shown in Appendix F.2, that at room temperature of 23ºC, the measured force error (%) at the inboard pad was about 2% comparing to the outboard pad which was about 1.6% whereas at the higher temperature of 200ºC, the measured force error (%) at the inboard pad was much higher in the range of 9% comparing to the outboard pad which was about 5%. It was confirmed that the pressure sensors are sensitive to the elevated brake temperatures and they should be used within the temperature range specified by the manufacturer to ensure accurate results. A detailed calibration results are displayed in Appendix F.1 and F.2.

3.5.2 Other Instruments

Disc temperature was measured using a non-contact laser infrared thermometer with a range of 0 to 250°C. According to the manufacturer, the accuracy of this thermocouple was approximately ±2% of the nominal range.

A condensing type microphone was placed at distance of 100mm outboard from the disc face and 500mm above and perpendicular to the centreline of the disc. The microphone was connected with the B&K FFT analyser type 2031 to identify the generated noise frequency.

3.6 Brake Tests

The following procedures were carried out to ensure that all the tests initiated with similar conditions.

3.6.1 Bedding-in Process

The bedding-in process involved a gradual build-up of heat in the brake disc and pad lining. This process laid down a thin layer of transfer film on to the rotor surface. All brake pads were fully “bedded in” with the brake disc before performing any noise tests to ensure consistent and reliable results. The bedding-in procedure involved performing short drag braking events at different speeds from 10-80 rev/min during

which the brake pressure was applied to varying levels, between 0-2MPa hydraulic pressure whilst allowing the brake disc temperature to steadily increase to 250°C. Temperature rise during each braking event was in the region of 10-20°C and the disc temperature at the beginning of the "bedding" procedure was 20°C. Once the disc temperature of 250°C had been reached, the disc was allowed to cool down to 20°C. Following this process the brake was examined visually and the disc and pad surfaces inspected to ensure full contact between disc and pad had been achieved and, by observation, that the surface transfer was complete around the disc rubbing surface.

3.6.2 System Stabilisation

This procedure was carried out to ensure that all the tests were carried out with similar conditions. The disc speed was set to 80 rev/min and a uniform hydraulic pressure of 0.7MPa was applied to the brake until the brake temperature was in the range of 200°C. Once the temperature exceeded 200°C, the disc speed was reduced to 60 rev/min and the hydraulic pressure in the caliper reduced to 0.3MPa until the disc cooled down to 100°C. This procedure can also be used to induce noise in a brake system. The squeal noise was checked during this cooling period by increasing the pressure quickly to 1.4MPa and then reducing it gradually to zero. The brake noise was audible readily below 100°C.

The brake squeal evaluation process was based on subjective rating for brake squeal annoyance. It provided a reliable prediction of the annoyance of brake squeal on a rating scale from 1 (very loud squeal) to 4 (no squeal) as shown in Table 3.1.

Table 3.1 Squeal annoyance rating scale

1	2	3	4
Very loud squeal	Squeal (moderate squeal)	Intermittent squeal	Quiet (no squeal)

3.7 Summary

In this chapter, a unique experimental technique was developed to measure the movement of the dynamic centre of pressure as well as contact pressure distribution

between friction pairs of disc/pad during braking events. A modified caliper and set of pads were developed, whilst a control panel was constructed to apply individual pressure at various pistons.

The pressure mapping system was evaluated prior to use and the pressure sensors were conditioned and calibrated to ensure accurate results. Once the calibration process was conducted and evaluated, an immediate insight into the behaviour of contact forces and pressure distribution of disc/pad interfaces could be examined. The next chapter is focused on the detailed experimental study of contact pressure distribution of the disc brake assembly and the dynamic movement of centre of pressure during braking events.

Chapter 4

Experimental Studies

4.1 Introduction

In this chapter, the results of experimental studies on contact pressure distribution of disc brake assembly are presented. A number of tests were carried out to measure the pressure distribution between friction pair of disc/pad under various conditions. The main experimental measurements conducted in this chapter are listed as follows:

- Contact pressure distribution measurements
- Effect of different parameters on contact pressure distribution
- Contact pressure distribution measurements during squeal

4.2 Contact Pressure Distribution Analysis

The pressure distribution measurements between friction pair of disc/pad were captured over a period of set time through a movie recording. The advantage of taking movie recording is that all the recorded information can be viewed in a variety of graphical representation and the measured results can be accessible at any time. A typical recorded image of force distribution can be seen in Figure 4.1. It should be noted that Figure 4.1 showing a single frame taken from the recorded movie and the centre of pressure is shown as a grey and white diamond as indicated.

In addition, the total contact force and contact area distribution could be measured and plotted under various conditions. The graphical images of contact pressure distribution map and force distribution map of both outboard and inboard pad were captured simultaneously to exhibit the characteristics behaviour of each of the pads as shown in Figure 4.1.

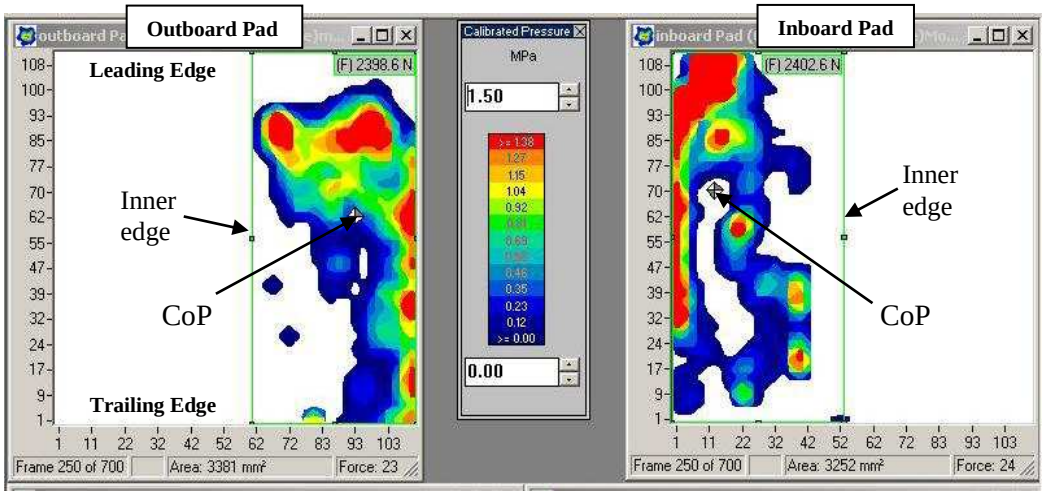

Figure 4.1 Typical display of a force distribution map reading for both outboard (LHS) and inboard (RHS) pad

4.2.1 Movement of Centre of Pressure (CoP)

The movement of centre of pressure (CoP) was measured for the duration of a recorded movie. The centre of pressure (CoP) can be tracked by playing, as a movie, one frame at a time.

In order to allow the movement of the centre of pressure to be plotted against brake pressure and disc speed, the centre of pressure (CoP) data was imported into a Microsoft Excel spread sheet programme. However the imported data was in unformatted text and it was therefore required to reformat the data to obtain meaningful results.

To undertake a meaningful investigation of the influence of variables, the investigation was divided into 3 parts, with each part subdivided into more detailed studies.

Speed - The first part, section 4.3, part 1a, was to determine the effect of speed and so the pistons were each set to a specific uniform pressure and the speed varied over a given range. The pressure was then adjusted and the tests repeated. This provided information on CoP movement with respect to speed and CoP movement with

respect to pressure variation. Section 4.3.1, part 1b was to use the same information to investigate the effect of CoP movement due to uniform pressure variation.

Pressure variation - Longitudinal – The speed was set at 10 rev/min and the pressure was principally varied along the length of the pad.

Pressure variation - Radial – The speed was set at 10 rev/min and pressure was varied principally in the radial direction.

4.2.2 Comparison of Static Pressure Measurements

These tests included static pressure measurements with the sensor film placed between the pad friction face and the disc. Total contact forces at each pad were measured at various brake pressures of 0.4, 0.6, 0.8, 1.0, 1.5, 2.0MPa. The graphical images of contact pressure distribution map of both outboard and inboard pad were captured to exhibit the characteristic behaviour of each of the pads.

The pressure sensor film was then embedded into the recess of the pads and the "plug" used to form a sandwich of the sensor. The entire test was then repeated as mentioned above and the contact forces obtained from the Tekscan system were compared with the initial static tests. The contact force measurement errors between these two tests were in the range of about ±8%. A detail comparison of static pressure measurements are shown in Appendix G.

4.3 Effect of Rotational Speed of the Disc and Contact Pressure on Contact Pressure Distribution – Part 1a

It was important to determine at the outset if disc speed had any effect on the centre of pressure. The reason for this was that a typical vehicle braking event is a variable speed event and if speed was an issue it would be necessary to establish the range of speeds of concern. In this section, the effect of the disc speed on the contact pressure distribution of disc/pad interface was investigated. The modified pads were initially calibrated to the static interface pressure measurements. Once the static characteristic

behaviour and sensitivity of the modified pads were established, the pressure distribution between disc/pad was measured under dynamic conditions.

The measurements were conducted at six different rotational speeds: 5, 10, 15, 20, 30 and 40 rev/min (this equivalent to vehicle speed of 2.6 km/h). The caliper pressure setting on all pistons was initially set at 0.2MPa. The static value was established initially and then the disc speed was increased in various stages, each stage being for the duration of 50 seconds. This provided 700 movie frames for each pressure setting with a period of 0.5 second between each frame. The recorded information provided seven sets of images of contact force, pressure and contact area distribution.

The same test was repeated again with various hydraulic pressures of 0.4, 0.6, 0.8, 1.0, 1.5, 2.0MPa.

The measured centre of pressure was plotted against a different set of disc speeds as shown in Figures 4.2 and 4.3 for the outboard pad longitudinal and radial movement and Figures 4.4 and 4.5 for the inboard pad. In all cases it can be seen from the Figures that disc speed does not appear to have any real noticeable effect on the position of centre of pressure. However it was noted that the centre of pressure of the outboard pad tended to be more erratic than the inboard pad, possibly because of the less rigid condition of the outboard pad. The similar movement was evident radially with the centre of pressure of the outboard pad. It was also observed that the fluctuation movement of the centre of pressure, of both outboard and inboard pad, tends to decrease with the higher caliper pressure. It is felt that this reduction may be as a result of the increased pad/carrier abutment force and so a greater damping effect on any movement.

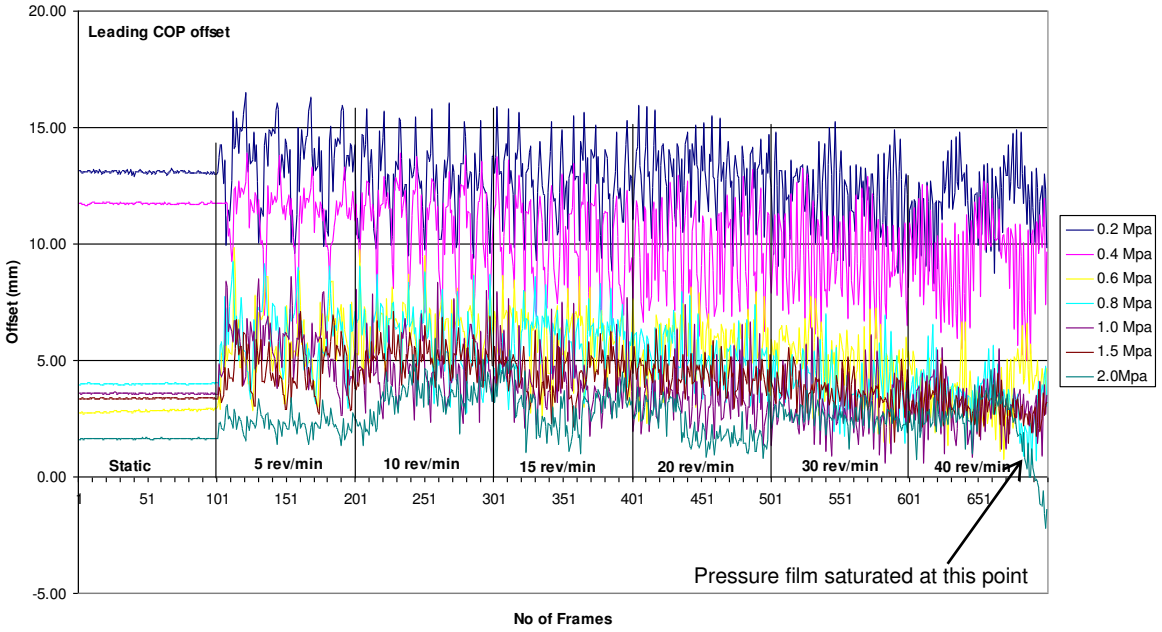

Figure 4.2 Variation of longitudinal centre of pressure with speed (Outboard Pad)

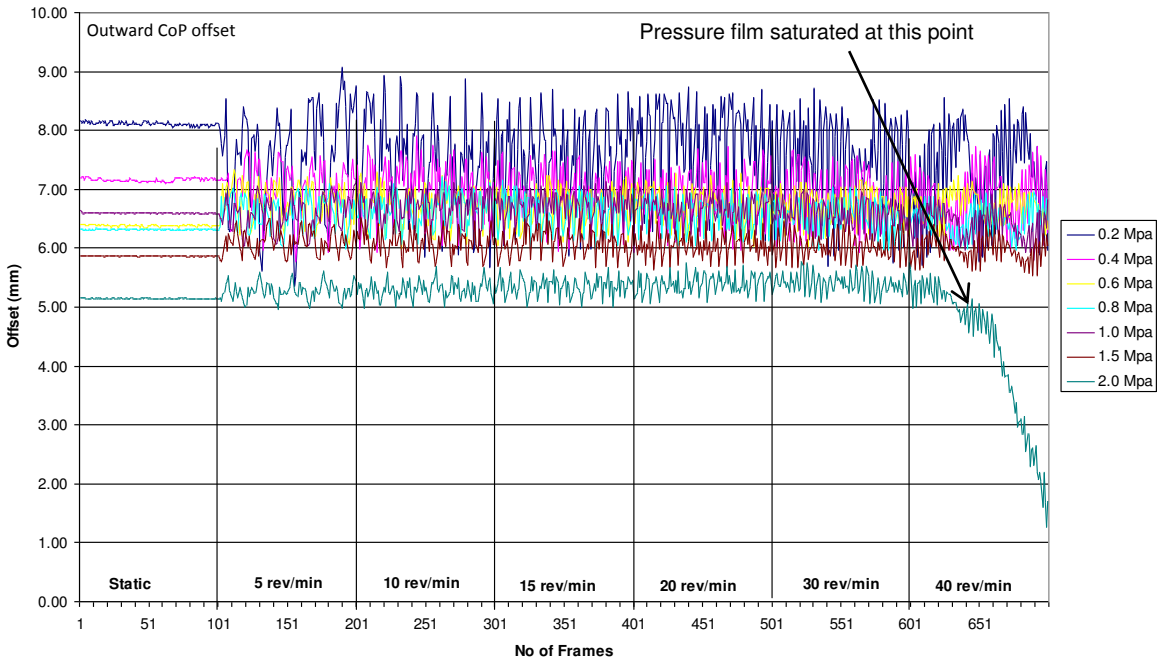

Figure 4.3 Variation of radial centre of pressure with speed (Outboard Pad)

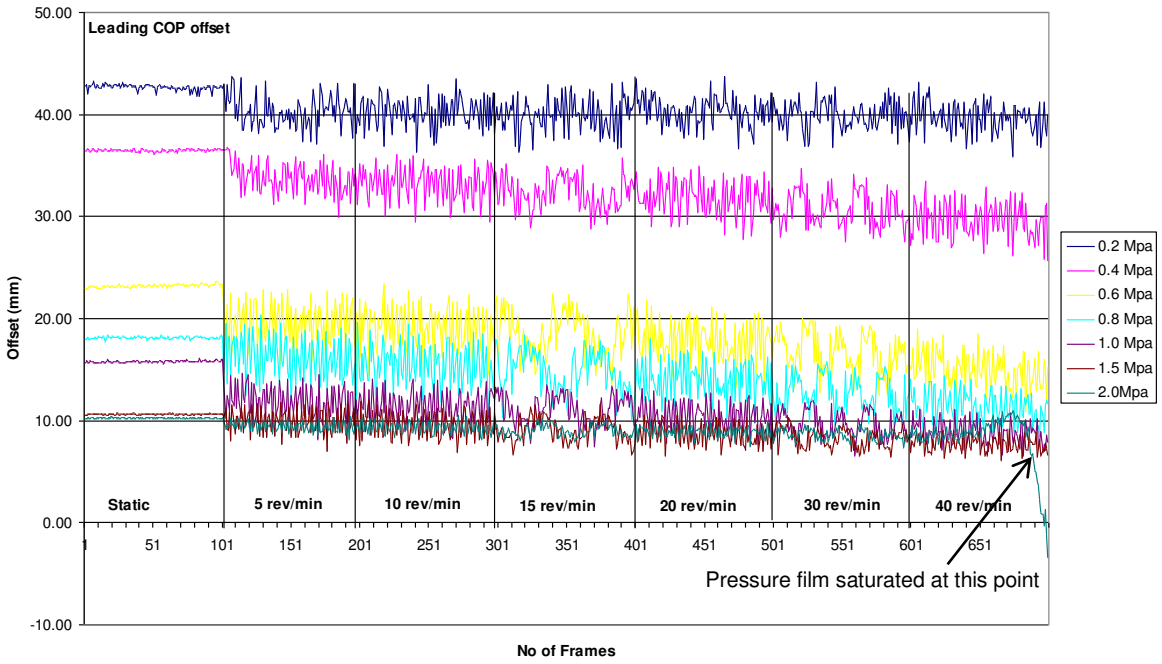

Figure 4.4 Variation of longitudinal centre of pressure with speed (Inboard Pad)

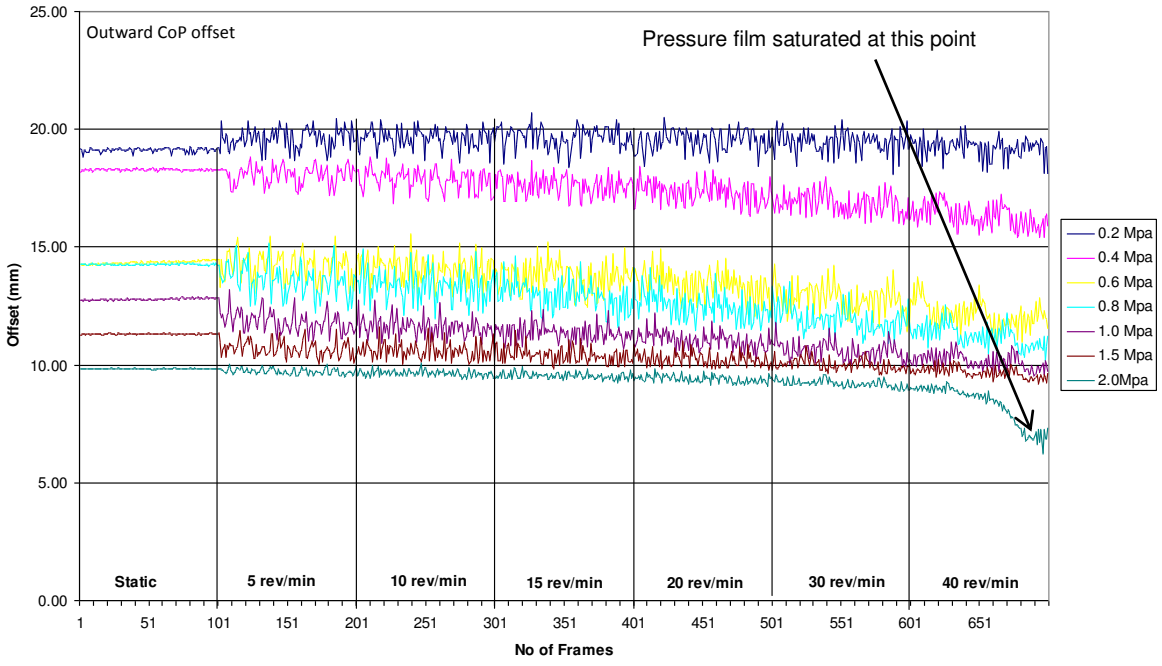

Figure 4.5 Variation of radial centre of pressure with speed (Inboard Pad)

4.3.1 Effect of Hydraulic Pressure of the Caliper on Contact Pressure Distribution – Part 1b

In this section, the effect of the caliper pressure on the contact pressure distribution of the disc/pad interface was examined. The same procedure used in the previous section 4.3 allowed movement of the centre of pressure (CoP) against various caliper pressures to be plotted. However in this particular test the hydraulic pressure was increased after an interval of 80 frames recording with a total of 560 frames being recorded (7 tests x 80 frames).

The measured centre of pressure was plotted against a different set of caliper pressures as shown in Figures 4.6, 4.7, 4.8 and 4.9. From the Figures, it is clearly evident that the centre of pressure (CoP) tended to be positioned towards leading offset at low brake pressure (0.2MPa). As the caliper pressure increased it was seen that the centre of pressure moved towards the central section of the pad (Figures 4.6 outer pad and 4.8 inner pad). It was also seen that by increasing the caliper pressure, the centre of pressure of both outboard and inboard pad, tended to move radially inwards (Figures 4.7 and 4.9). From the results it was apparent that the longitudinal centre of pressure (CoP) of the inboard pad tended to have more leading offset compared to the outboard pad. Similar results can be seen for the radial centre of pressure (CoP). It was also evident that the centre of pressure (CoP) of the outboard pad moved more erratically than the inboard pad, as seen with Figures 4.2 to 4.5.

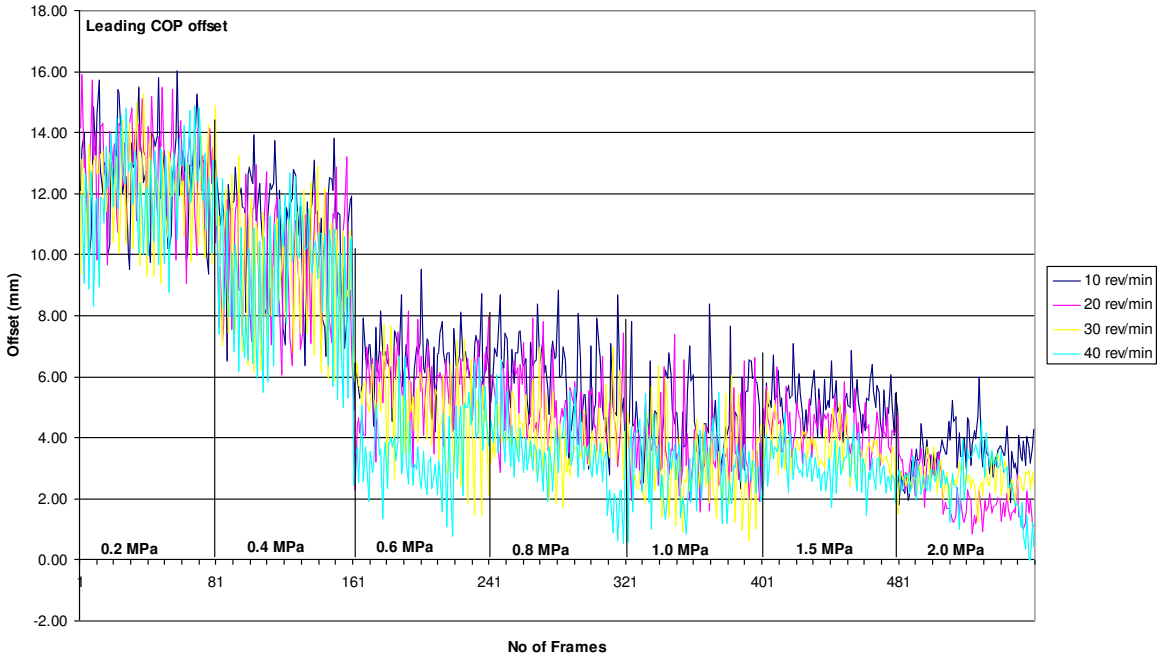

Figure 4.6 Movement of longitudinal centre of pressure with different hydraulic pressures (Outboard Pad)

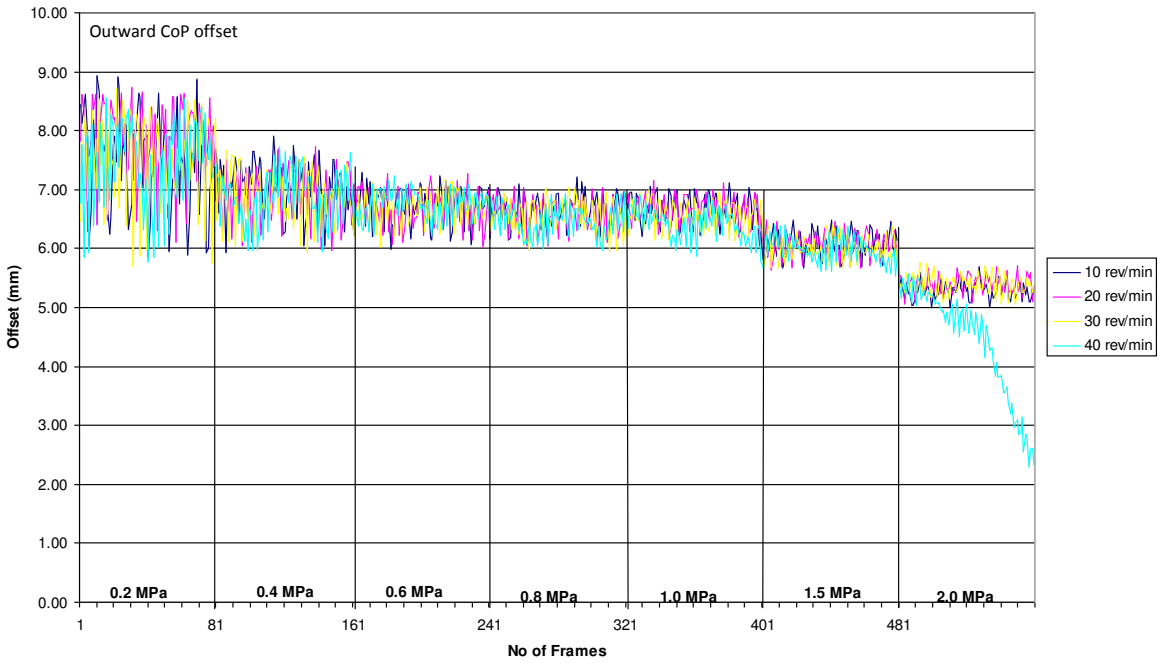

Figure 4.7 Movement of radial centre of pressure with different hydraulic pressures (Outboard Pad)

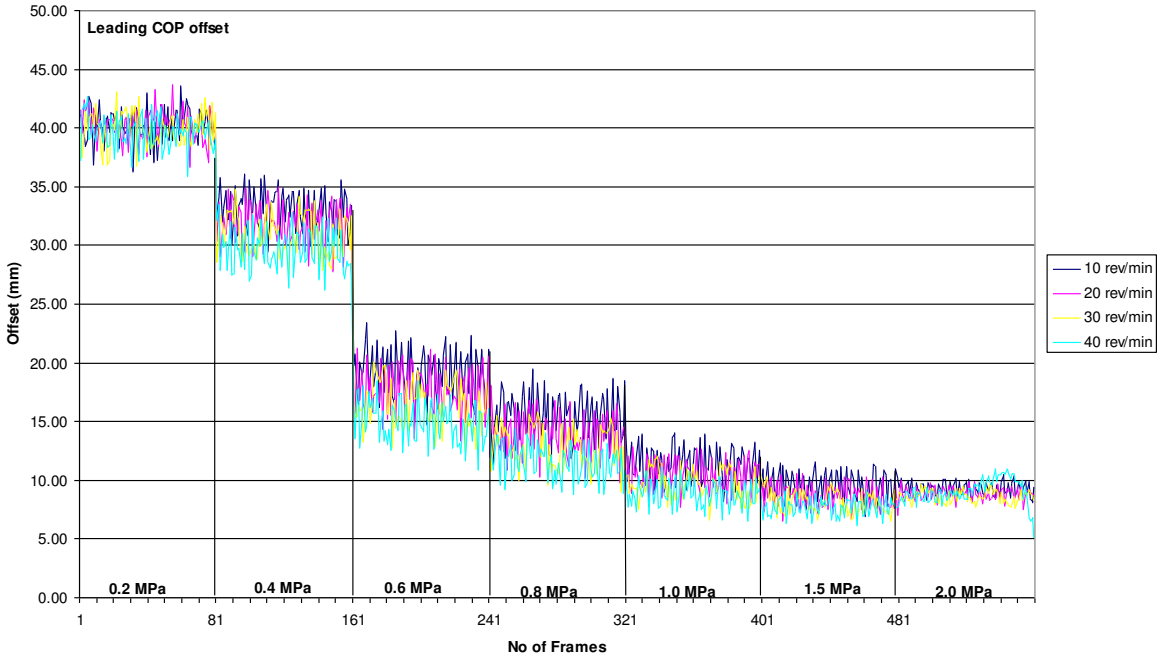

Figure 4.8 Movement of longitudinal centre of pressure with different hydraulic pressures (Inboard Pad)

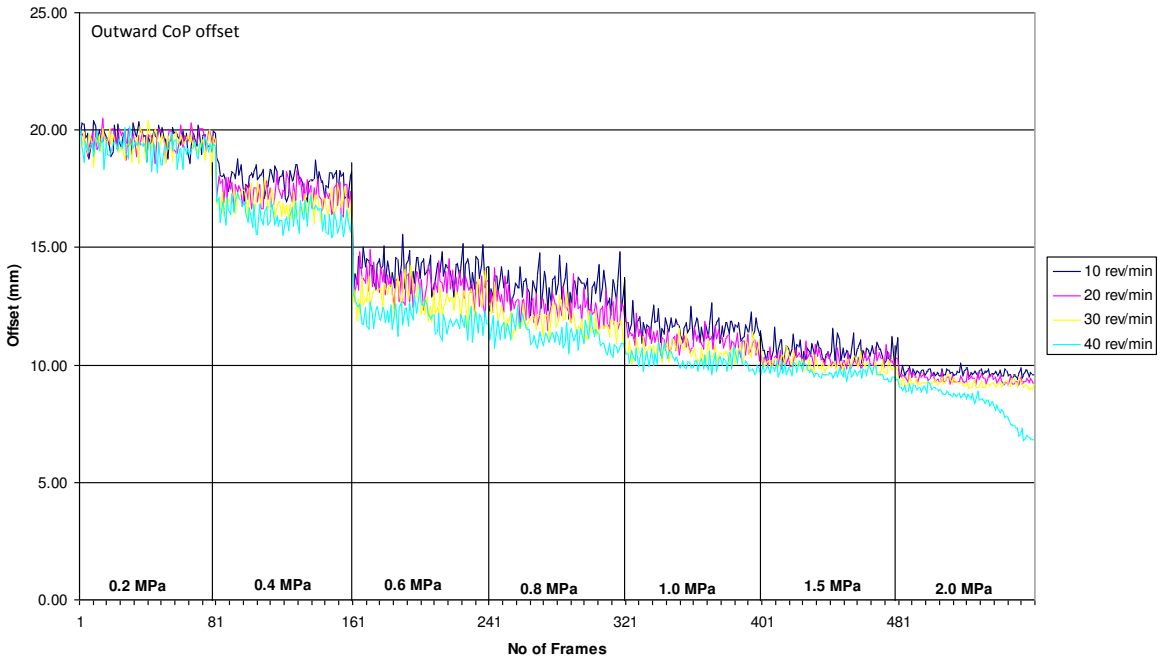

Figure 4.9 Movement of radial centre of pressure with different hydraulic pressures (Inboard Pad)

The averages of each of the pressure settings in Figure 4.8 were calculated and re-plotted. A clearer trend of CoP movement was seen as shown in Figure 4.10 whereby as pressure increased the CoP moved towards the pad centre.

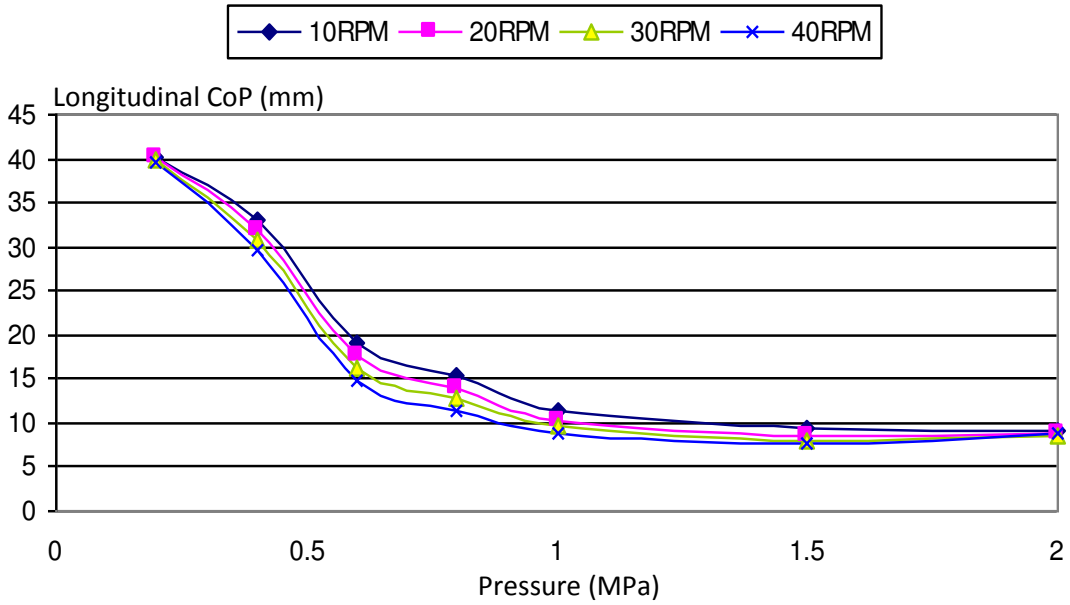

Figure 4.10 Average CoP for pressure series shown in Figure 4.8

Each of these curves can be represented a cubic equation of the form:

$$y = ax^3 + bx^2 + cx + d \qquad (4.1)$$

with the constants for each of these curves being as shown in Table 4.1

Table 4.1 Constants in cubic equation (longitudinal) for each speed setting

Speed Constant	10 RPM	20 RPM	30 RPM	40 RPM
a	-10.16	-11.95	-13.32	-14.68
b	51.86	58.98	64.13	69.84
c	-86.78	-94.65	-99.89	-105.95
d	56.76	57.93	58.40	58.98

If these constants are plotted against speed then it is possible to better evaluate the effects of speed and so extrapolate the curves to determine the constants at any other speed, and thus predict the position of the CoP due to speed variation.

The plots for the constants shown in Table 4.1 are presented in Figure 4.11.

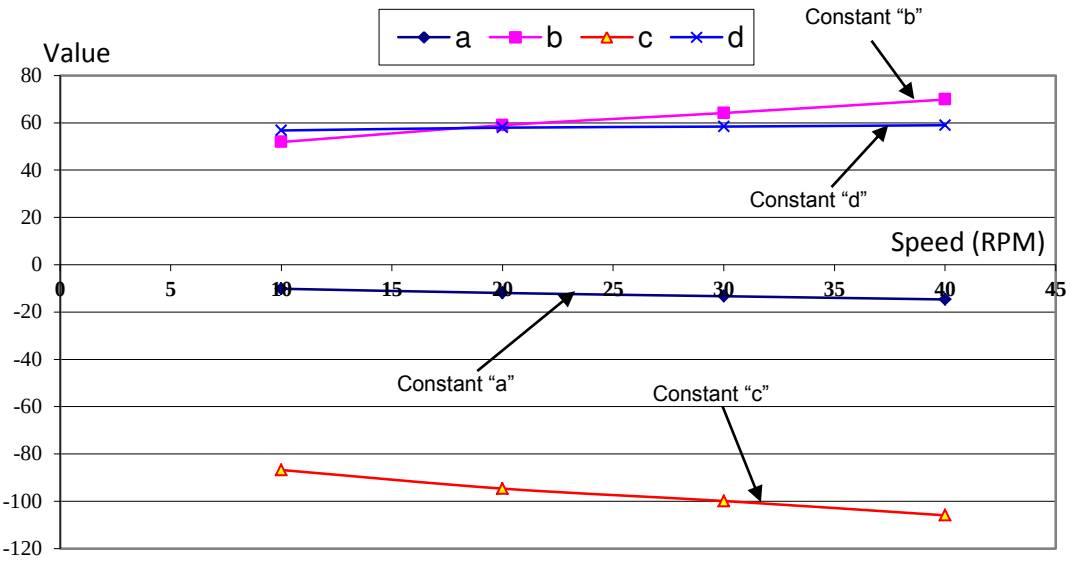

Figure 4.11 Plots of cubic equation constants (longitudinal) against disc speed (Refer to Table 4.1)

Note how constant "d" is almost level whereas constants "a" and "c" tend to have a negative gradient whereas "b" has a positive gradient. The gradient variations in the constants would tend to compensate for each other and so indicate an overall independence of speed regarding the CoP, supporting the general observation made earlier on Figures 4.2 to 4.5.

If an overall average of the curves shown in Figure 4.10 is calculated (that is the influence of speed is considered minimal) and the result is then plotted then Figure 4.12 provides the general equation as

$$y = -12.53x^3 + 61.20x^2 - 96.82x + 58.02 \qquad (4.2)$$

where "y" is the offset and "x" is the overall applied piston pressure.

If this is then compared to the actual theoretical cubic curve a comparison of accuracy may be made as shown in Figure 4.12. Accepting this as correct then the

CoP for any reasonable pressure setting may now be calculated where “y” being the longitudinal CoP and “x” being the applied piston pressure.

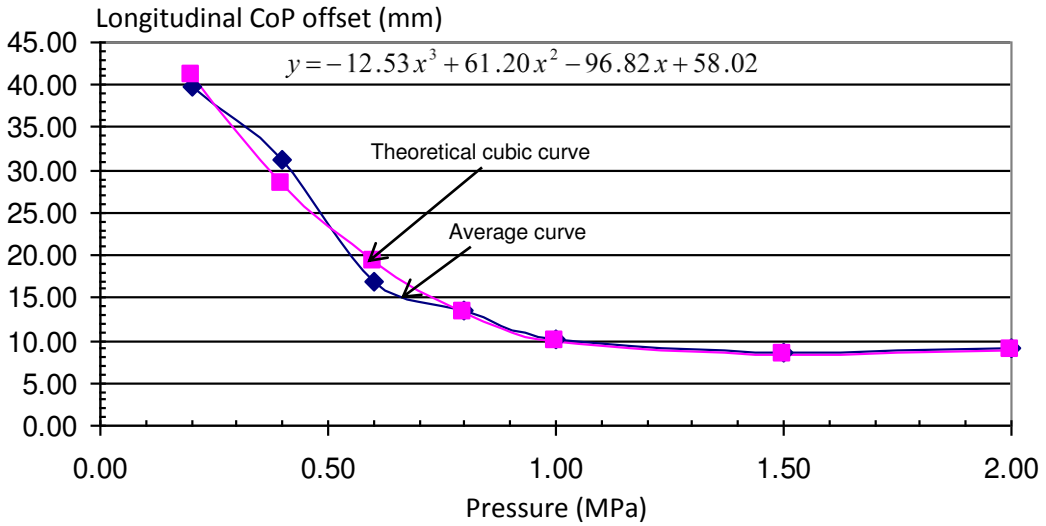

Figure 4.12 Overall average curve for all speeds at varying pressures

If this is accepted then there is now an equation that will allow the longitudinal CoP to be predicted if the pressure is known.

A similar analysis was carried out for the radial movement as shown in Figure 4.13 that shows the average CoP radial movement of the curves shown in Figure 4.9. Again the constants may be determined for each curve, these being shown in Figure 4.14 and listed in Table 4.2. By observation it can again be inferred that speed has minimal effect on the radial CoP, as with the longitudinal CoP.

Table 4.2 Constants in cubic equation (Radial) for each speed setting

Speed Constant	10 RPM	20 RPM	30 RPM	40 RPM
a	-10.16	-3.26	-3.67	-5.85
b	16.22	15.41	17.14	24.52
c	-25.86	-25.17	-27.27	-34.61
d	25.01	24.19	24.53	26.01

If an overall average of the curves shown in Figure 4.13 is calculated (that is the influence of speed is considered minimal) and the result is then plotted then Figure 4.15 provides the general equation as

$$y = -4.09x^3 + 18.32x^2 - 28.23x + 24.93 \qquad (4.3)$$

where "y" is the radial offset from pad centre, in this case, and "x" is the overall applied piston pressure.

If this is then compared to the actual theoretical cubic curve a comparison of accuracy may be made as shown in Figure 4.15. Accepting this as correct then the CoP for any reasonable pressure setting may now be calculated where "y" being the radial CoP and "x" being the applied piston pressure.

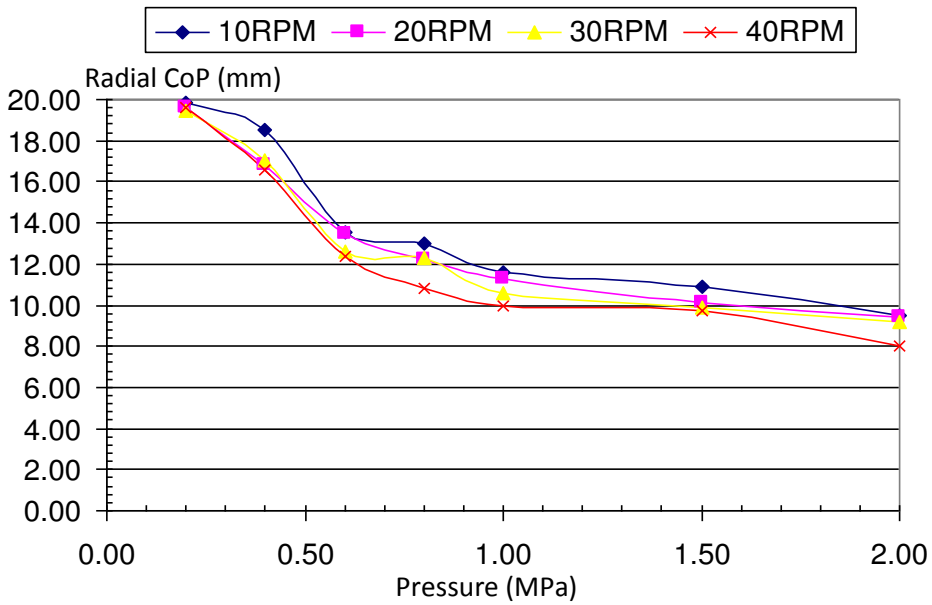

Figure 4.13 Plots of radial movement with speed

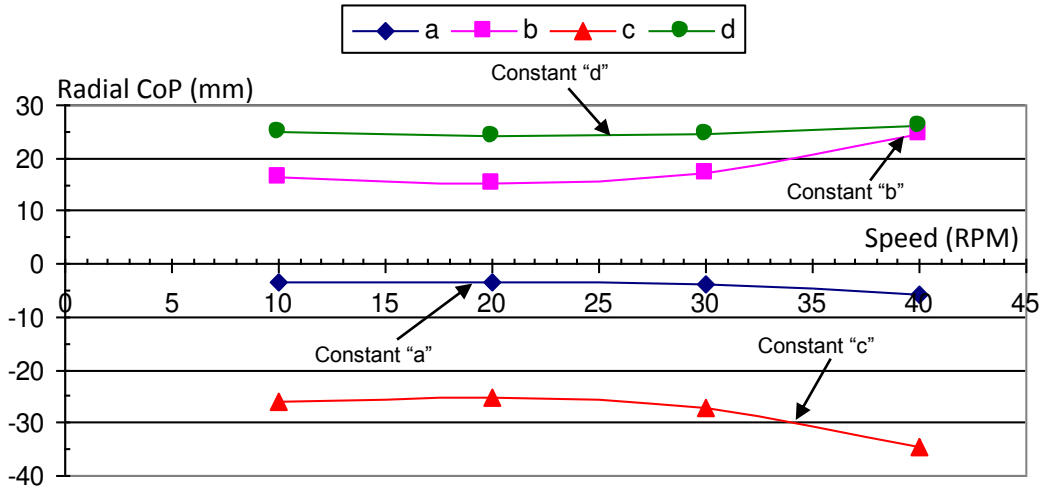

Figure 4.14 Plots of cubic equation constants (Radial) against disc speed. (Refer to Table 4.2)

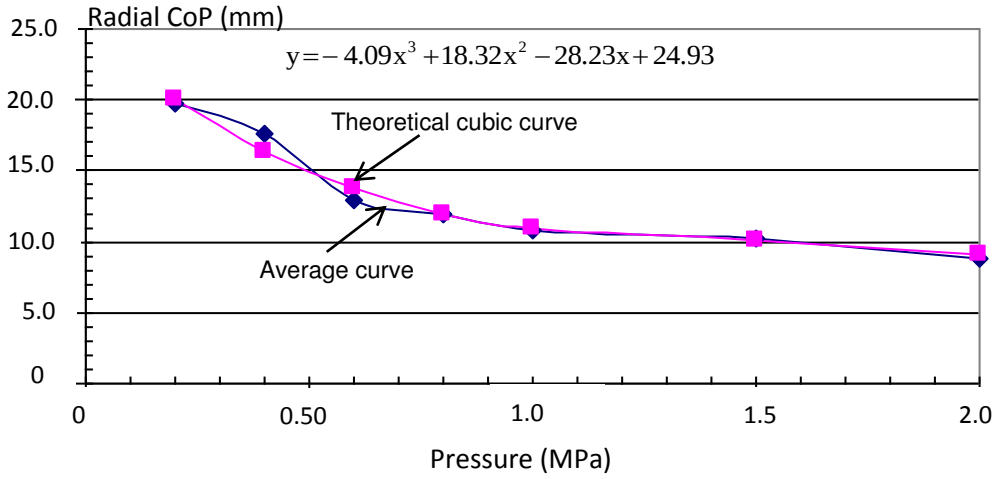

Figure 4.15 Overall average curve for all speeds at varying pressures.

The effect of hydraulic pressure on the contact force distribution with various caliper pressures was also examined. Figure 4.16 shows that as the caliper pressure increased, the total contact force also increased as would be expected. The magnitude of the applied hydraulic pressure was relatively proportional to the total contact force. Both inboard and outboard pads demonstrated the same effect. The curves plotted were not strictly linear because of the higher force measurement error (%) at the pressure of 2MPa as shown in Appendix F.1. If the last reading at the pressure of

2MPa is excluded from the overall results, the curve would be linear and the brake line pressure would be proportional to the total contact forces.

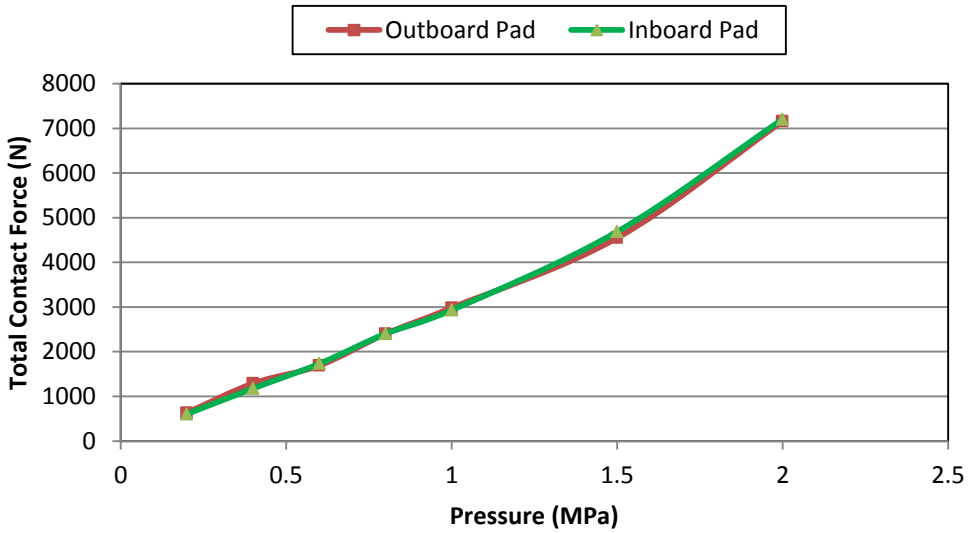

Figure 4.16 Total contact force at various brake hydraulic pressures

Total contact area was also plotted against different hydraulic pressures as shown in Figure 4.17. The results clearly demonstrate that the interface contact area between the disc/pad interfaces does vary with the different brake hydraulic pressures and the relation between the total contact areas and applied hydraulic pressure is not strictly linear. Both inboard and outboard pads exhibited a similar trend.

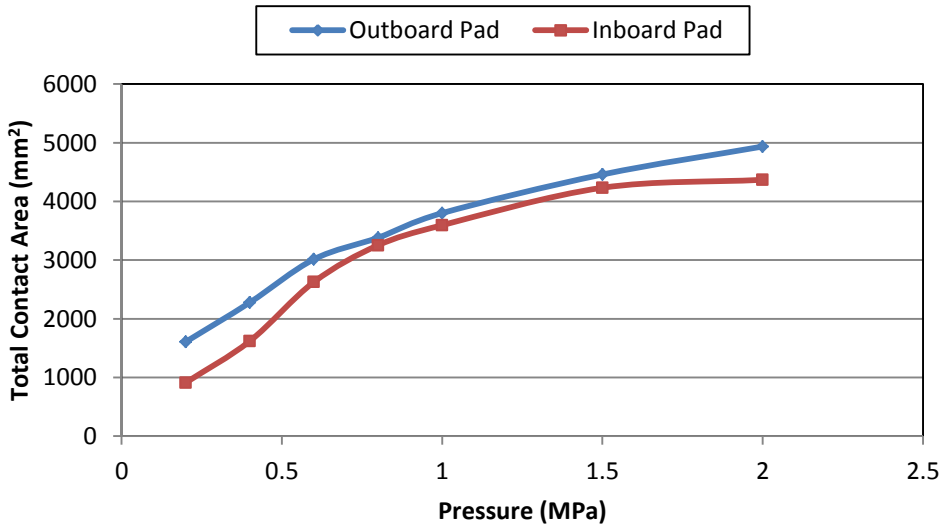

Figure 4.17 Total contact area at various hydraulic pressures

4.4 Contact Pressure Distribution Measurements during Squeal

In this section, the pressure applied to the pistons was adjusted to various settings to observe its effect on the squeal characteristics. Two different sets of test were carried out with the pressure varied along the length of pad and also radially. The movement of centre of pressure for both outboard and inboard pads was plotted at different stages.

The total contact force and contact area distribution were also measured and plotted at various stages. In this investigation, the total contact force and contact area distribution was measured from the centre of the pads to display the characteristics behaviour of both leading and trailing side of the pads under various caliper pressure settings.

4.4.1 Condition 1 – Movement of Longitudinal Centre of Pressure

The test was carried out in eight different stages as shown in Table 4.3. At each stage, the piston pressure was adjusted by four master cylinders to offset the position of the centre of pressure at the disc/pad interface. The focus was on varying the longitudinal pressure and so the longitudinal position of the CoP. The movement of centre of pressure for both outboard and inboard pads was plotted at different stages as presented within Table 4.3.

The brake was stationary (without any rotation) and the static pressure measurements at disc/pad interface were obtained (Stage 1). A disc speed of 10 rev/min was selected for use throughout the test (stage 2). Immediately the disc was rotated a squeal noise in the region of 1820 Hz could be heard. This frequency eventually became sustained and remained the dominant frequency generated throughout the rest of the test. The other apparent frequencies generated by the brake system were 3042Hz, 4150Hz, 4835Hz and 6430Hz. Although these additional frequencies are not discussed in more detail in this chapter, they have been used for validation of the FE models and are discussed further in Section 6.4.

At stage two, the pair of leading and outer centre pistons were pressurised to 1.4Mpa and the pairs of trailing and inner centre pistons were adjusted to 0.1MPa as shown in Table 4.3. The pressure settings are represented as a bar chart in Figure 4.18 where it is seen more clearly that a leading CoP leads towards brake noise.

Table 4.3 Details of variation of pressure at each cylinder position and affect on noise propensity

Caliper piston numbering:
1 - Both leading piston pairs are connected.
4 - Both trailing piston pairs are connected.
2 & 3 - The two central pistons may be pressurised independently.

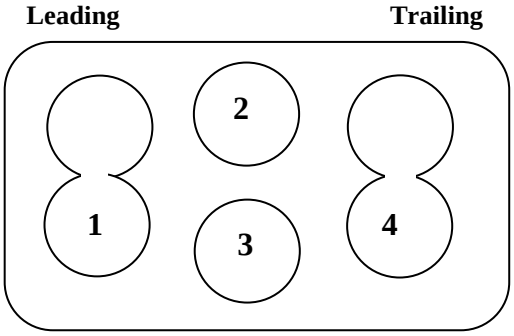

	Pressure (MPa) – for each piston set				Speed (rpm)	Comments
Stage	**1**	**2**	**3**	**4**		
1	1.4	1.4	0.1	0.1	Static	N/A
2	1.4	1.4	0.1	0.1	10	Squealing
3	1.4	1.4	1.4	0.1	10	Very loud squealing
4	1.4	1.4	1.4	1.4	10	Intermittent noise
5	1.4	1.4	1.4	2.0	10	Quiet
6	1.4	1.4	0	1.4	10	Intermittent noise
7	1.4	1.4	2.0	2.0	10	Quiet
8	0.7	0.7	2.0	2.0	10	Quiet

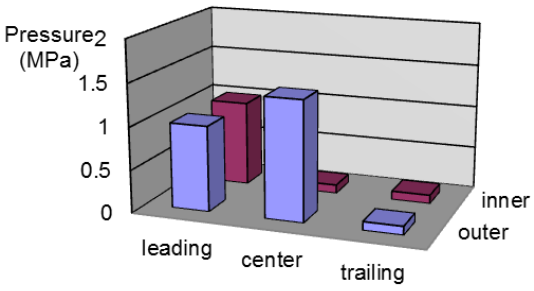

Stage 1 - Static

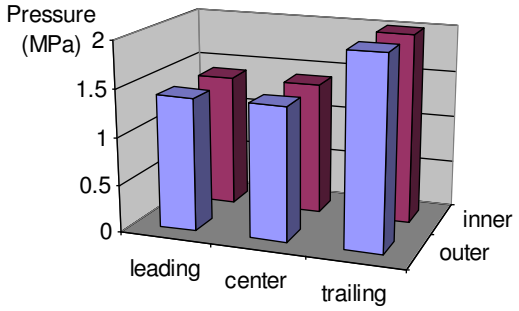

Stage 5 - Quiet

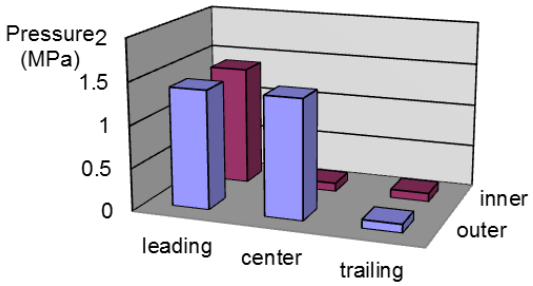

Stage 2 - Squealing

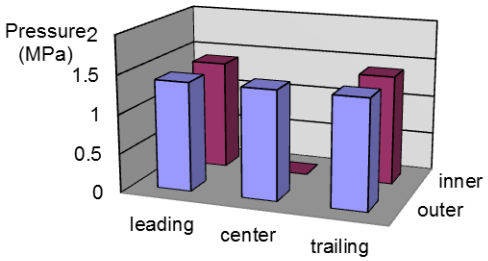

Stage 6 - Intermittent

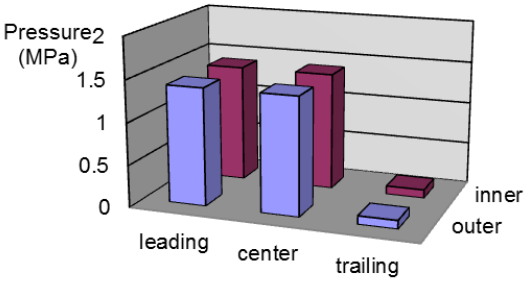

Stage 3 – Very Loud Squealing

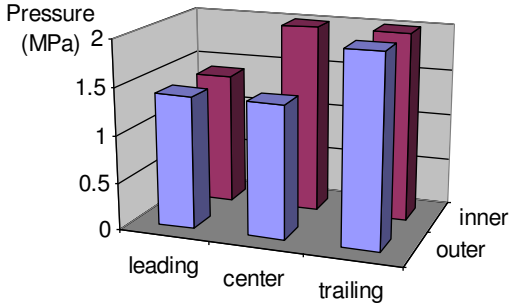

Stage 7 - Quiet

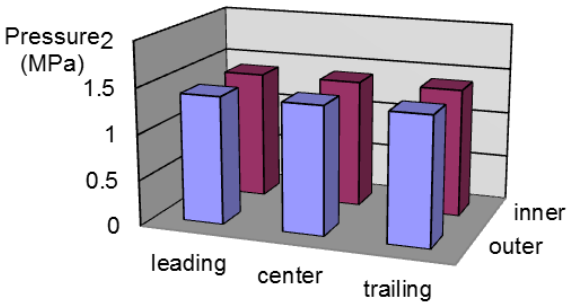

Stage 4 – Intermittent Noise

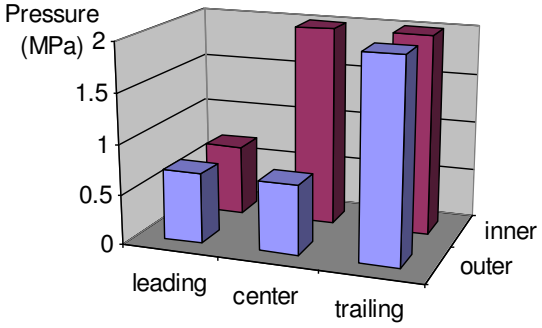

Stage 8 - Quiet

Figure 4.18 Piston pressure settings as listed in Table 4.3

At stage three, the pressure was increased on Piston 3 (inner centre pistons) from 0.1 to 1.4MPa so causing the centre of pressure (CoP) shift more towards the centre of the pad. This setting generated an increased squeal and was categorised as a “very

loud" squeal noise. This can be explained by looking at Figure 4.19. It is evident that the centre of pressure (CoP) offset towards the leading side of the pad. This increased leading offset of around 15mm on the inboard pad results in more instability and promotes most noise in the brake.

At stage four, a uniform pressure of 1.4MPa was applied to all pistons and it is clear from Figure 4.19 that the CoP reduced immediately to around 6mm leading. It is apparent from the result that by applying a uniform even pressure along the length of the pad it does tend to provide a leading offset, of about 6mm in this case, resulting in intermittent noise. It is suggested that the movement towards the centre of the pad is tending towards stability – hence the intermittent noise as opposed to continuous noise.

At stage five, the pressure was increased to 2.0MPa at the pair of trailing pistons, pistons 4. This induced a trailing CoP and as such the brake was quiet. It is concluded that an induced trailing CoP would promote a more stable and quiet brake.

At stage six, the pressure on Piston 3 was reduced to zero. This arrangement tended to re-establish the 6mm leading CoP on the inboard pad and the intermittent noise returned. At the same time, Figure 4.20 shows the radial movement of the CoP, when piston 3 set to zero, to move radially out towards the centre of pad. It is suggested that an arrangement with a leading CoP, and it being central to the pad, would tend towards a more unstable system and so noisy brake hence intermittent noise.

For the final two stages (7 & 8), the hydraulic pressure at the trailing pistons (4) was maintained high. It is most apparent from the results that by establishing more pressure towards the trailing edge of pads the brake tends more towards stability and thus a quiet brake. It is noticed that the position of centre of pressure (CoP) remains either very close to the centre of pad or towards the trailing edge of pad.

Although it is not felt that the pressure distribution on the outboard pad is such a significant influence it is also observed that in general the centre of pressure (CoP) of

the outboard pad tends to trail more than the inboard pad and both inboard and outboard pad follow the similar trend.

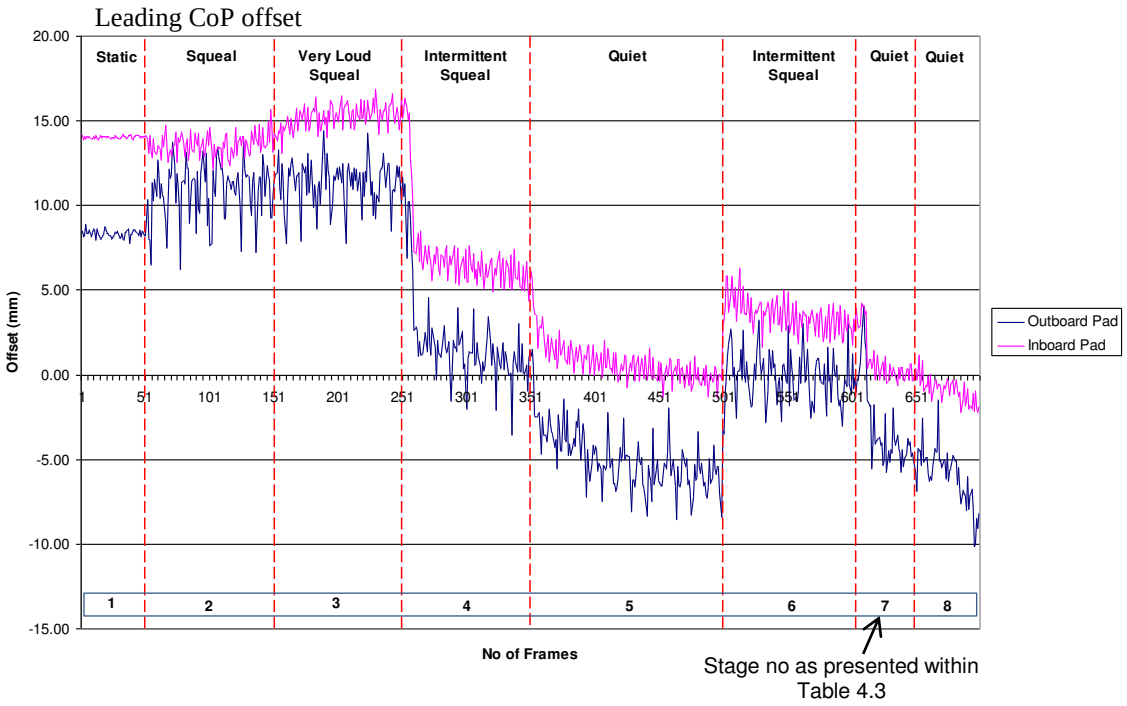

Figure 4.19 Longitudinal centre of pressure with varying pressure along the pad

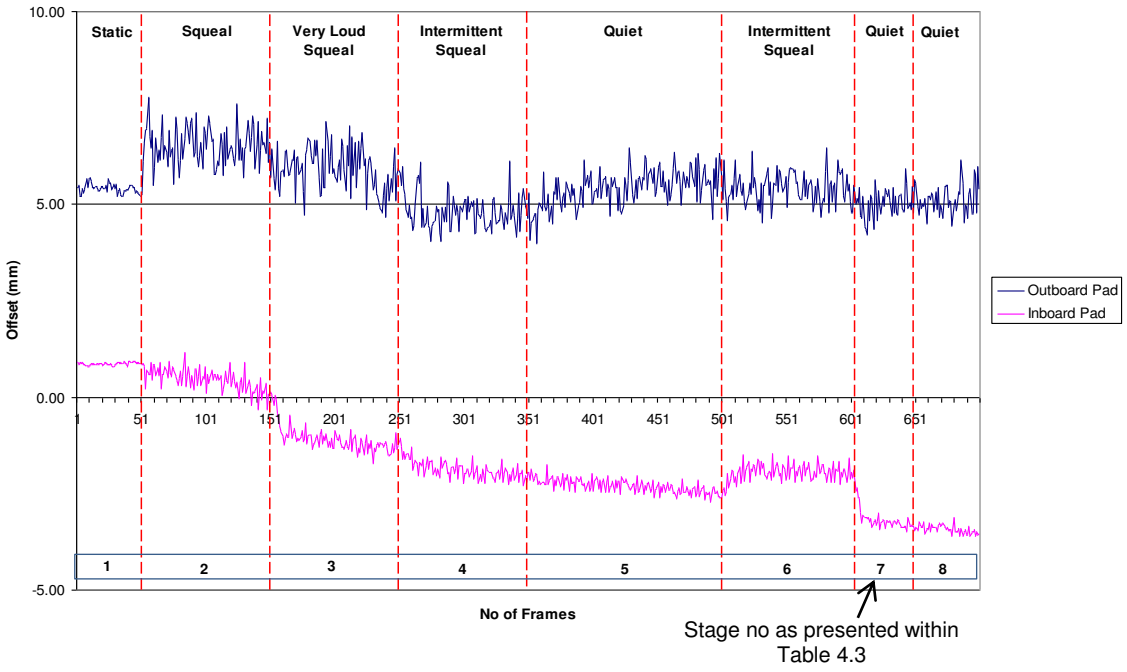

Figure 4.20 Radial centre of pressure across pad with varying pressure along the pad

4.4.1.1 Contact Force Measurements

To complement the CoP results in Figure 4.19 it is possible to show the disc/pad interface contact forces of the leading and trailing ends of both the inboard and outboard pads. In this section, the total contact force and contact area distribution was measured from the centre of the pads to display the characteristic behaviour of both leading and trailing side of the pads under various caliper pressure settings. Figure 4.21 and 4.22 clearly demonstrate that the intensity of the squeal noise increased as the total contact force distribution towards the leading side of the pad increased. Again it must be noted that the brake was very noisy at condition 3 and quiet at conditions 5, 7, and 8. It is particularly noticeable in Figure 4.22 that when the contact force was greatest within the trailing section the brake was quiet. When marginal, as in condition 6, as shown in Figure 4.22, the noise was intermittent. It was evident from the results that the brake tended to be quiet with higher contact force distribution towards the trailing side of the pad. It was also visible from the graphs that the brake would be more stable if the total contact force was more evenly distributed between the leading and trailing sides. Appendix H displays full graphical images of pressure mapping for both pads.

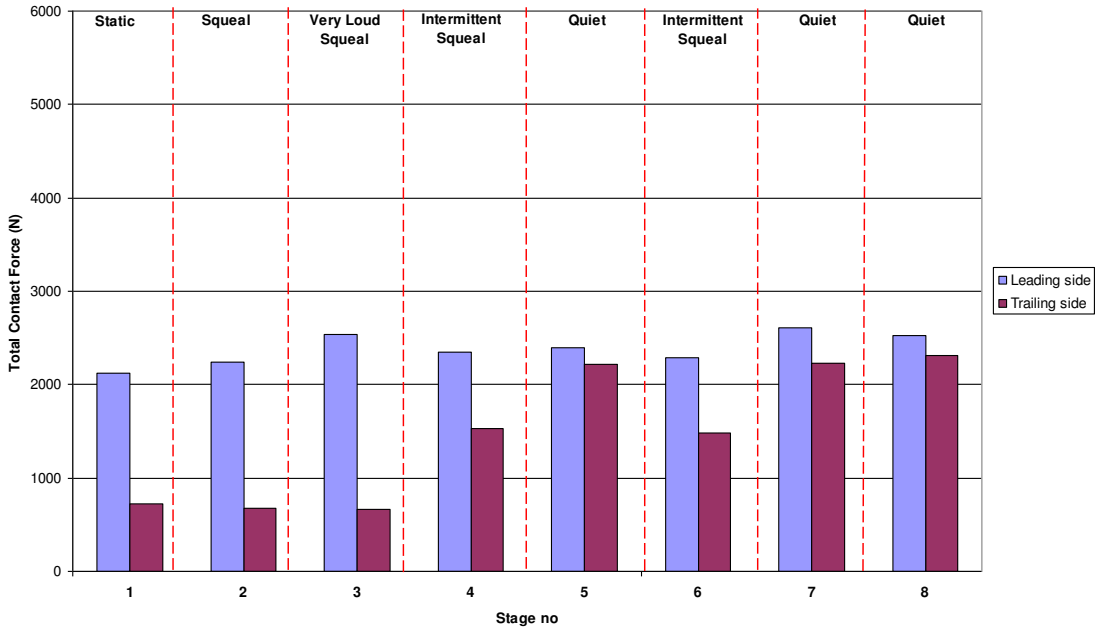

Figure 4.21 Total contact forces at leading and trailing section of pad (Outboard pad)

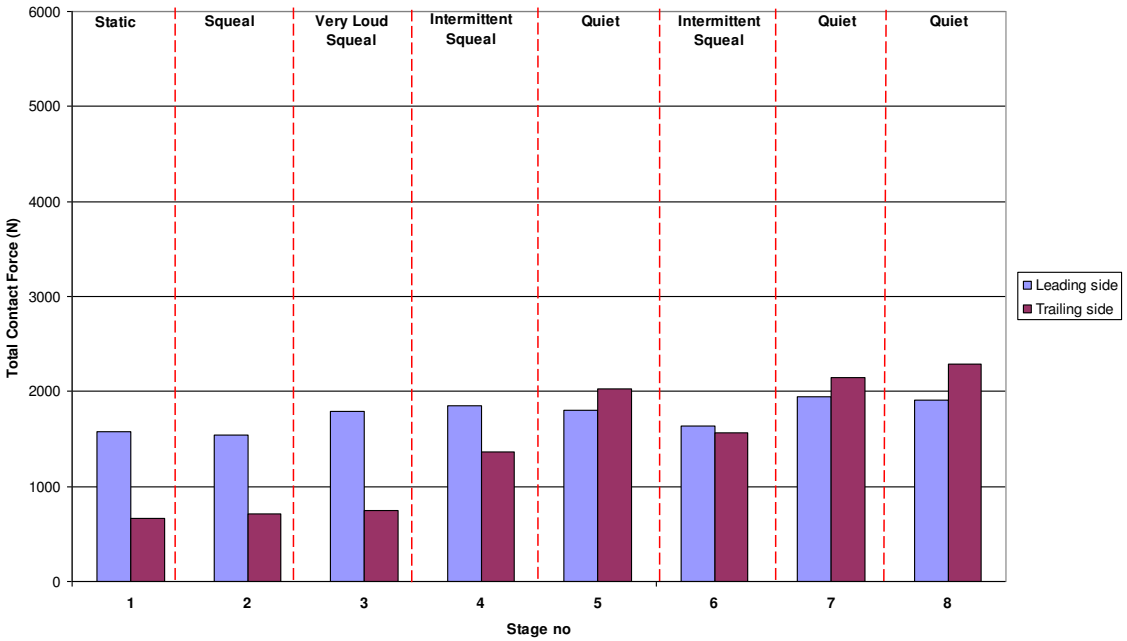

Figure 4.22 Total contact forces at leading and trailing part of pad (Inboard pad)

4.4.1.2 Contact Area Measurements

The total contact area was also measured at leading and trailing side of the pads. Figures 4.23 and 4.24 shows that the instability within the brake system tended to increase as the contact area variation between the leading and the trailing side of the pad increased. The brake system tended to be unstable with the higher contact area towards the leading side of the pad. Both outboard and inboard pads exhibited a similar trend. Appendix H displays full graphical images of pressure mapping of both pads at various stages.

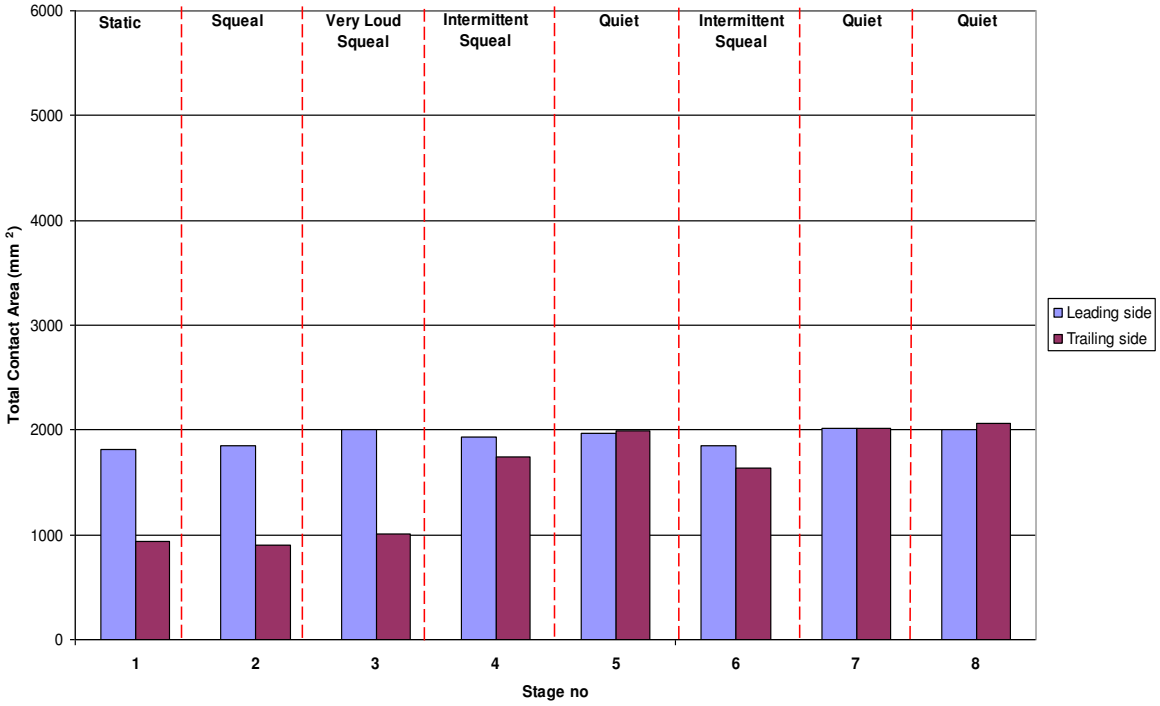

Figure 4.23 Total contact area at leading and trailing section of pad (Outboard pad)

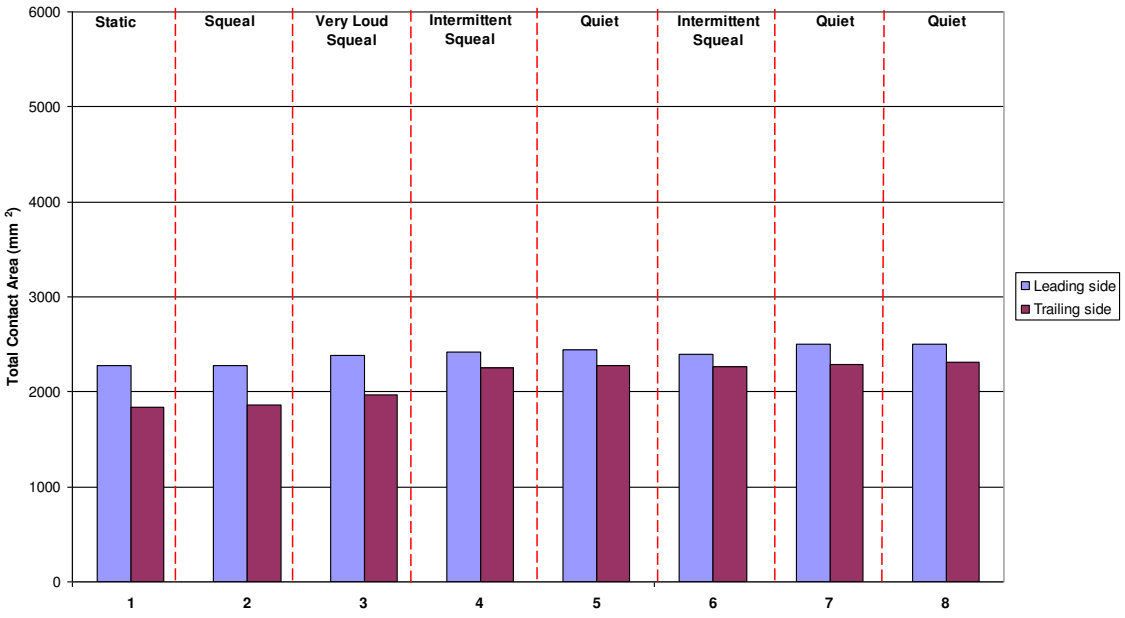

Figure 4.24 Total contact area at leading and trailing section of pad (Inboard)

4.4.2 Condition 2 – Movement of Radial Centre of Pressure

This test varied the pressures in each caliper piston as indicated in Table 4.4. In this investigation the focus was on varying the radial pressure and therefore the radial position of the CoP. It can be seen that pistons 1 and 2 remained constant at 1.0MPa and pistons 3 and 4 were used to vary the radial and longitudinal CoP.

Table 4.4 Details of variation of pressure at each cylinder position and affect on noise propensity (emphasis on radial variation)

	Pressure (MPa) – for each piston set				Speed (rpm)	Comments
Stage	**1**	**2**	**3**	**4**		
1	1.0	1.0	0.4	0.3	Static	N/A
2	1.0	1.0	0.4	0.3	10	Squeal
3	1.0	1.0	2.0	0.3	10	Very loud squealing
4	1.0	1.0	2.0	0.5	10	Squeal
5	1.0	1.0	0	0.3	10	Squeal
6	1.0	1.0	0.5	0.3	10	Squeal
7	1.0	1.0	2.0	0	10	Squeal
8	1.0	1.0	0.4	0.7	10	Intermittent squeal
9	1.0	1.0	0.4	1.4	10	Quiet

The piston pressure settings are shown in Figures 4.25 for stages 2 to 9, stage 1 being the same as stage 2. The longitudinal offset plot during each pressure setting/stage shown in Figure 4.26 and the radial offset shown in Figure 4.27.

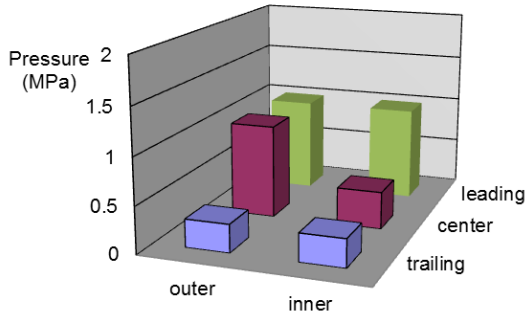

Stage 2 - Squeal

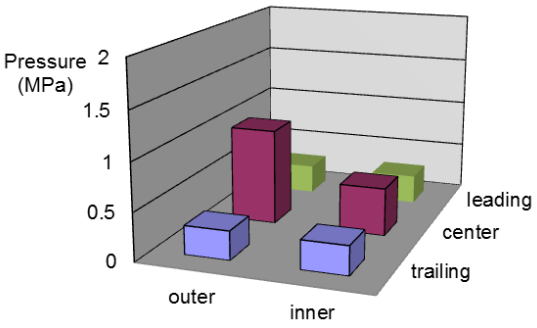

Stage 6 - Squeal

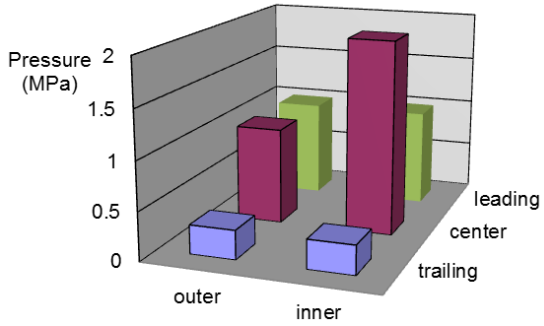

Stage 3 – Very Loud Squealing

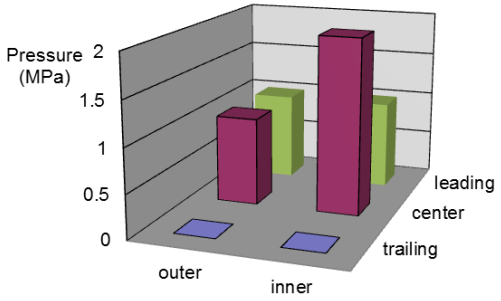

Stage7 - Squeal

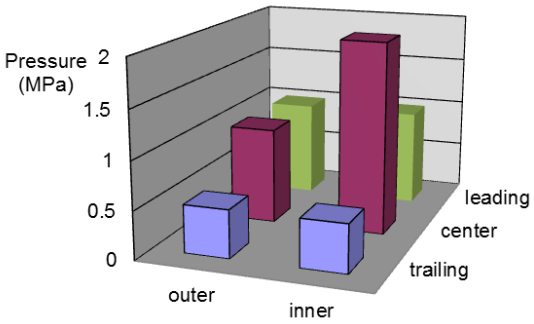

Stage 4 – Squeal (little squeal)

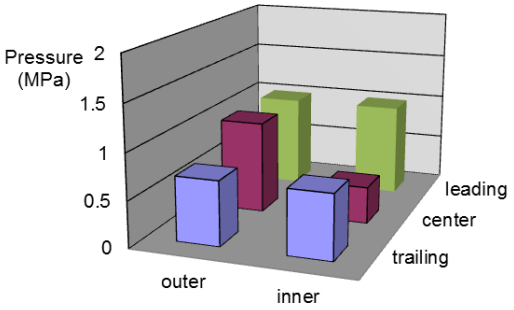

Stage 8 – Intermittent squeal

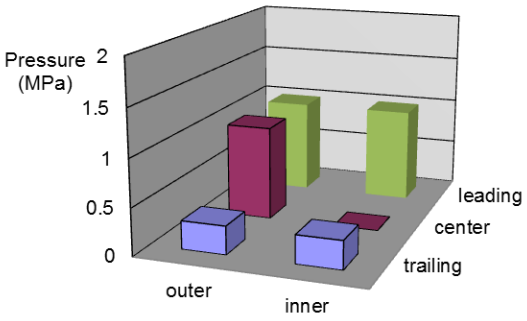

Stage 5 - Squeal

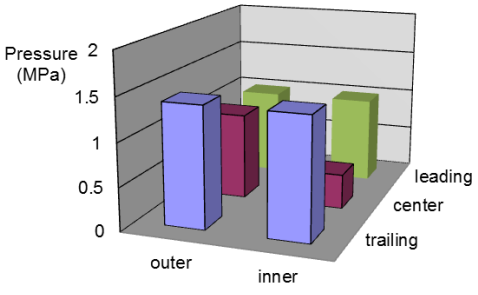

Stage 9 - Quiet

Figure 4.25 Piston pressure settings as listed in Table 4.4

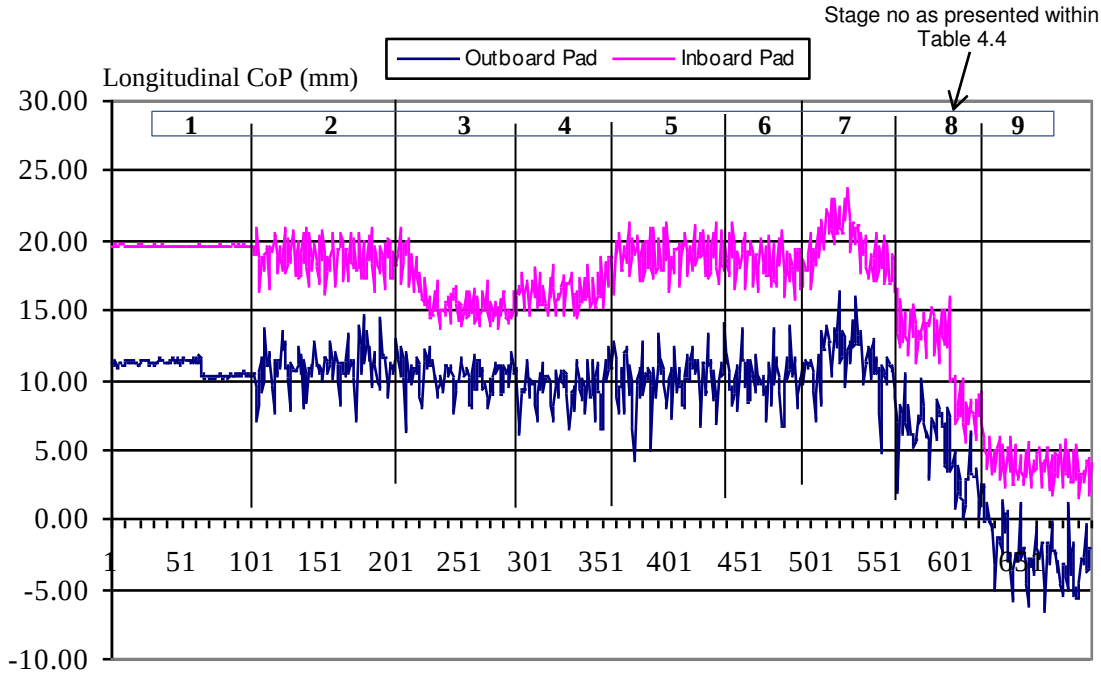

Figure 4.26 Longitudinal centre of pressure with varying pressure along the pad - emphasis on radial pressure adjustment (Refer to Table 4.4)

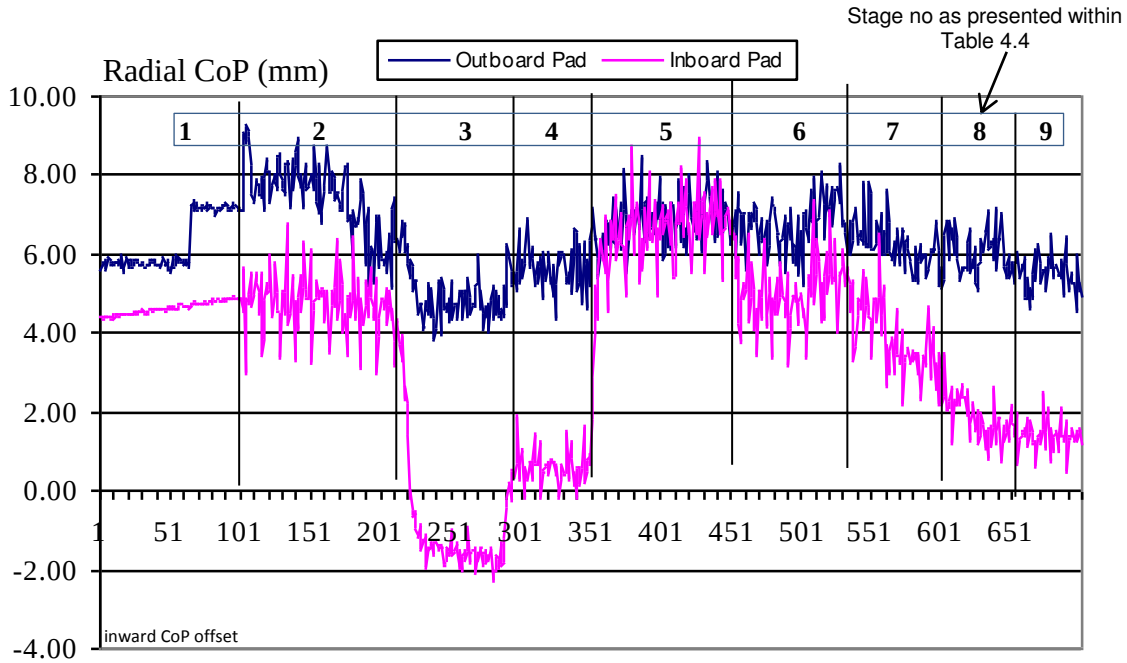

Figure 4.27 Radial centre of pressure across pad with varying pressure along the pad - emphasis on radial pressure adjustment (Refer to Table 4.4)

Considering Figure 4.26, it is seen that when the longitudinal offset is around 15mm for the inboard pad, the brake is very noisy. When this increases in stage 4 the brake

becomes less noisy and when the offset reduces in stages 7, 8 & 9 the noise becomes intermittent and then quiet. With radial offset, Figure 4.27, it is seen that when the loudest squeal was experienced at stage 3 the CoP was deliberately induced towards a zero (centre of pad) – that is radially towards the centre of the disc. If this offset was increased to become positive, as with case 4, the brake was less noisy. The radial offset in the case of stage 7 was not so appartent but the audible squeal noise was still evident. The quietest arrangement appears to be when the CoP was generally close to 2mm positive offset (radially outwards) and 5mm leading. As the CoP migrates further radially outwards the noise begins to become re-established (stage 5 & stage 6). The reason for this is still unclear.

Overall it is seen that the outboard pad is less sensitive to pressure variations. It is apparent from Figure 4.27 that the radial centre of pressure (CoP) of the inboard pad tended to offset more with various pressure settings comparing to the outboard pad.

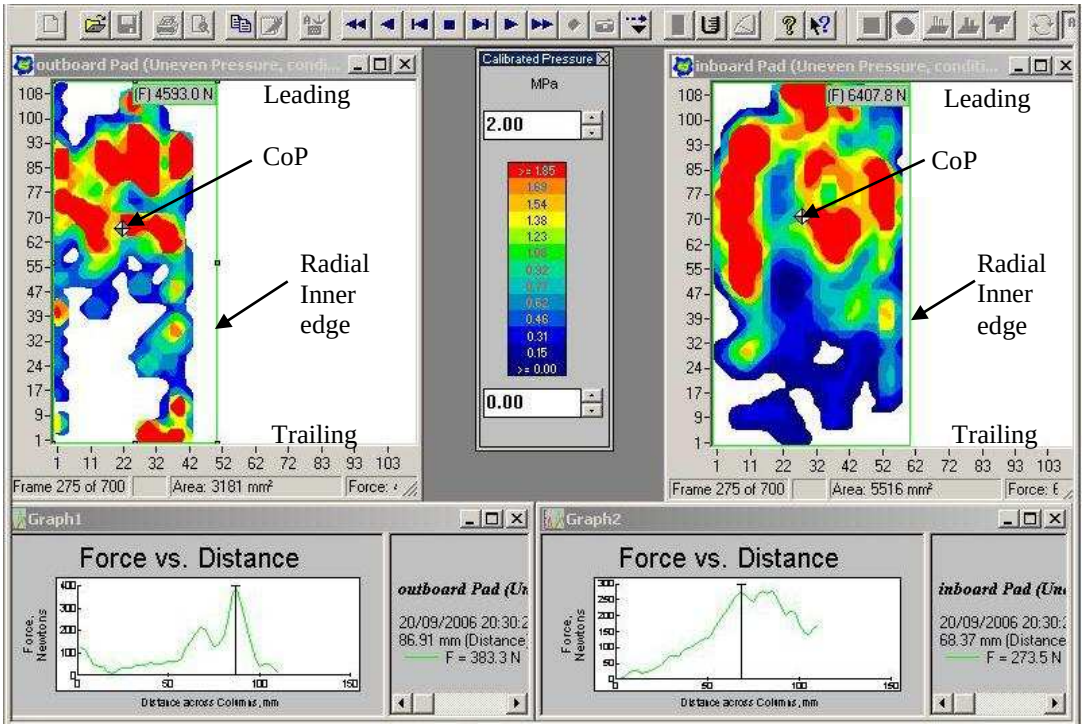

Figure 4.28 Pressure map of outboard (left) and inboard pad (right),
Pressure **1.0 (1), 1.0 (2), 2.0 (3), 0.3 (4)** MPa
Very loud noise, Refer to Table 4.4, Stage 3

It can be seen from the pressure map of both pads as shown in Figure 4.28 that the inboard pad appeared to carry significantly more load than the outboard pad. Without further evidence it is suggested that the outboard pad transmits less force than the inboard pad. This can be explained as “lost energy" or “lost load” in straining the caliper. The more rigid the caliper the more force is transferred to the outboard pad. An infinitely rigid caliper will give an equal and opposite force whereas the sliding fist caliper will lose energy in deforming the relatively weak pins. In the case of Brabus/Alcon caliper (12 pistons caliper), it is two halves bolted together so less rigid and therefore less load at the outboard pad. Such a situation can lead to possible thermal issues and cross disc thickness temperature gradient.

4.5 Discussion of Results

In the first study described in section 4.3 the effect of disc speed on contact pressure distribution was investigated. It was found that the disc speed had very little effect on the position of centre of pressure. It was also observed that the disc speed did not have any significant effect on the total contact force and contact area distribution. The overall contact area and the pressure distribution mapping remained almost same for different disc speeds.

In the next study described in section 4.3.1 the effect of uniform hydraulic pressure on contact pressure distribution was studied. It was apparent from the results that with uniform caliper pressure, the position of the centre of pressure was always towards the leading edge of the pad resulting in squeal. It was found that as the caliper pressure increased the longitudinal centre of pressure tended to move towards the centre of the pad and at the same time move radially inward towards the centre of the disc. It was also confirmed that the magnitude of applied hydraulic pressure was proportional to the total contact force which gave good confidence in the results. The results also showed that the contact area also fluctuated with the applied pressure. The overall results illustrated that the longitudinal centre of pressure (CoP) of the inboard pad tended to have more leading offset comparing to the outboard pad.

In section 4.4 the piston pressures were adjusted to various settings to observe the effect on the squeal characteristics. It was found that centre of pressure was a very important factor to control the noise of the brake system. The disc brake was more prone to noise when the centre of pressure was towards the leading edge of the pad. It was noticed that when the centre of pressure (CoP) was close to the centre of the pad or trailing then the brake was quiet. In order to reduce the intensity of noise within the brake system, the position of the centre of pressure must be towards the trailing edge of the pad. This can be achieved successfully by offsetting the pistons towards the trailing end of the pad. It is observed that in order to ensure consistent disc brake performance with regards to taper wear, the interface distribution must be carefully controlled to maintain a uniform pressure distribution along the length of pad.

It was also apparent that the centre of pressure (CoP) of the outboard pad moved more vigorously than the inboard pad as indicated by the graphical traces in Figures 4.19 and 4.20. It is felt that this was due to the caliper construction with the inboard pad being closer to the mounting plane so more robust and able to “apply” a greater load. This tended to be supported by observation of the pressure maps, typically Figure 4.29, which showed a greater loading on the inboard pad. Further investigation of the pressure maps, as shown in Figure 4.29, exhibits the inboard pad which showed a more uniform distribution of load whereas the outboard pad showed high concentrations of loading. Variations of loading within these high concentrations will have a greater effect on the CoP position and as a result a more vigorous movement of the CoP. Conversely, the inboard pad, with its more uniform loading, will be less susceptible to such concentrated pressure changes. The other possible explanation is due to the spragging effect which cannot be established with the outboard pad, the resulting load acting away from the caliper mounting plane. The mounting plane of the caliper bracket relative to the disc surface is important as this forms the “spragging” angle along with the position of the CoP. Theoretically it should be very close to the disc surface to minimise the potential “sprag” angle.

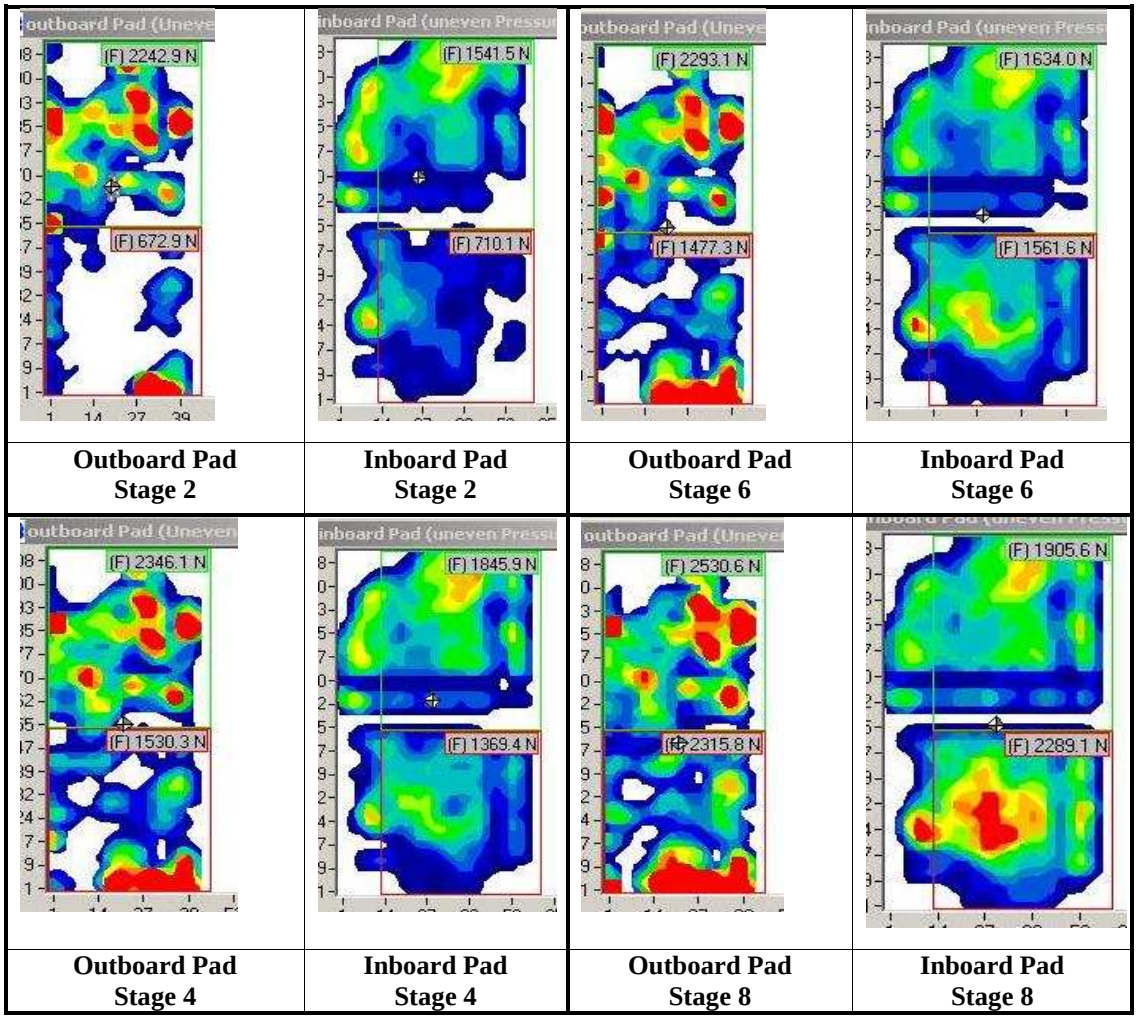

Outboard Pad Stage 2	Inboard Pad Stage 2	Outboard Pad Stage 6	Inboard Pad Stage 6
Outboard Pad Stage 4	**Inboard Pad Stage 4**	**Outboard Pad Stage 8**	**Inboard Pad Stage 8**

Figure 4.29 Force distribution map for both outboard and inboard pad at various stages (Refer to Table 4.3)

It was also shown that the brake was quiet if the contact area and contact force was equally distributed towards the leading and trailing side of pads as shown in Figure 4.21 and Figure 4.23.

Analysis shown in Appendix A may be elaborated by reference to Figure 4.30 which shows a trailing pad abutment arrangement and Figure 4.31 shows the variation in the pad abutment force over a full cycle, starting at minimum pad displacement. This force will be influenced by the μ/velocity interface friction coefficient characteristic and as such only a nominal gradient is shown in the graph. The smallest abutment

force will be at maximum velocity which is at minimum pad displacement (when horizontal). The extreme of pad displacement will be maximum force as abutment velocity differential is zero. The interface force then reverses direction. The gradients of the graph are due to the μ_2/velocity characteristics of the interface friction coefficient. At maximum speed differential between pad and abutment the force is at its minimum (0˚, 180˚ & 360˚).

If a co-planar analysis is performed, and considering the reaction force "R" to be varying due to the pad cyclical and reversing abutment force, a general equation for the position of the CoP may be derived.

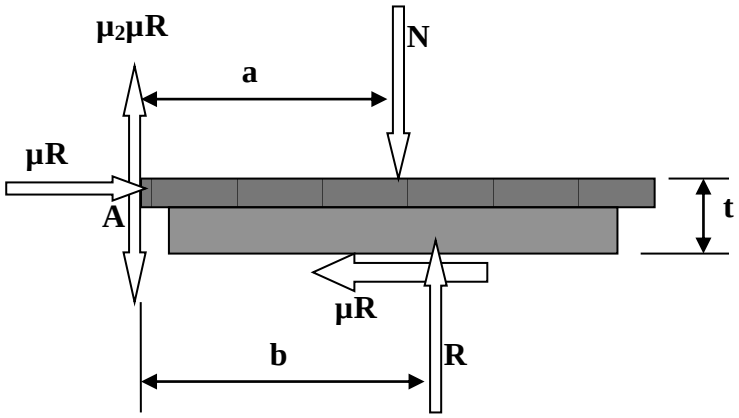

Figure 4.30 Free body diagram of trailing abutment arrangement

where:

N	Caliper piston force
R	Reaction force at the disc/pad interface
μ	Disc/pad interface friction coefficient
μ_2	Pad abutment interface friction coefficient
t	Pad thickness (mm)
a	Distance of caliper piston force (N) from pad abutment face
b	Distance of reaction force (R) from pad abutment face

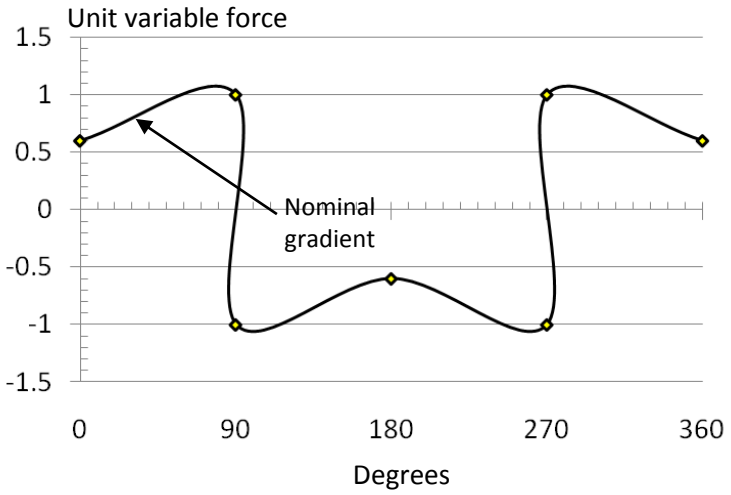

Figure 4.31 Representation of variable abutment force at trailing end of pad

In this case the system is not balanced as "N" is not equal to "R" and the relationship between the two may be determined by resolving forces vertically as follows:

If a co-planar analysis of the trailing abutment is performed, with reaction force "R" and abutment force μR and varying force due to the pad vibration abutment force "$\pm R\mu\mu_2$", then

$$R = N \pm \mu\mu_2 R \tag{4.4}$$

or

$$\frac{N}{R} = \left(1 \pm \mu\mu_2\right) \tag{4.5}$$

Furthermore, by taking moments about the abutment face "A", equilibrium will be attained if:

$$\mu Rt + Na = Rb \tag{4.6}$$

that is

$$\frac{N}{R} = \frac{\left(b - \mu t\right)}{a} \tag{4.7}$$

or

$$b = a\frac{N}{R} + \mu t \tag{4.8}$$

Substituting for N/R from equation (4.5) gives

$$b = a\left(1 \pm \mu\mu_2\right) + \mu t \qquad (4.9)$$

If the offset of the resultant force "R" to the piston force "N" (b - a) is δ then from equation (4.9):

$$\delta = (b - a) = [a\left(1 \pm \mu\mu_2\right) + \mu t] - a \qquad (4.10)$$

$$\boldsymbol{\delta = \mu t \pm a\,\mu\mu_2} \qquad (4.11)$$

Typically for a high aspect ratio pad

a = 70mm; μ = 0.4; μ_2 = 0.25 (Steel on steel); t = 15mm

Giving δ = 6.0 ± 7

δ = + 13mm to -1mm

and as μ_2 tends to zero the offset tends to +6mm (μt), leading.

If "t" reduces, the offset reduces and the tendency to sprag reduces, resulting in less noise due to this mechanism. Such analysis is supported by other researchers who have observed that noise propensity reduces as the pad wears [43].

When such a centre of pressure was imposed on a braking arrangement it was found that noise could be readily generated [18].

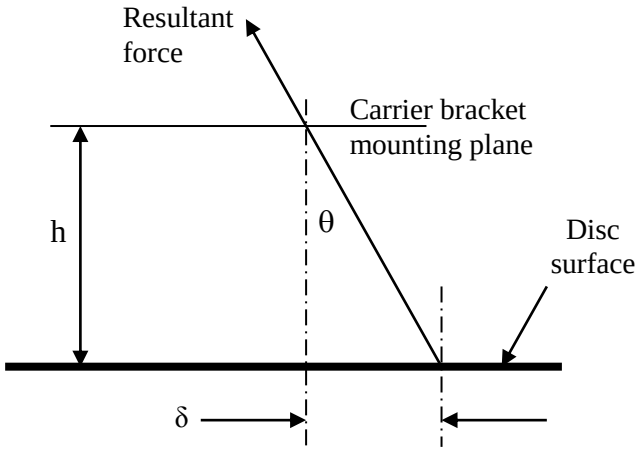

Figure 4.32 Sprag angle (θ) relates to the disc/pad friction coefficient where $\theta = \tan^{1}\mu$

With reference to Figure 4.32

$$\tan \theta = \mu = \delta / h \quad (4.12)$$

giving

$$h = \delta / \mu \quad (4.13)$$

From equation (4.11) this gives

$$h = t \pm a\ \mu_2 \quad (4.14)$$

so for the given parameters with μ_2 = 0.25 and considering only the positive as possible:

h = 32.5mm

If this height "h" can be related to the brake geometry (this value is for this size of pad), and it is known that noise is an issue, then spragging effect may be the source of noise and may be avoided at the design stage by addressing the mechanics at the pad abutment interface.

In general the analysis shows that the CoP is given by equation (4.9) and (4.11). From the above equations it is seen the CoP would vary by $b = a(\pm \mu \mu_2)$

For a brake pad used in this study

Assuming μ = 0.4, μ_2 = 0.25 and "a" = 86mm (half pad length) then the movement of the CoP during braking is **±8.6mm.**

Reference to case study presented in Appendix A (Figure A.10) shows this to be a viable range of movement, particularly at low pressures. By inference it is suggested that if μ_2 reduces to zero then the CoP movement tends to zero. It is known that a lubricant added to the abutment face can reduce the propensity for a brake to generate noise. In addition as "t" reduces to zero, as the pad wears, then the CoP offset reduces, an observation supported by Liles [43].

4.6 Summary

This chapter has generally concentrated on the experimental study of the contact pressure distribution and the dynamic movement of the centre of pressure. This chapter has demonstrated many new aspects that have not been considered in previous research and has made significant contributions to the knowledge in the area of brake noise. A number of tests were carried out to measure the centre of pressure and contact pressure distribution between the friction pair of disc/pad under various conditions. It was apparent from the results that the disc speed did not have any profound effect on the position of the centre of pressure. However as the brake hydraulic pressure increased the centre of pressure tended to moves towards the central section of the pad. It was also observed that the centre of pressure tended to be positioned towards leading offset at low brake pressure. It has been demonstrated for the first time in this thesis that as the brake hydraulic pressure increased the centre of pressure of both the outboard and inboard pad tended to move radially inwards. The effect of hydraulic pressure on the contact force distribution was also examined. It was established that the magnitude of the applied hydraulic pressure was linearly proportional to the total contact force. It was also evident from the results that the centre of pressure of the outboard pad moved more erratically than the inboard pad. It was concluded that in order to reduce the intensity of noise within a brake system, the position of centre of pressure must be towards the trailing edge of the pad. The ideal position for the centre of pressure of the pad would be longitudinally central to trailing and radially out from the pad centre. After extensive experimental studies on contact pressure distribution, following chapters are focused mainly on the development of a finite element model of a disc brake assembly. A finite element model was developed to accommodate both contact pressure distribution analysis as well as complex eigenvalue analysis. Finite element results were then compared with the experimental results to verify the accuracy of the FE method.

Chapter 5

Finite Element Method

5.1 Introduction

The finite element method is considered as one of the most well-established techniques for the computational solution of complex problems in different fields of engineering. The success of the finite element method is based largely on the basic finite element procedure, the finite element discretisation of formulation and the effective solution of the resulting finite element equations [51].

Crolla and Lang [52] emphasised that the key to further progress in analysing the brake noise problem lies in developing better finite element models and in particular in finding an accurate way of representing the frictional coupling terms at the rubbing surface. It was further established that the accuracy of disc brake instability from the eigenvalue analysis exclusively depends on the frictional contact interface behaviour.

One of the main purposes of the work presented in this thesis was to develop a representative finite element model of a disc brake to examine the contact pressure distribution between disc/pad interfaces. In order to obtain the dynamic characteristics of the disc brake components, a modal analysis at the component level was performed and was then correlated with the real brake components. The modal analysis study enables the mass and stiffness distribution in the model to be 'tuned' to that of the actual components. A number of contact methods were exploited to determine the pressure distribution, interfacial contact area and normal contact forces under frictionless and frictional braking conditions. The effects of varying friction coefficients and the brake hydraulic pressure were also investigated. Finite element results of contact pressure distribution were validated with the experimental results and then a comprehensive modal analysis of the disc brake assembly was performed

using the complex eigenvalue method to predict the natural frequencies and the mode shapes of the brake components. Furthermore a stability analysis of the brake assembly was carried out to distinguish the unstable frequencies.

A number of parametric studies were also performed to understand the characteristic behaviour of disc brake system in terms of squeal noise performance.

ANSYS finite element software package is used throughout this study to examine the brake squeal. ANSYS software package was selected at the request of Alcon Brakes Components, sponsors of this research project.

5.2 Development of Finite Element Model

The development of an accurate finite element model is a significant and crucial part of any linear and nonlinear analyses. This section describes in detail the development of a disc brake model. All the analyses were conducted under isothermal conditions.

In these analyses, the finite element model of the rotor differs from that used in the experimental work. The former is solid whilst the latter is vented. The finite element model of disc brake assembly consisted of a solid disc, and the inboard and outboard pad assembly as shown in Figure 5.1 & Figure 5.2. The pad assembly was made of a backplate and a friction lining. Dimensions and basic data for the brake components are shown in Appendix I. A fixed type caliper comprising 12 pistons (6 pistons per side) was assumed in the finite element model. The caliper and the pistons were not present in the finite element model. It was also assumed that the contacts at the disc/pad interfaces are even and the friction material surfaces were smooth without any irregularity.

A mapped mesh was chosen for the finite element analysis. The mapped volume mesh contained hexahedral elements with a regular pattern with noticeable rows and columns. The finite element model of the disc brake assembly was therefore built as a series of regular volumes that could accept the mapped mesh easily. The Solid45 hexahedral element was selected from the ANSYS elements library to mesh the disc

brake assembly. The Solid45 element is defined by eight nodes having three degrees of freedom at each node; a translations in the nodal x, y and z directions [53].

Mesh density is an extremely important factor for any finite element model. If the mesh is too coarse, the final results can contain serious errors. Conversely, a very fine mesh can lead to waste of computer resources resulting in excessively long run time. A study on mesh sensitivity was performed to confirm the validity of the mesh employed in the current analysis. Disc models with different mesh densities were considered to establish a mesh convergence. The frequencies, obtained from the finite element of the disc were then plotted against their respective diametral modes of vibration to indicate when convergence had been achieved or how far away the most refined mesh was from full convergence as shown in Appendix J. From this study, a disc model with 5520 elements, shown in Figure 5.1, was selected to ensure accurate finite element results.

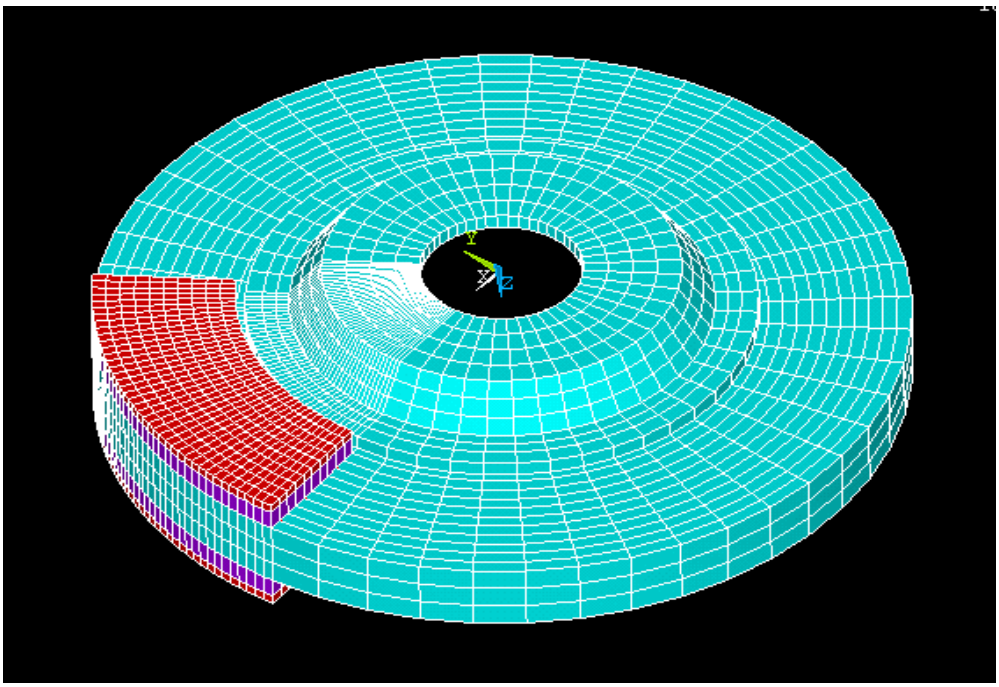

Figure 5.1 3D representation of the brake assembly used in the FE analysis

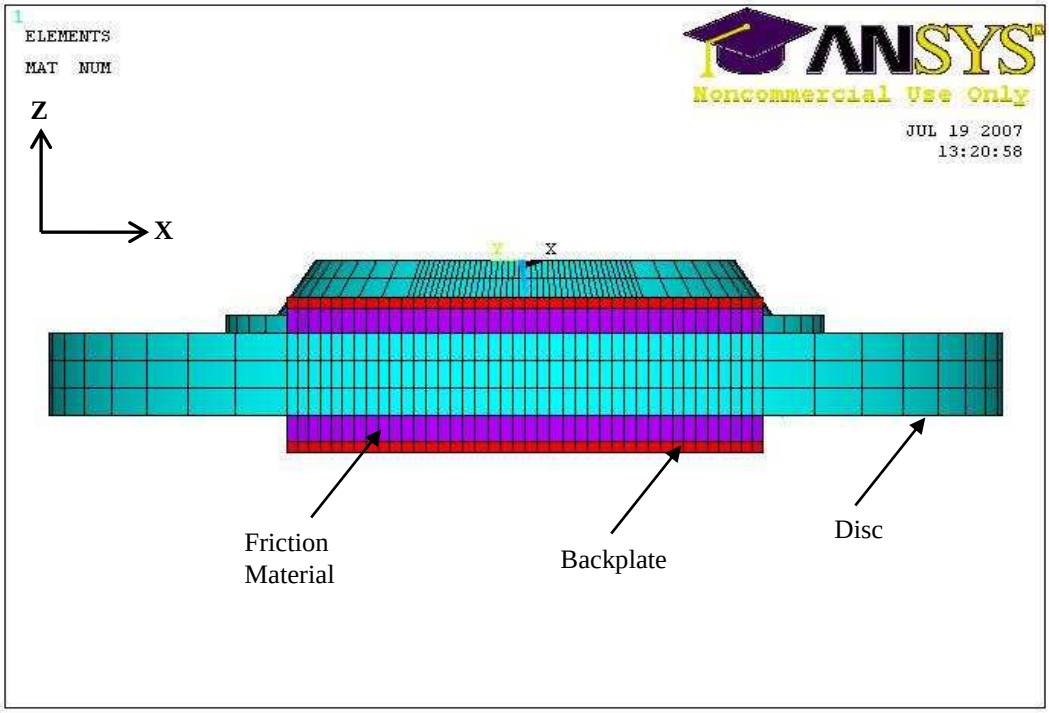

Figure 5.2 Side view of brake assembly used in the FE analysis

One of the primary functions of finite element analysis is to examine how a structure responds to certain loading conditions. It was therefore important to specify the loading conditions accurately in this finite element analysis. The loads could be applied either on a solid model (lines or areas) or finite element model such as nodes or elements. In the current analysis all the loads were applied on the finite element model of the disc brake. This was primarily because of more flexibility in selecting the desired nodes and specifying the appropriate constraints [53].

The brake pressure was applied as an equivalent force on each node of the backplate of both outboard and inboard pads which were in contact with the piston nodes, as shown in Figure 5.3. This established contact between the disc/pad interfaces which allowed the contact pressure distribution to establish on the friction lining surface when the disc was not rotating. It was ensured that the position of the piston loadings on the backplates was similar to the actual loading of disc brake system. In the current analysis, automatic time stepping was selected which adjusted the time step size as needed, gaining a better balance between accuracy and CPU time. In automatic time stepping, the time step size was automatically determined in response to the current state of the analysis under consideration.

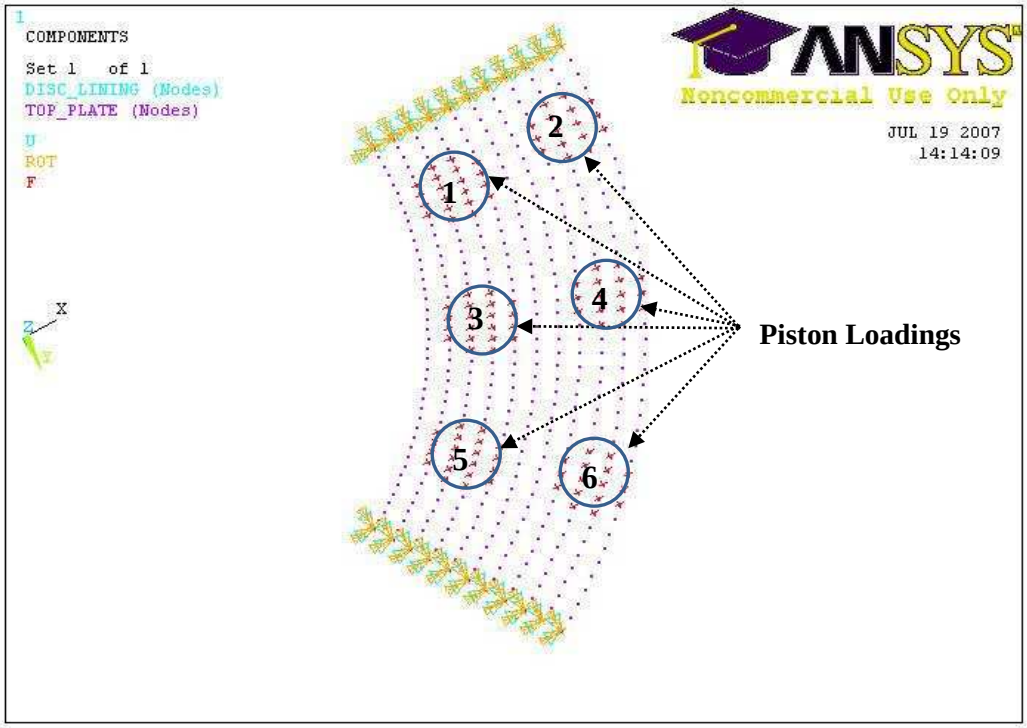

Figure 5.3 Actual positions of the piston loading at the pad backplate

A number of researchers have previously studied the effect of abutment constraints on contact force distribution. It has been established by Ripin [54] that the abutment arrangement does not substantially alter the contact force distribution. It was concluded by Ripin [54] that number of nodes in contact and the pressure distribution patterns remained the same for different abutment arrangements. However, Lee [55] also investigated the effect of abutment conditions using the FE method and found that combined abutment restraints can provide greater interfacial contact area compared to either leading or trailing abutments and this specific arrangement could provide more uniform interfacial contact pressure distribution. It was further established by Lee [55] that the trailing abutment had the lowest interfacial contact area but that the stability results were relatively good, hence, the model with the trailing abutment was the least likely to simulate squeal [55].

Although not practical, in the current FE model the constraints were applied at the leading/trailing edges of the pad to ensure uniform contact pressure distribution between the disc/pad interfaces. The leading and the trailing edges of the both pads were constrained in the X and Y direction only. However no constraint was applied

in the Z direction, normal to the disc surface, allowing the pads to move freely in the direction normal to the disc as shown in Figure 5.4. Initially, under frictionless conditions (μ=0), the disc was fully constrained at the inner radius of the top hat in all translation and rotation directions however in order to perform a forced sliding contact analysis between a brake pad and the associated disc rotor these constraints were subsequently altered to permit rotation of the disc as discussed in section 5.3.

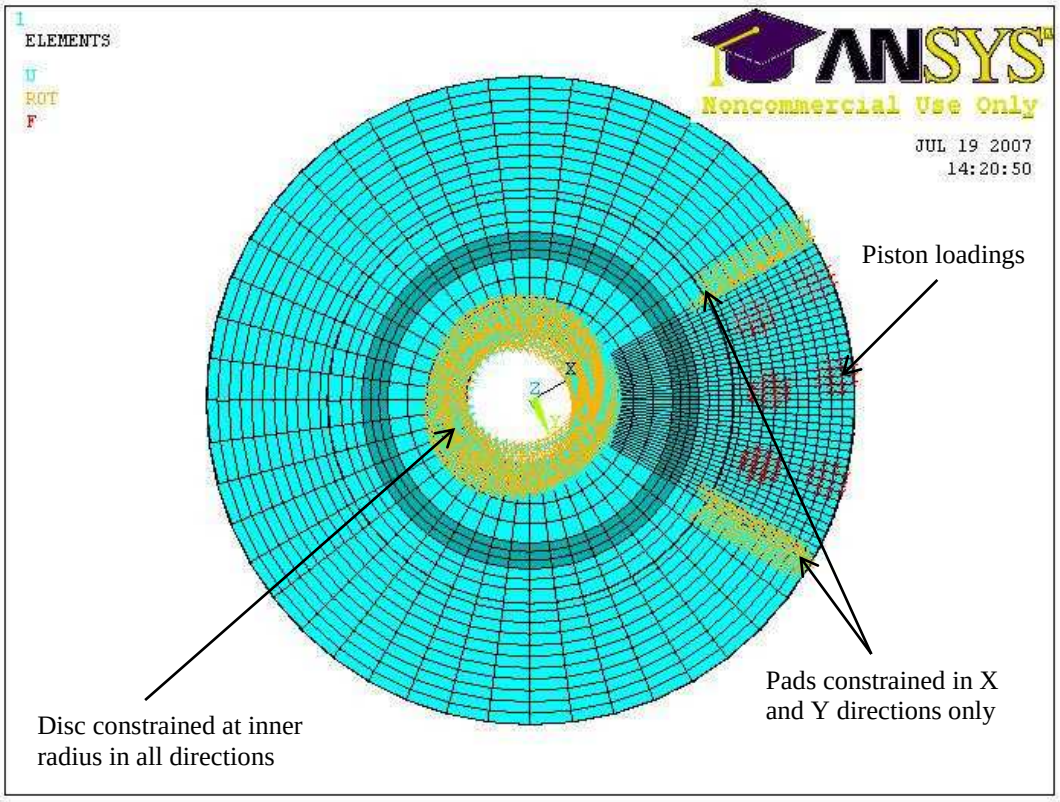

Figure 5.4 Piston loadings and the applied constraints

5.3 Finite Element Contact Analysis

The main components of a brake system where the sliding contact can occur are the disc and the pads. ANSYS software offers four different contact algorithms. These are node to node, surface to surface, beam to beam and surface to node contact models. The surface to surface contact model was chosen for the current analysis. This was mainly because it provided better contact results, such as normal contact forces, interfacial friction forces and stresses between the friction pair of disc/pad

interfaces, and supported large deformation with significant amount of sliding and friction efficiency. It was also known from previous experiences [56] that surface to surface model leads to less disk space and lower CPU usage and provides better visualisation. A table showing capabilities of various methods is presented in Appendix K.1.

The disc was defined as a target surface due to its stiffer material properties and the pad friction material is defined as a contact surface because it was much softer than the target surface (disc). Contact occurs when one of the contact elements penetrates one of the target segment elements on the specified target surface. CONTA173 and TARGE170 elements were selected from the ANSYS elements library, to generate the element between the disc/pad interfaces. After defining the element type, the real constant sets were selected. Each contact pair was referenced by its own real constant number. Contact elements were generated using automatic generation as this approach was simpler and more consistent. ANSYS automatically defined a default value for sliding (tangent) contact stiffness that was proportional to the coefficient of friction and the normal stiffness. For surface to surface analyses, ANSYS used Gauss integration points as a default, which generally provided more accurate results than the nodal detection scheme, which used the nodes themselves as the integration points.

The initial gap between two rubbing interfaces was very importance in terms of its effect on the magnitude of contact area and subsequently the brake system's stability. It has been identified by Ioannidis [57] that the open gap represents the un-burnished state of the lining's surface on assembly while a closed gap (perfect initial contact) simulates the fully worn state. He further elucidated that the perfect initial contact can simulate the relative thermal expansion in the model that the brake components undergo during a braking operation. Therefore in this thesis the initial gap between the friction material and the disc surface is assumed to be closed in the FE model.

The interfacial pressure distribution and the normal contact force were calculated by simply applying the piston loading on both the outboard and the inboard backplate under frictionless conditions ($\mu = 0$). But once the friction force was introduced to

the rubbing surface of the lining and disc, the resulting contact boundary and normal forces required rebalancing. At this instant, the friction and normal contact forces calculated are no longer related by Coulomb's Law [46]. Therefore a further loadstep was required to restore the equilibrium by rotating the disc rotor, to apply torque, about the Z axis (normal to the disc brake). In order to perform a forced sliding contact analysis between a brake pad and the associated disc rotor, additional elements were created about the inner radius of disc developing an umbrella shape at the centre of the disc as shown in Figure 5.5. BEAM4 element was chosen from the ANSYS library. BEAM4 is a uniaxial element with torsion, and bending capabilities. It has six degrees of freedom at each node: translations in the nodal x, y and z directions and rotations about the nodal x, y and z axis [53]. All earlier constraints were removed at the inner radius of the top hat and then constraints were applied in the x, y and z direction at the centre node of the disc and then rotating the target surface (disc) about the centre node of the disc. After imposing a rotational displacement to the brake assembly, a new set of normal contact forces was obtained.

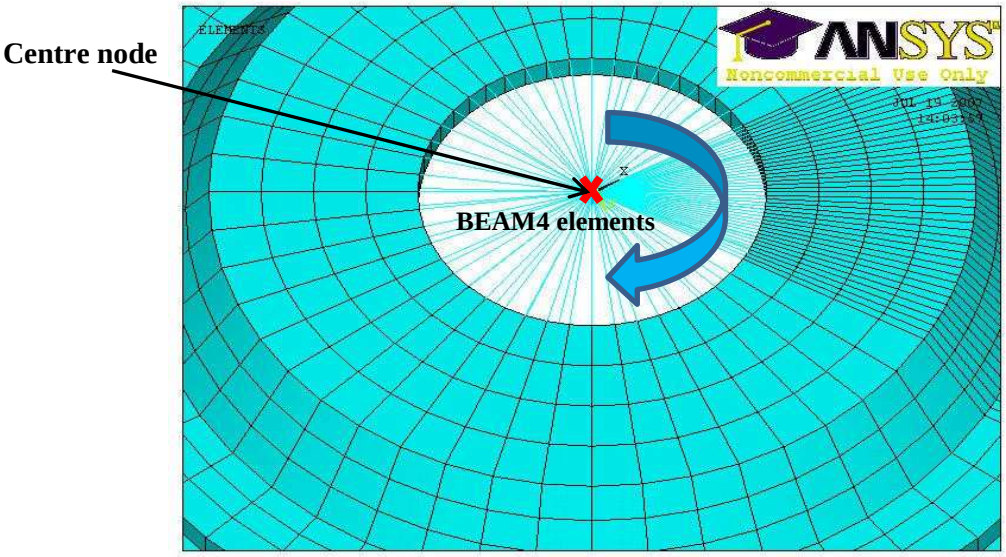

Figure 5.5 Showing the construction of BEAM4 elements

5.3.1 Confirmation of Friction Equilibrium

Disc brake torques obtained from the finite element results were compared with the analytical results to verify that the FE friction model has stabilised successfully and

the additional load step restored the equilibrium effectively. For surface to surface contact analysis, the torque of the disc brake was determined by rotating the disc about the centre node of the disc.

The torque of the disc was also found analytically by using the simple formula as shown below:

$$T_B = F_c R_E \tag{5.1}$$

$$T_B = \left[2 P_H \; A_P \; \mu\right] R_E \tag{5.2}$$

where

T_B Torque generated by the caliper on the rotor

F_c Clamp force

R_E Effective radius of the brake pads from the centre of the disc

P_H Hydraulic pressure of brake system

A_P Total area of pistons in one half of caliper

μ Coefficient of friction

It was established from the finite element results that the brake torque obtained from ANSYS was within the range of approximately 3.7% of the analytical results as shown in Table 5.1. That implied that the additional loadstep restored the equilibrium effectively. It was also apparent from the FE results that as the value of coefficient of friction increased in the FE model, the brake torque also increased. It was noted that the disc torque was linearly proportional to the coefficient of friction as shown in Table 5.1.

Table 5.1 Comparison of analytical and FE torque of disc brake

Hydraulic Pressure (MPa)	Coefficient of Friction, μ	Analytical Torque (Nm)	Torque (Nm) calculated from ANSYS	Torque Calculated Error (%)
1.00	0.20	164.59	158.71	3.70
1.00	0.30	246.89	238.53	3.50
1.00	0.40	329.18	317.42	3.70
1.00	0.50	411.48	396.78	3.71
1.00	0.60	493.77	476.13	3.70

5.4 Methodology of Contact Analysis

Contact problems are inherently nonlinear and present significant difficulties because of the unknown contacting zone prior to analysis. They also involve a variety of geometric and kinematic situations. For the frictionless condition, the contact element stiffness matrices were symmetric and only normal components of the traction force (normal to the contact surface) were present in the model. However once friction was incorporated in the model, the tangential traction to the surface was also generated. The simplest model for friction conditions is Coulomb friction where:

$$\left|t_s\right| \le \mu \left|t_n\right| \tag{5.3}$$

where

t_s Tangential traction

μ Coefficient of friction

t_n Normal traction

In the basic Coulomb friction model, friction pairs can carry shear stresses up to a certain magnitude across their interface before they start sliding relative to each other. This state is known as sticking where t_s is less than the limit condition, whereas if the magnitude is at the limit condition sliding occurs with an imposed tangential traction on each surface opposite to the direction of slip and equal to $\mu\left|t_n\right|$.

5.4.1 The Newton-Raphson Method

ANSYS employs the Newton-Raphson approach to solve nonlinear contact problems. The Newton-Raphson method is the most rapidly convergent process for solutions of problems in which only one evaluation of a function is made in each iteration. In this approach, the load is subdivided into a series of load increments and then solves a set of simultaneous algebraic equations of the form [53].

$$[K]\{x\} = \{F^a\} \tag{5.4}$$

where

$[K]$ System stiffness matrix

$\{x\}$ Global displacement vector

$\{F^a\}$ Vector of applied loads

5.4.2 Contact Methods

ANSYS offers a number of contact methods for surface to surface contact elements. In the current research, the augmented Lagrangian and the penalty method were considered and compared to observe the behaviour of the contact pressure distribution between the disc/pad interfaces.

5.4.2.1 The Penalty Method

The penalty method uses a contact "spring" to establish a relationship between the friction material and the disc surfaces. In a penalty method approach the final gap between the disc/pad interfaces is not zero but becomes a small number depending on the value of the parameters selected. Therefore, the advantage of the penalty method is somewhat offset by a need to identify the value of parameter that gives an acceptable solution [53].

5.4.2.2 Augmented Lagrangian Method

The augmented Lagrangian method is an iterative series of penalty methods. The contact pressure and frictional stresses are augmented during equilibrium iterations so that the final penetration is smaller than the allowable tolerance. The augmented Lagrangian method usually leads to better conditioning and is less sensitive to the magnitude of the contact stiffness [53].

5.4.3 Comparison of Augmented Lagrangian and Penalty Method

The main purpose of comparing these two contact methods was to evaluate the capabilities of these methods in terms of disk space and CPU usage, which can lead

to more efficient and user friendly nonlinear contact method resulting in accurate computation of contact pressure distribution between the disc/pad interfaces.

It was found that the pressure distribution, contact normal forces and interfacial contact areas were almost identical for both methods however the Penalty method required more computational time to solve comparing to the Augmented Lagrangian method. It was noted that the CPU time for the Penalty method (CPU = 250s) was about 20% higher compared to the Augmented Lagrangian method (CPU = 200s). It was therefore concluded that the Penalty method was more expensive in terms of computation cost and would therefore result in more CPU time.

The Augmented Lagrangian scheme was selected for the analysis in this thesis. This was because of its less CPU time usage and the method was less sensitive to contact stiffness compared to the Penalty method.

5.5 Finite Element Modal Analysis

5.5.1 Modal Analysis of Disc Rotor

Due to the time and computational power constraints, a number of simplifications were made to the finite element model. In the current study, a solid disc was considered. Therefore tuning of the mass and stiffness distribution was required to reduce the relative errors between the FE and experimental results.

In the first stage, the disc rotor was simulated in the free-free boundary condition and natural frequencies up to 8 kHz were considered and then the finite element model of the disc was validated with the experimental modal analysis of the disc rotor.

The roving impact hammer technique was employed to extract the natural frequencies of the disc rotor. The accelerometer was connected directly to the data acquisition system of the LMS hardware. The responses obtained from the accelerometer were very clear and the dominant frequencies are presented in Table

5.2. In the final stage, tuning of the density and stiffness distribution of the FE model was performed to reduce relative errors between the two sets of results.

Table 5.2 Calculated and measured natural frequencies of disc

Mode Order	Experimental Modal Analysis	FE Modal Analysis
	Frequencies (Hz)	Frequencies (Hz)
2	630	627
3	1629	1558
4	2594	2768
5	3791	3948
6	4589	4890
7	6132	5980

The frequencies, obtained from the finite element and the hammer tests of disc rotor were then plotted with the respective modes of vibration to derive a relation between the noise frequency and mode shape. There were various mode shapes exhibited in the FE results. However, only diametrical modes were considered because they are considered to be dominant ones in the squeal events [3]. The calculated and measured natural frequencies are given in Table 5.2, which includes 2^{nd} diametrical mode up to 7^{th} diametrical mode. The number of diametrical modes based on a number of nodes and anti-nodes appearing on the rubbing surfaces of the disc.

The results obtained in Table 5.2 exhibited good correlation between the predicted and measured natural frequencies of the disc rotor. It provided confidence on the validity of the disc rotor results. A graph was plotted from the second mode (two-diameter) to the seventh mode of vibration of the disc rotor as shown in Figure 5.6. The trend line showed a constant deviation as the mode of vibration became higher. It can be inferred from the graph that a reasonable convergence was achieved between the finite element modal analysis and the hammer test. It was found that the relation between noise frequency and mode of vibration was fairly linear as shown in Figure 5.6. The experimental modal analysis of the pad was not undertaken since the eigenvalue analysis of the brake pad was not considered in the current studies.

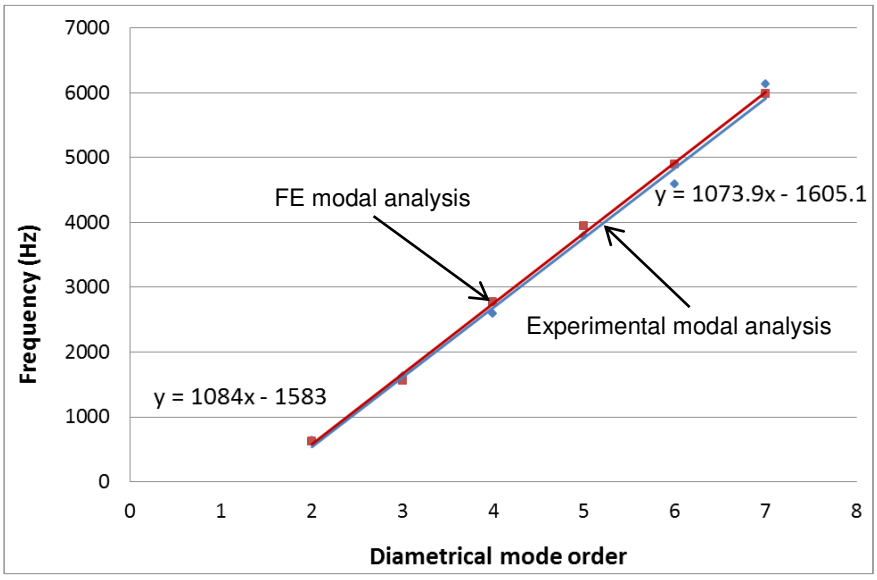

Figure 5.6 Plot of disc frequencies against diametrical mode order

5.5.2 Finite Element Modal Analysis of Disc Brake Assembly

The non-linear contact analysis provided information on the normal contact forces, interfacial friction forces, contact areas and contact pressure distribution of disc/pad interfaces. In order to investigate the mode shapes, natural frequencies and instability measurements in the dynamic modal analysis, the existing nonlinear structural system needed to be linearised. This meant replacing only those nonlinear contact elements which were closed as a result of the applied loads with the equivalent linear elements. In the current study, MATRIX27 interfacial stiffness elements were applied over the effective contact areas predicted by the existing nonlinear contact analysis. The unsymmetric stiffness matrix for each contacting interfacial element was calculated by coupling normal contact forces and friction forces according to Coulomb's law [45]. It should be noted that the linear elements had to have the capability to transform the symmetric structural system matrix to an unsymmetric matrix and the interfacial coupling behaviour must continue to observe Coulomb's law [53].

The unsymmetric matrix was solved using the direct solver method by specifying the unsymmetric option for the Newton-Raphson method. It was found that by simply defining the friction, the unsymmetric matrices could not be produced. The two

conditions needed to be met for the unsymmetric matrices. First, the unsymmetric stiffness had to be requested with the unsymmetric option for the Newton-Raphson method. Secondly, the frictional sliding between friction pair of disc/pad had to occur for the matrices to be unsymmetric. ANSYS calculated the unsymmetric stiffness terms due to frictional sliding, and then included the unsymmetric matrices in the eigensolution.

5.5.2.1 Complex Eigenvalue Method

A complex eigenvalue analysis was performed and is detailed in Chapter 6. This method used the Lanczos algorithm from which the instability measurement, natural frequency and the mode shape information was extracted. This section briefly explains the background theory of the complex eigenvalue method exploited in the current simulation.

In the current study, viscous damping was not considered in the FE model. The equations of motions for a system in the absence of damping can be expressed as shown by Liles [43]:

$$[M]\{\ddot{x}\} + [K]\{x\} = \{F_f\} \tag{5.5}$$

where:

$[\mathrm{M}]$ System Mass matrix

$\{\ddot{x}\}$ Global acceleration vector

$[\mathrm{K}]$ System stiffness matrix

$\{\mathrm{F_f}\}$ Interfacial force vector

$\{\mathrm{x}\}$ Global displacement vector

The resulting frictional forces can be written in term of the relative displacement between the contacting surfaces [45]:

$$\{\mathrm{F_f}\} = [\mathrm{K_f}]\{\mathrm{x}\} \tag{5.6}$$

Where $[K_f]$ is the Friction stiffness matrix associated with the MATRIX27 interface element. Rearranging the equation gives [45]:

$$[M]\{\ddot{x}\} + [K - K_f]\{x\} = \{0\} \quad (5.7)$$

The solution of the above second order matrix differential equation can be described as follows:

$$\{x\} = \{\phi\}e^{\gamma t} \quad (5.8)$$

where:

γ Complex eigenvalue

$\{\phi\}$ Complex eigenvector

t Time

The eigenvalue problem then becomes

$$\left([M]s^2 + [K - K_f] \right)\{\phi\} = \{0\} \quad (5.9)$$

in which $\{\phi\}$ is the scaled eigenvector revealing the relative shape of the oscillatory motion for each mode of vibration.

The complex eigenvalue extracted from equation (5.9) consist of real and imaginary parts. For the particular ith mode, the eigenvalue pair is described as [45]:

$$\gamma_i = \sigma_i \pm j\omega_i \quad (5.10)$$

Here σ_i is the real part and ω_i is the imaginary part of the ith eigenvalue and $j = \sqrt{-1}$.

The unsymmetric method, which also uses the full [K] and [M] matrices, was employed to analyse the instability in disc brake assembly where the stiffness and mass matrices are unsymmetric [53]. In this particular solver (contrary to classical mechanical theory), the real part of the eigenvalue represented the natural frequency and the imaginary part was a measure of the instability of the system. A negative value of the imaginary part meant the system was stable while a positive value meant

the system was an unstable mode of vibration that are likely responsible for squeal noise.

5.6 Instability Analysis

The degree of instability in a brake system can be measured by calculating the standard deviation of the damping coefficient. Liles [43] established that a higher number of unstable modes or larger damping magnitude can actually increase the standard deviation about the mean value of zero. It was further emphasised by Lee [45] that the stability of a system can be quantified by measuring the distribution of the instability measurements. It was found that the greater the standard deviation of the instability measurements, the greater the propensity of the disc brake system to squeal.

The standard deviation of normal contact forces can also be employed to represent the non-uniformity of contact pressure distribution. The standard deviations of friction forces and normal contact forces are related by a factor which is exactly to the coefficient of friction [43]. It was also clear that the smaller the standard deviation of the normal contact forces, the more uniform was the interfacial pressure distribution [43].

5.7 Summary

In this chapter, a detailed FE model of disc brake was constructed to examine the contact pressure distribution between disc/pad interfaces. A number of contact methods were examined to determine the interfacial pressure distribution, interfacial contact area and normal contact forces under both frictionless (μ) and frictional braking conditions. In order to investigate the mode shapes, natural frequencies and instability measurements in the dynamic modal analysis, the existing nonlinear structural system was linearised by replacing the nonlinear contact elements with the corresponding linear elements over the effective contact areas. This chapter also briefly examined the background theory of the complex eigenvalue method exploited in the current simulation. In the next chapter, the finite element results are presented and compared with the experimental results.

Chapter 6

Finite Element Results

6.1 Introduction

In this chapter the finite element model, developed in Chapter 5, was used to understand the characteristic behaviour of brake squeal noise. The coefficient of friction (μ) of pad material and hydraulic brake pressure was varied to observe its effects on various modes of vibration and possible modal coupling between the out-of-plane modes of the rotor. This was used to determine which modes of vibration (frequencies) were unstable and potentially a source of audible discomfort. A range of experimental tests, performed in Chapter 4, were compared to validate the FE contact results. A complex eigenvalue analysis was also performed to ascertain the instability measurement of the disc brake assembly. Furthermore the predicted mode shapes from the FE results were studied and compared with the experimental results.

6.2 Effect of Hydraulic Pressures

The effect of different hydraulic pressure was studied with various piston pressure settings of 0.4, 0.6, 1.0, 1.5, 2.0MPa. The piston loadings were applied at both the outboard and the inboard pad backplates and the value of the coefficient of friction kept constant at $\mu = 0.4$ (a value specified by manufacturer for these particular pads) for different pressure settings. The contact force distribution for the different hydraulic pressure was determined along an arc at mean rubbing radius of both the outboard and inboard pad friction lining respectively as shown in Figure 6.1 and Figure 6.2. It was found from Figure 6.1 and Figure 6.2 that as the hydraulic pressure increased, the normal contact force also increased. Both the inboard and the outboard pads demonstrated a similar trend.

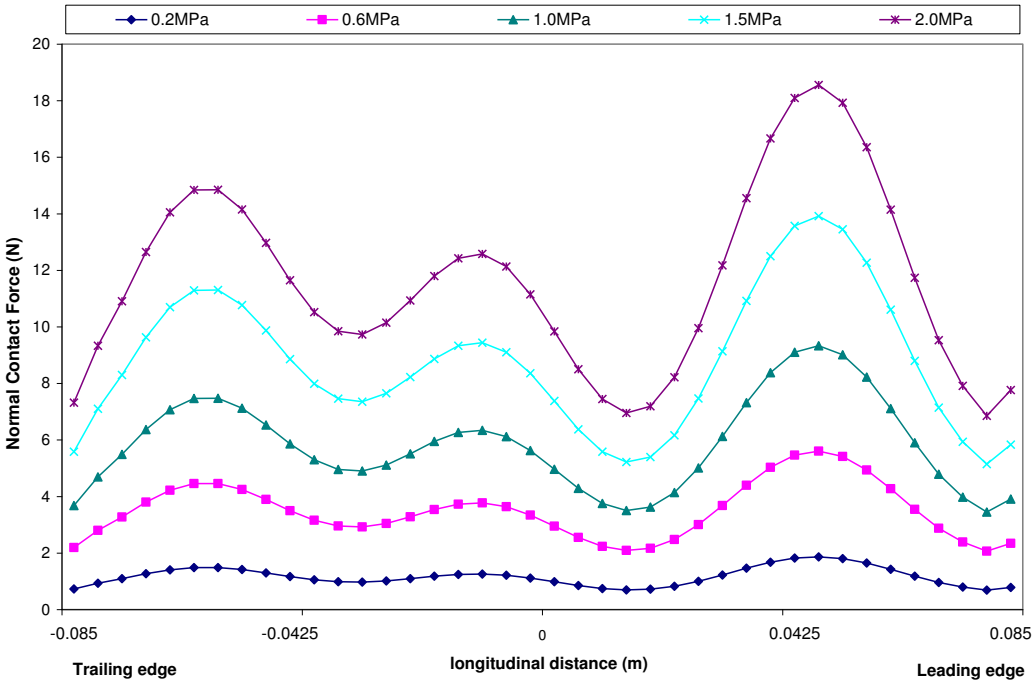

Figure 6.1 Contact force distribution at outboard pad for various hydraulic pressures

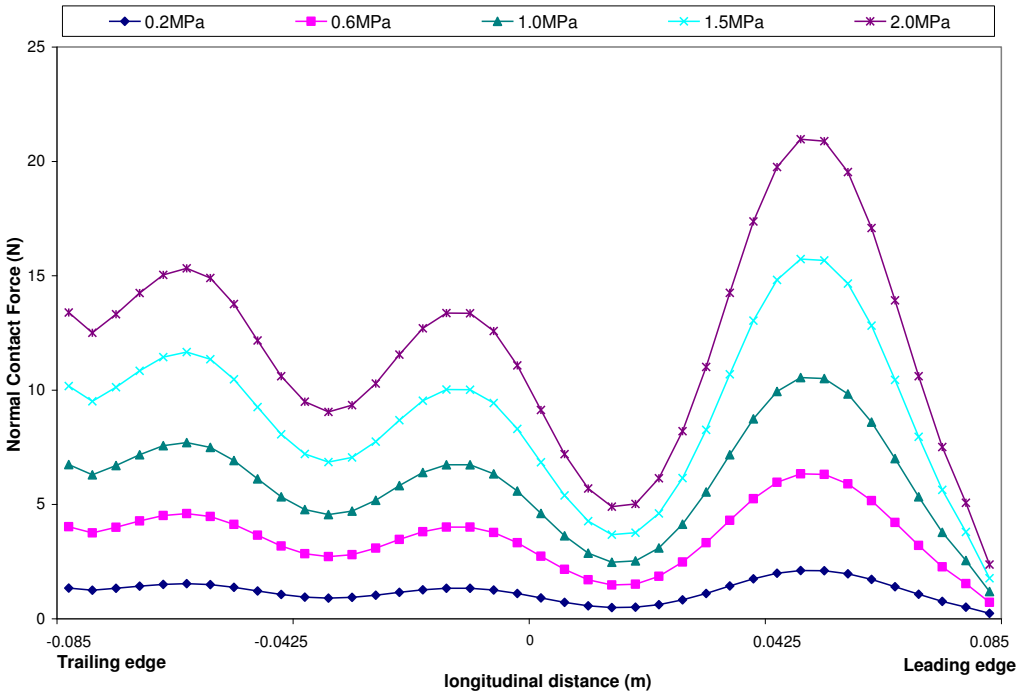

Figure 6.2 Contact force distribution at inboard pad for various hydraulic pressures

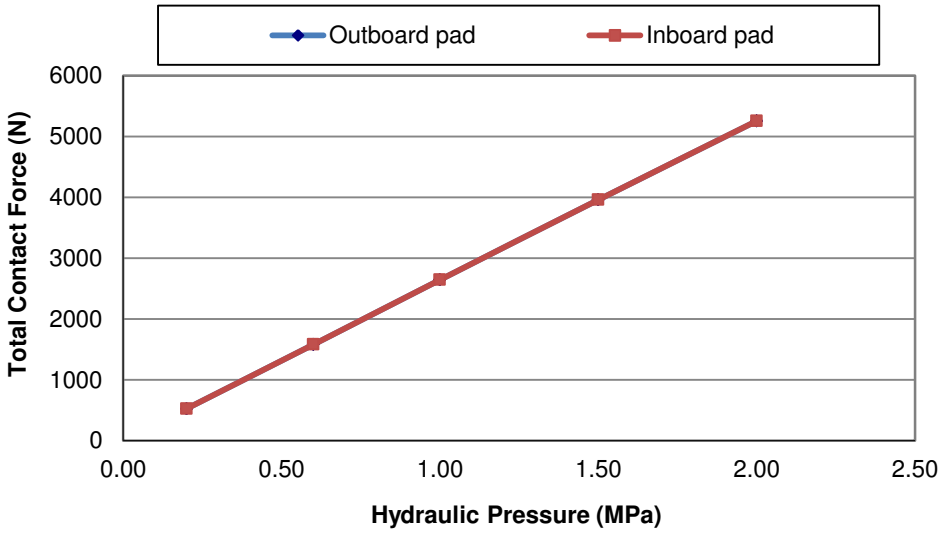

Figure 6.3 Total contact forces at various hydraulic pressures for outboard and inboard pads

It can be seen from Figure 6.3 that as the hydraulic pressure increased at the outboard and the inboard pads, the value of the normal contact force also increased. The FE results showed that the magnitude of interfacial contact force was linearly proportional to the hydraulic pressure but the contact areas did not alter with different values of hydraulic pressures as shown in Figure 6.4. These findings correlate well with the finite element results of other researchers such as Lee [46] and Ripin [57].

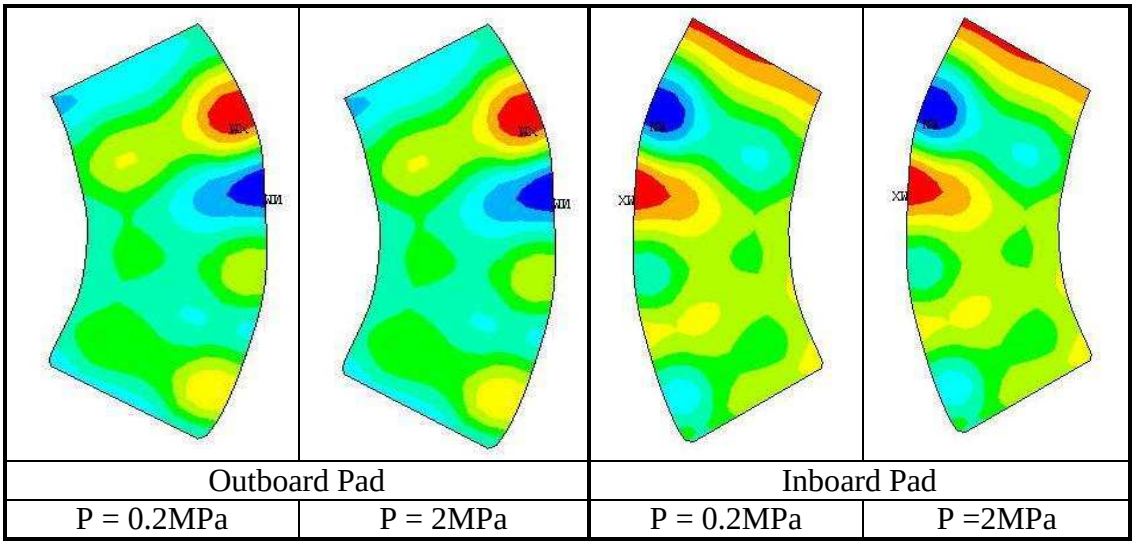

Outboard Pad		Inboard Pad	
P = 0.2MPa	P = 2MPa	P = 0.2MPa	P =2MPa

Figure 6.4 Comparison of FE images of contact pressure distribution for different hydraulic pressure settings

A complex eigenvalue analysis was also performed to measure the instability of the disc brake assembly. The standard deviation of the instability measurements up to 15 kHz was considered and compared with various FE models. The standard deviation value was used as index to quantify the squeal propensity of the system. It must be remembered that the real part of the eigenvalue represented the natural frequency and the imaginary part was a measure of the instability of the system. The degree of instability for FE models with different hydraulic pressures was found by plotting the standard deviation of the instability measurements versus natural frequency as shown in Figure 6.5.

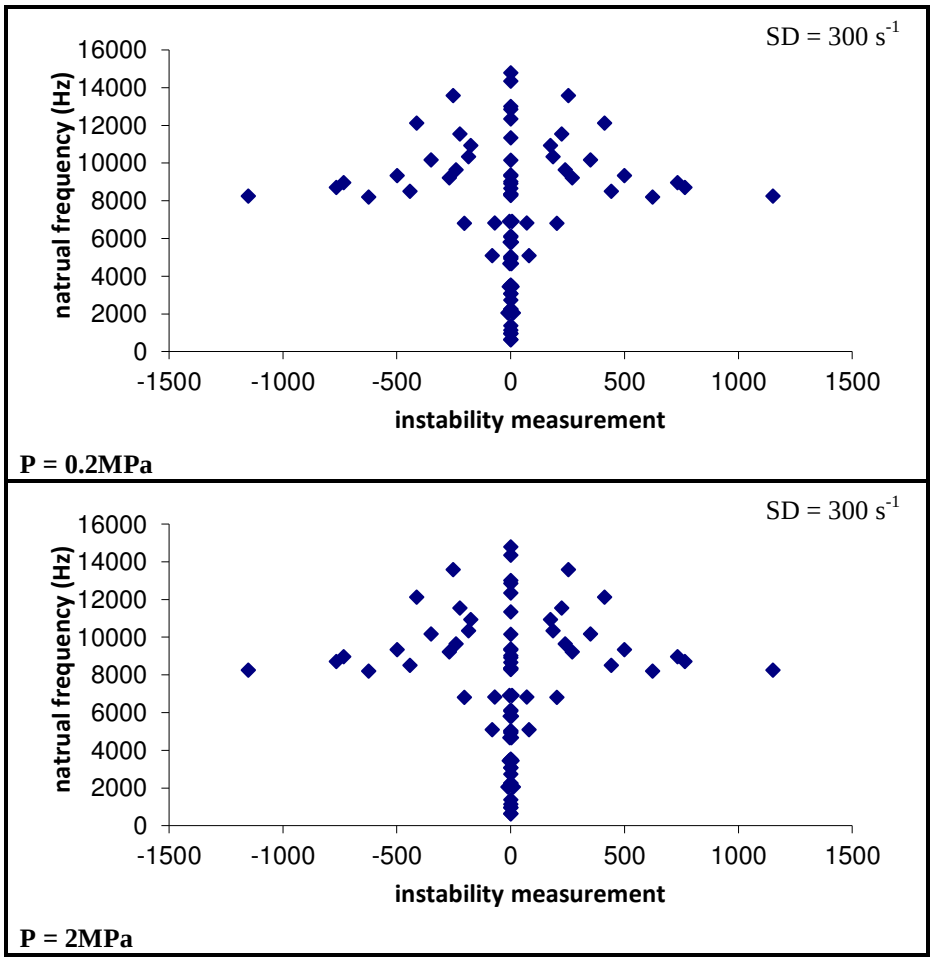

Figure 6.5 Instability measurements versus natural frequency for different hydraulic pressure settings

It can be seen from Figure 6.5 that the different value of hydraulic pressures did not affect the instability measurements of disc brake. The instability measurements were

almost identical for different hydraulic pressure settings and the complex eigenvalue results displayed a similar number of unstable modes and natural frequencies. This was due to the fact that the contact area did not change with the different value of hydraulic pressures therefore the generated unsymmetric stiffness matrix which couples the contact forces and their induced friction forces remained unchanged [45].

6.2.1 Comparison with the Experimental Results

Part 1a- The validation process is an essential procedure of any finite element analysis to confirm the accuracy of FE results. This practice confirms that the finite element results correlated well with the experimental results. Therefore a range of experimental tests performed earlier in Chapter 4; Section 4.3 was compared to validate the FE contact results. The contact pressure distribution images of both outboard and inboard pads were compared with the experimental results as shown in Figure 6.6 to Figure 6.10.

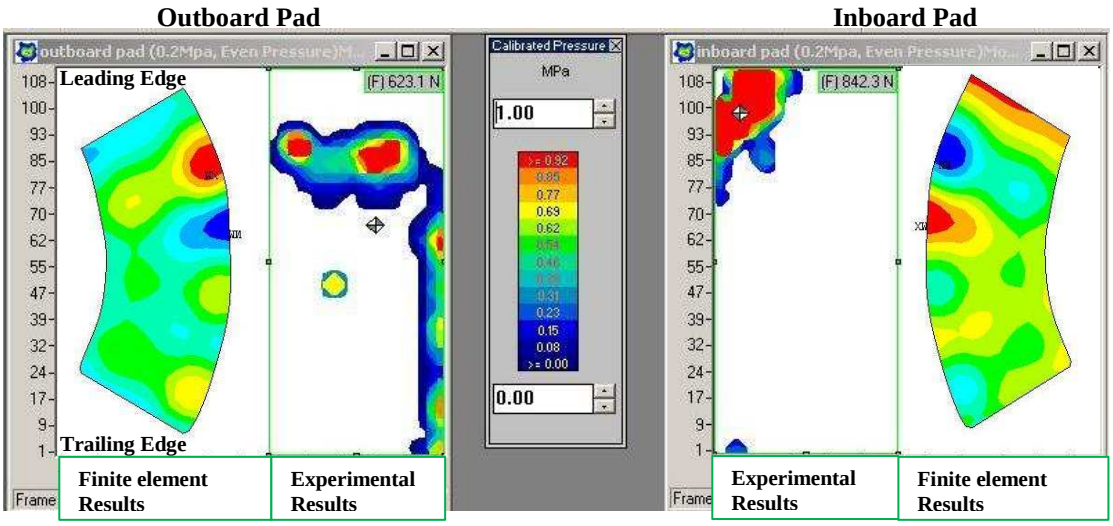

Figure 6.6 Comparison of finite element results with the experimental data at hydraulic pressure of 0.2MPa

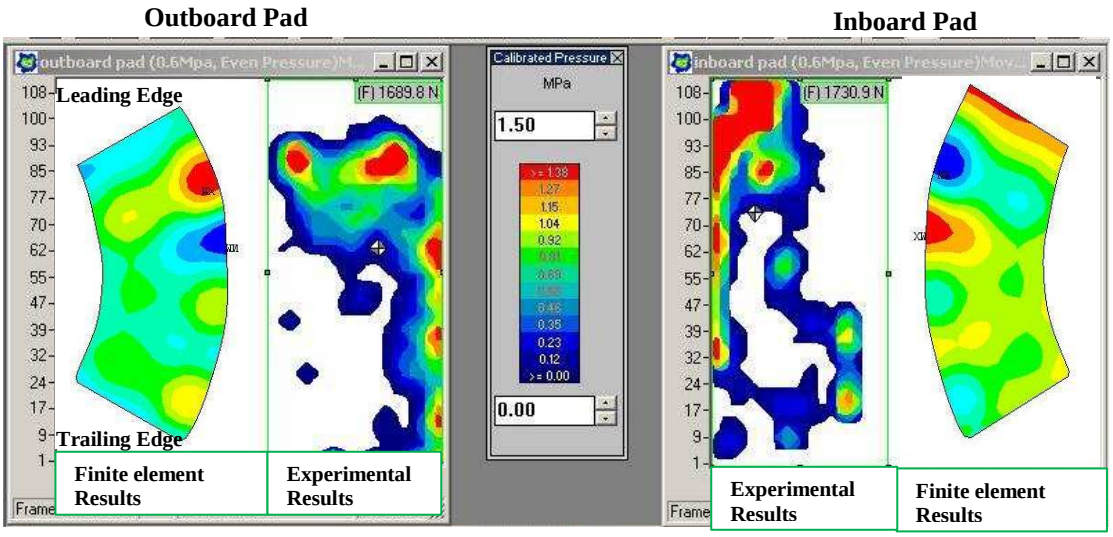

Figure 6.7 Comparison of finite element results with the experimental data at pressure of 0.6MPa

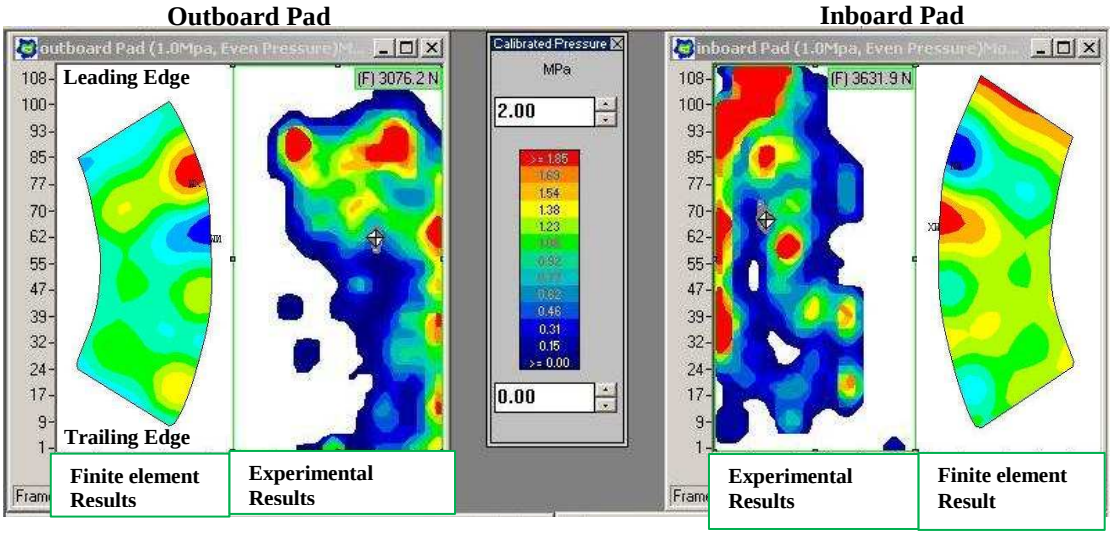

Figure 6.8 Comparison of finite element results with the experimental data at pressure of 1.0MPa

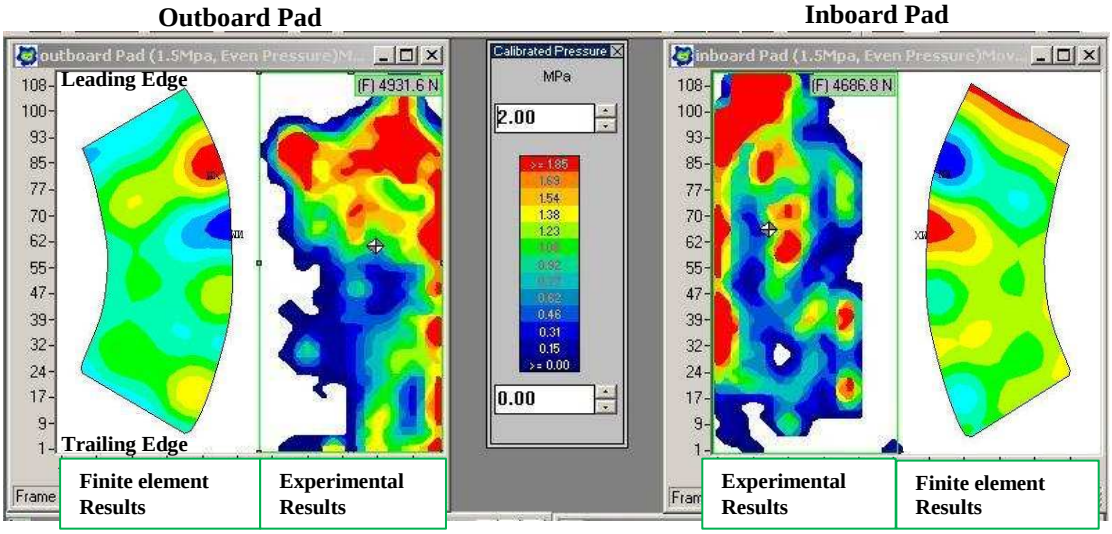

Figure 6.9 Comparison of finite element results with the experimental data at pressure of 1.5MPa

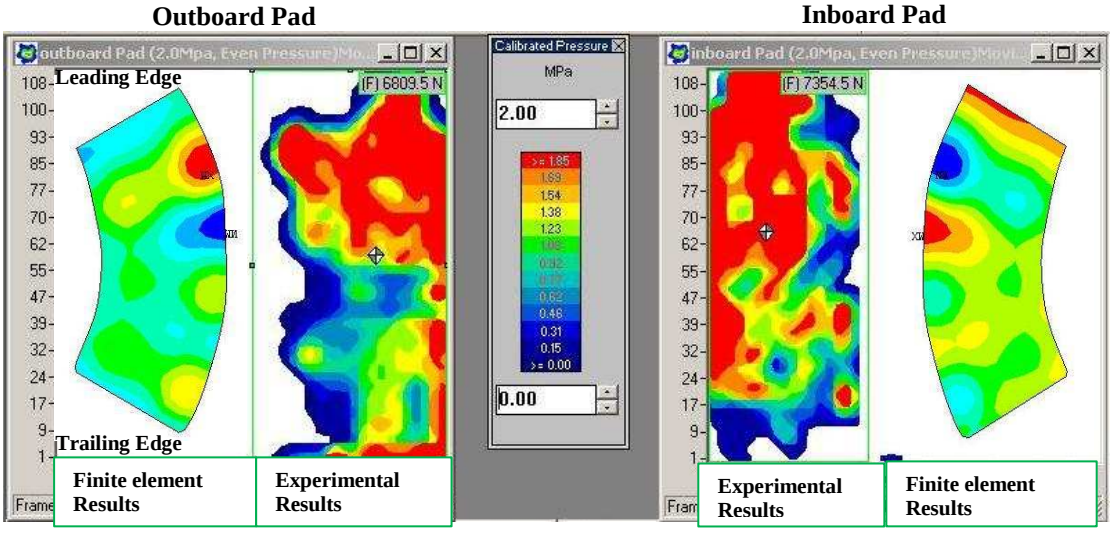

Figure 6.10 Comparison of finite element results with the experimental data at pressure of 2.0MPa

It was apparent from the experimental results that the magnitude of the interfacial contact force increased with the higher caliper pressures settings. This correlated

well with the finite element results however it was also obvious from the experimental results that the contact pressure distribution and contact area does vary with different hydraulic pressure and therefore does influence the squeal propensity. This latter finding from the experimental results did not correlating well with the finite element results, where the contact area boundary remained similar for each pressure settings as shown in Figure 6.6-6.10. It was felt that the discrepancy in the FE results could be due to the fact that in reality the actual rubbing surfaces of disc/pad interfaces was not perfectly smooth and in addition the thermal effects can cause distortion of actual brake structures under braking events causing the contact pressure distribution to change as the hydraulic pressure is increased.

Part 1b- An additional study of finite element contact analysis was performed with similar conditions as mentioned in Chapter 4, section 4.4.1. The piston pressure was adjusted to various settings, in eight different stages as shown in Table 4.3 (page 64). At each stage, the piston pressure was adjusted by applying various hydraulic pressures along the length of the pads. Contact force and pressure distribution was measured from the centre of the pads to display the characteristic behaviour of both leading and trailing side of the pads under various caliper pressure settings. It was established that the finite element results correlated well with the experimental results and the total contact force and pressure distribution towards the leading and trailing edge of the pads followed a similar trend as established in the experimental results. Comparison of the contact pressure distribution images of both experimental and FE results are shown in Appendix K.2.

It was found from Figure 6.11 and Figure 6.12 that overall the FE results correlated well with the experimental results. It was apparent especially from Figure 6.12 that when the brake was prone to squeal, stage 3, contact force distribution was higher towards leading side of the pads whereas when the brake was quiet, stage 8, the contact force distribution was generally towards the trailing side of the pads indicating good correlation between the results.

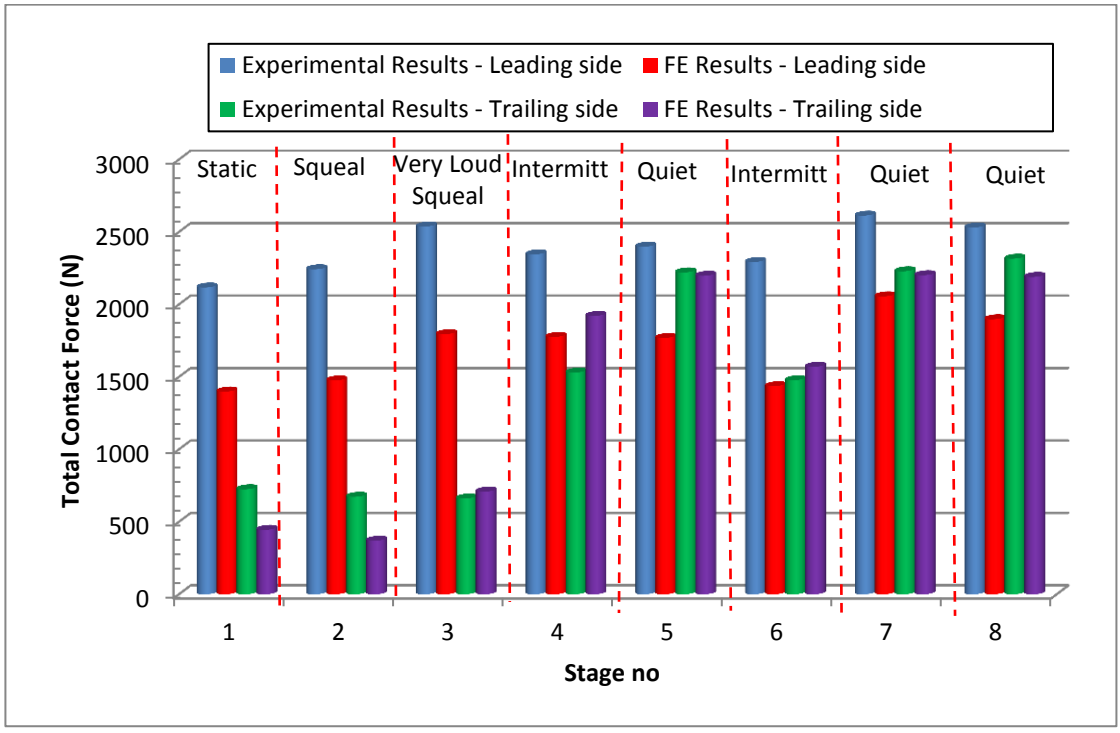

Figure 6.11 Comparison of total contact force at leading and trailing section of pad (Outboard pad)

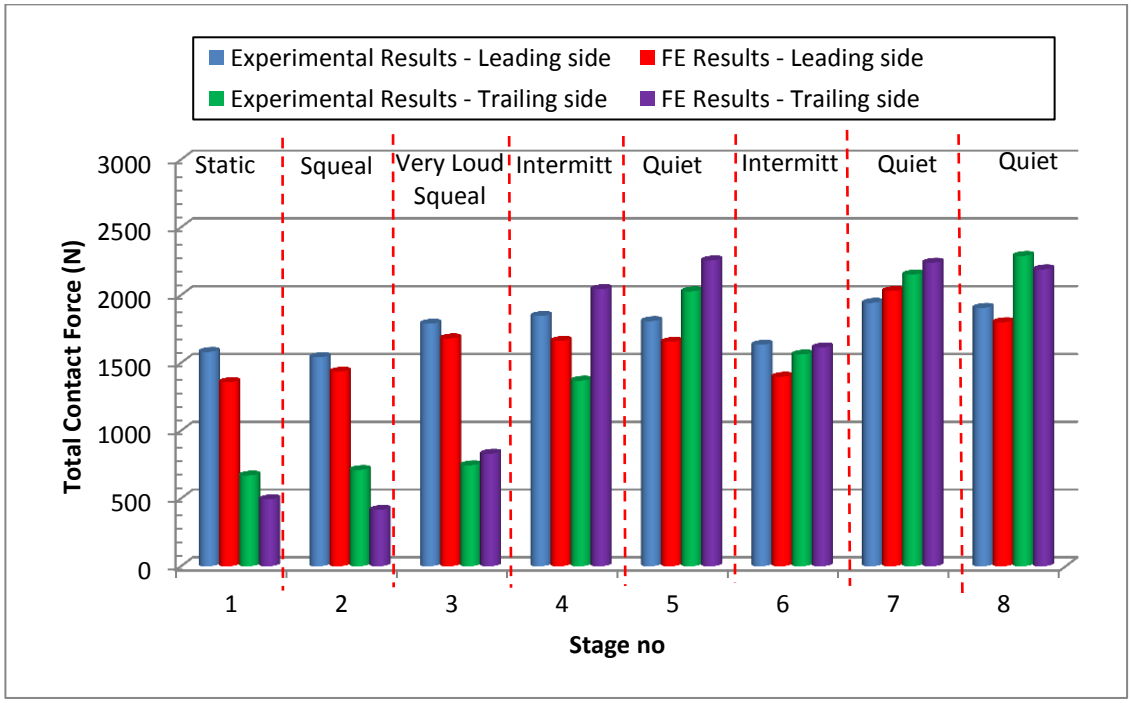

Figure 6.12 Comparison of total contact force at leading and trailing section of pad (Inboard pad)

6.3 Effect of Coefficient of Friction

The coefficient of friction is one of the most important parameter that has significant influence on squeal propensity [40]. The purpose of this investigation was to identify the effect of various coefficients of friction on the disc brake squeal. In this analysis, the coefficient of friction between the disc/pad interfaces was varied from $\mu = 0$ to $\mu = 0.6$. The hydraulic brake pressure of 1.0MPa was kept constant throughout this study. The analysis was initially performed under a frictionless condition ($\mu = 0$). It was found from Figure 6.13 and 6.14 that under frictionless conditions, the magnitude of the normal contact force, along an arc at mean rubbing radius of the pad, was higher towards the leading edge of the pad and the magnitude of contact force at the centre of the pad was much lower compared to both the leading and the trailing edge of the pad. The pressure distribution and the magnitude of the normal contact force at both the outboard and the inboard interfaces were almost similar to each other. However when the coefficient of friction of $\mu = 0.2$ was introduced in the FE model, the interfacial pressure distribution shifted towards the leading edge of the pad resulting in more contact area towards the leading edge of the pad. Conversely, more separation occurred towards the trailing region of the pad. It is again shown in Figure 6.13 and Figure 6.14 that with an increase in the coefficient of friction, the contact pressure distribution shifted more towards the leading edge of the pad and therefore more separation occurred toward the trailing end of the pad. These findings were in good agreement with the results of Tirovic et al [17] and Lee [46].

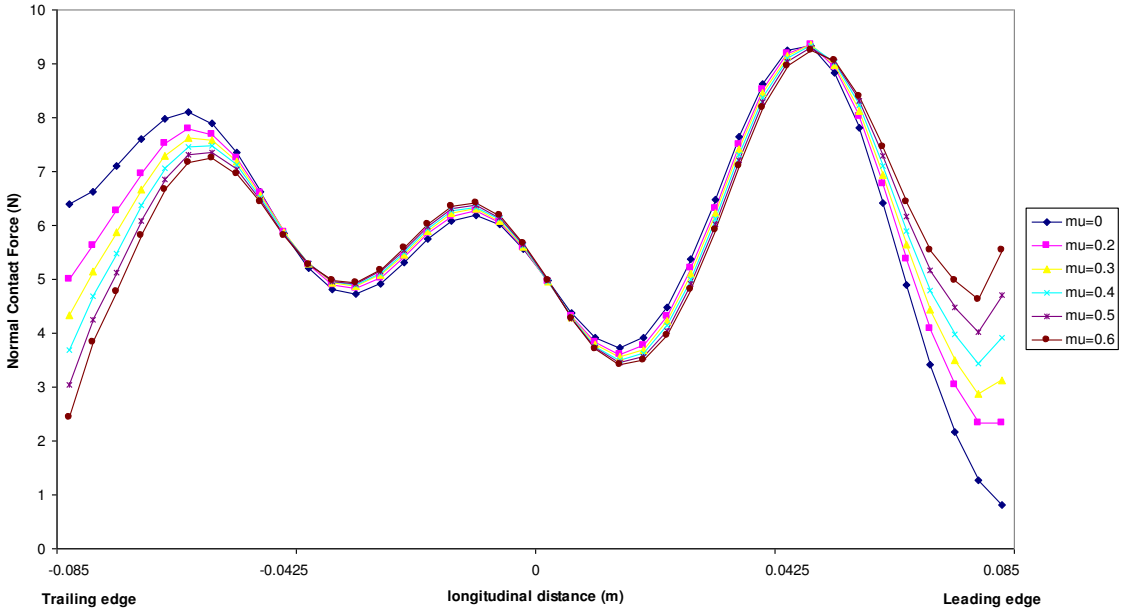

Figure 6.13 Contact force distribution along an arc at mean rubbing radius of outboard pad for various coefficients of friction (Brake line pressure= 1.0MPa)

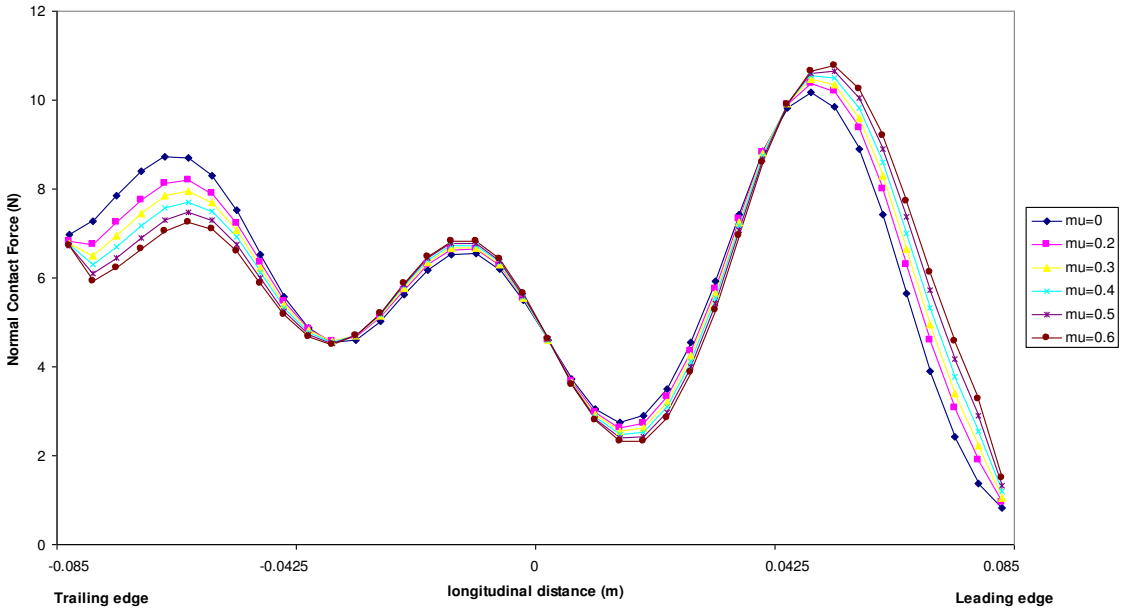

Figure 6.14 Contact force distribution along an arc at mean rubbing radius of inboard pad for various coefficient of friction (Brake line pressure= 1.0MPa)

The standard deviation of the normal contact forces was also measured to observe the non-uniformity of the interface pressure distribution for different coefficients of friction as shown in Figure 6.15. It was found that for the frictionless model ($\mu = 0$), the standard deviation of the normal contact force was 2.70 N. Once the friction was

included in the model (μ= 0.4), the standard deviation of contact forces was reduced to 2.40 N which was a reduction of 11%. It was apparent from the standard deviation measurements of contact forces and the pressure distribution contours, as shown in Appendix L, that as the value of coefficient of friction increased, there was a more uniform contact pressure distribution between the disc/pad interfaces.

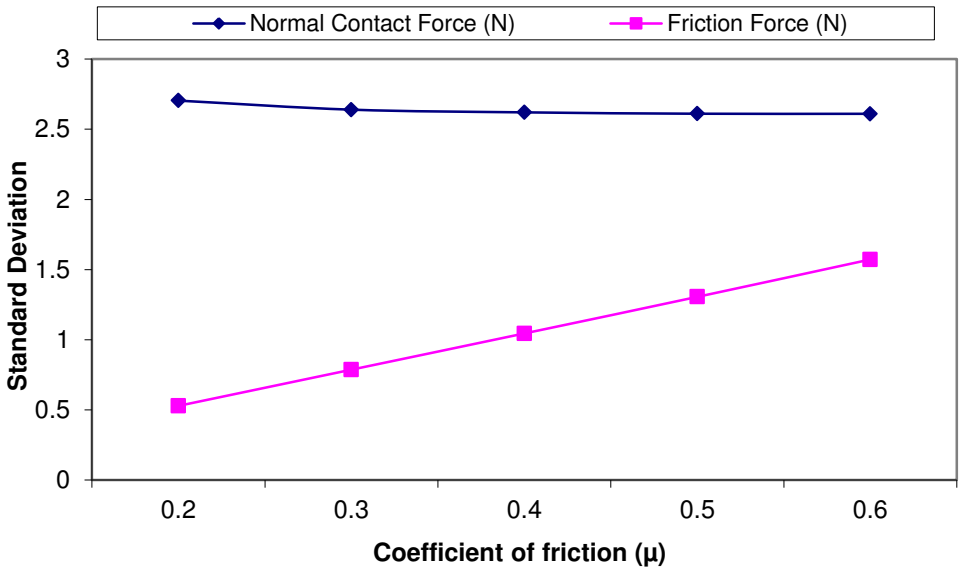

Figure 6.15 Sensitivity studies showing the effect of various coefficients of friction on contact forces

A sensitivity analysis showing the effect of coefficient of friction on the standard deviation of the friction forces was also measured as shown in Figure 6.15. It was found that when the friction coefficient was μ=0.2, the measured standard deviation was about 0.53N however with the friction coefficient of μ=0.6 the standard deviation was at 1.57N which was 66% higher than friction coefficient of μ = 0.2. It is shown in the Figure 6.15 that the standard deviation of the interfacial frictional forces was directly proportional to the friction coefficient. It was observed that a higher coefficient of friction resulted in a higher amount of interfacial friction forces and thus causing more instability in a brake assembly. This implies that the most fundamental method of eliminating brake squeal is to reduce the friction between the disc/pad interfaces. However, this may reduce braking performance and is not a preferable method to employ.

A complex eigenvalue analysis was also performed to measure the instability of the disc brake assembly. The degree of instability for different coefficient of friction models was found by plotting the standard deviation of the instability measurements versus natural frequency as shown in Figure 6.16.

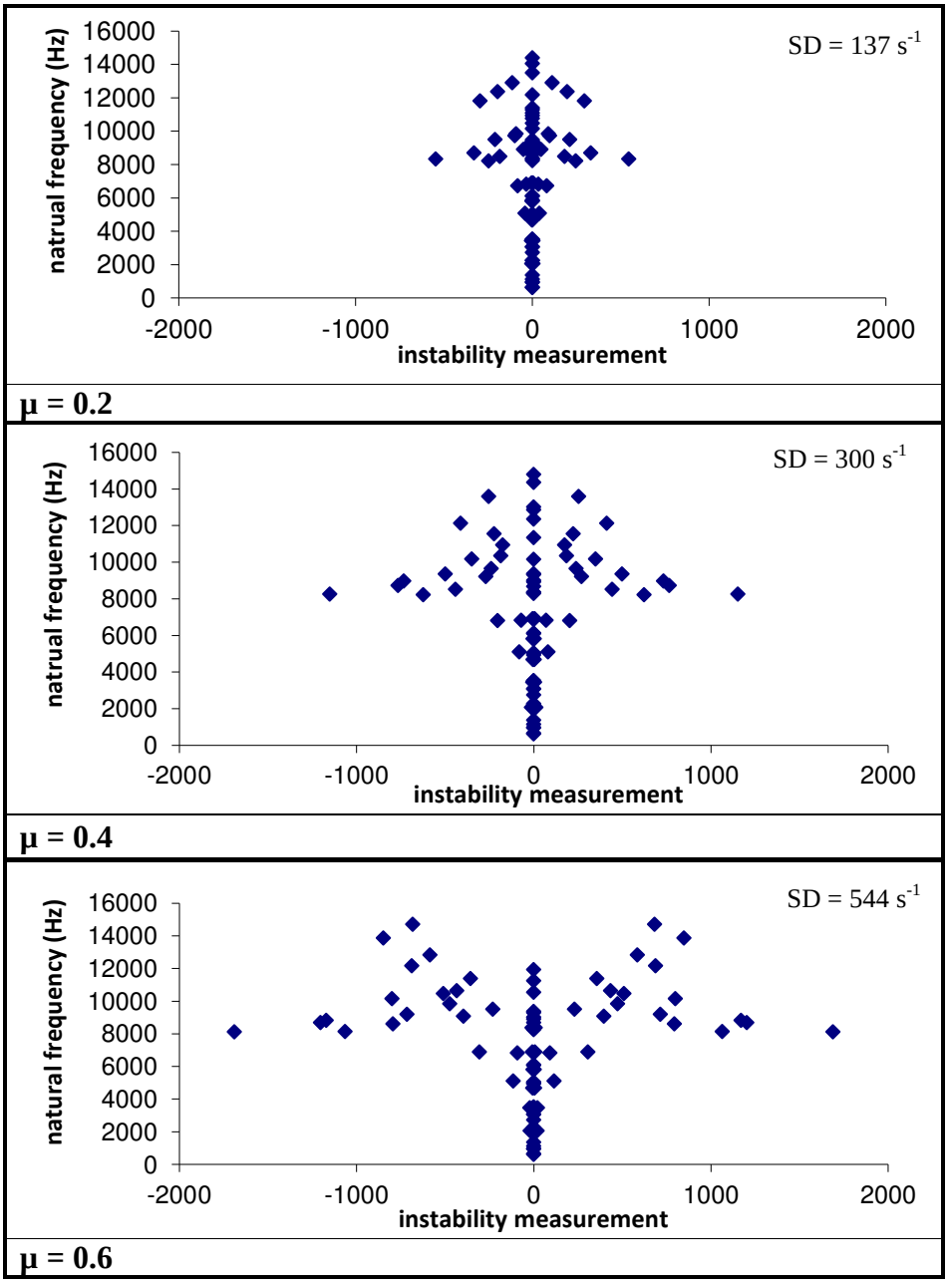

Figure 6.16 Standard deviation of the instability measurements versus natural frequency for various frictional conditions

It was found from Figure 6.16 that for the lower value of coefficient of friction (μ=0.2), the standard deviation of the instability measurement was 137s^{-1} and the standard deviation of instability measurement of the model with μ=0.40 was measured as 300s^{-1} whilst the standard deviation of the instability measurement of the model with coefficient of friction μ=0.6 was calculated as 544s^{-1}. It was observed that the calculated standard deviations of instability measurement were approximately proportional to the coefficient of friction as shown in Figure 6.17. It is apparent that as the coefficient of friction increased, the propensity towards instability also increased. In other words, the higher the value of coefficient, the greater the calculated standard deviation of instability and therefore it was more likely for instability to take place in the brake assembly. These findings are in good agreement with the previous studies presented by Liles [43] and Lee [46].

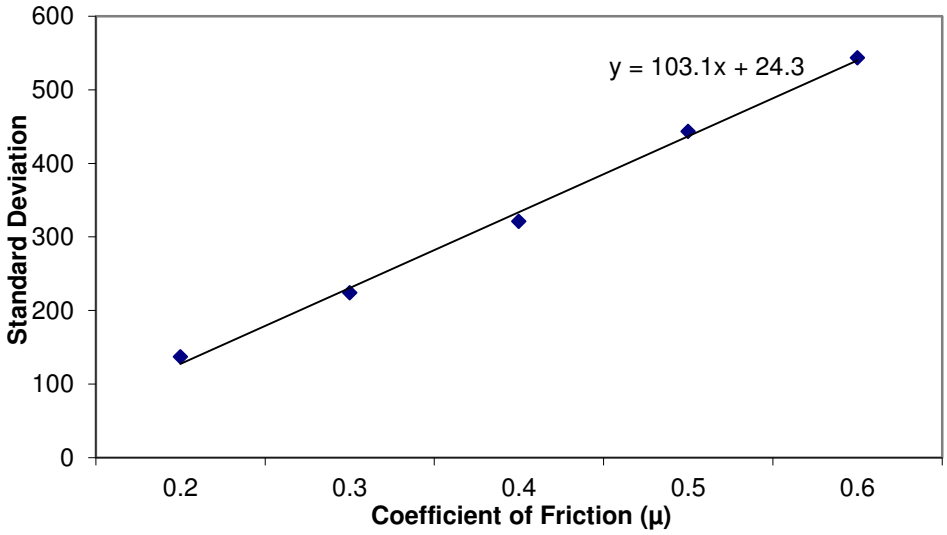

Figure 6.17 Plot of coefficient of friction vs. instability measurement

6.4 Study of Modes of Vibration

A finite element model with coefficient of friction of μ = 0.4 was used to study the mode shapes and the excited frequencies of the disc brake. A hydraulic pressure of 1.0MPa was applied at the backplate of both the outboard and the inboard pads. A complex eigenvalue analysis was performed to ascertain the instability measurements, natural frequencies and the modes of vibration up to 8 kHz as shown in Table 6.1.

Table 6.1 Natural frequency and mode shapes of disc brake assembly

Mode Order	Frequency (Hz)	Instability Measurements (1/second)	No of Diametral Lines (Disc Surface)
1	623	0	1
2	650	0	1
3	942	0	2
4	972	0	2
5	1130	0	1
6	1369	0	1
7	2058	12.277	3(R); 3(I)
8	2058	-12.277	3(R); 3(I)
9	2246	0	1
10	2261	0	1
11	2733	0	1 (circumferential)
12	3064	0	2
13	3077	0	2
14	3447	2.081	4(R); 4(I)
15	3447	-2.081	4(R); 4(I)
16	3503	0	1
17	3530	0	1
18	4674	-2.9604	3(R); 3(I)
19	4674	2.9604	3(R); 3(I)
20	4928	0	2
21	4994	0	1
22	5047	0	2
23	5103	-73.745	5(R); 5(I)
24	5103	73.745	5(R); 5(I)
25	5812	2.7973	1(R); 1(I)
26	5812	-2.7973	1(R); 1(I)
27	6082	0	1
28	6120	0	6
29	6823	-71.66	6(R); 6(I)
30	6823	71.66	6(R); 6(I)
31	6838	159.37	6(R); 6(I)
32	6838	-159.37	6(R); 6(I)
33	6902	-5.9149	5(R); 5(I)
34	6902	5.9149	5(R); 5(I)
35	8287	0	2
36	8355	6.1398	7(R); 7(I)
37	8355	-6.1398	7(R); 7(I)
38	8403	528.5	7(R); 7(I)
39	8403	-528.5	7(R); 7(I)
40	8417	0	8

Note: R indicates real part of a complex mode

I indicates imaginary part of a complex mode

- indicates complex mode with a negative instability measurement

+ indicates complex mode with a positive instability measurement

There were a number of normal modes found within the frequency range of 8 kHz. The first normal mode of disc occurred at a frequency of 622 Hz which was clearly the 1st diameteral mode of vibration as shown in Figure 6.18. The second mode of vibration occurred at a frequency of 942 Hz and exhibited a 2nd diametral mode as shown in Figure 6.19. A normal mode with zero instability measurement is in general a stable mode and therefore is not accountable for brake noise.

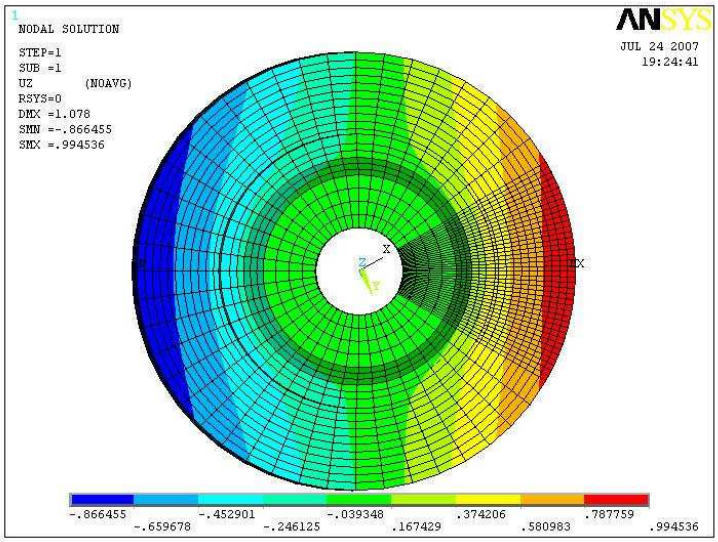

Figure 6.18 Mode shapes of disc surface at 622 Hz with 1st nodal diameter

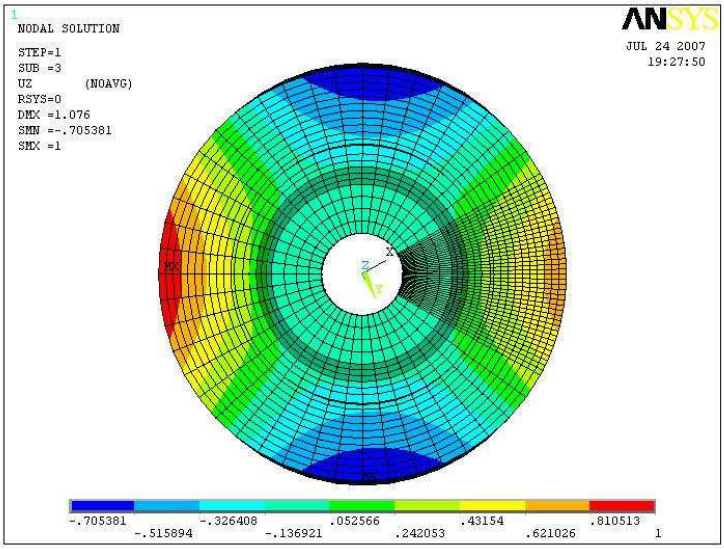

Figure 6.19 Mode shapes of disc surface at 942 Hz with 2nd nodal diameter

A complex mode always appears in pairs with the same natural frequency. A negative value means the system is stable, whereas a positive value means the system is unstable indicating tendency to generate noise. The first such mode was at the

frequency of 2058 Hz with an instability measurement of ±12.3 as shown in Figure 6.20 and 6.21. It was established from the finite element results that it was a 3rd diametral mode of vibration. It can be seen from Figure 6.20 and 6.21 that pattern of imaginary parts was similar to the real parts and that the imaginary parts of two complex modes shows the same magnitude of amplitude with opposing signs which suggested that they were 180° out of phase with each other. It should be noted again that the positive sign of the instability measurement contributes to unstable modes resulting in instability within the brake system however a negative sign leads to stable modes promoting quiet brakes.

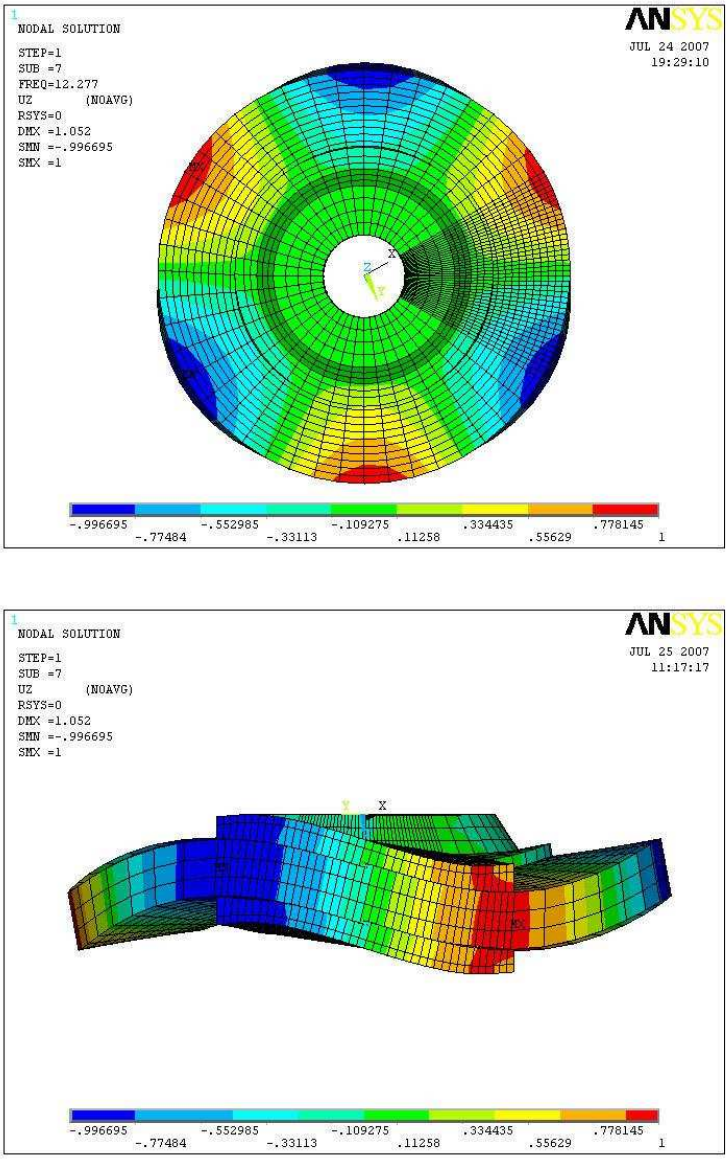

Figure 6.20 Mode 7 showing unstable mode of disc surface at 2058 Hz with 3rd nodal diameter

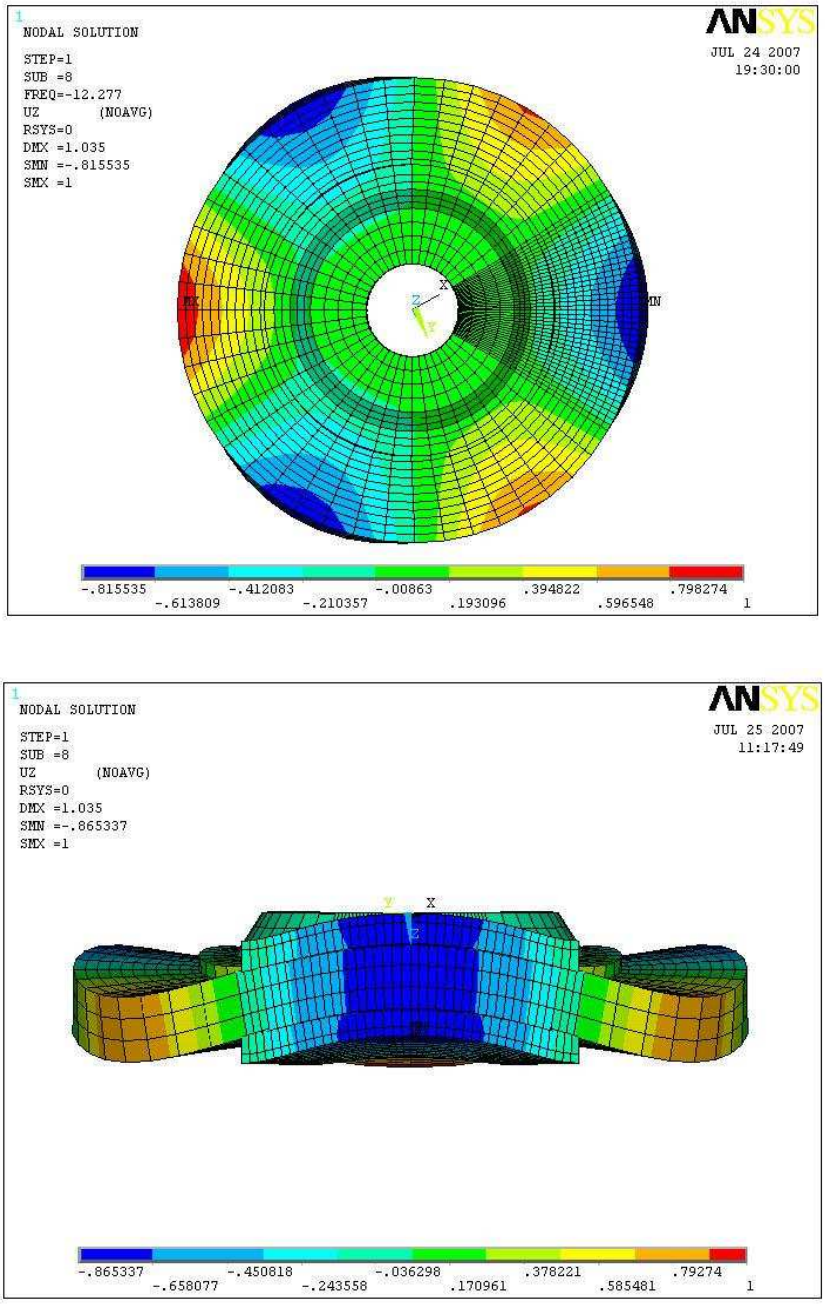

Figure 6.21 Mode 8 showing unstable mode of disc surface at 2058 Hz with 3rd nodal diameter

The second complex mode occurred at a frequency of 3447 Hz with an instability measurement of ±2.1 as shown in Figure 6.22 and Figure 6.23. This was the 4th diameteral mode of the disc. There were a few other similar type of complex modes present in the finite element results, the most obvious were at the frequencies of 5103Hz (5th diameteral mode) and 6823 Hz (6th diameteral mode) with the

instability measurements of ±73 and ±71 respectively as shown in Figure 6.24 to Figure 6.27.

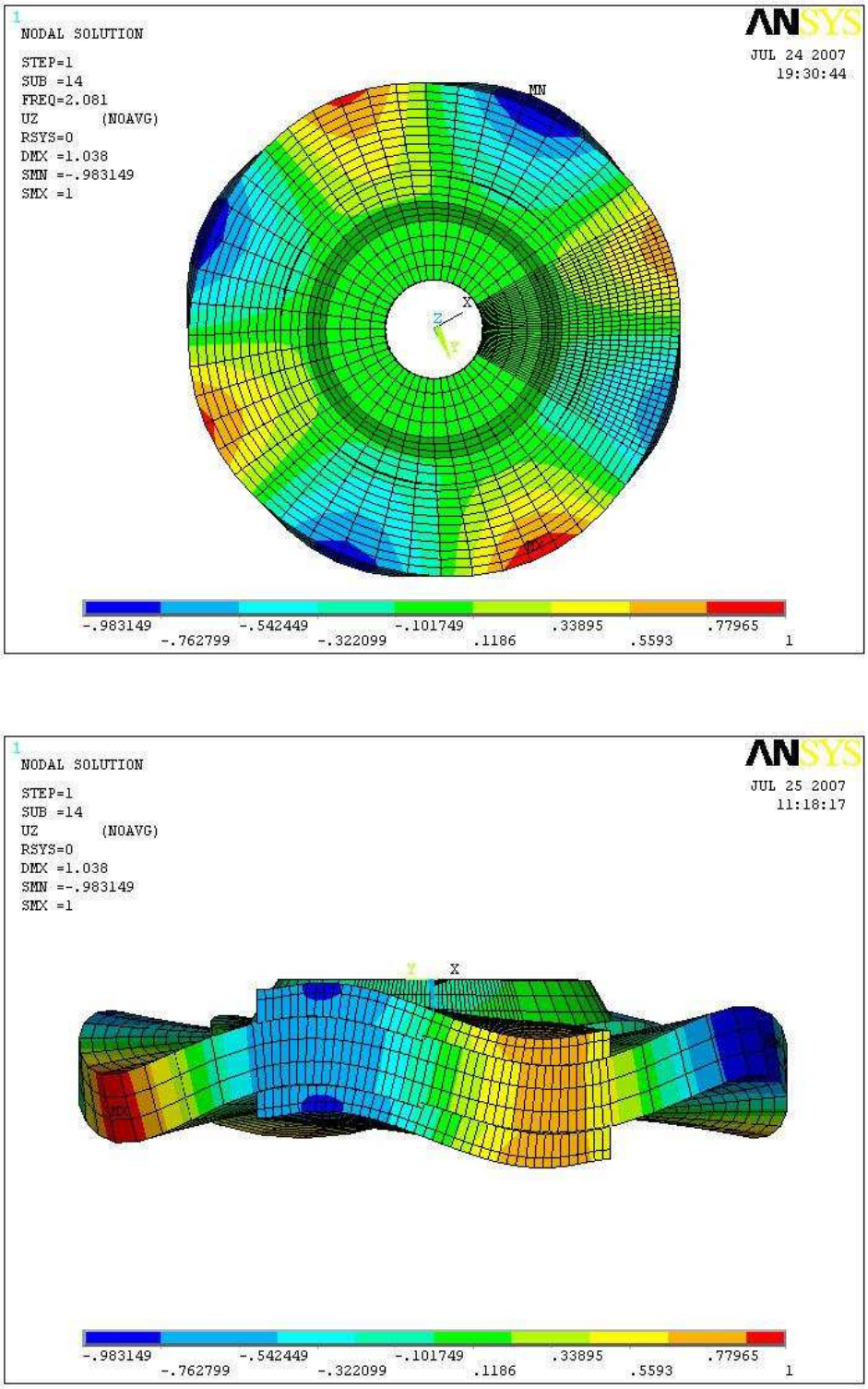

Figure 6.22 Mode 14 showing unstable mode of disc surface at 3447 Hz with 4th nodal diameter

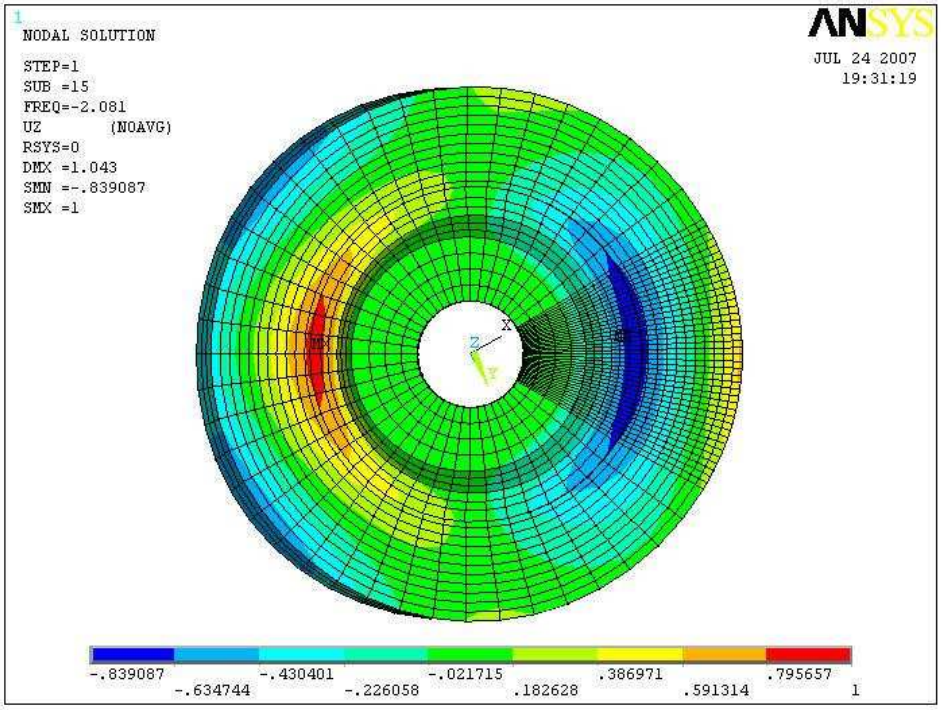

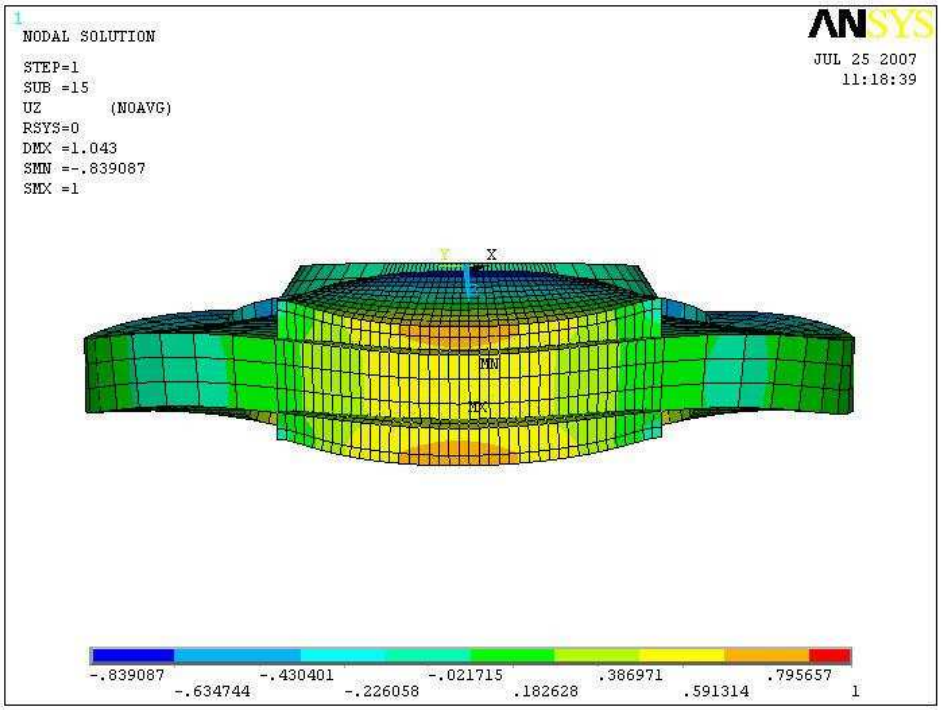

Figure 6.23 Mode 15 showing unstable mode of disc surface at 3447 Hz with 4th nodal diameter

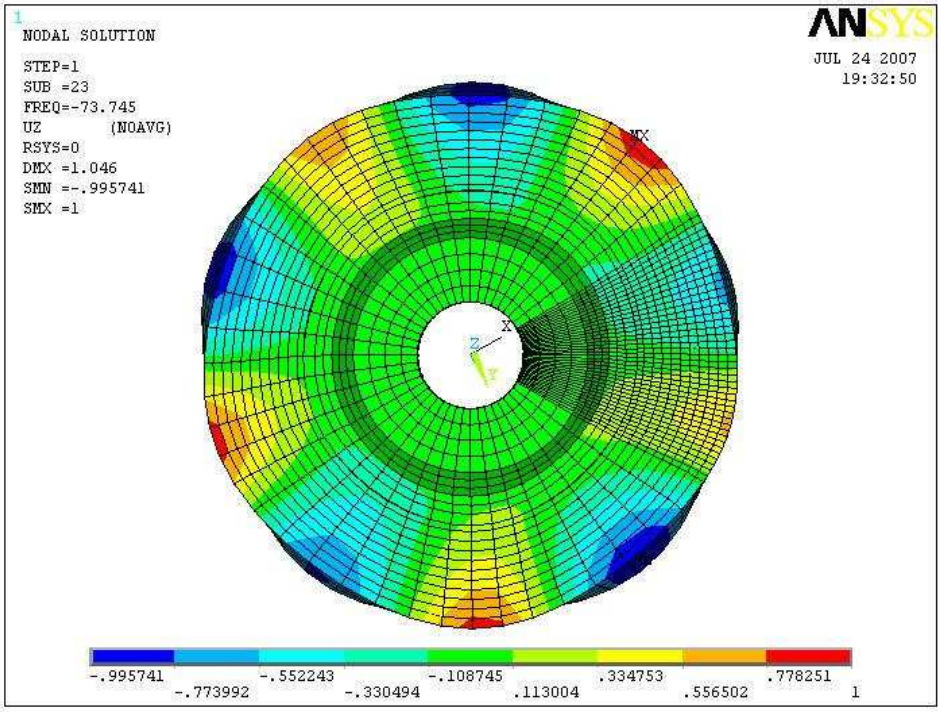

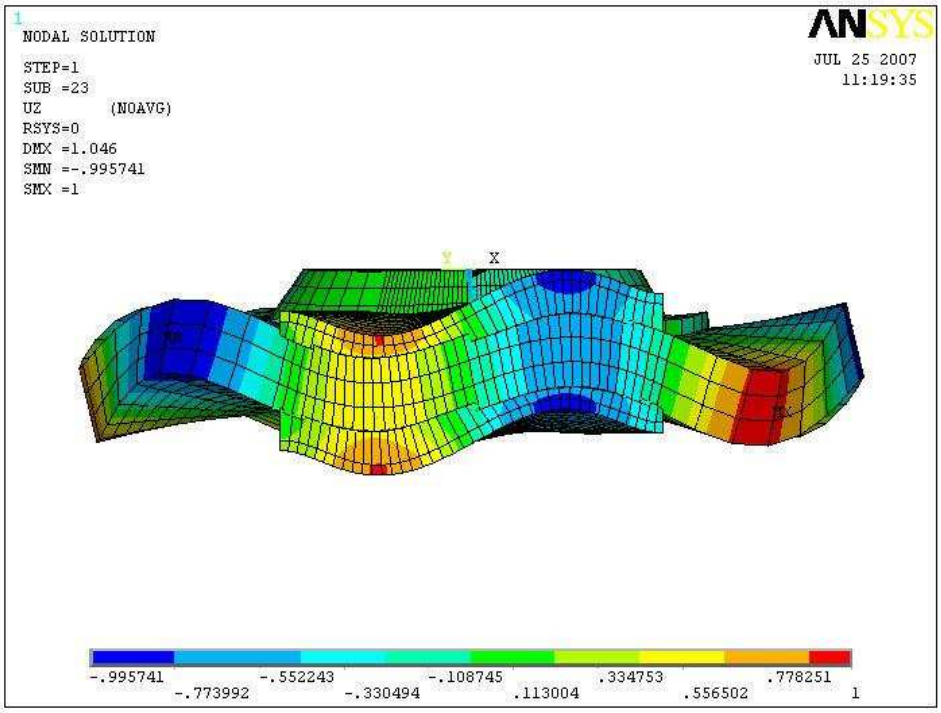

Figure 6.24 Mode 23 showing unstable mode of disc surface at 5103 Hz with 5th nodal diameter

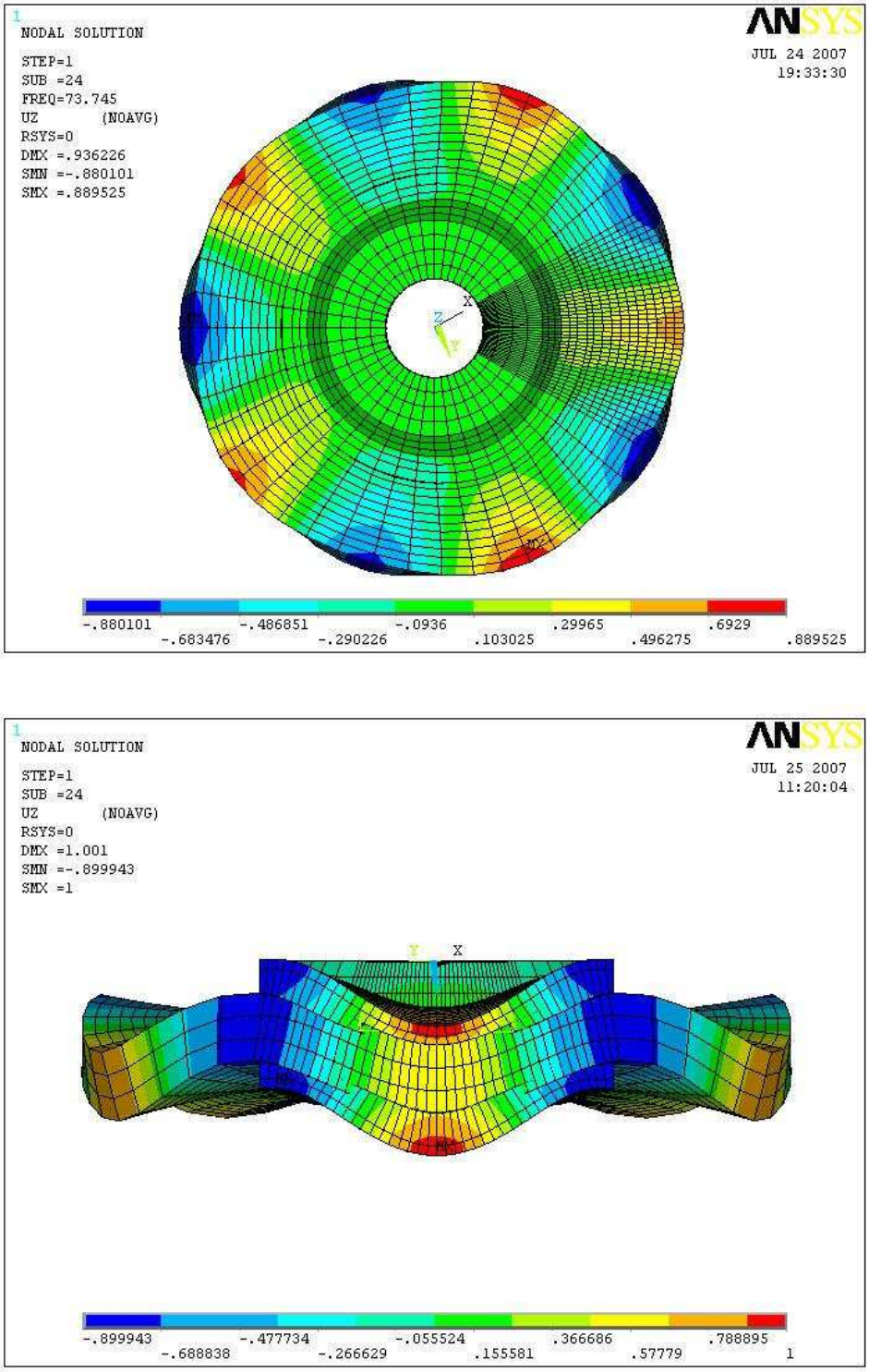

Figure 6.25 Mode 24 showing mode shapes of disc surface at 5103 Hz with 5th nodal diameter

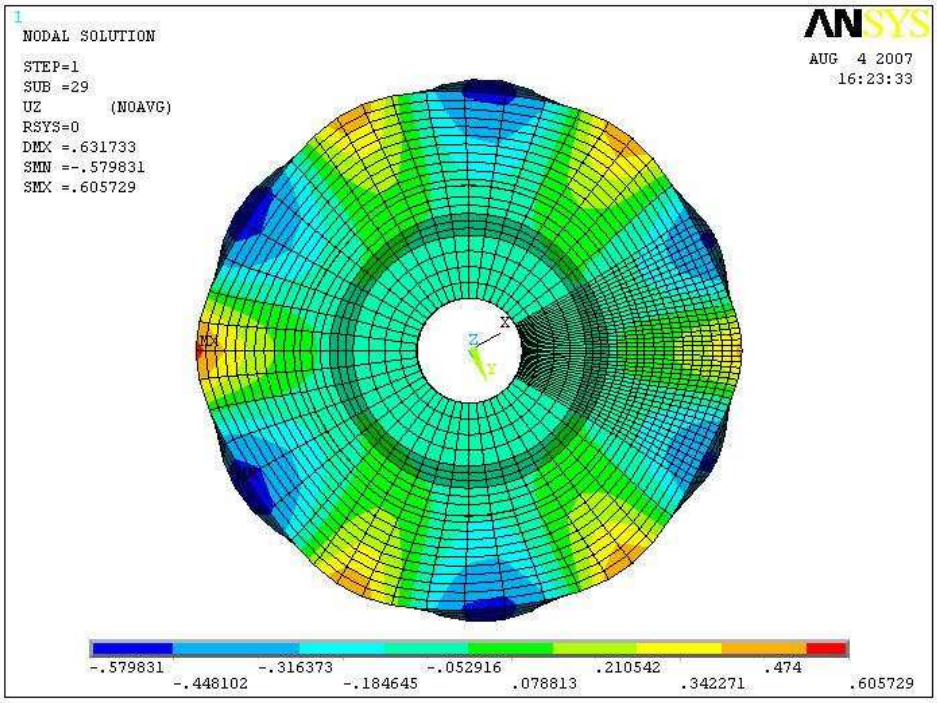

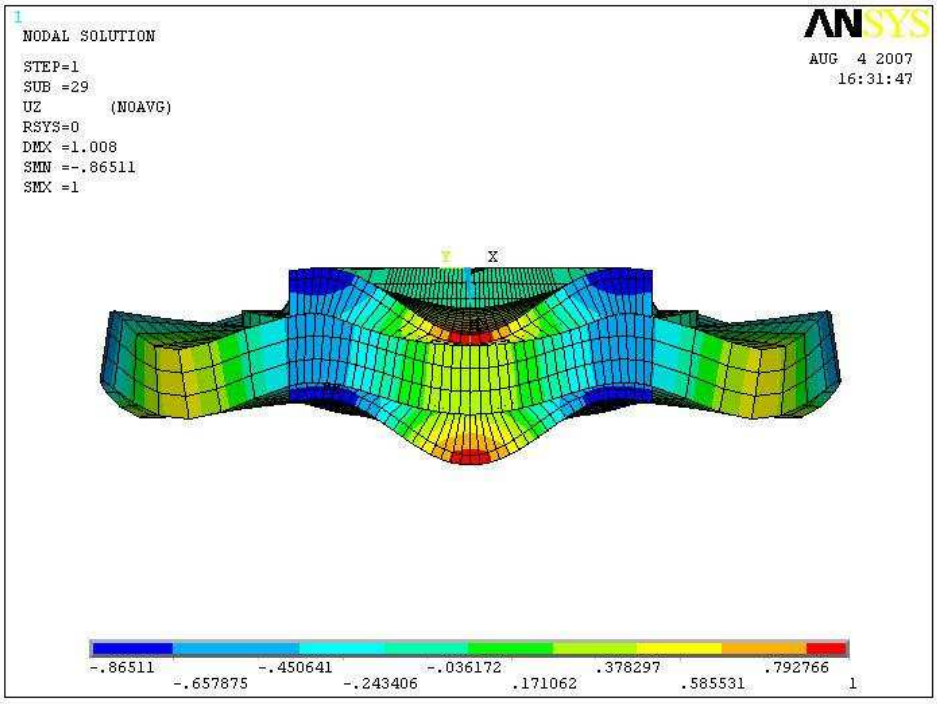

Figure 6.26 Mode 29 showing mode shapes of disc surface at 6823 Hz with 6th nodal diameter

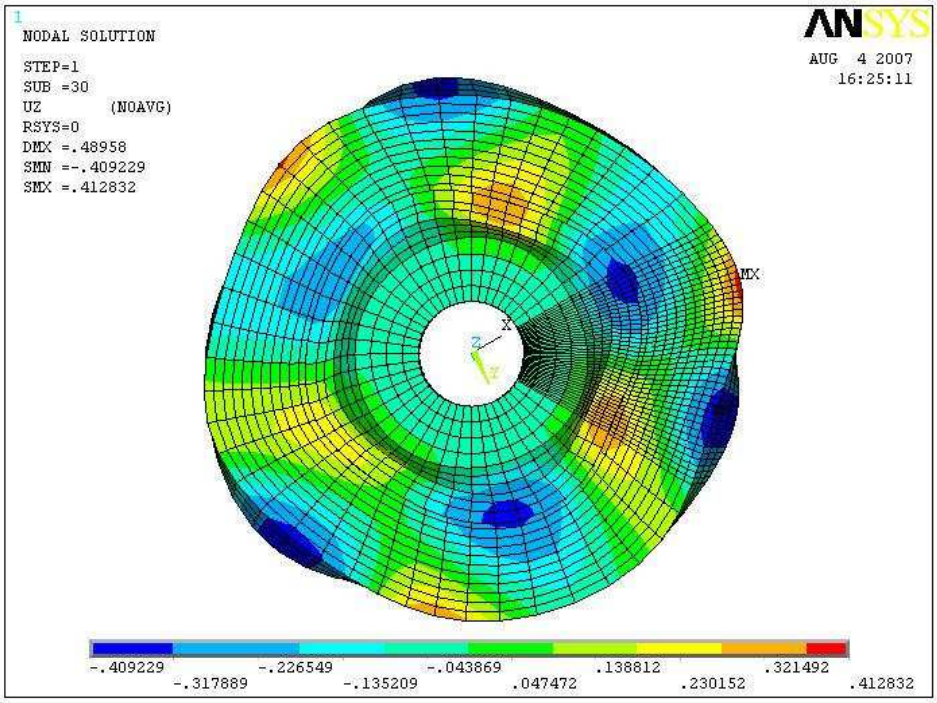

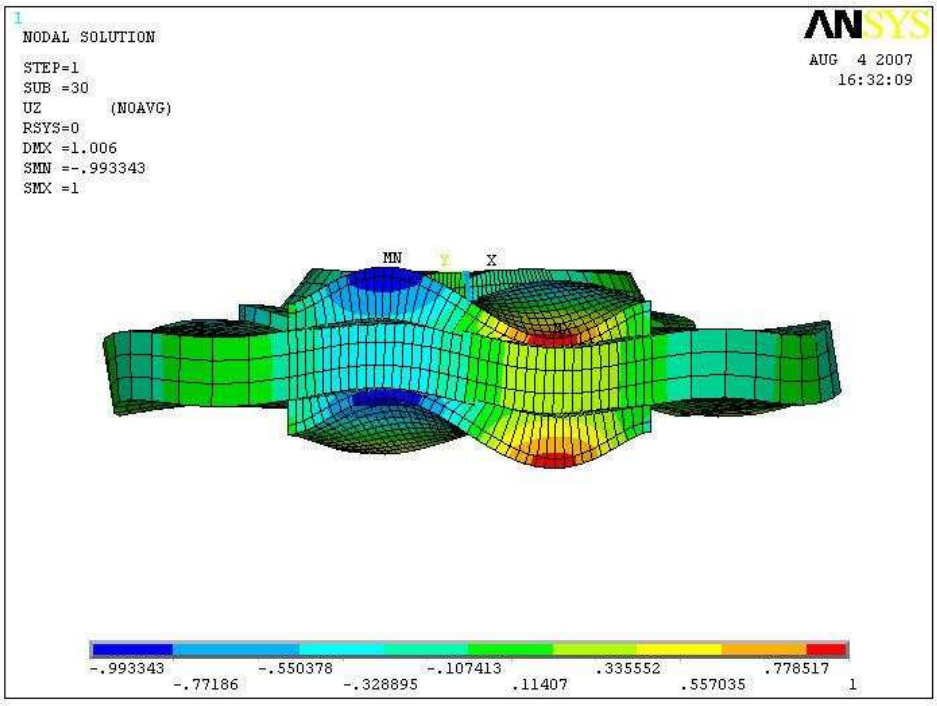

Figure 6.27 Mode 30 showing mode shapes of disc surface at 6823 Hz with 6th nodal diameter

From the experimental results, it was established that the disc brake became unstable at frequencies of 1820Hz, 3042Hz, 4150Hz, 4835Hz and 6430Hz. Although the experimental results did not reveal any information on disc diameteral modes they did confirm the squeal frequencies of noisy brake which was measured using a FFT analyser. Therefore the frequencies obtained from the experimental results were compared with the FE results to provide better insight into unstable modes of the disc brake as shown in Table 6.2. It should be noted that only complex modes with a positive instability measurement (unstable modes) were considered for comparison purposes.

Based on the experimental results, the first unstable frequency (squeal noise) was observed at a frequency of 1820 Hz. It was also confirmed by the manufacturer in a private conversation that this frequency was in accordance with the manufacturer's recorded squealing frequency. Finite element results also exhibited the first unstable mode (real parts) at a frequency of 2058 Hz with an instability measurement equal to + 12.3, which was characterised by 3 nodal diameters as shown in Figure 6.20. From the above results it was established that the 3rd diametral mode was most likely to be accountable for brake squeal in the current brake system.

Table 6.2 Comparison of finite element results with the experimental results

Experimental Results (Hz)	Finite Element Results (Hz)	Error (%)	Mode Order from FE Results
1820	**2058**	**11.56**	**3**
3042	3447	11.75	4
4150	4674	11.21	3
4835	5103	5.25	5
6430	6823	5.76	6

The overall finite element results correlated well with the experimental data. Although not the focus of the experimental work in Chapter 4, there were other apparent squeal frequencies observed during the experimental tests which were also compared with the FE results. It was found that the simulated unstable frequencies were within the range of 12% of experimental results as shown in Table 6.2. It was established that the instability analysis using the complex eigenvalue method was

able to predict unstable modes of vibration at frequencies which were fairly similar to the squealing frequencies obtained during the tests on the test rig and on-vehicle testing by the manufacturer.

6.5 Summary

In this chapter, the effects of varying the friction coefficient and the brake hydraulic pressure were investigated. It was established from the FE results that the brake pressure was linearly proportional to the normal contact forces and that the magnitude of the interfacial contact forces increased with the higher caliper pressures. It was also confirmed that a higher coefficient of friction resulted in a high amount of interfacial friction forces and thus the potential to cause more instability in a brake assembly.

A modal analysis of the disc rotor was performed and then compared with the real brake rotor. Finite element results of contact pressure distribution were validated with the experimental results and then a comprehensive modal analysis of disc brake was performed using the complex eigenvalue method to predict the natural frequencies and the mode shapes of the disc rotor. Furthermore a stability analysis of the brake assembly was performed to determine the unstable frequencies in the current brake assembly. It was noted that the overall finite element results correlated well with the experimental data and the measured unstable frequencies were within the rage of 12% of the experimental results. Following on from the CEA model, the next chapter details a number of parametric studies which were performed to examine the effect of material attributes on the contact pressure distribution and squeal propensity.

Chapter 7

Parametric Studies

7.1 Introduction

In this chapter, the effort is primarily focused on the sensitivity studies of brake assembly which can lead to improvements in the stability of the system and consequently assist to reduce the squeal propensity of the brake. The effects of the material attributes for the pad backplate, friction material and the disc rotor are investigated in this chapter.

7.2 Methodology

The FE model consisted of a solid disc and two complete pads with backplate assemblies. A brake hydraulic pressure of 1.0MPa was chosen for parametric studies since the experimental results at this pressure were comparable to the FE simulation as shown in Figure 6.8. The hydraulic pressure was applied to the nodes associated with both the outboard and the inboard pistons and kept constant for various sensitivity studies. The coefficient of friction between the friction pairs of disc/pad was also kept constant ($\mu = 0.4$) throughout these studies. The material properties of the brake components are shown in Appendix I. The contact force distribution was measured along an arc at mean rubbing radius of both the outboard and the inboard friction lining. The standard deviation of normal contact force was also calculated to examine the non-uniformity of the contact pressure distribution between the friction pairs of disc/pad. In addition a further complex eigenvalue analysis was performed to evaluate the unstable mode of the system which allowed prediction of the degree of instability present in the brake assembly under various conditions.

7.3 Effect of Modulus of Elasticity of Pad Friction Material

It has been found that the effect of pad friction material is one of the major factors influencing the pressure distribution at the disc/pad interfaces. It has been established

by many researchers [17, 46, 54] that a softer more compressible friction material can reduce the squeal propensity. In this section, the effect of the pad friction material has been studied by varying the stiffness of the friction material. The stiffness was altered by changing the value of modulus of elasticity (E) of the friction material. A finite element model with different values of elastic modulus equal to 1.0, 1.5, 2.0 GPa was analysed. The brake hydraulic pressure and the coefficient of friction between the disc/pad interfaces were kept constant for all three conditions.

The graphical images of the contact pressure distribution for friction lining with different modulus of elasticity (E) are shown in Appendix M. The contact force distribution for different values of modulus of elasticity (E) was measured along an arc at mean rubbing radius of both the outboard and the inboard friction lining as shown in Figure 7.1 and Figure 7.2.

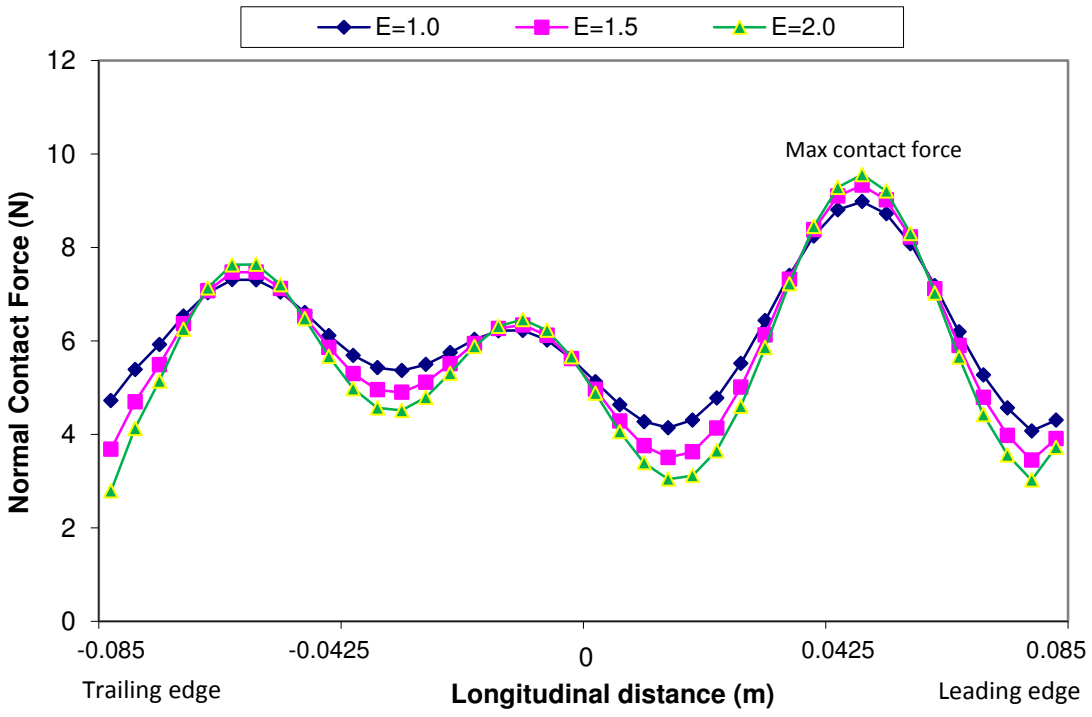

Figure 7.1 Contact force distribution along an arc at mean rubbing radius of outboard pad for various modulus of elasticity

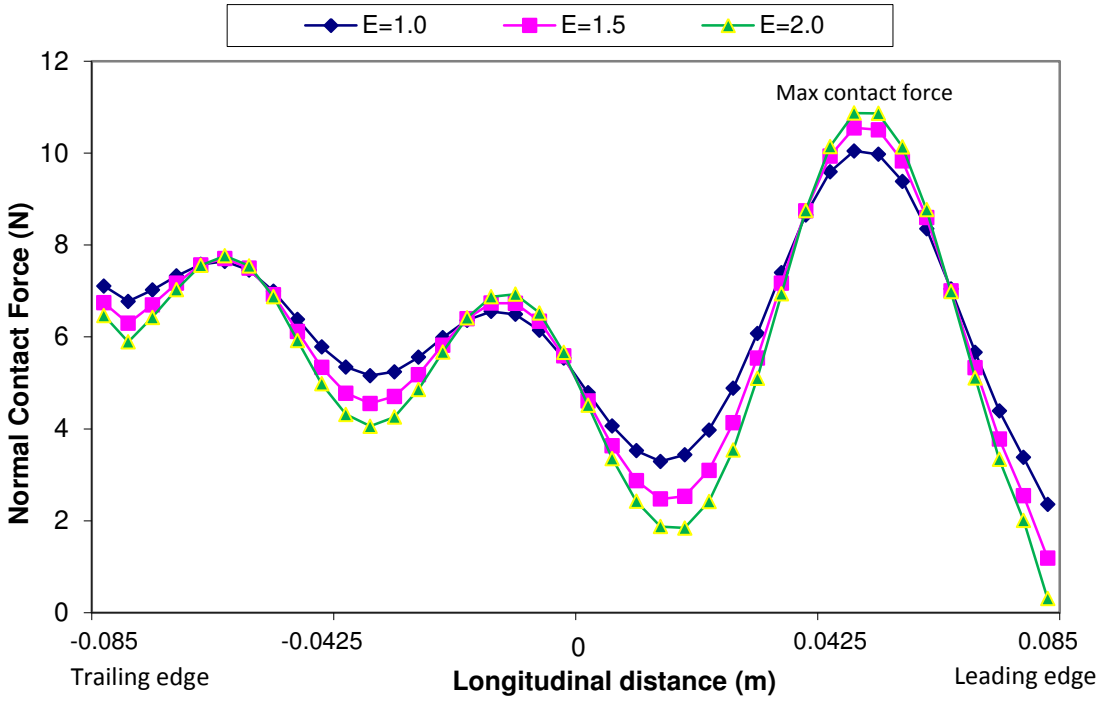

Figure 7.2 Contact force distribution along an arc at mean rubbing radius of inboard pad for various modulus of elasticity

It was found from Figure 7.1 that when the value of the modulus of elasticity of the friction material was increased from 1.5GPa to 2.0GPa, the maximum normal contact force on the outboard pad interface was increased from 9.3N to 9.6N which was an increase of about 3% whereas with a lower value of modulus of elasticity (E=1.0GPa), the maximum contact force was 8.93N which was about 4% lower than the initial model (E=1.5GPa). It was also observed from the graphical images of the contact pressure distribution (Appendix M) that FE model with the stiffer friction material (E=2.0GPa) provided less uniform (more concentrated) contact pressure distribution while the model with the softer friction material (E=1.0GPa) provided a more uniform interface pressure distribution at the disc/pad interfaces. Both the outboard and the inboard pads demonstrated similar characteristic behaviour.

The standard deviation of normal contact forces and interfacial friction forces were also plotted against various values of modulus of elasticity (E). It can be seen from Figure 7.3 that when the modulus of elasticity was E=1.5GPa, the standard deviation of normal contact force for this model was 2.40N. However once the elastic modulus

was reduced to the value of E=1.0GPa, the standard deviation of the normal contact force was also reduced to 1.99N which was about 17% lower than the initial model (E=1.5GPa). Conversely, with a higher value of elastic modulus (E=2.0GPa) the standard deviation of the normal contact force was 2.72N which was an increase of about 12%.

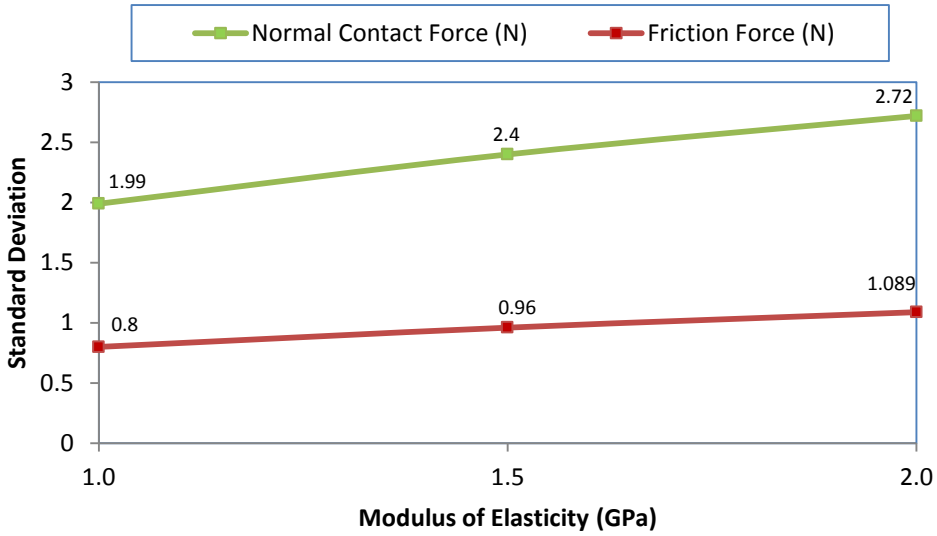

Figure 7.3 Standard deviation of normal contact forces and interfacial friction forces for friction material with different modulus of elasticity

The standard deviation of interfacial friction forces (μ x SD of normal contact forces) also demonstrated that the stiffer friction material resulted in higher localised forces at the disc/pad interfaces. The relationship between the elastic modulus of the friction material and the standard deviation of interfacial friction forces was found to be directly proportional to each other as shown in Figure 7.3.

Furthermore, the distributions of instability measurement against natural frequencies were plotted for different friction linings models as shown in Figure 7.4. It is found that for the initial model (E=1.5GPa), the standard deviation of the instability measurements was about $300s^{-1}$. However with the lower value of elastic modulus (E=1.0GPa), the magnitude of the unstable modes presented in the system was reduced and the standard deviation of the instability measurements reduced to $266s^{-1}$ which was a reduction of about 11% whilst with the higher value of modulus of elasticity (E=2.0GPa), the standard deviation increased to $320s^{-1}$ which was an

increase of almost 6%. It was yet again confirmed that the degree of instability was decreased by reducing the elastic modulus of the friction lining and that the softer more compressible friction material provided more uniform interface pressure distribution which may assist to reduce the squeal propensity. The above FE results are in good agreement with the previous work of Tirovic [17], AbuBakar [48] and Lee [55].

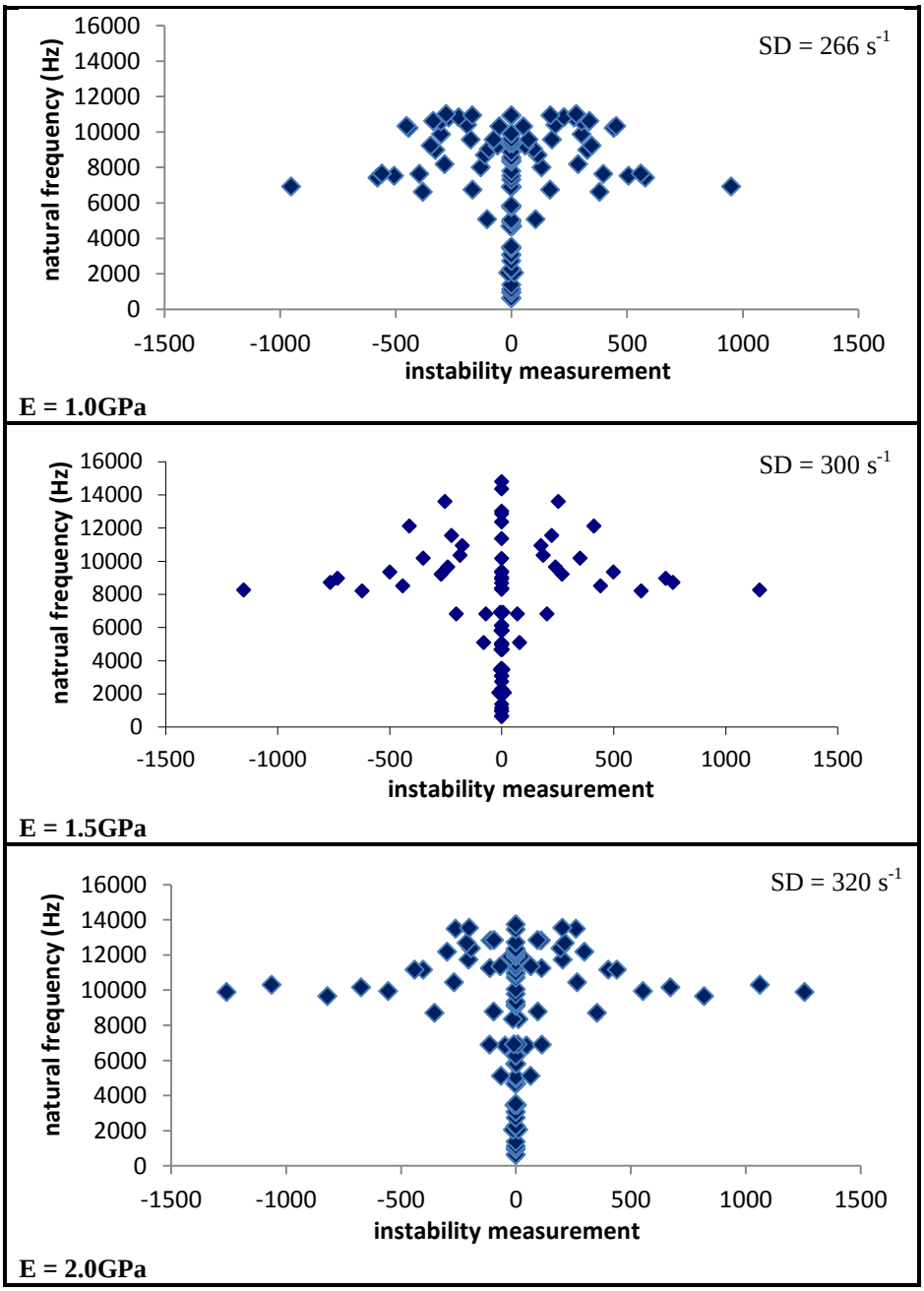

Figure 7.4 Instability measurements versus natural frequency for friction material with different modulus of elasticity

7.4 Effect of Backplate Material

An automotive pad assembly is made of a backplate and a friction lining. A stiffer backplate generally give more uniform pressure distribution between the disc/pad interfaces however recently most of the pads are made of thinner backplate (about 5mm thick) to achieve the lower mass and to reduce the cost of the pad assembly [17]. In this section, the effect of the backplate material on brake squeal noise is investigated. For the initial FE model, the pad backplate was made of mild steel with elastic modulus of 200GPa. Two further models with different backplate materials were analysed to observe their effect on the squeal propensity as shown in Table 7.1.

Table 7.1 Material properties for different backplates

Material	**Modulus of Elasticity (GPa)**	**Density (kg/m^3)**	**Poisson's Ratio**
Grey Cast Iron (CG-20)	96	7200	0.25
Steel	**200**	**7827**	**0.27**
Steel Alloy (MMC)	300	8000	0.33

The graphical images of the contact pressure distribution for various backplate materials are shown in Appendix N. The contact force distribution was measured along an arc at the mean rubbing radius of both the outboard and the inboard friction lining as shown in Figure 7.5 and Figure 7.6. It was apparent from Figure 7.5 that when the elastic modulus of the backplate was reduced from E=200GPa (steel) to E=96GPa (grey cast iron), the maximum contact force on the outboard pad interface was increased from 9.3N to 10.1N which was an increase of about 8% whereas with a higher modulus of elasticity E=300GPa (steel alloy), the maximum contact force was 8.3N which was a reduction of about 4%. It was also noted from the graphical images of the contact pressure distribution (Appendix N) that the backplate with lower elastic modulus (E=96GPa) provided less uniform (more concentrated) contact pressure distribution while the backplate with the higher modulus of elasticity (E=300GPa) provided a more uniform interface pressure distribution at the disc/pad

interfaces and this promote stability in the brake assembly. Both the outboard and the inboard pads demonstrated similar characteristic behaviour.

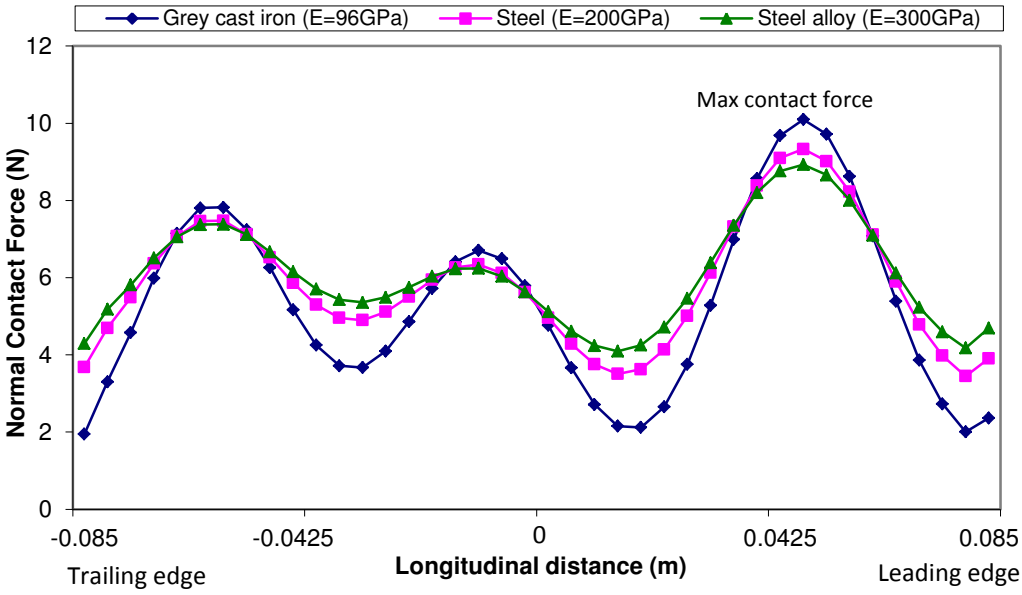

Figure 7.5 Contact force distribution along an arc at mean rubbing radius of outboard pad for various backplate materials

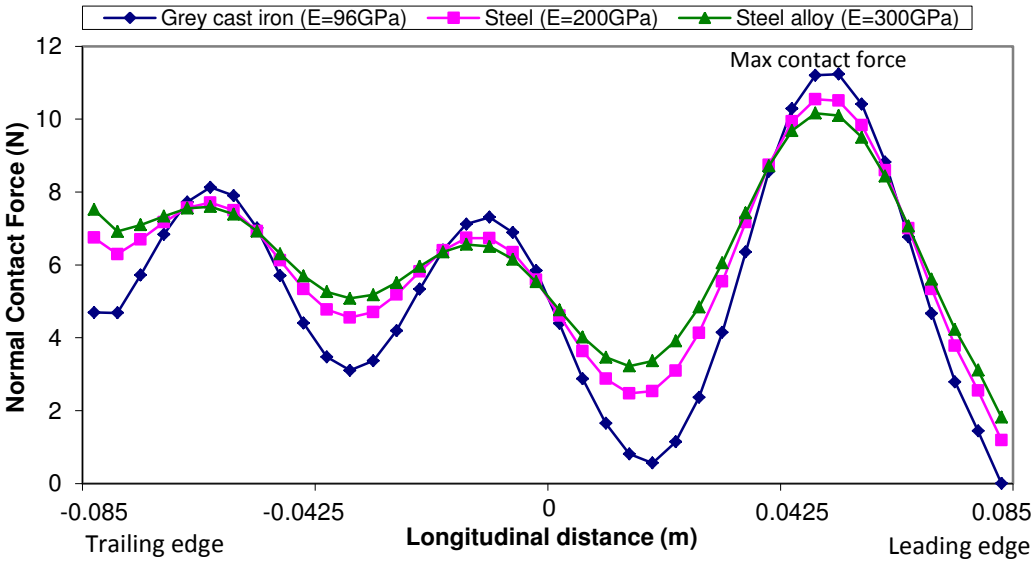

Figure 7.6 Contact force distribution along an arc at mean rubbing radius of inboard pad for various backplate materials

The standard deviation of normal contact forces and interfacial friction forces were also plotted against various backplate materials. It was apparent from Figure 7.7 that when the modulus of elasticity of the backplate was increased from the initial model

E=200GPa (steel) to E=300GPa (steel alloy), the standard deviation of the normal contact force was measured at 2.00N which was a reduction of 20%. However when the stiffness of the backplate was reduced to E=96GPa (grey cast iron), the standard deviation of the normal contact force was measured at 3.36N which was an increase of 40% from the initial condition.

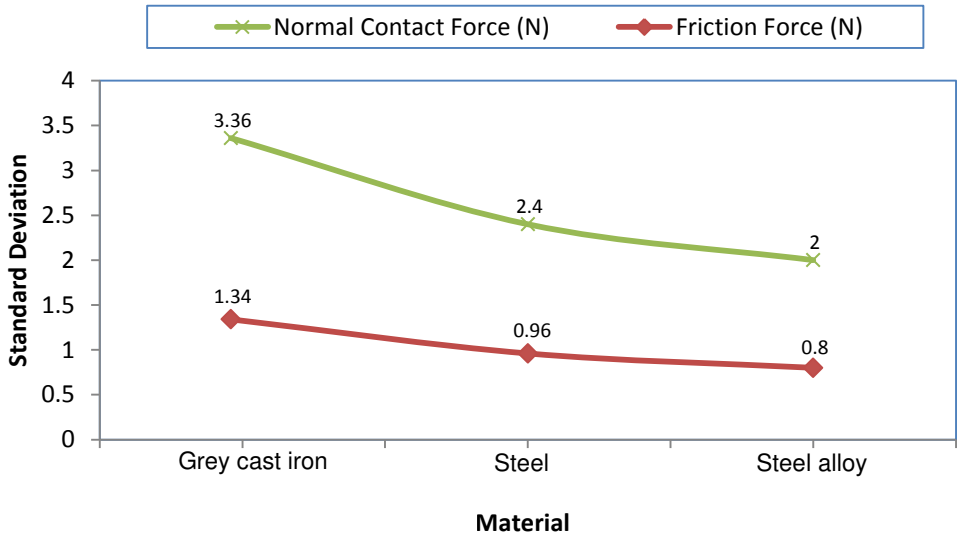

Figure 7.7 Standard deviation of normal contact forces and interfacial friction forces for various backplate materials

The standard deviation of interfacial friction forces was also investigated to observe its effect on the stability of the system. It is shown in Figure 7.7 that when the modulus of elasticity was increased from the initial model E=200GPa (steel) to E=300GPa (steel alloy), the standard deviation of friction forces was measured at 0.80N whereas with the elastic modulus of 96GPa (grey cast iron), the standard deviation was 1.34N. It was found that the standard deviation of interfacial friction force is inversely proportional to the elastic modulus of backplate.

The standard deviation of instability measurements was also calculated to quantify the squeal propensity as shown in Figure 7.8. It was found that for the initial model (E=200GPa), the standard deviation of the instability measurements was $300s^{-1}$. When the elastic modulus of the backplate was increased to E=300GPa, the standard deviation of the instability measurements was $281s^{-1}$ which was an increase of 6%. Conversely, with the value of E=96GPa, the standard deviation of the instability measurement was 343 s^{-1} which is an increase of 13%. The simulation results clearly

demonstrated that as the elastic modulus of the backplate was increased, the degree of instability in the brake assembly reduced. On the other hand, a softer more compressible backplate tended to introduce more uneven deformation causing more instability in the brake assembly and therefore more prone to squeal propensity. These findings correlated well with the previous work studied by AbuBakar [48] and Lee [55].

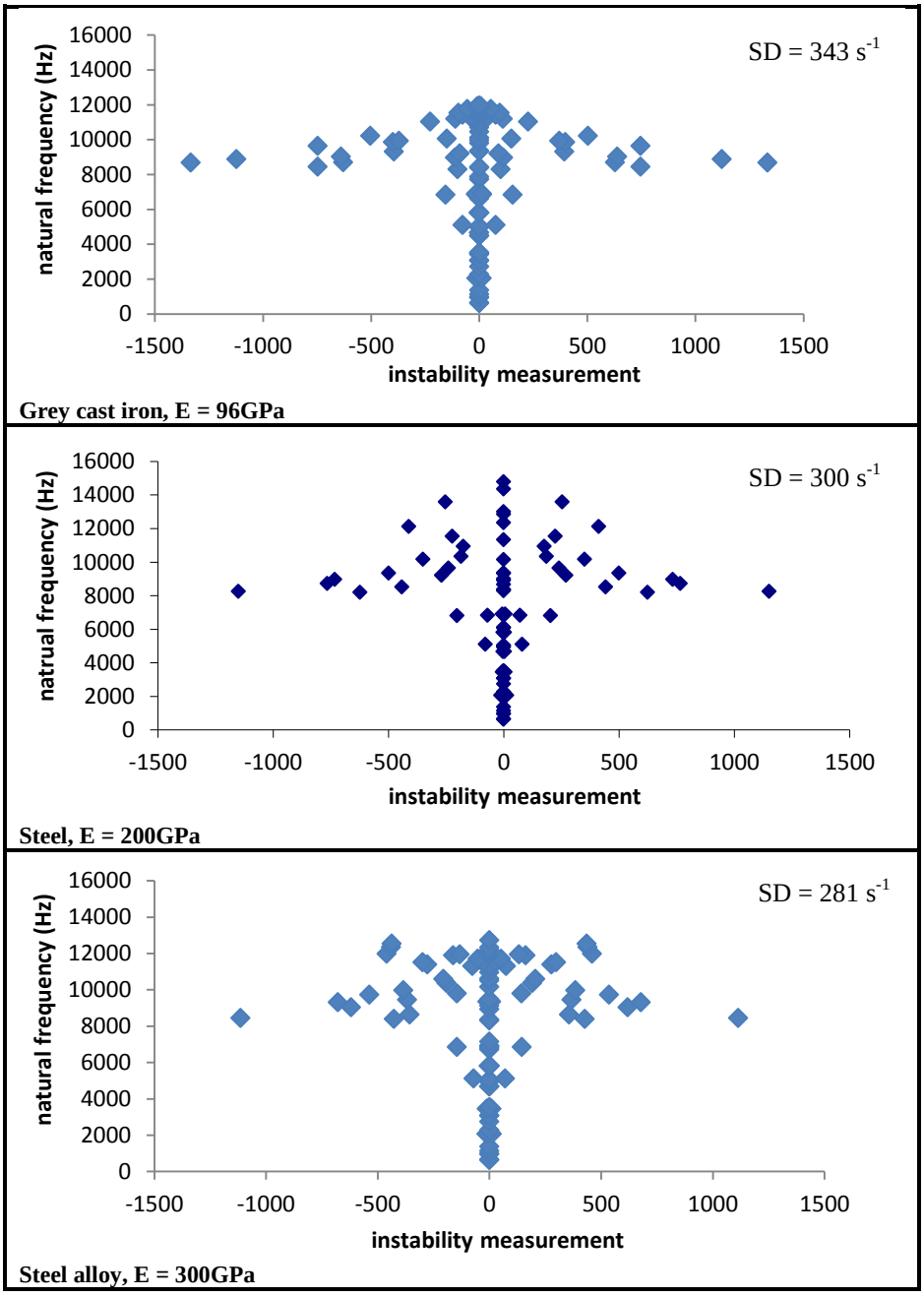

Figure 7.8 Instability measurements versus natural frequency for various backplate materials

7.5 Effect of Disc Material

The effect of the stiffness of the disc on brake squeal propensity was studied by changing the material properties of the disc. For the initial model, the disc was modelled with grey cast iron and its modulus of elasticity was 96GPa however in this study four different disc materials were considered to observe their effect on the brake instability as shown in Table 7.2.

Table 7.2 Typical properties of the disc materials analysed

Material	**Modulus of Elasticity (GPa)**	**Density (kg/m^3)**	**Poisson's Ratio**
Carbon-Ceramic (C/SiC)	29	2400	0.06
Aluminium Alloy (AMC1)	73	2794	0.33
Grey Cast Iron (GG-20)	**96**	**7200**	**0.25**
Steel	200	7827	0.27

The graphical images of the contact pressure distribution for various disc materials are shown in Appendix O. The contact force distribution for different values of modulus of elasticity were measured along an arc at the mean rubbing radius of both the outboard and the inboard friction lining as shown in Figure 7.9 and Figure 7.10.

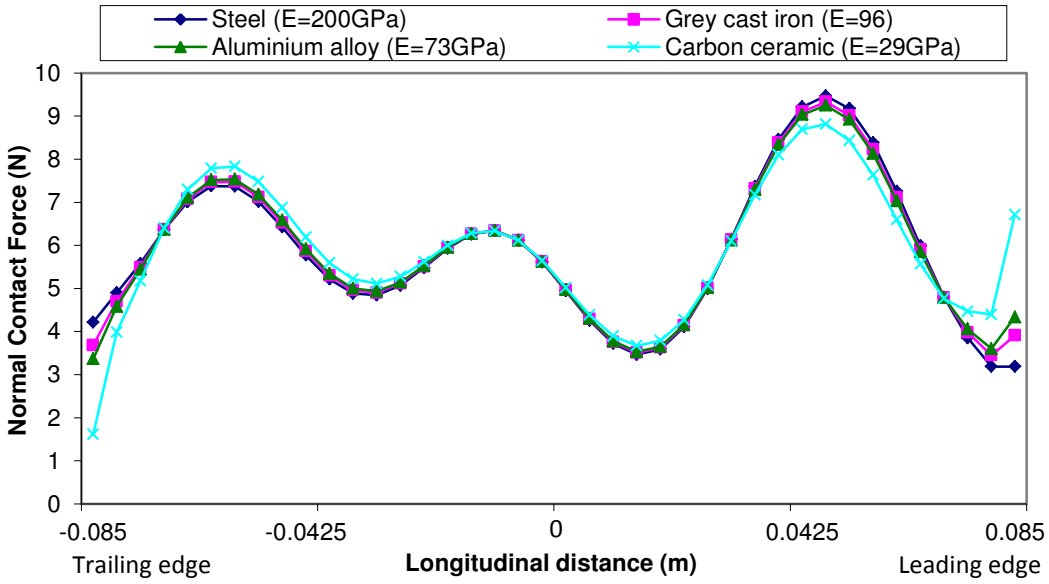

Figure 7.9 Contact force distribution along an arc at mean rubbing radius of outboard pad for various disc materials

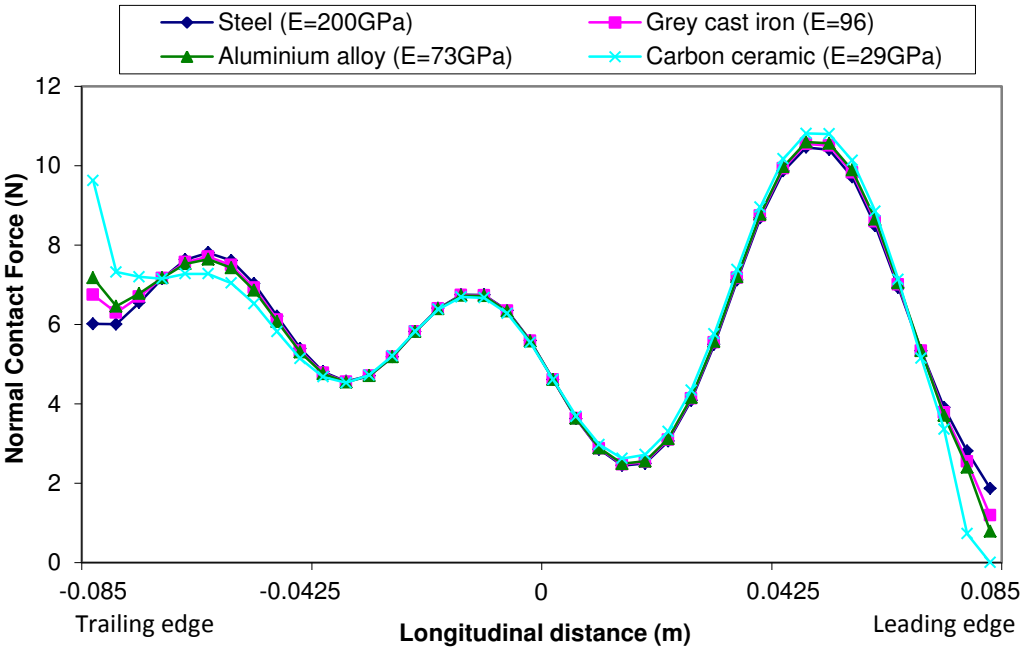

Figure 7.10 Contact force distribution along an arc at mean rubbing radius of inboard pad for various disc materials

There was no significant variation in the FE results of the contact force distribution for different disc materials as shown in Figure 7.9 and 7.10. The standard deviation of normal contact forces and interfacial friction forces were also plotted against various disc materials as shown in Figure 7.11. The standard deviation of the normal contact forces and the interfacial friction force was found to be directly related to the value of modulus of elasticity (E) of the disc however there was little variation in the overall results.

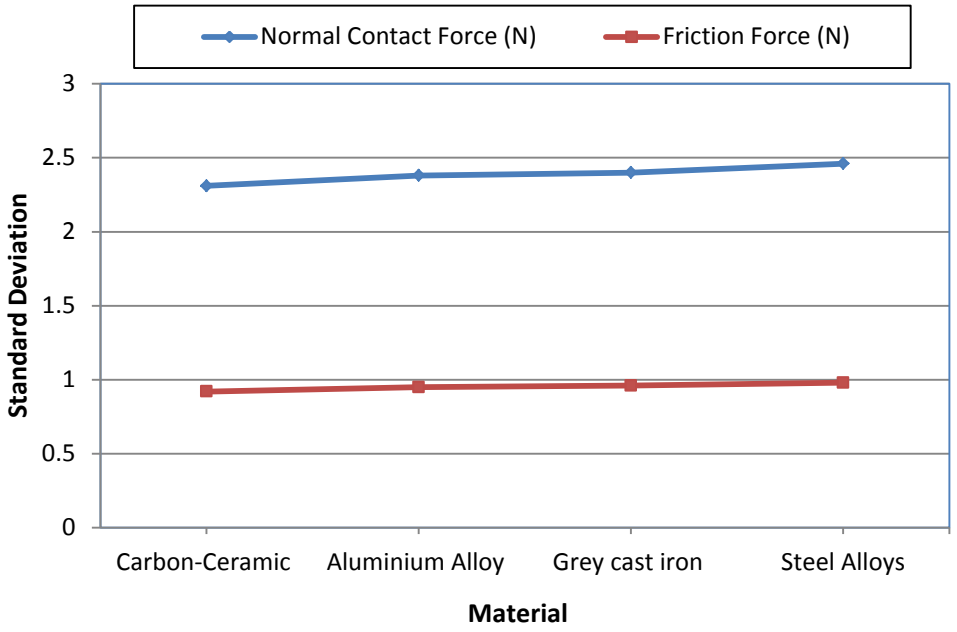

Figure 7.11 Standard deviation of normal contact forces and interfacial friction forces for various disc materials

The distribution of the instability measurement versus the natural frequencies for various disc materials was plotted. It is shown in Figure 7.12 that for the initial model (E=96GPa); the standard deviation of the instability measurements was measured at $300s^{-1}$. When the value of elastic modulus of the disc was increased to E=200GPa (steel), the magnitude of the unstable modes present in the system also increased and the standard deviation of the instability measurements was $336s^{-1}$. This was an increase of almost 11%. However, when the material of the disc was modelled as carbon ceramic (E=29GPa), the standard deviation was at $238s^{-1}$ which was a reduction of almost 21%. It was obvious from Figure 7.12 that as the stiffness of the disc (carbon ceramic) was increased the degree of instability was reduced. This was because the magnitude of unstable modes of the disc was decreased significantly by introducing a lower value of elastic modulus. These findings correlated well with the previous work studied by AbuBakar [48] and Lee [55]. However it must be noted that in practise the effect of the disc material plays an insignificant role comparing to the lining and backplate material. It is known that varying the disc material properties does not affect the squeal propensity very effectively although it may change the squeal frequency range.

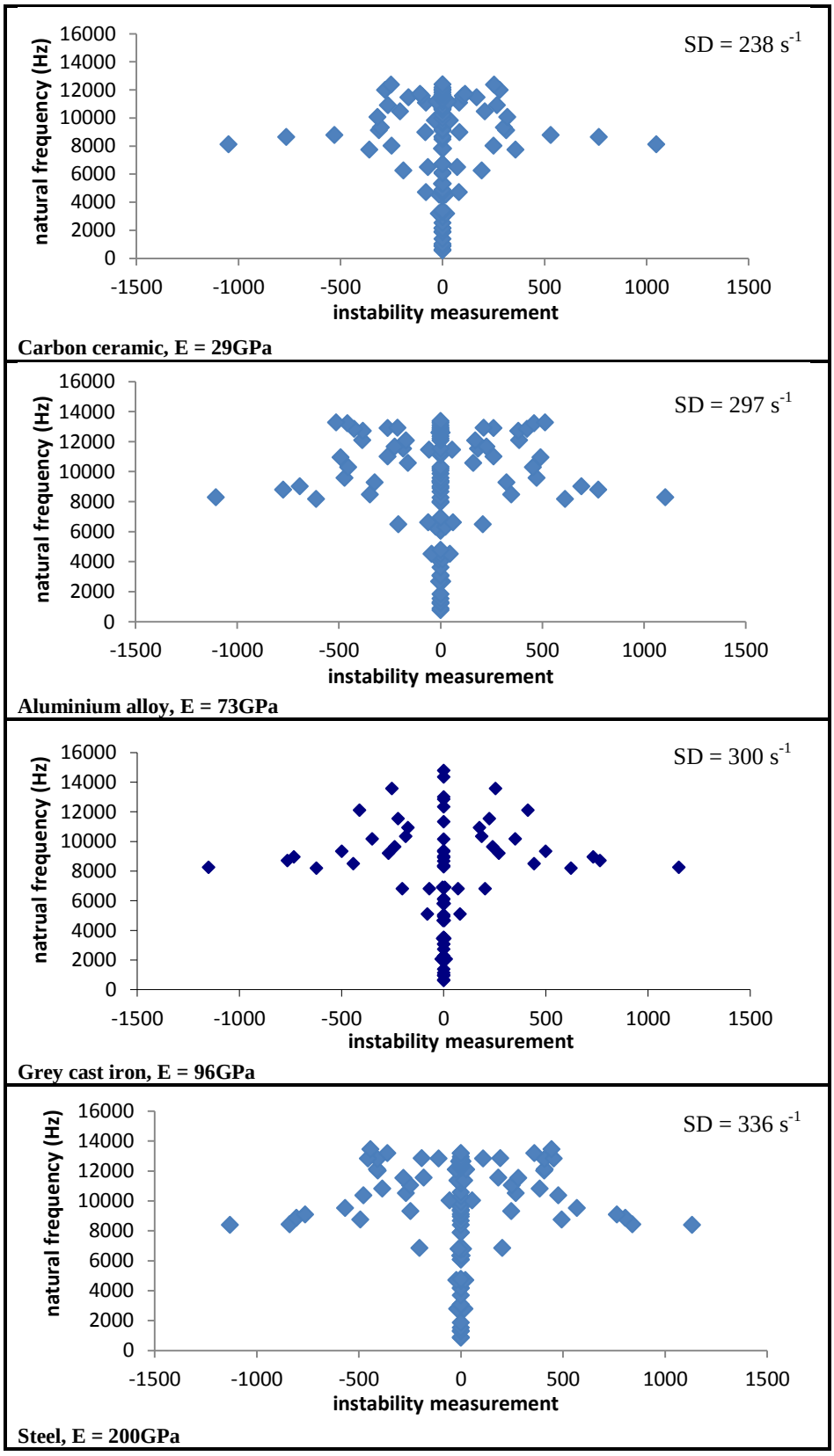

Figure 7.12 Instability measurements versus natural frequency for various disc materials.

7.6 Summary

A number of parametric studies were undertaken to investigate the effect of different material attributes on contact pressure distribution and on brake squeal. It was demonstrated that the degree of instability was sensitive to these variations. It was apparent from the FE results that a lower value of elastic modulus (E) of friction lining increased the uniformity of the contact pressure distribution and therefore improved the degree of stability in a brake assembly. On the other hand, a higher value of elastic modulus (E) of the backplate tended to increase the uniformity of the contact pressure distribution and consequently reduced the degree of instability.

Chapter 8

Conclusions and Recommendations for Future Work

8.1 Summary of the Work Done

In this section, a summary of the work performed during the course of this thesis is outlined. The main conclusions and contributions to the brake industry will be described in the next section. The overall objective of this project, as stated in the introduction, was to gain insight into the influence of the friction pair contact pressure distribution on disc brake squeal which would provide the basic understanding of the contributing mechanisms which cause the brake instability. It is a well-known phenomenon within the brake industry that movement of the CoP is a very important factor to control the noise in disc brakes, and that the brake system becomes unstable when the CoP is towards the leading side of the pads. A number of researchers [18, 20, 43, 46] have conducted a detailed study on this subject but still there is a knowledge gap that the present work contributes towards. The preliminary work carried out by Bosch Braking Systems [20] indicated that the centre of pressure did move noticeably during the application of the brake but the work was unable to consider how it moved during a brake application. This thesis examined the analysis and measurement of the dynamic centre of pressure of a brake pad during a normal braking event. A novel method was employed using laminated film in conjunction with an opposed 12 piston caliper to predict the dynamic contact pressure distribution between disc/pad interfaces. The technique was unique in its design and implementation. The process was progressive whereby the interface static measurements were first taken and then dynamic testing was performed during braking events.

The overall objective has been successfully accomplished by carrying out a number of actions which are summarised below.

In Chapter 1 and Chapter 2, the problem of disc brake squeal was introduced and a comprehensive literature review of previous work was discussed. In Chapter 3, the design and development of the test rig was presented. A unique method was employed to predict the dynamic contact pressure distribution between disc/pad interfaces. The caliper and set of pads were modified to allow the measurement of the movement of the CoP during braking events. Chapter 4 focused on the measurements of CoP during braking events. A number of tests were carried out at varying speeds and with varying (but uniform) pressures along the length of the pad. In all cases the centre of the pad was the reference (zero) position with positive being measured towards to outer edge of the pad/disc and negative radially inwards. The second part of the experimental investigations was aimed at obtaining the contact pressure distribution of disc/pad interfaces at various variable pressures during squeal events. Two different set of tests were carried out with the pressure varied along the length of the pad and radially respectively. The piston pressures were adjusted to different actuating settings to observe the effect on the squeal characteristics. The movement of the centre of pressure for both outboard and inboard pads was plotted at different stages. In Chapter 5 and Chapter 6, a detailed finite element model of a disc brake assembly was developed. A modal analysis at component level was performed and then compared with the real brake components. The work continued by conducting a contact analysis between the brake pads and disc and the FE results were compared with the experimental results. Once the FE contact analysis was successfully validated with the experimental results, a modal analysis of the brake assembly was carried out to predict the natural frequencies and the mode shapes of the disc brake. The effects of varying both friction coefficient and the brake hydraulic pressure on disc brake squeal were also examined to confirm a number of studies discussed throughout this thesis. A complex eigenvalue analysis was also performed successfully to ascertain the instability measurement, natural frequency and the modes of vibration up to 8 kHz. Chapter 7 considered a number of parametric studies of the disc brake as a possible way of eliminating/reducing squeal vibration. Structural modifications such as the effect of disc material, friction material and stiffness of the backplate were investigated to understand the characteristics of the disc brake system in terms of squeal noise performance.

8.2 Main Conclusions and Contributions to Knowledge

The main conclusions drawn from the current research and the contributions to the brake industry are described below.

It has been demonstrated that disc rotational speed has limited effect on the CoP and that contact pressure distribution remained unchanged with various rotational speeds. The degree of offset does not appear to be influenced significantly by the speed of disc rotation. The experimental results also clearly showed that with low brake hydraulic pressures (but uniform pressure at each piston) there was a leading offset at the disc/pad interface, hence, an increased propensity to generate noise; but as the pressure was increased the centre of pressure moved towards the centre of the pad, leading to stability. It was observed that under light braking, with uniform pressure at each piston, the centre of pressure (CoP) will always tend to be leading. Whether this will actually result in noise depends on the various factors such as coefficient of friction, pad wear and caliper mounting geometry. The experimental results also showed that a trailing centre of pressure will tend towards a stable, quiet brake. This is substantiated by general observation, when the brake pressure is increased during normal braking, noise reduces. To ensure a leading centre of pressure is not established on an existing brake it may be necessary to introduce a stepped shim at the piston/pad interface. The experimental results compared well with the theoretical approach explained by Fieldhouse [18, 20] and showed that when a leading centre of pressure was introduced at the disc/pad interface then squeal propensity increased.

It was shown for the first time in this research that noise would be more likely if the CoP moves radially inwards towards the centre of the pad. The ideal position for the centre of pressure of the pad is longitudinally central to trailing and radially outwards from the pad centre.

It was also established that when the centre of pressure (CoP) was close to the centre of the pad, or trailing, then the brake was quiet. In order to reduce the intensity of

noise within the brake corner assembly, the position of the centre of pressure must be towards the trailing edge of the pad. The FE results also verified that the magnitude of interfacial contact force was much higher towards the leading side of the pads. It was obvious from the FE results that the magnitude of interfacial contact force increased with the higher caliper pressures settings. The overall FE results correlated well with the experimental results.

It was observed from the experimental results that the centre of pressure of the outboard pad moved more vigorously than the inboard pad. This was due to the caliper construction with the inboard pad being closer to the mounting plane so more robust and able to apply a more uniform load. It was established that the inboard pad had a general overall equal distribution of load whereas the outboard pad showed high concentrations of loading. Variations of loading within these high concentrations had a greater effect on the CoP position and as a result generated a more vigorous movement of the CoP. Conversely, the inboard pad, with its more uniform loading, was less susceptible to such concentrated pressure changes. This was also related to the spragging effect which cannot be established with the outboard pad as the resulting load acts away from the caliper mounting plane. The mounting plane of the caliper bracket relative to the disc surface is important as this forms the spragging angle along with the position of the CoP. Theoretically it should be very close to the disc surface to minimise the potential sprag angle as shown by Fieldhouse [18].

It was apparent from the experimental results that the inboard pad appeared to carry significantly more load than the outboard pad. Such a situation can lead to possible thermal issues and cross disc thickness temperature gradients. This observation will be the subject of further investigation.

It was found that complex eigenvalue results compared well with the experimental results. The measured unstable frequencies were within the range of 12% of the experimental results.

As a final conclusion, the FE simulations conducted in the current research have shown that the friction coefficient, brake hydraulic pressure and friction material can all influence the squeal characteristics. It has been established that to promote stability a disc brake requires a low friction coefficient between the disc/pad interfaces. This can be justified by referring back to equation (4.9) in Chapter 4. It was shown that $b = a(1 \pm \mu\mu_2)+\mu t$ and the oscillation will increases if μ is high and conversely the initial leading offset μt is reduced if μ is low.

8.3 Future Work

It is recommended to machine the caliper so that all the pistons in the caliper can be controlled independently to each other. This would provide extensive functionality to the test rig and therefore would provide an increased database of results.

The work carried out during the course of this project has provided an increased understanding of the mechanism for instability generation. However, the FE simulations were performed using a solid disc which has some noticeable geometry differences to the actual brake assembly, which used a vented disc. Thus, it would provide valuable information towards quantifying the error by applying the modelling technique described in the thesis to actual brake components.

In the present work, the finite element model considered a smooth and flat surface for the friction material whereas in reality the pad surface is irregular and rough. It is therefore recommended to model the brake pad from information extracted from real surface of pads.

It was found that FEM contact area was insensitive to change in hydraulic pressure however in practical situation the contact area does vary with different hydraulic pressures and therefore does influence the squeal propensity. It is therefore recommended to undertake further FE analyses to understand the main reason for this.

The modal analysis performed in this research is based on the assumption that the effect of the disc damping is negligible. It is therefore recommended to consider the damping in the FE model to perceive its effect on system instability.

8.4 Final Remarks

The overall objective of this project was to gain a greater insight into the influence of the friction pair contact pressure distribution on disc brake squeal, and that this would provide additional understanding of the contributing mechanisms which cause the brake instability. This has been achieved by using both experimental tests and FE models. Due to the time, financial constraints and computational power constraints, a number of simplifications have been made to both experimental equipment and the finite element model. However, the research presented in this thesis has still demonstrated a significant contribution towards a better understanding of brake squeal and, thus, the goal of ensuring quiet brakes.

APPENDIX A CASE STUDY 1

A.1 - Method of Measuring Dynamic Pressure

Measurement of the dynamic centre of pressure during braking is difficult. The unique technique was to use an embedded pressure sensitive film within the pad. To allow this the film was first bonded to a smooth pressure plate as shown in Figure A.1.

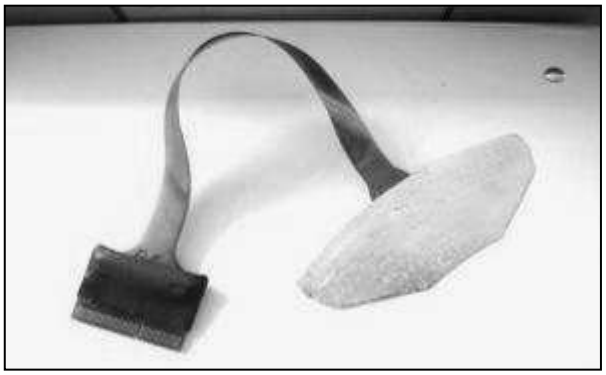

Figure A.1 Pressure sensitive film bonded to metal support plate

A pad was prepared to receive the laminate by machining a recess and "plug" as shown in Figure A.2. The film laminate was then fitted to the recess and the "plug" used to form a sandwich of the film laminate as shown in Figure A.3. The pad was machined to give a level rubbing surface and the assembly used to measure the dynamic centre of pressure on a test rig.

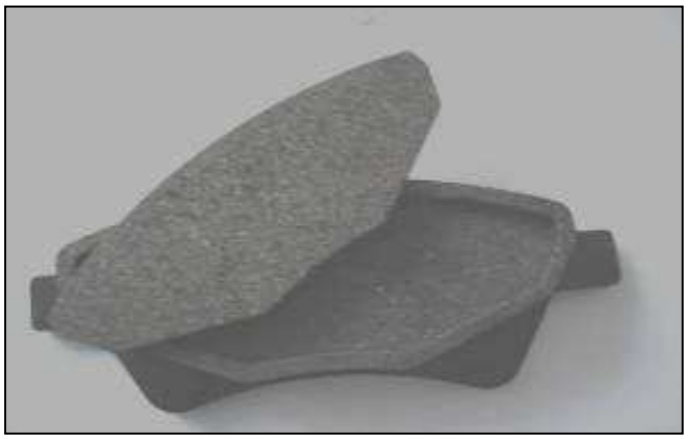

Figure A.2 Recessed pad and associated "plug"

Figure A.3 Pad assembly with film laminate sandwiched within pad

A.2 Analysis

In a practical situation there will be an interaction between frictional effects (forces) at the pad abutment/caliper interface with the geometric features of the brake pad when it is in equilibrium. A measure of the relationships involved for the different types of abutment may be established and compared if it is assumed that the various forces acting on the pad are coplanar as shown in the brake caliper in Figure A.4 and the free-body diagrams of the abutment arrangement in Figure A.5.

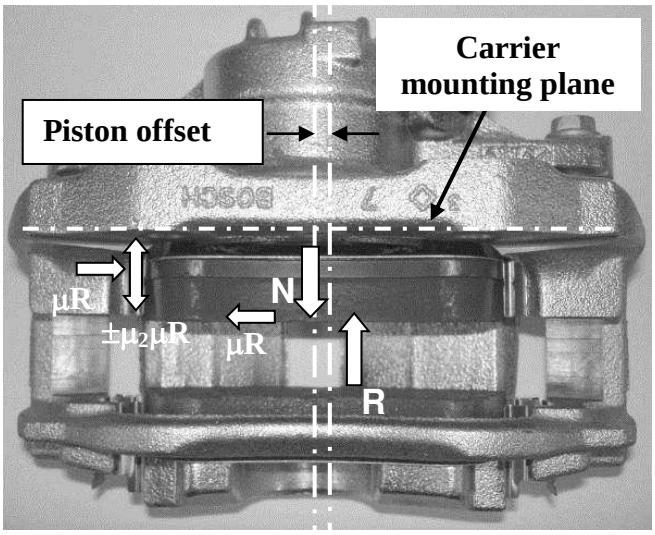

Figure A.4 Co-planar forces added to piston pad [20]

The force at the abutment face must equal the frictional force (μR) if the horizontal reaction at the piston/backplate interface is neglected. It should be noted that the position of reaction "R" (centre of pressure) to provide equilibrium depends on direction and magnitude of abutment force which in turn is dependant of friction level of friction material (μ) and friction level at abutment interface (μ_2).

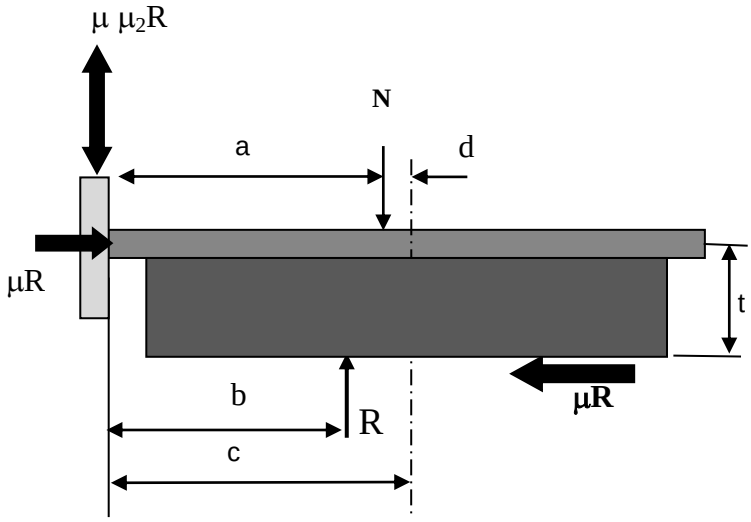

Figure A.5 Free body diagram of trailing abutment [20]

If the pad end tends to move in a vertical plane it will have a resistive force equal to the friction force and friction coefficient between pad and carrier finger (μ_2). This vertical force ($\mu\ \mu_2$ R) will change direction as the pad end reverses direction.

In this case the system is not balanced and hence "N" is not equal to "R" and the relationship between the two may be determined by resolving forces vertically to give:

$$R = N \pm \mu \mu_2 R \qquad (A.1)$$

or

$$\frac{N}{R} = (1 \pm \mu \mu_2) \qquad (A.2)$$

Furthermore by taking moments about the abutment, equilibrium will be attained if:

$$\mu Rt + Na = Rb \qquad (A.3)$$

that is

$$\frac{N}{R} = \frac{(b - \mu t)}{a} \qquad (A.4)$$

or

$$b = a\frac{N}{R} + \mu t \qquad (A.5)$$

giving

$$b = a(1 \pm \mu\mu_2) + \mu t \qquad (A.6)$$

as $\mu_2 \Rightarrow 0$ then $b \Rightarrow a + \mu t$ giving a maximum leading offset, $\delta_{max} = \mu t$ where 5mm is piston offset

Given $\mu = 0.45$, a = 63.49mm, t = 18.15mm, h = 23.18mm
then the above equation (A.6) becomes

$$b = 71.66 \pm 28.57\mu_2 \qquad (A.7)$$

Consider the condition when "b" is a maximum, i.e. a leading centre of pressure.

$$b = 71.66 + 28.57\mu_2 \qquad (A.8)$$

From given pad friction coefficient and known h = 23.18mm

Sprag angle = Tan $\theta = \mu = \delta / 23.18 = 0.45$ (given)

To sprag this gives leading offset, δ = 10.43 mm

$$\delta = b - a - d \qquad (A.9)$$

where piston offset, d = 5mm

$$\delta = 71.66 + 28.57\mu_2 - 63.49 - 5 \qquad (A.10)$$

$$\delta = 3.17 + 28.57\mu_2 \qquad (A.11)$$

if δ = 10.43mm

then $\mu_2 = 0.254$ maximum

This is a realistic value for the pad/abutment finger interface friction coefficient.

A stability envelope may be plotted for the varying characteristics as shown in Figure A.6. This indicates a low μ_2 would tend towards a more stable system.

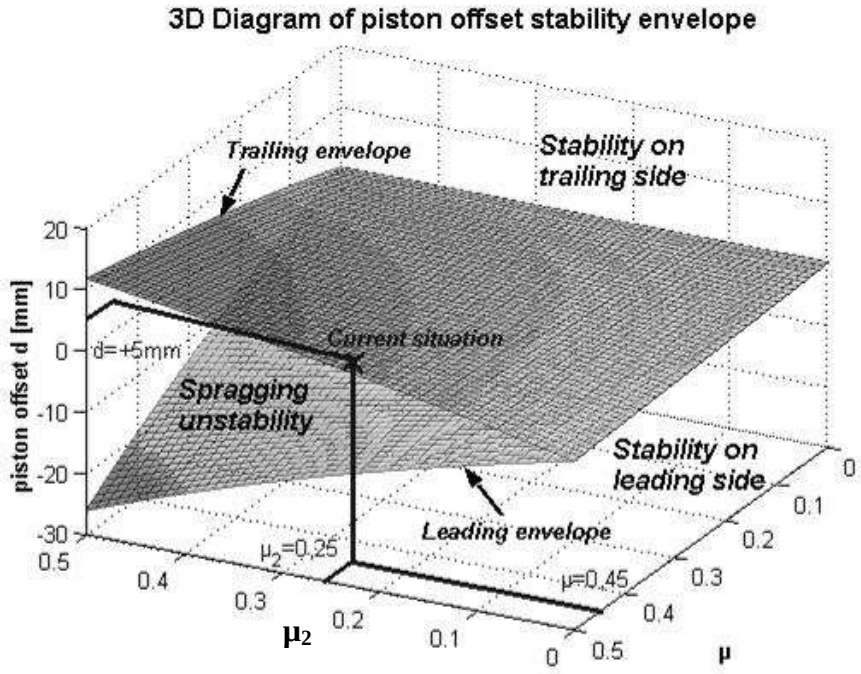

Figure A.6 Plotted stability envelope for varying parameters, μ, μ_2 & piston offset [20]

If this situation of a moving centre of pressure is accepted then it may be related back to caliper mounting as follows. This may be extended by considering the effect of the reversing force at the pad abutment as indicated in Figures A.7 (a-c) showing the carrier/caliper mounting. The disc is moving left to right and the forces are indicated.

In Figure A.7a, the centre of pressure is leading and as such the resultant force causes the mounting to rotate clockwise. If the centre of pressure is less leading then the resulting force causes the mounting to rotate counter-clockwise as indicated in Figure A.7b. Clearly if the centre of pressure "hunts" between these two extremes it will pass a point where the resultant will cause the mounting to physically move axially (vertical in diagram) against the mounting points, as shown in Figure A.7c spragging at its worst. In this case the normal force at the disc/pad interface will increase because of the increased stiffness of the mounting and as such the disc will

experience a variable and periodical out-of-plane excitation force. It is suggested this could be the source of noise generation.

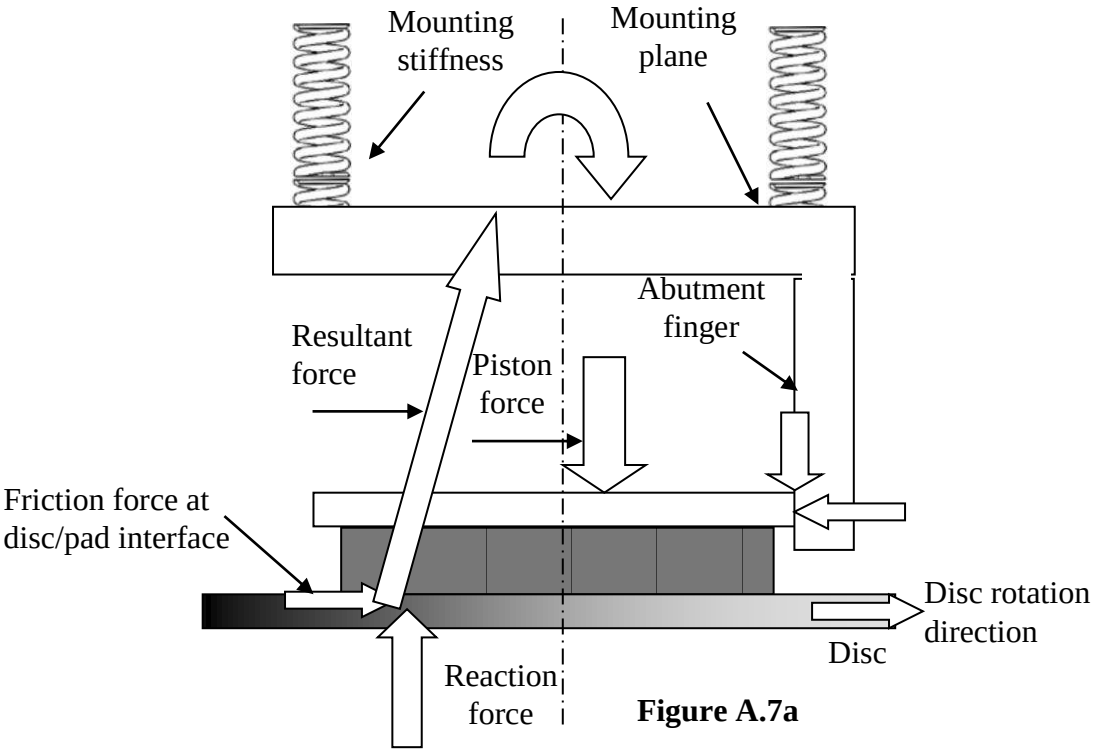

Figure A.7a

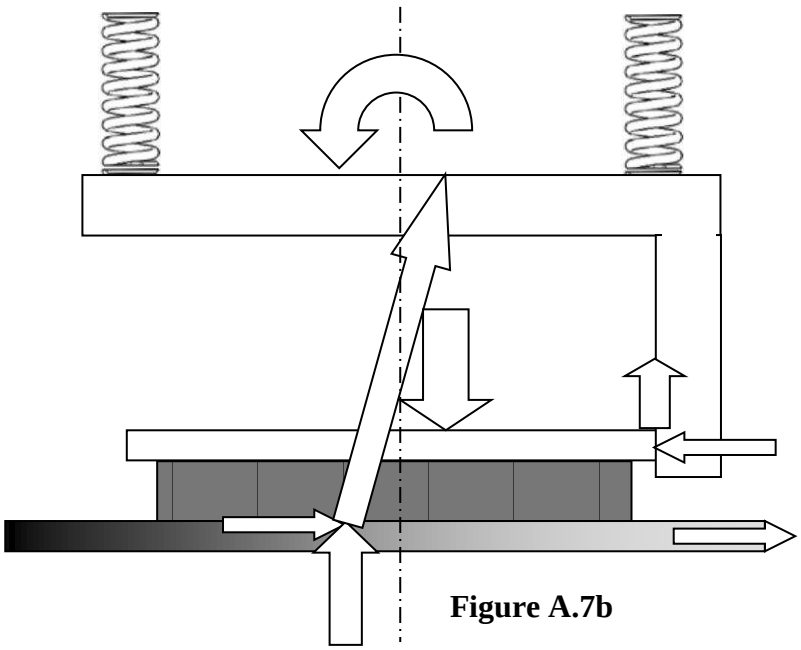

Figure A.7b

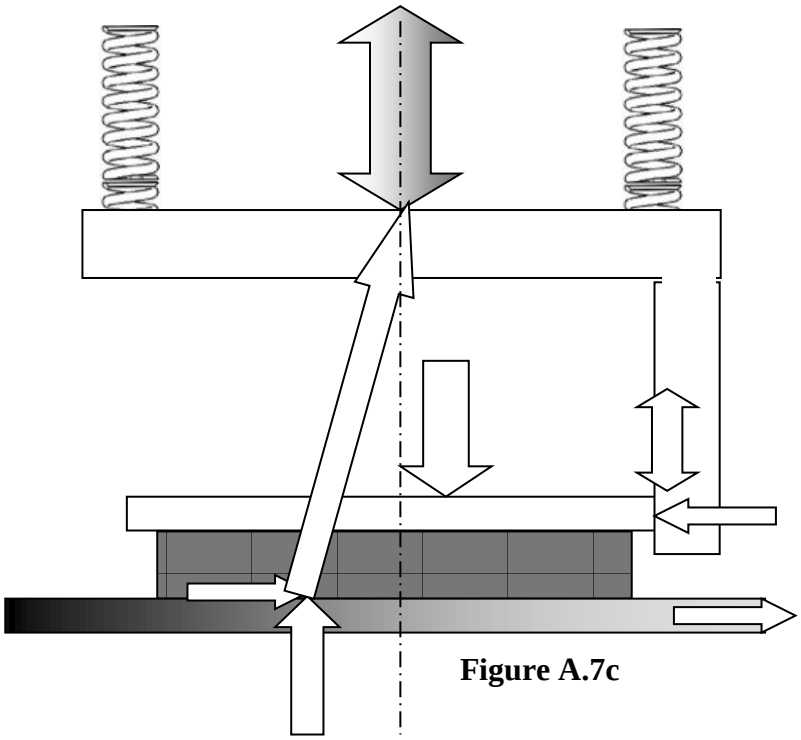

Figure A.7c

Figure A.7 Diagram of pad and carrier/caliper mounting plane with varying abutments force directions influencing position of resultant force

A.3 Measured Results

The results are dynamic and as a consequence the centre of pressure moves constantly as the pad wears and as the pressure varies. Figure A.8 shows an instantaneous shot of the results from a dynamic recording where the path of the centre of pressure (CoP) may be seen as a white trace. Figure A.9 shows plots of centre of pressure during braking under various braking pressures. It can be seen clearly from Figure A.9 that the maximum and minimum centres of pressure (CoP) vary most at low pressures but tend to be less erratic as pressure increases. It is important to note that the tangential offset is generally leading, around 11 mm maximum leading, even though the piston arrangement is such as to provide a 5 mm trailing offset. It is noticed that as the brake line pressure increases, the tangential offset envelop decreases. The calculations also indicated spragging would occur with a 10.43mm leading offset. Figure A.10 again illustrates the visulisation of centre of pressure movement on the actual pad surface. It is apparent from Figure A.10 &

Figure A.11 that the movement of CoP inclines more towards the leading side of the pad and the dynamic behavior of CoP is more erratic at low pressure.

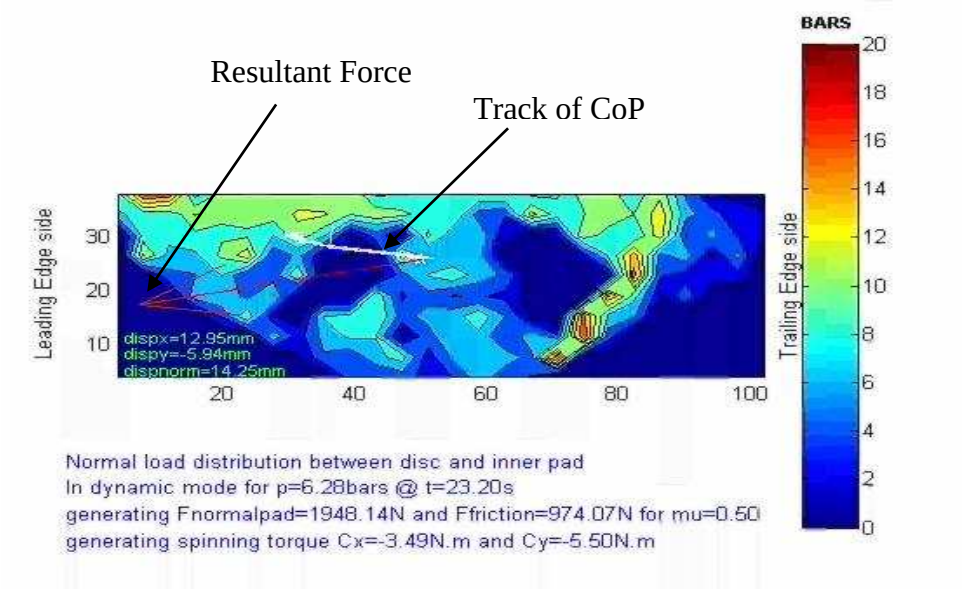

Figure A.9 Typical pressure distribution during braking

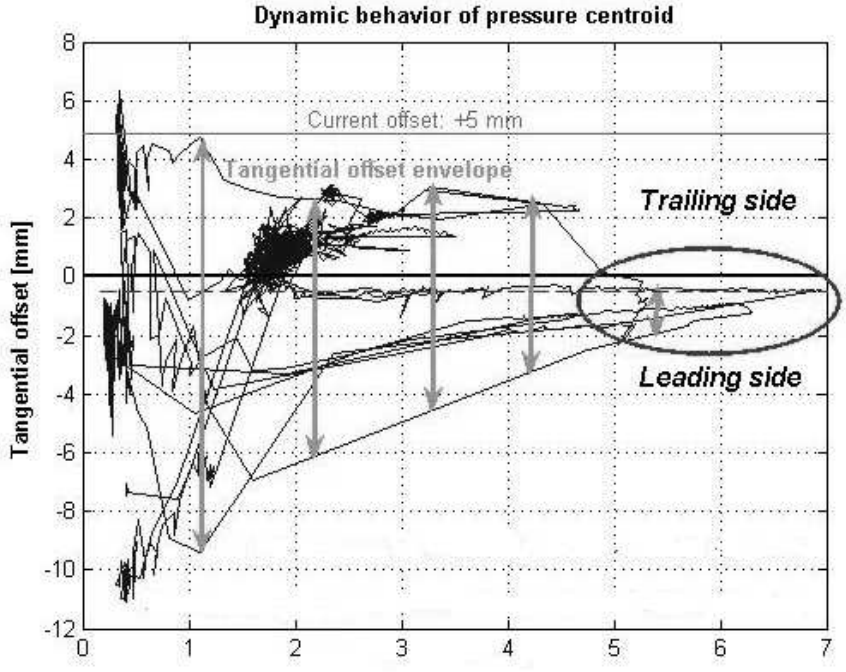

Figure A.10 Plots of centre of pressure during braking under variable braking pressures [20]

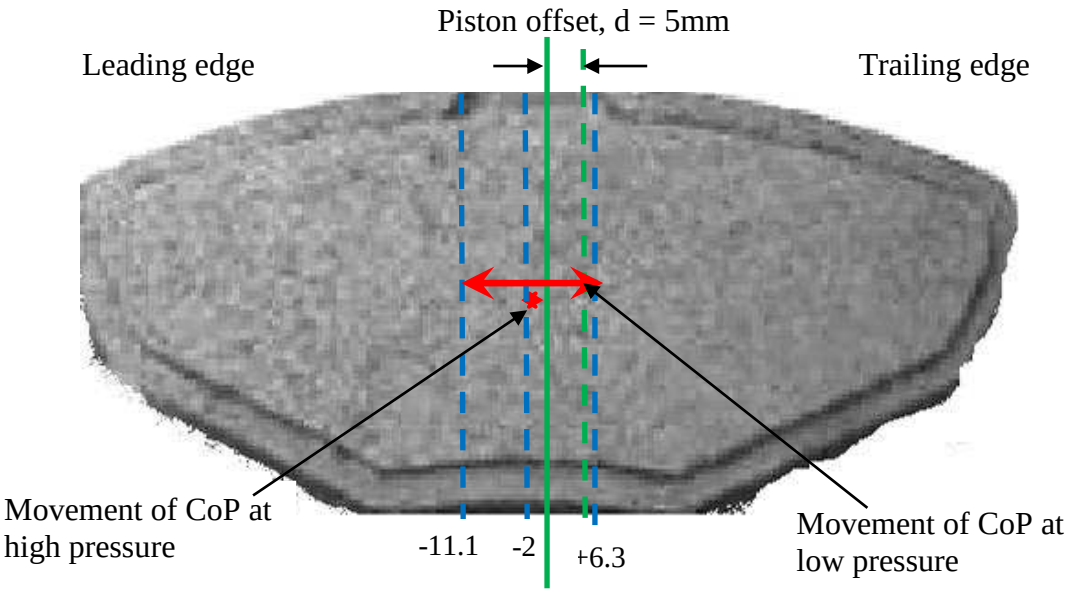

Figure A.11 Visualisation of tangential offset on the actual pad surface

A.4 Discussion of Preliminary Results

Figure A.10 shows the trace (or movement) of the centre-of-pressure as brake pressure is varied. The vertical axis represents the offset with, in this case, the piston offset trailing by +5mm. Even with this trailing (positive) piston offset it can be seen that the centre of pressure tends to be leading the piston and the majority leading the centre of the pad. In addition it must be noted that low brake pressure levels leads to greater leading centre of pressure and greater instability. The pressure is hardly ever transmitted on the trailing side of piston centre. This is generally what is experienced on a vehicle, noise most prevalent as brake pressure is reduced. During pressure application, the centre of pressure moves between -11.1 mm and +6.3 mm as shown in Figure A.10 and Figure A.11. This benchmark may be used to plot an instability diagram as shown in Figure A.12 with an assumed μ_2 = 0.3 and known pad friction level of 0.45. Additional envelopes for pad friction 0.35 and 0.45 are included to indicate sensitivity to friction level changes. It generally stays in the "spragging instability" area and as a consequence the brake generates noise. The spragging instability area for (μ ; μ_2) = (0.45 ; 0.3) gives δ between -13.3 mm and +6.2 mm.

Measured tangential pressure centroid seems to let the system stay in the spragging instability region (based on static model).

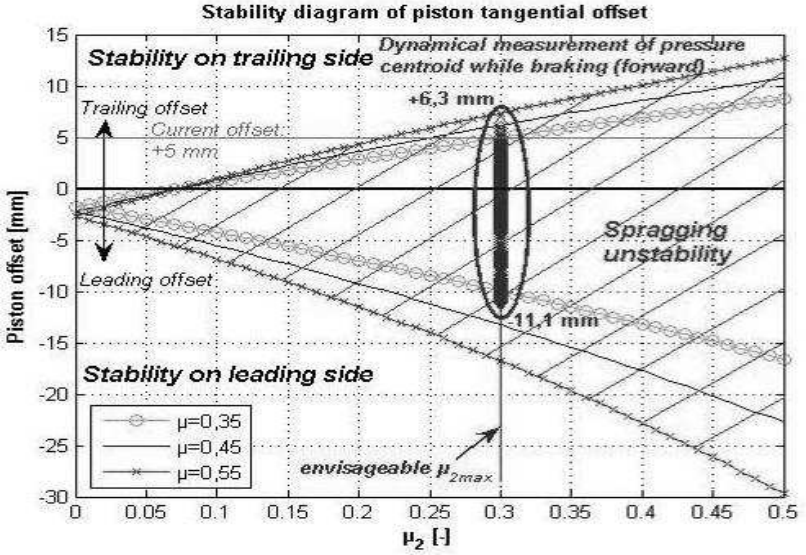

Figure A.12 Instability diagram indicating variation in envelope for different pad abutment friction levels (μ_2) [20]

Appendix B

Description of Piezoelectric beams

Piezoelectric sensors are used to measure vibration/displacements and have the ability to vibrate or deform when a sinusoidal signal is applied to them due to the piezoelectric effect, this can have benefits in the micro-actuator field. However, piezoelectric materials also have the benefit that when the materials are sheared they give off a small voltage which is proportional to the applied shear stress. Therefore if a piezoelectric beam is rigidly attached to a vibrating object it will provide a voltage signal which is proportional to the shear stress and at the same frequency of oscillation. Piezoelectric materials generate an electric potential when mechanically strained, and conversely an electric potential can cause physical deformation of the material. The principle of operation is that when an asymmetrical crystal lattice is distorted, a charge reorientation takes place, causing a relative displacement of negative and positive charges. The displaced internal charges induce surface charges of opposite polarity on opposite sides of the crystal. Surface charge can be determined by measuring the difference in voltage between electrodes attached to the surfaces. Using this principle it is possible to record the vibration of different components of the braking system simultaneously. The piezoelectric beams had a size of 25x6.35x0.5mm; this small size allowed their positioning on the brake components. This has benefits when compared to non-contacting measurement systems such as holographic interferometry or electronic speckle pattern interferometry which must have a clear view of the component in order to be able to measure the vibration and/or displacement. The piezoelectric beams were mounted at the relevant points on the brake components using epoxy resin, making sure that there was good contact between the beam and the pads to provide an adequate response. The resonant frequency of the beams was in the region of 56 kHz which was much higher than the measurement frequency (32 kHz) and therefore did not have any influence on the actual measurements. There are various modes of operation of piezoelectric sensors, depending on the material and the crystallographic orientation of the plate. These modes include the thickness or longitudinal compression, transversal compression, thickness-shear action, and face-shear action.

Appendix C

Case Study 2 – Summary of Analysis of Abutment Effects

Table C.1 Summary of analysis of abutment affects giving details of minimum value of μ_2 to avoid offset pressure compensation, δ, to achieve equilibrium and also maximum offset as the pad/calliper finger interface coefficient of friction, μ_2, tends to zero [18].

Abutment	**Min μ_2**	**Offset δ**	**Max Offset**
Combined	0.214	$\delta = \mu[t - (a + b)\mu_2 / 2]$	μt leading
Trailing	0.200	$\delta = \mu(t - a\mu_2)$	μt leading
Leading	0.231	$\delta = \mu(b\mu_2 - t)$	μt leading

Appendix D Case Study 3

D.1 Analysis Demonstrating Relationship Between Sprang Angle and Centre of Pressure

Analysis of the variable offset and the sprag angle (friction angle), shows that the offset coincides approximately with the line of resultant force between the induced centre of pressure and the intersection between the piston centreline at the carrier mounting plane as indicated in Figures D.1 and D.2.

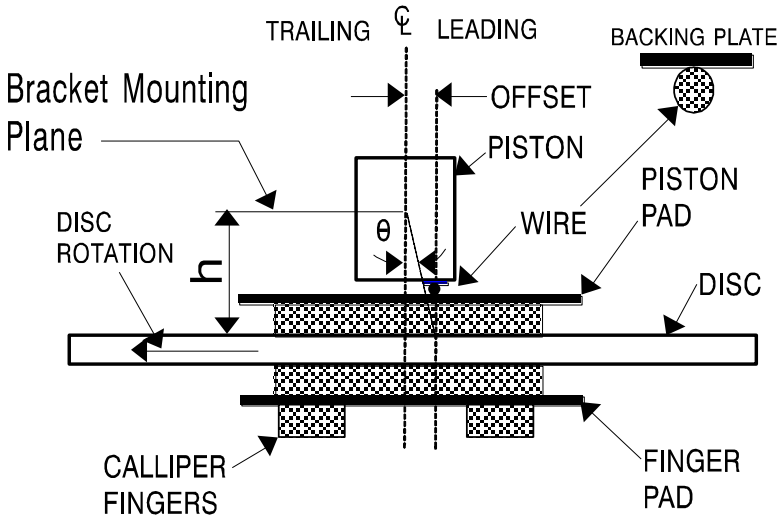

Figure D.1 Diagram showing wire offset contact position relative to caliper piston centreline [18]

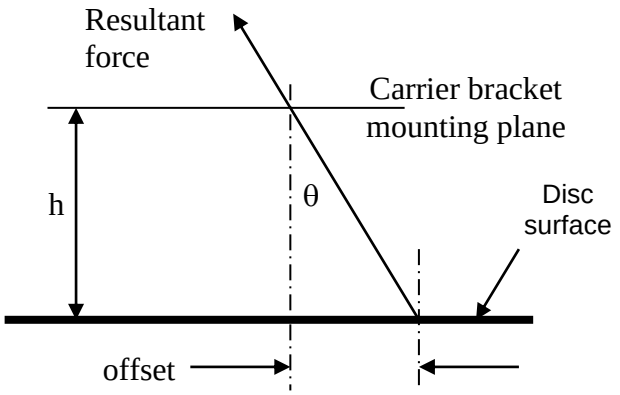

Figure D.2 Sprag angle coincides with angle between line of resultant force and intersect between centreline of piston and carrier bracket mounting plane [13]

In this instance interface coefficient of friction [18] was around 0.7 which leads to a spragging angle:

$$\theta = Tan^{-1}\mu \qquad (1)$$

As the critical offset, δ, is from 12 to 15mm then from Figure 1.12 the height "h" is

$$h = \delta / tan\ \theta \qquad (2)$$

Therefore for 12 and 15mm offset, δ, the distance "h" is 17.1 and 21.4mm respectively.
The actual distance "h" for this brake was 19mm.

D.2 Test Rig Validation

This relation between sprag angle and observation centre of pressure (as determined by pad wear) was evaluated against a commercial disc brake. The coefficient of friction for these tests is quoted by the brake manufacturers as 0.34. The distance from the disc face to the caliper mounting bracket face was 37.5mm. This was mounted to an adaptor 26mm thick as shown in Figure D.3.

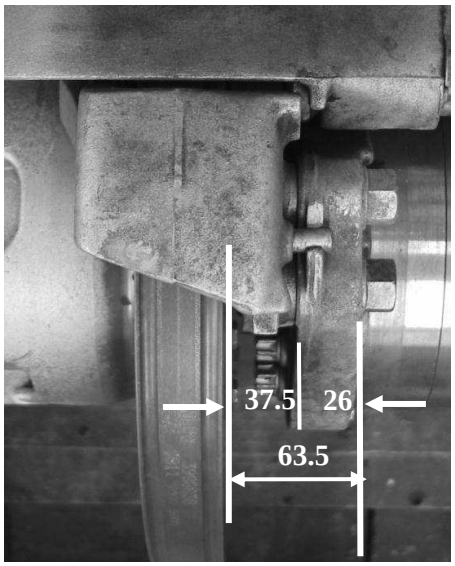

Figure D.3 Side view of commercial disc brake and relevant dimensions [13]

The total distance from the disc to the adaptor mounting face was 63.5mm as shown in Figure D.3. To determine the centre of pressure, wear measurements were made on the pad, this being shown in Figure D.4.

The centre of wear (pressure) or offset, δ = 23mm

This gives: $\mu = \tan\theta = \frac{23}{63.5} = 0.36$ (compare with 0.34 as given by brake suppliers)

This observation on a completely different disc arrangement goes some way to support the spragging theory.

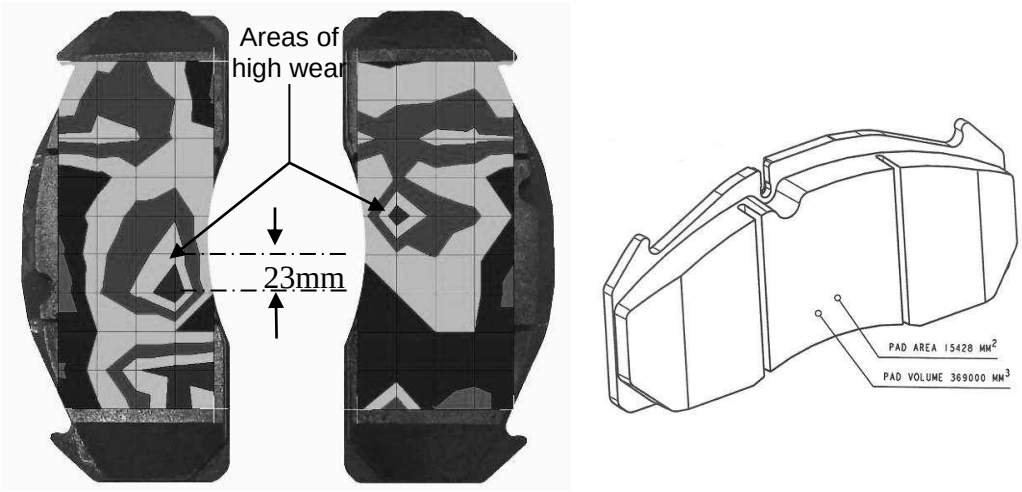

Figure D.4 Wear pattern on surface of pad indicates centres of pressure & also general view of pad [13]

D.3 On-Vehicle Validation

In this study, noise was an issue following the release of a limited numbers of high performance versions of a high volume commercial "sports" type car. A trailing centre of pressure was induced by the introduction of a 10mm chamfer on the leading edge of pad, the results as indicated in Table D.1.

Table D.1 Results of inducing trailing CoP by leading edge chamfer [13]

	Original	**With chamfer**	**Wet Test**
Pad Effective Length (mm)	96 mm	86 (Trailing CoP)	89
Effective Radius (mm)	124.2		
Pad Angle (deg)	45	40.5	42
Frequency (Hz)	2150	Difficult to get noise	2250

When the chamfer reduced to 6mm, through natural wear, the noise returned but when the chamfer of 10mm was re-established the noise was again eradicated. It will be noted that the original pad angle corresponds to the free mode antinode angular pitch for a 4^{th} diametral mode order. As such the brake would be more likely to generate noise with this mode order. The introduction of the chamfer introduces two changes, that of a trailing centre of pressure but also the disc/pad interface geometry is altered. Regardless the effects of inducing a trailing centre of pressure is, to some degree, an indication that such a design parameter should be considered at the design stage.

Appendix E

Appendix E.1 Data Sheet for Sensor Type 5101

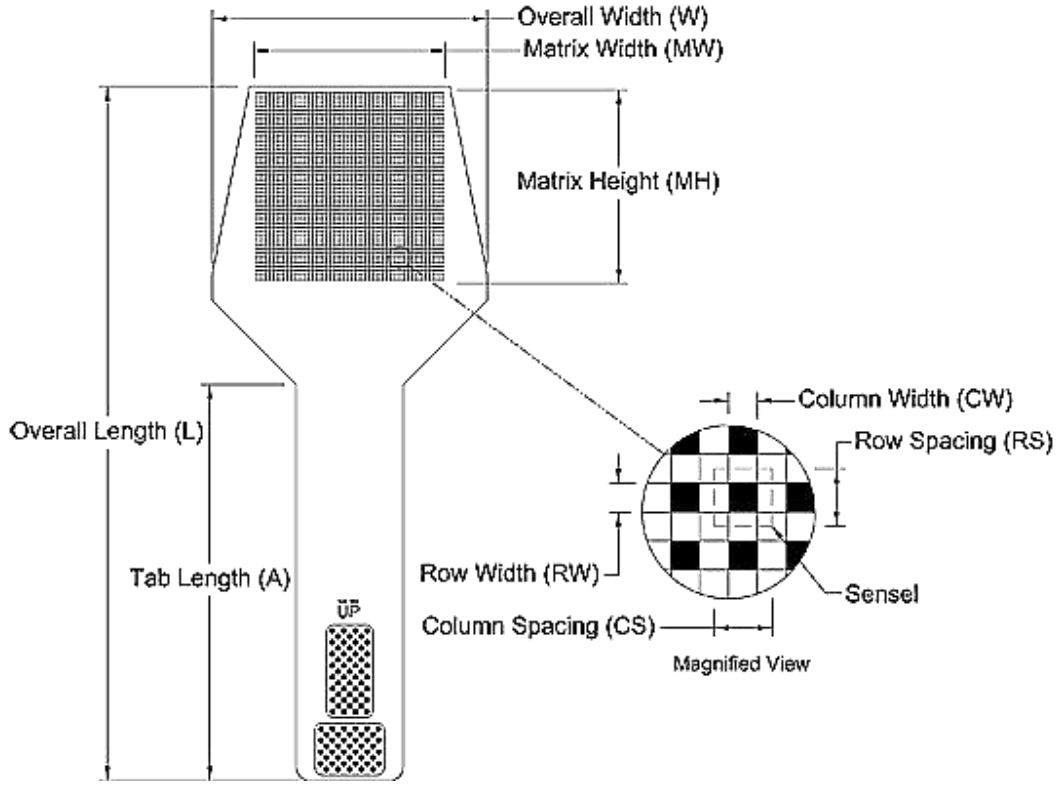

	General Dimensions			Sensing Region Dimensions								Summary	
Model	Overall Length L	Overall Width W	Tab Length A	Matrix Width MW	Matrix Height MH	Columns CW	Columns CS	Columns Qty.	Rows RW	Rows RS	Rows Qty.	Total No.of Sensels	Sensel Spatial Resolution
US	(in)	(in)	(in)	(in)	(in)	(in)	(in)		(in)	(in)			(sensel per sq-in)
5051	9.9	3.2	6.5	2.2	2.2	0.03	0.05	44	0.03	0.05	44	1936	400
5076	12	4.8	6.9	3.3	3.3	0.04	0.08	44	0.04	0.08	44	1936	178
5101	13.4	5.9	6.6	4.4	4.4	0.05	0.1	44	0.05	0.1	44	1936	100
Metric	(mm)	(mm)	(mm)	(mm)	(mm)	(mm)	(mm)		(mm)	(mm)			(sensel per sq-cm)
5051	252.5	81.3	166.2	55.9	55.9	0.76	1.27	44	0.76	1.27	44	1936	62
5076	305.5	121.3	175.9	83.8	83.8	1.02	1.91	44	1.02	1.91	44	1936	27.6
5101	340	149	167.3	111.8	111.8	1.27	2.54	44	1.27	2.54	44	1936	15.5

Figure E.1 Dimensions and layout of sensor type 5101

Appendix E.2

Cutting Process of Brake Sensor, 5105

The trimmed dimension of the sensor was determined by counting the numbers of horizontal rows, with reference to the exact dimensions of brake pad cavity. The sensors were trimmed between the rows and connecting tracks as shown by the red line in Figure E2.

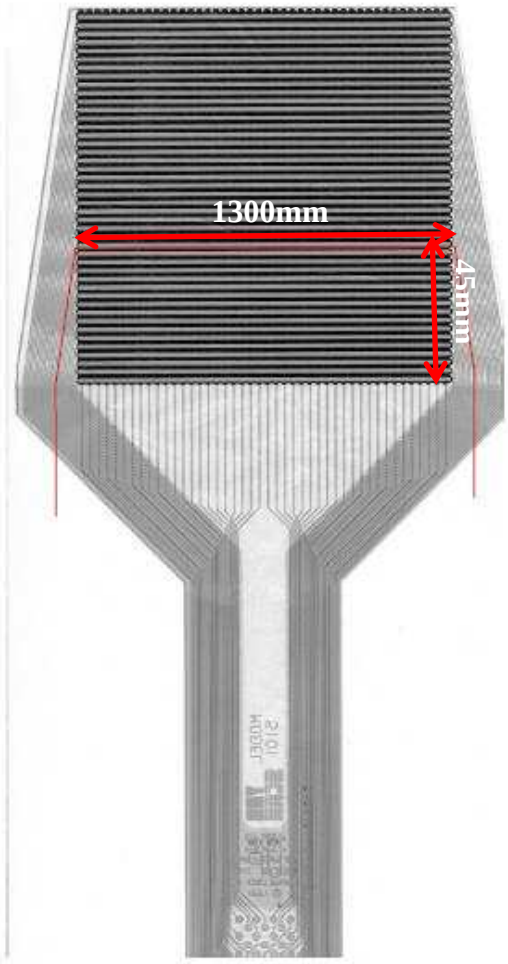

Figure E.2 Displaying the dimension of trimmed sensor

Note that alternate rows have connecting tracks at opposite ends. In this sensor the two Mylar films are stuck down round the edge only, not throughout the sensor matrix. It is ensured that the two layers are held firmly together to prevent movement whilst cutting. Sensors were carefully trimmed using guillotine to fit the recess pads. In general it is required to seal the cut edges with adhesive or tape to preclude dust and prevent relative movement of the two polyester films during handling and use. However, in this case the added thickness of adhesive or tape would probably affect the accuracy of pressure distribution results. As there are small shear forces involved once the brake pad is assembled, it was decided not to seal the edges.

Appendix F

Appendix F.1 Calibration of Pressure Sensors

For the calibration process, a uniform pressure was applied along the length of the sensor. A two-point calibration was performed by applying two different loads to the sensor (20% and 80% of the 2MPa). Using these data Tekscan software performs a power law interpolation for overall sensor based on zero load and the two known calibration loads [49].

The data is presented in Table F.1.

Table F.1 Contact force measurement error (%)

Pressure Applied (MPa)	Force Applied (N) to each sensor	Tekscan Results		Force Measurement Error (%)	
		Total Contact Force (N) (Outboard Pad)	Total Contact Force (N) (Inboard Pad)	Outboard Pad	Inboard Pad
0.5	1520	1589	1567	-4.34	-3.00
1	3040	2990	3105	1.64	-2.09
1.5	4560	4540	4527	0.44	0.72
2	6080	6588	6831	-7.71	-10.99

Appendix F.2

Temperature Sensitivity Studies of Pressure Sensors

Table F.2. Pressure sensors response at various brake temperatures

Pressure Applied (MPa)	Force Applied (N) to each sensor	Temperature °C	Tekscan Results		Force Measurement Error (%)	
			Total Contact Force (N)			
			Outboard Pad	Inboard Pad	Outboard Pad	Inboard Pad
1.0	3040	23	2990	3105	1.64	-2.09
		100	2948	3219	3.03	-5.56
		150	2901	3307	4.60	-8.07
		200	3199	3370	-4.97	-9.79

Appendix G

Comparison of Static Pressure Measurements

Table G.1 Force Measurement Error (%)

Pressure Applied (MPa)	Force Applied (N) to each Sensor	Tekscan Results				Force Measurement Error (%)				**Differences (%)**	
		Total Contact Force (N)									
		Outboard Pad		Inboard Pad		Outboard Pad		Inboard Pad		**Outboard Pad**	**Inboard Pad**
		Disc/Pad Interface	Embedded Pad	Disc/Pad Interface	Embedded Pad	Disc/Pad Interface	Embedded Pad	Disc/Pad Interface	Embedded Pad		
0.4	1258	1203	1290	1163	1178	4.37	-2.48	7.55	6.36	**6.85**	**1.19**
0.6	1781	1805	1690	1792	1731	-1.33	5.11	-0.61	2.81	**-6.44**	**-3.42**
0.80	2410	2394	2399	2559	2403	0.66	0.46	-6.18	0.29	**0.21**	**-6.47**
1	3040	2990	2983	3105	2932	1.64	1.88	-2.14	3.55	**-0.23**	**-5.69**
1.5	4560	4540	4932	4527	4686	0.40	-7.54	0.66	-2.69	**7.94**	**3.35**
2	6080	6588	7161	6831	7205	-7.71	-15.10	-10.99	-15.61	**7.38**	**4.62**

Appendix H

Showing Full Graphical Images of Pressure Mapping of Both inboard and outboard Pads at Various Stages

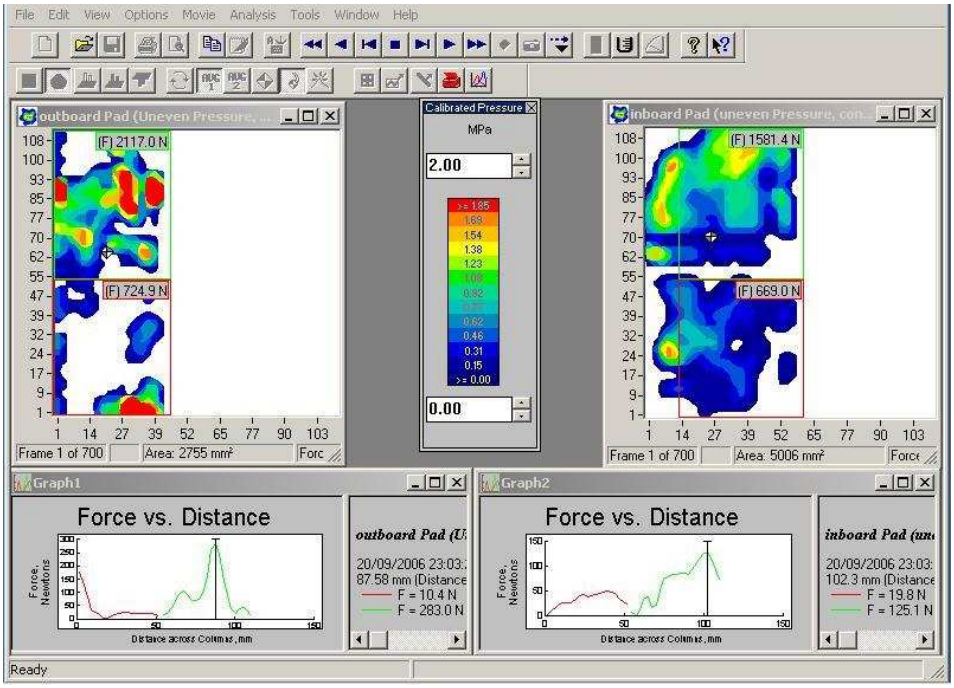

Figure H.1 Force distribution map for both outboard and inboard pad at Stage 1

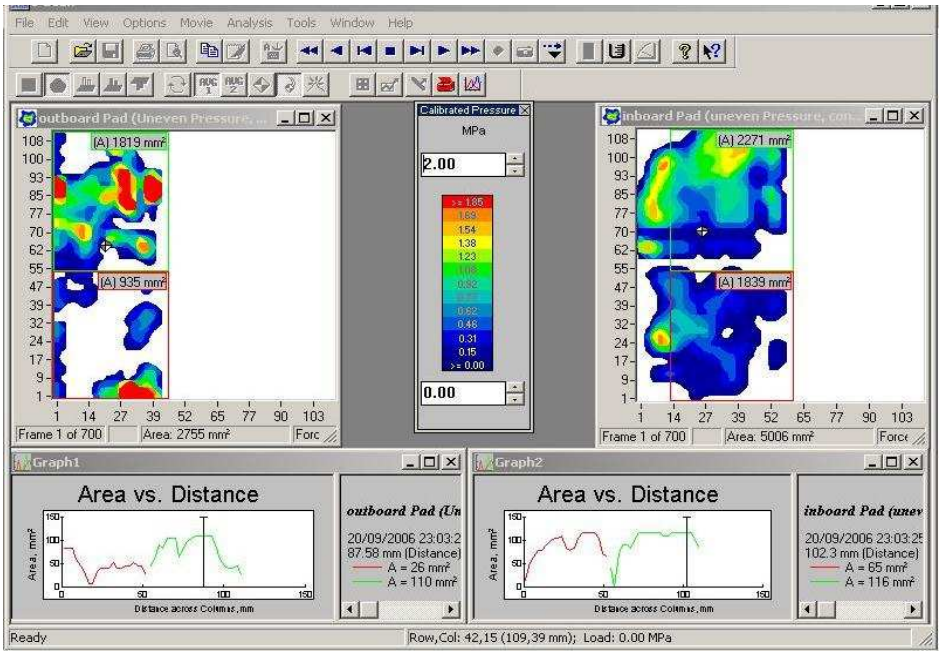

Figure H.2 Area distribution map for both outboard and inboard pad at Stage 1

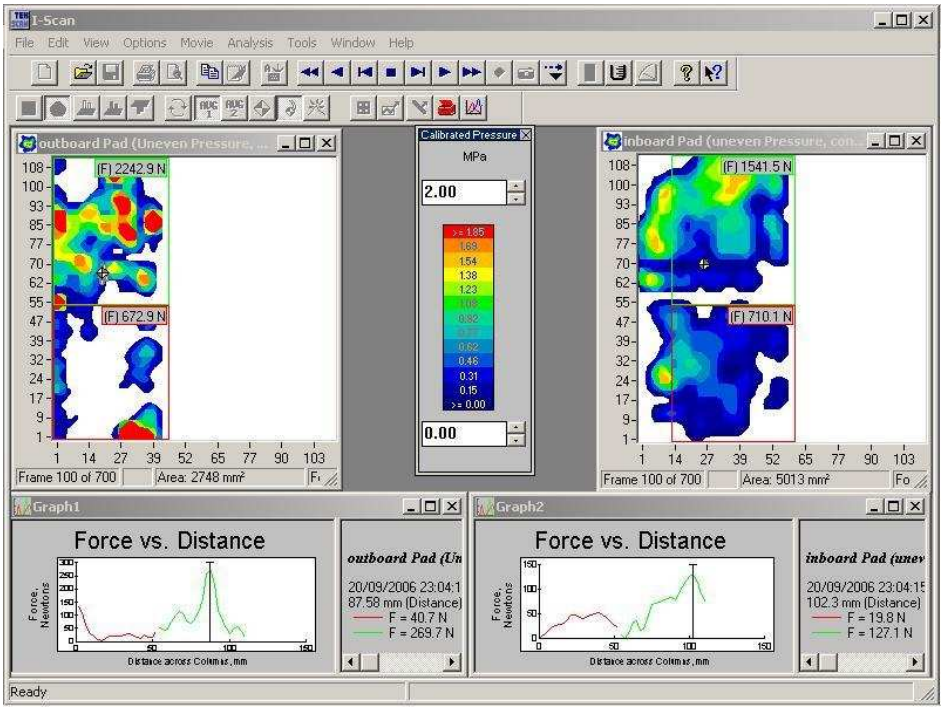

Figure H.3 Force distribution map for both outboard and inboard pad at Stage 2

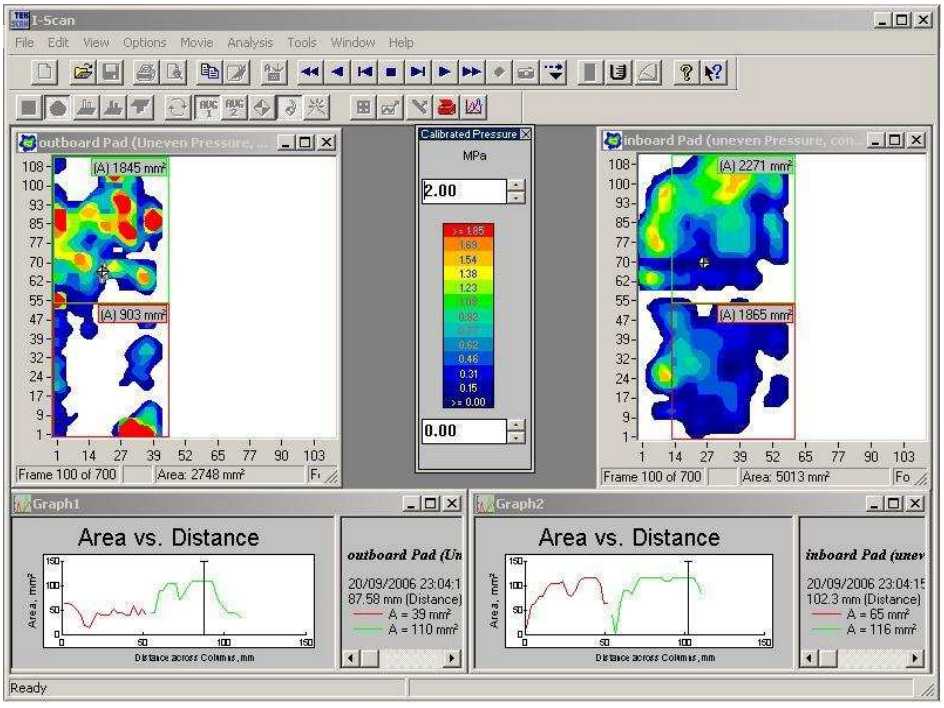

Figure H.4 Area distribution map for both outboard and inboard pad at Stage 2

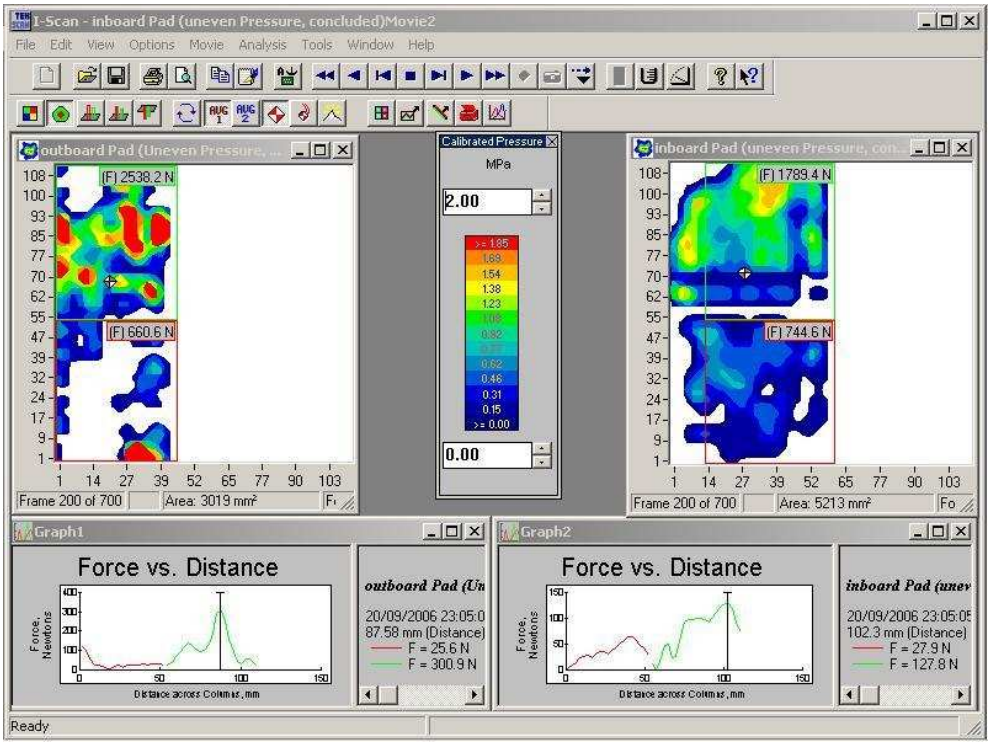

Figure H.5 Force distribution map for both outboard and inboard pad at Stage 3

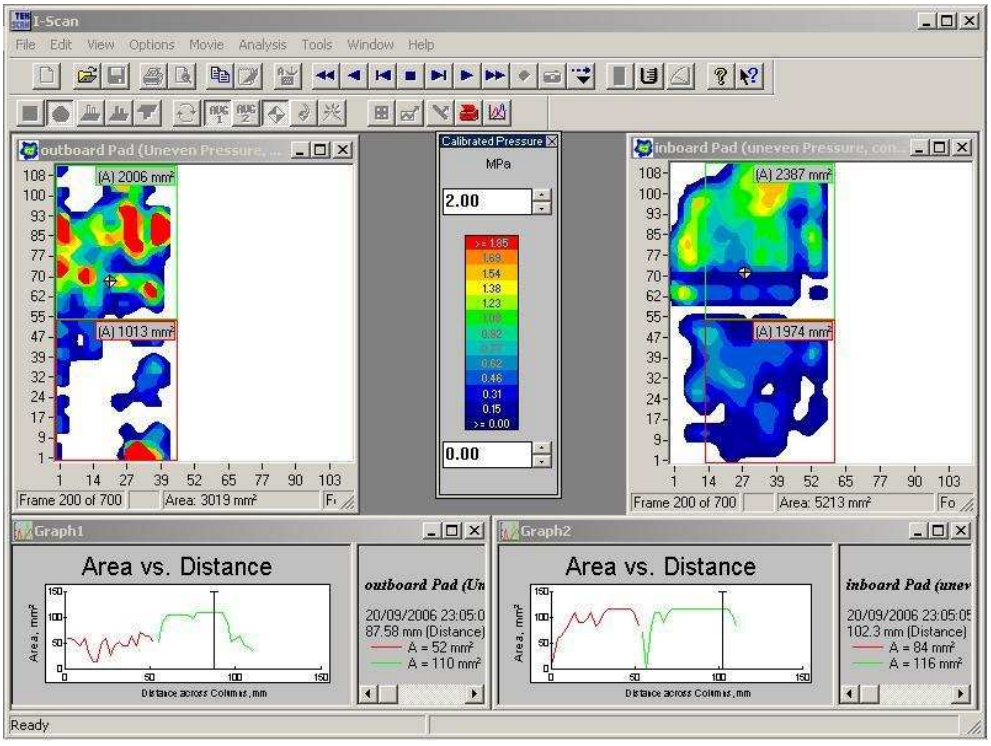

Figure H.6 Area distribution map for both outboard and inboard pad at Stage 3

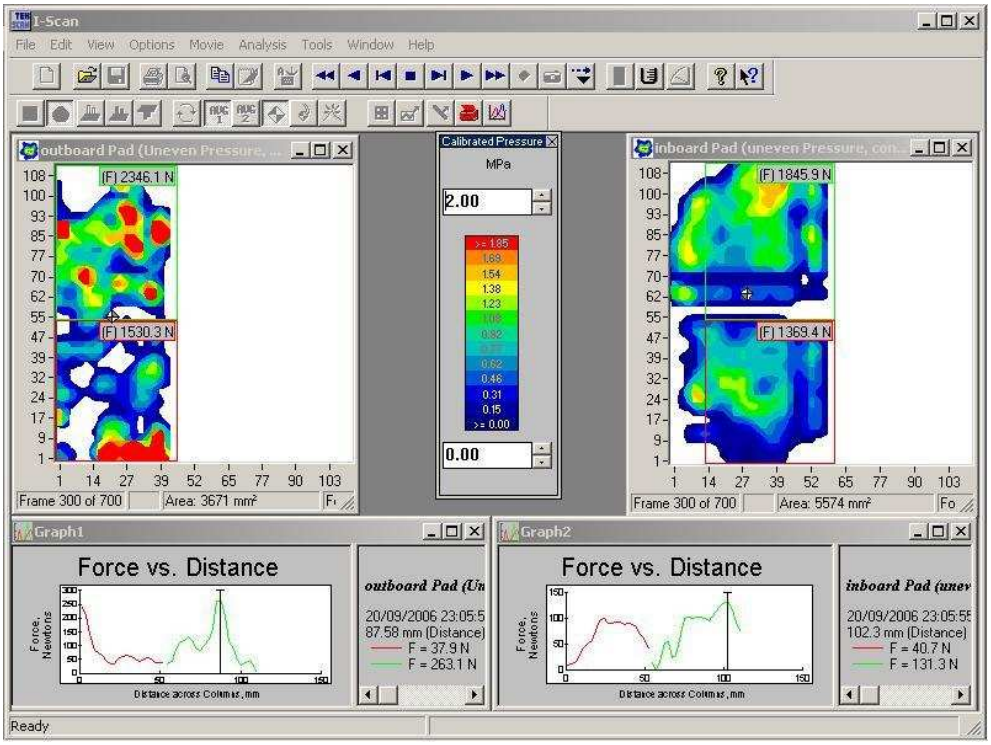

Figure H.7 Force distribution map for both outboard and inboard pad at Stage 4

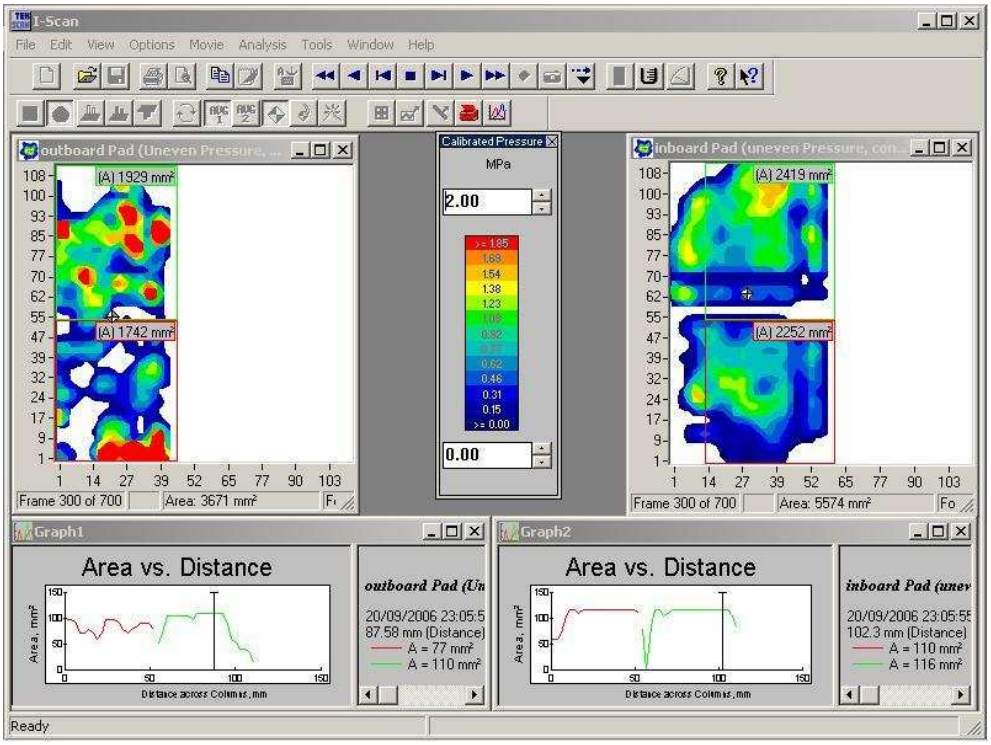

Figure H.8 Area distribution map for both outboard and inboard pad at Stage 4

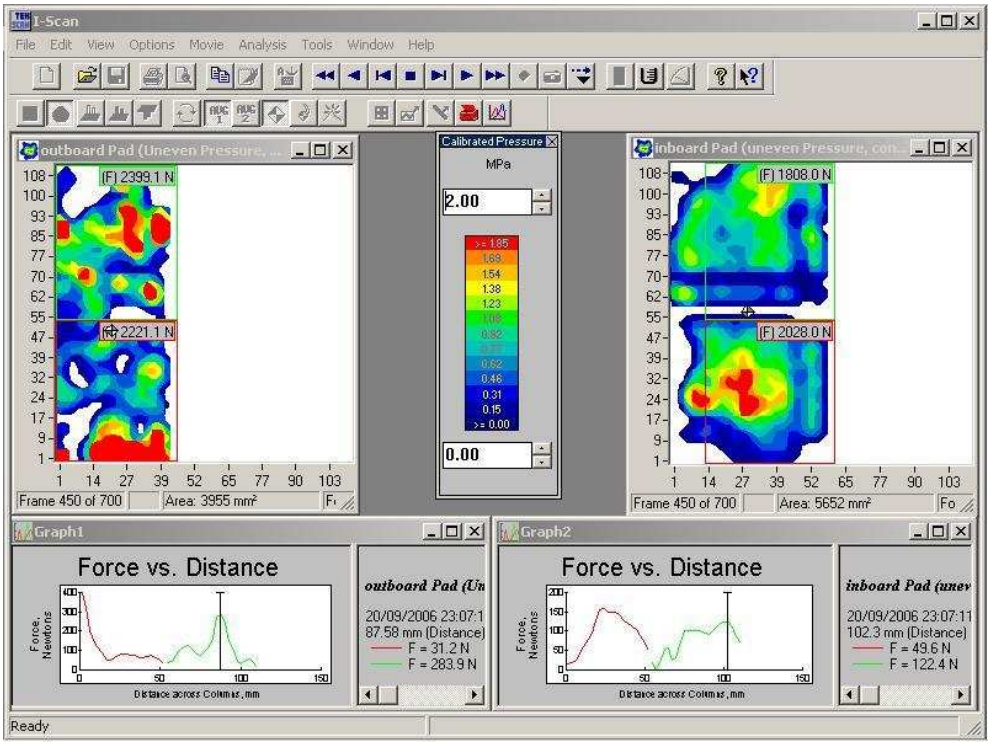

Figure H.9 Force distribution map for both outboard and inboard pad at Stage 5

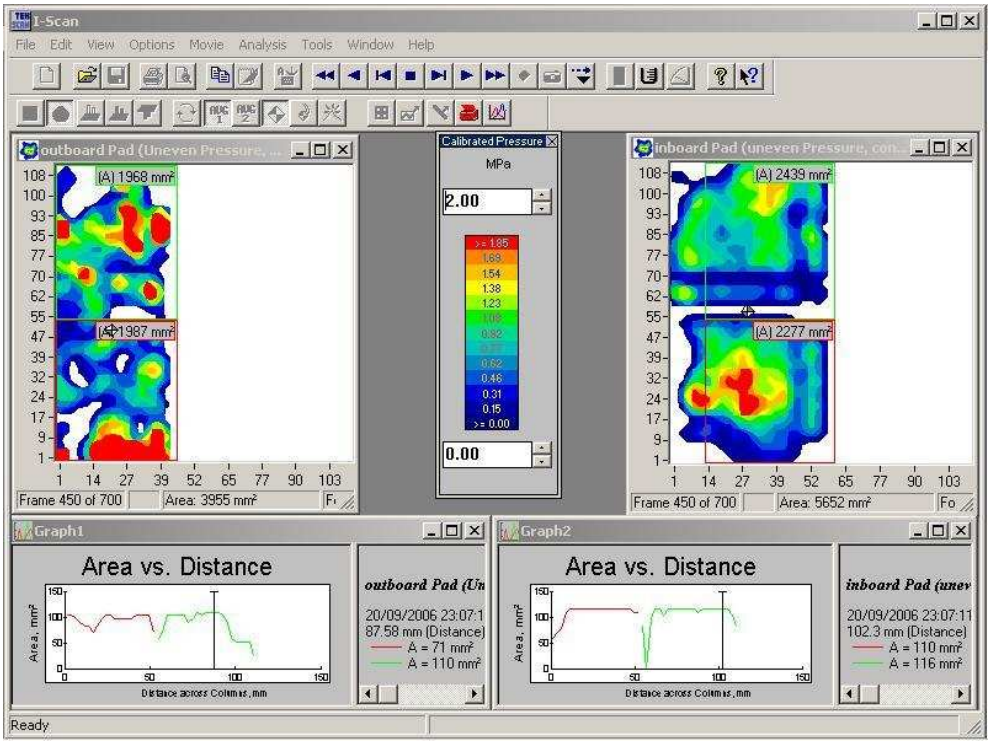

Figure H.10 Area distribution map for both outboard and inboard pad at Stage 5

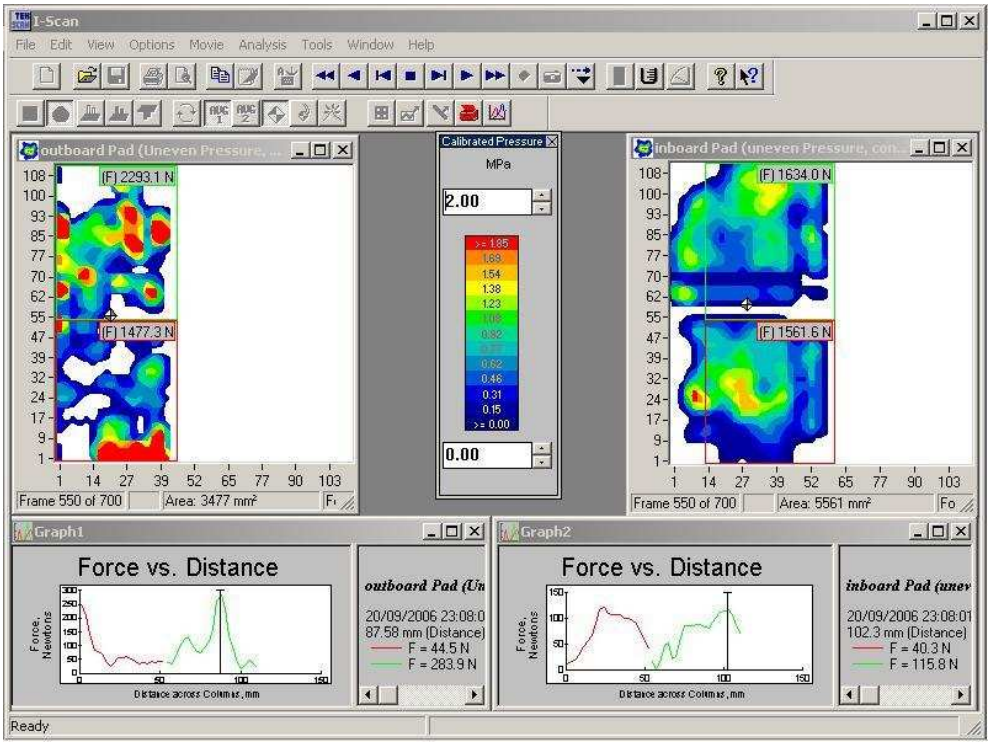

Figure H.11 Force distribution map for both outboard and inboard pad at Stage 6

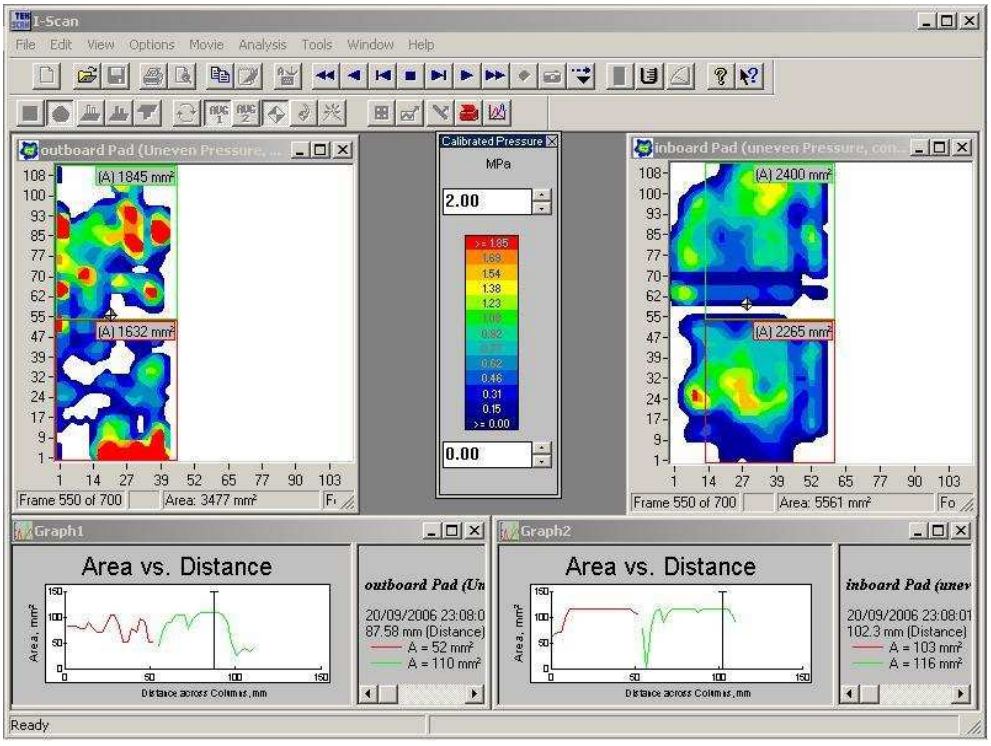

Figure H.12 Area distribution map for both outboard and inboard pad at Stage 6

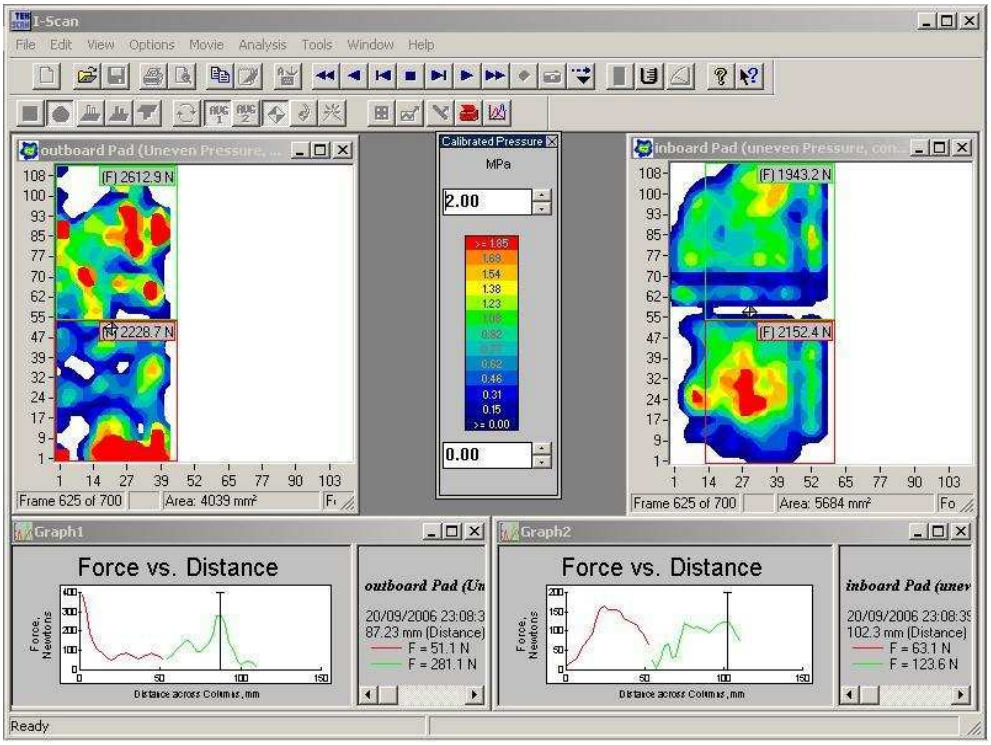

Figure H.13 Force distribution map for both outboard and inboard pad at Stage 7

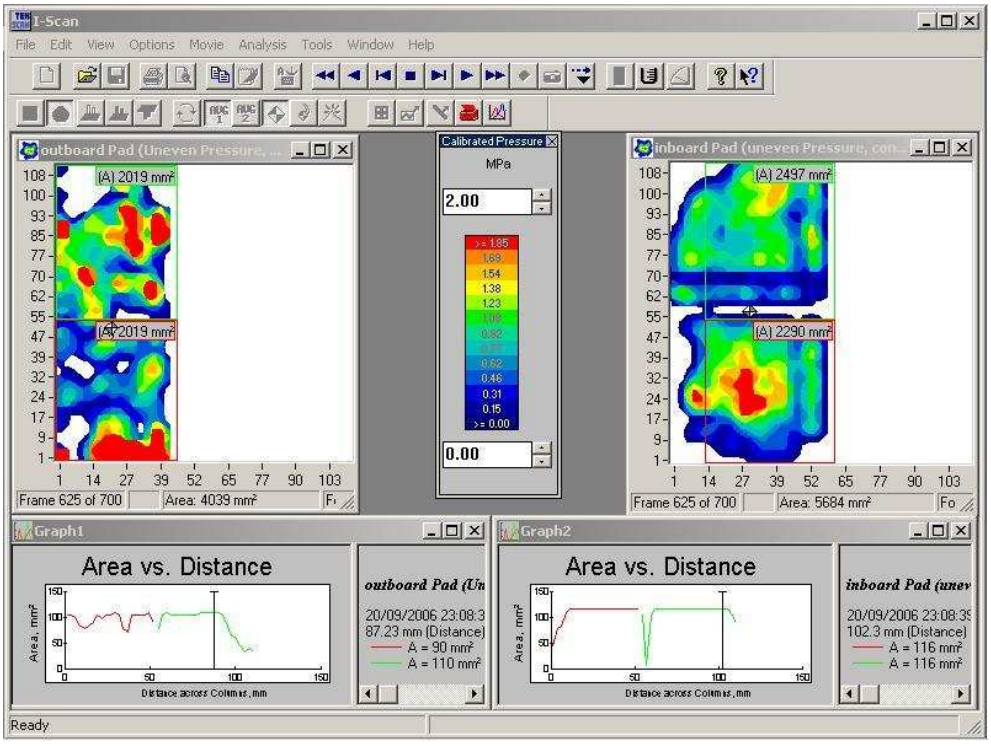

Figure H.14 Area distribution map for both outboard and inboard pad at Stage 7

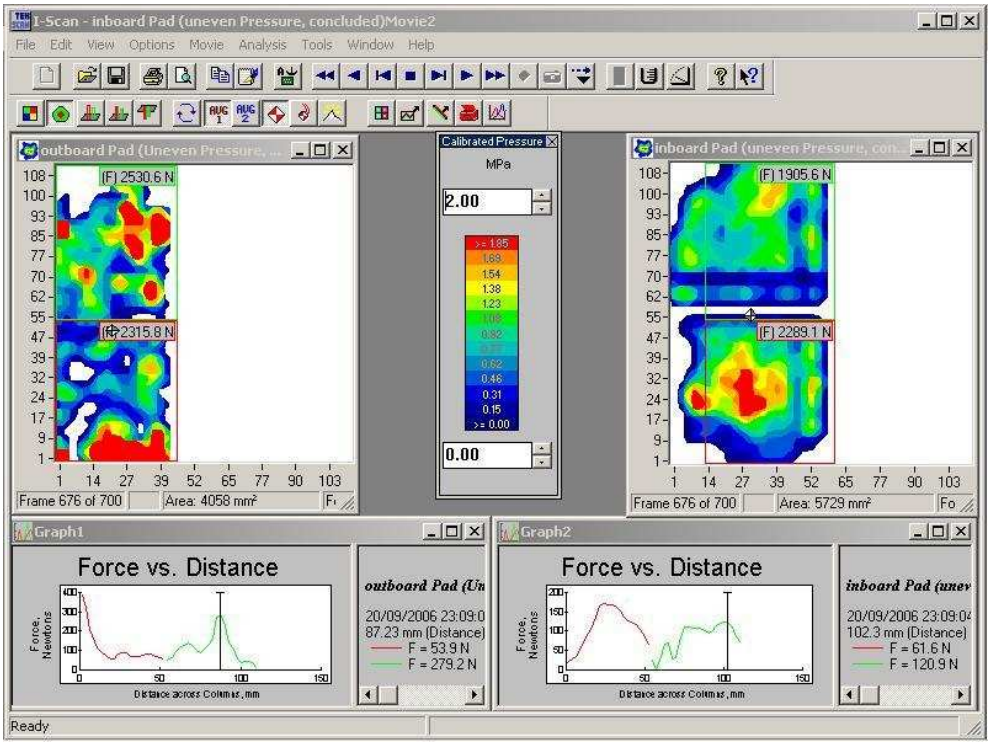

Figure H.15 Force distribution map for both outboard and inboard pad at Stage 8

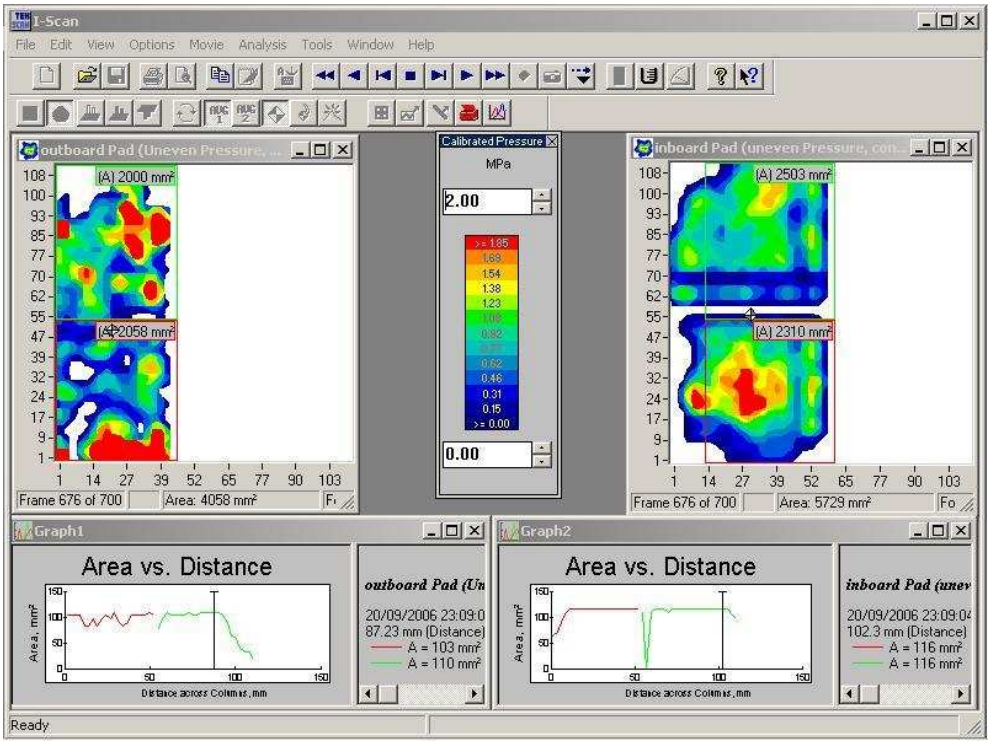

Figure H.16 Area distribution map for both outboard and inboard pad at Stage 8

Appendix I

Dimensions and Data of Disc Brake Components

Table I.1 Displaying the data of disc brake components

	Disc	Friction material	Backplate
Modulus of Elasticity (Gpa)	96	1.0	200
Density (kg/m^3)	7200	3000	7800
Poisson's ratio	0.25	0.25	0.30
Disc diameter (mm)	375		
Thickness of disc (mm)	36		
Pad length (mm)	172		
Thickness of friction material (mm)	10		
Thickness of backplate (mm)	5		
Piston diameter (mm)	25		
Caliper loading configuration	6 pistons on each side of the pad		
Abutment arrangement	Combined abutments		

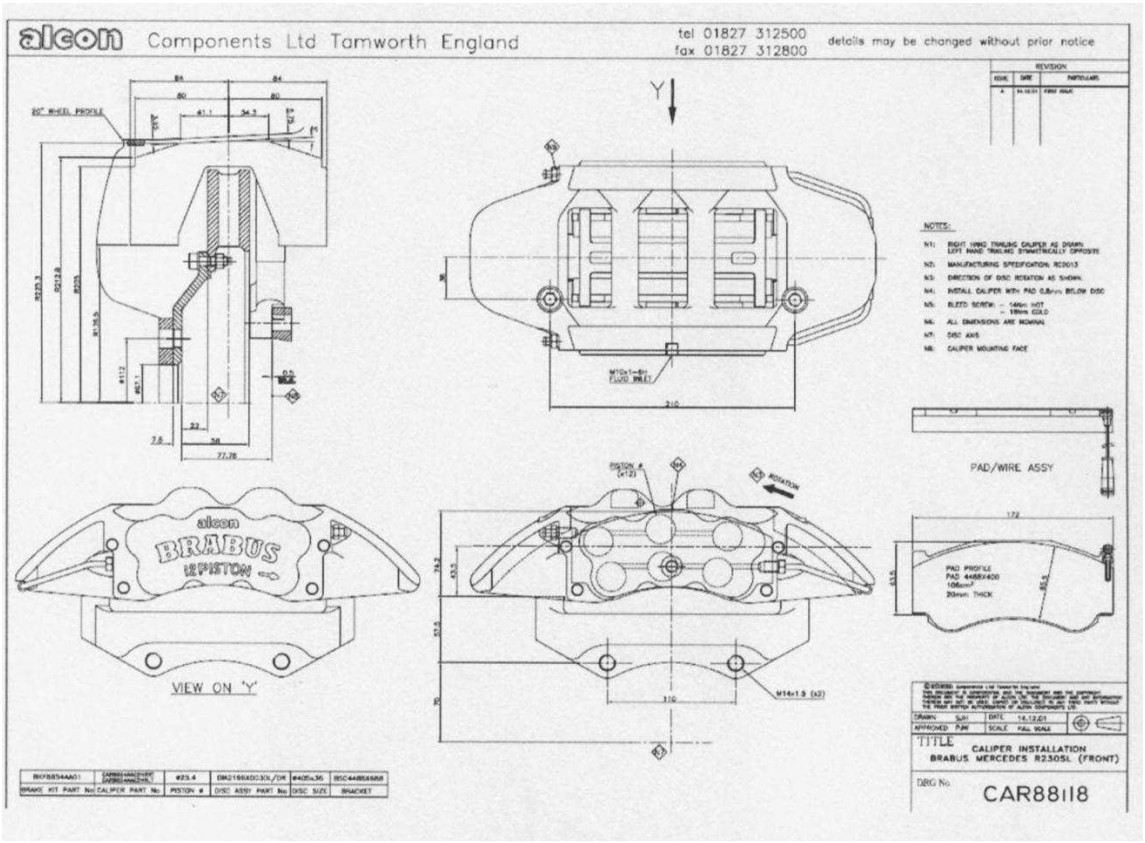

Figure I.1 Detailed drawing of the caliper

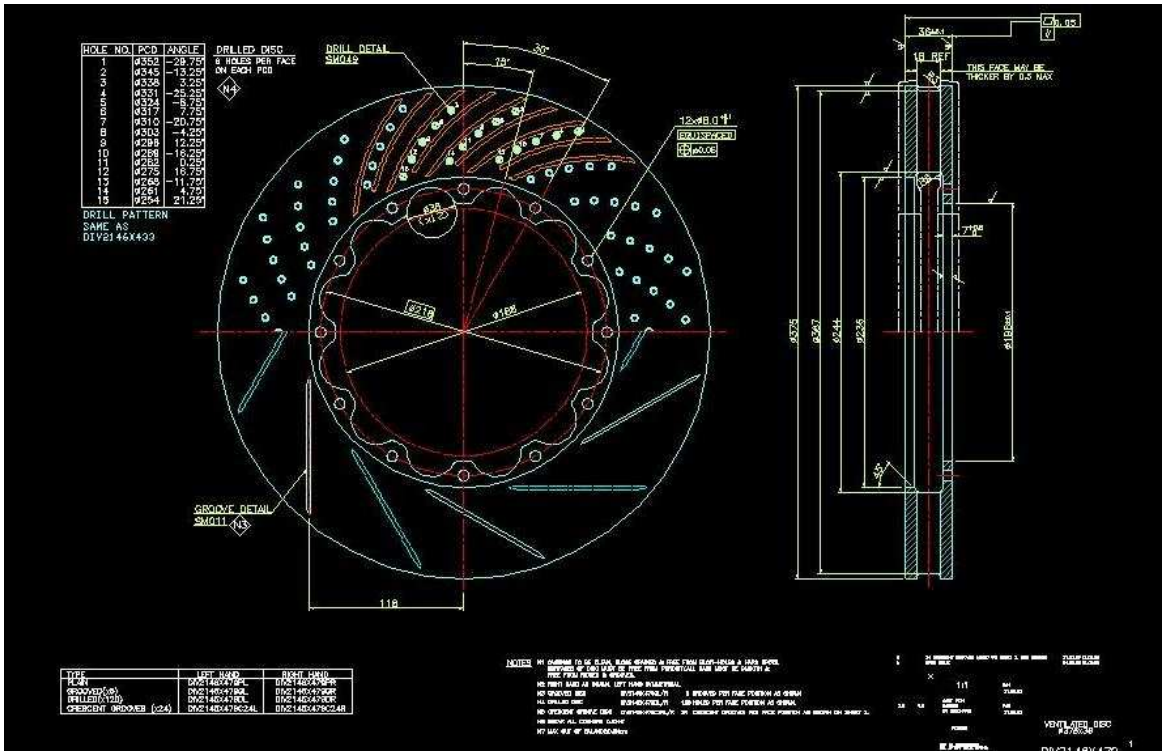

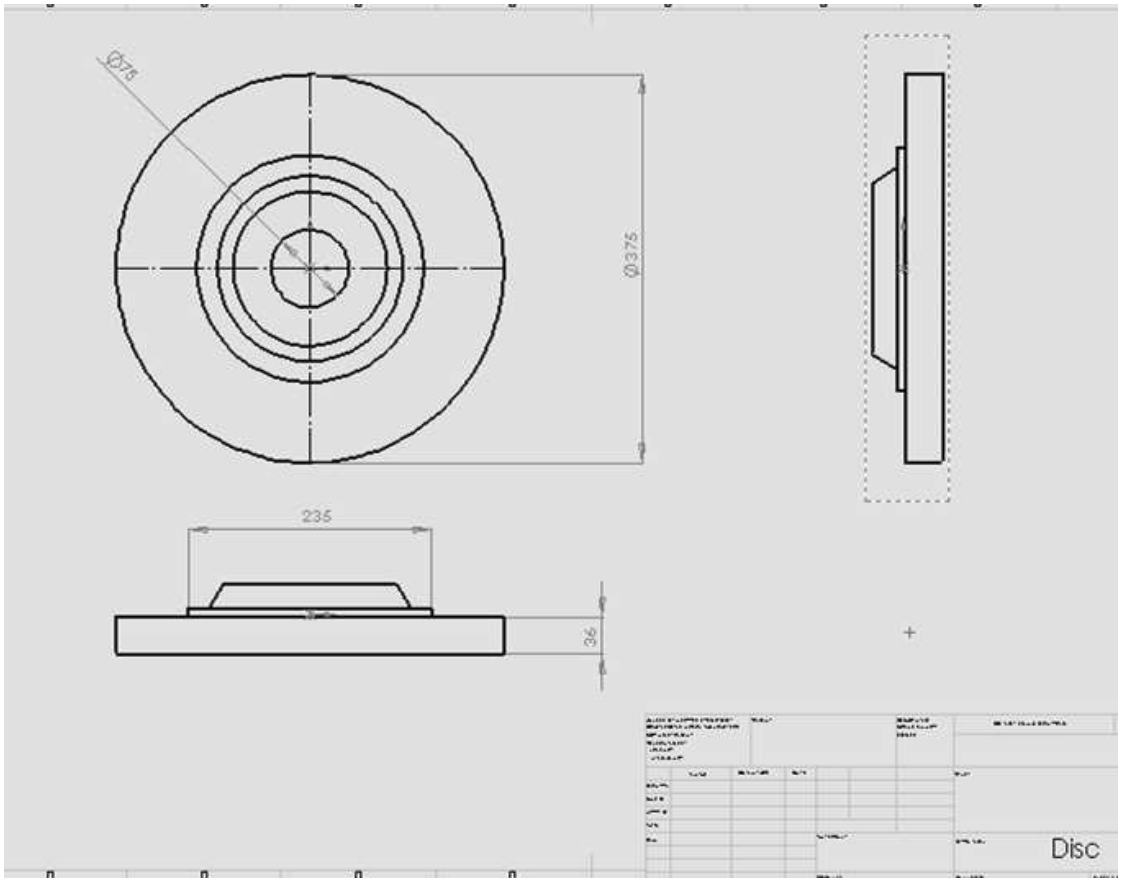

Figure I.2 Detailed drawings of the disc rotor

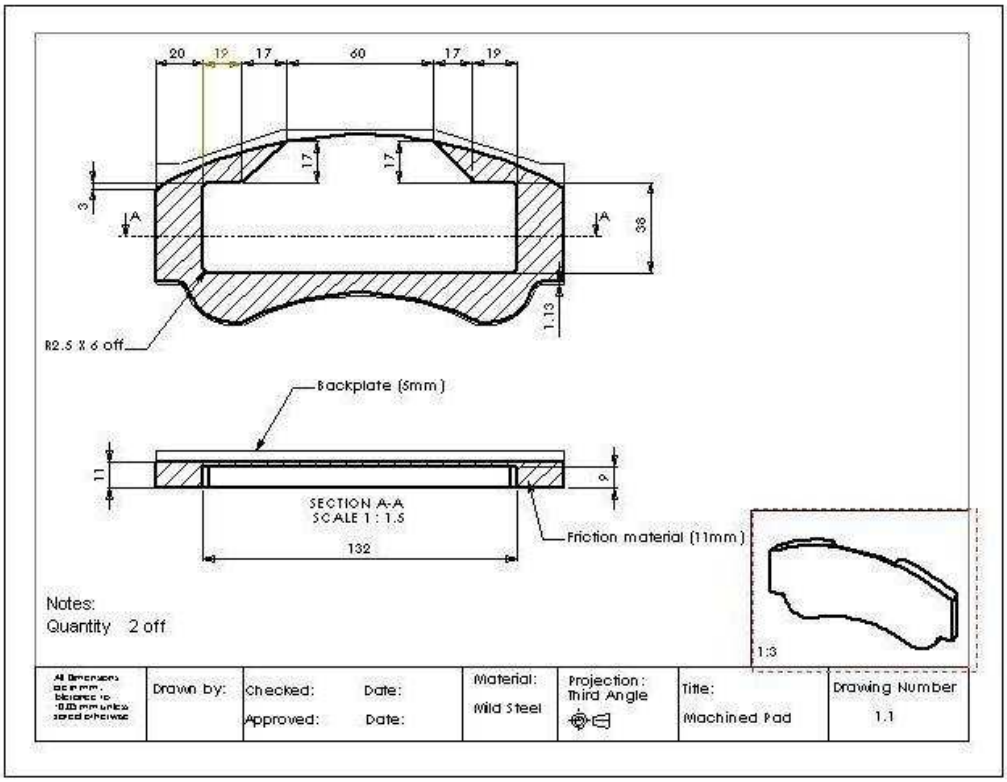

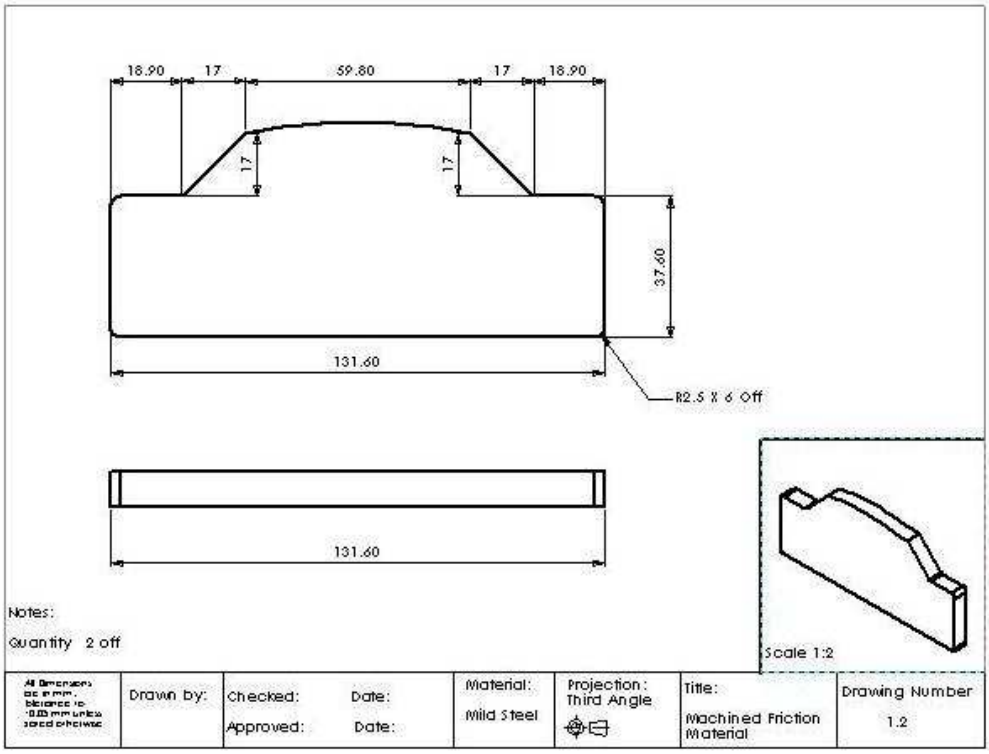

Figure I.3 Pad drawings with "recess" and "plug"

Appendix J

FE Models of Disc with Various Mesh Densities

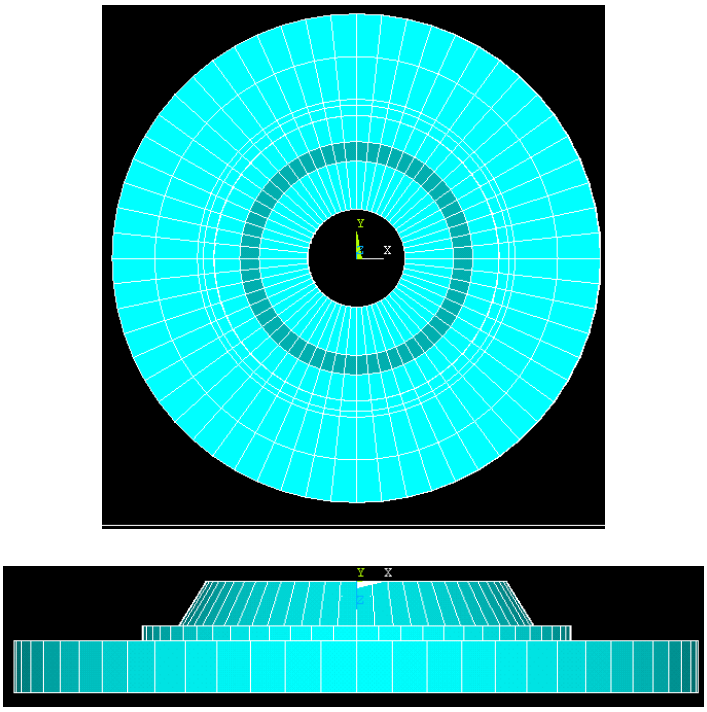

Figure J.1 **Model 1 - Coarse Mesh with 480 elements**

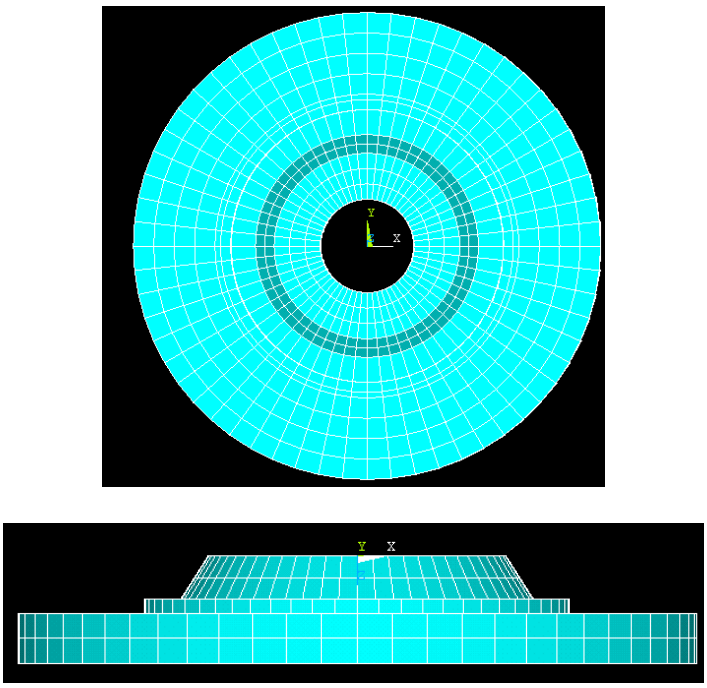

Figure J.2 Model 2 - Mesh density with 1140 elements

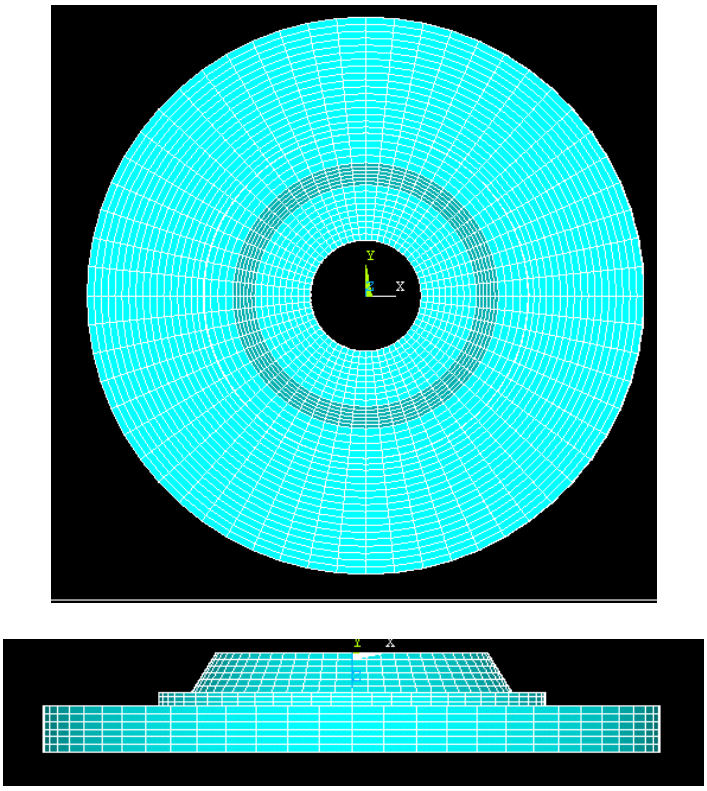

Figure J.3 Model 3 - Fine Mesh with 9900 elements

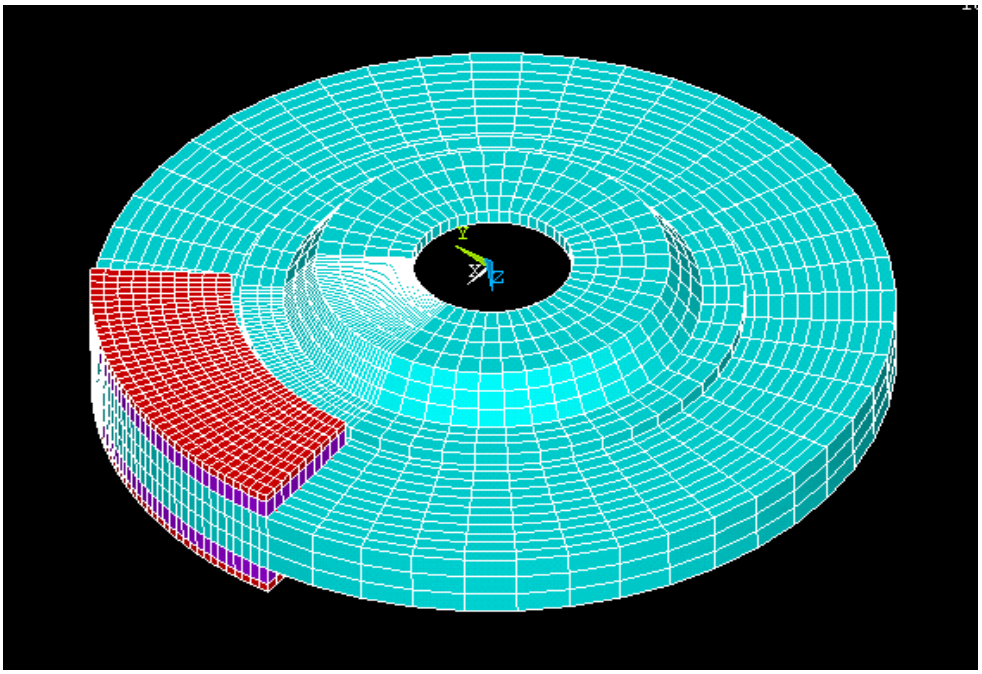

Figure J.4 Model 4 - Fine mesh with 5220 elements

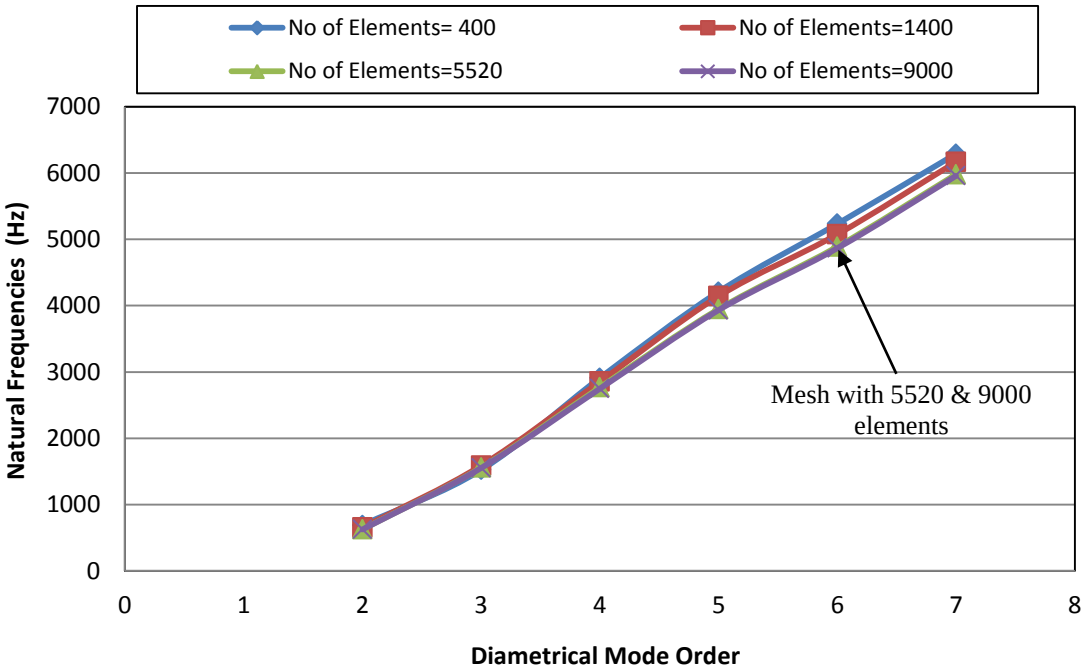

Figure J.5 Displaying convergence curve for various mesh densities (Fine mesh with 5520 elements were chosen in the current FE simulation)

Appendix K

Appendix K.1 Capabilities of Various Methods

Table K.1 A Table showing capabilities of various algorithms

	Node-to-Node			Node-to- Surface	Surface-to-Surface		Line-to-Line	Line-to- Surface
Contact Element No.	**12**	**52**	**178**	**175**	**171, 172**	**173, 174**	**176**	**177**
Target Element No.				**169, 170**	**169**	**170**	**170**	**170**
2-D	Y		Y	Y	Y			
3-D		Y	Y	Y		Y	Y	Y
Sliding	small	small	small	large	large	large	large	large
Cylindrical Gap	Y		Y					
Pure Lagrange Multiplier			Y	Y	Y	Y	Y	Y
Augmented Lagrange Multiplier			Y	Y	Y	Y	Y	Y
Lagrange Multiplier on Normal and Penalty on Tangent			Y	Y	Y	Y	Y	Y
Internal Multipoint Constraint (MPC)				Y	Y	Y	Y	Y
Contact Stiffness	user-defined	user-defined	semi-auto	semi-auto	semi-auto	semi-auto	semi-auto	semi-auto
Auto-meshing Tools	**EINTF**	**EINTF**	**EINTF**	**ESURF**	**ESURF**	**ESURF**	**ESURF**	**ESURF**
Lower-Order	Y	Y	Y	Y	Y	Y	Y	Y
Higher-Order				Y (2-D only)	Y	Y	Y	Y
Rigid-Flexible	Y	Y	Y	Y	Y	Y	Y	Y

Appendix K.2

Comparison of Pressure Distribution Map with the Experimental Results at Various Stages (Stage 1-8)

Outboard Pad **Inboard Pad**

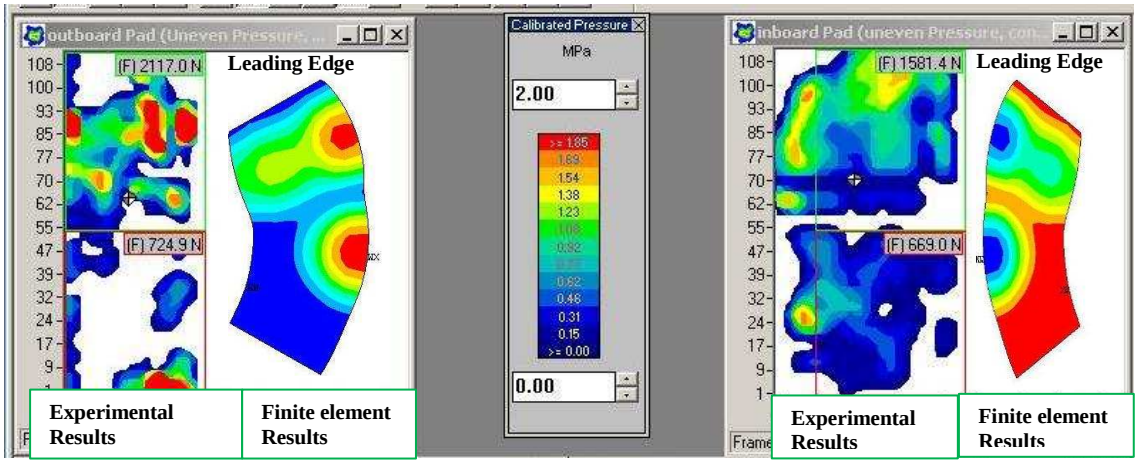

Stage 1

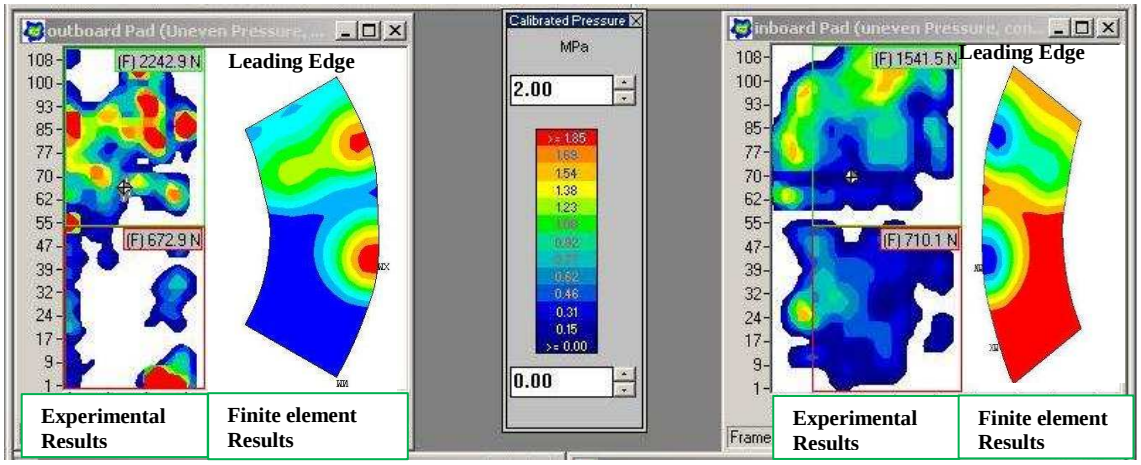

Stage 2

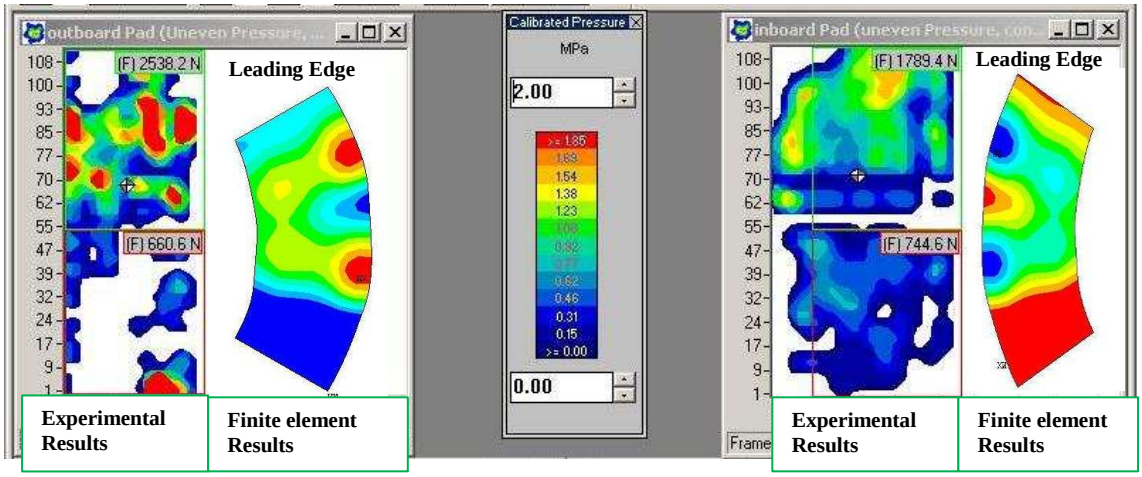

Stage 3

Outboard Pad **Inboard Pad**

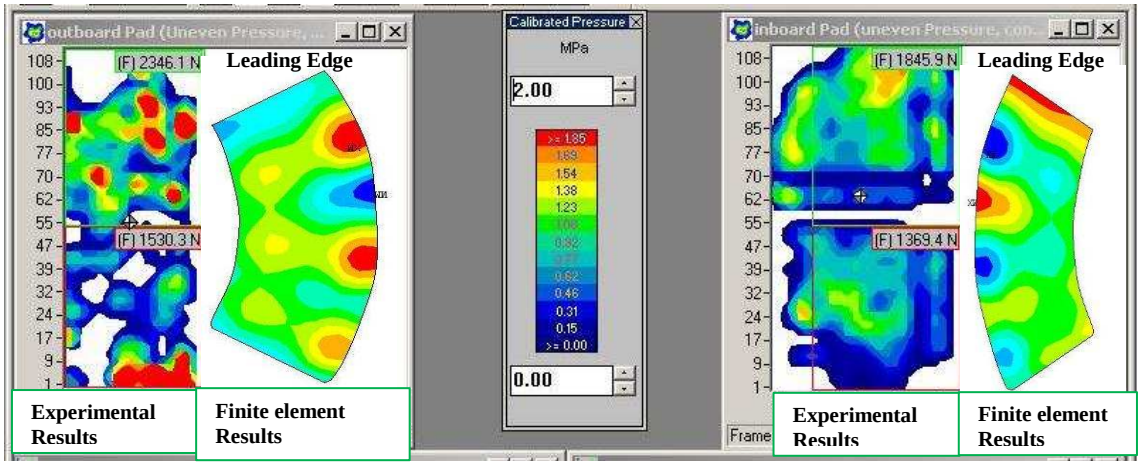

Stage 4

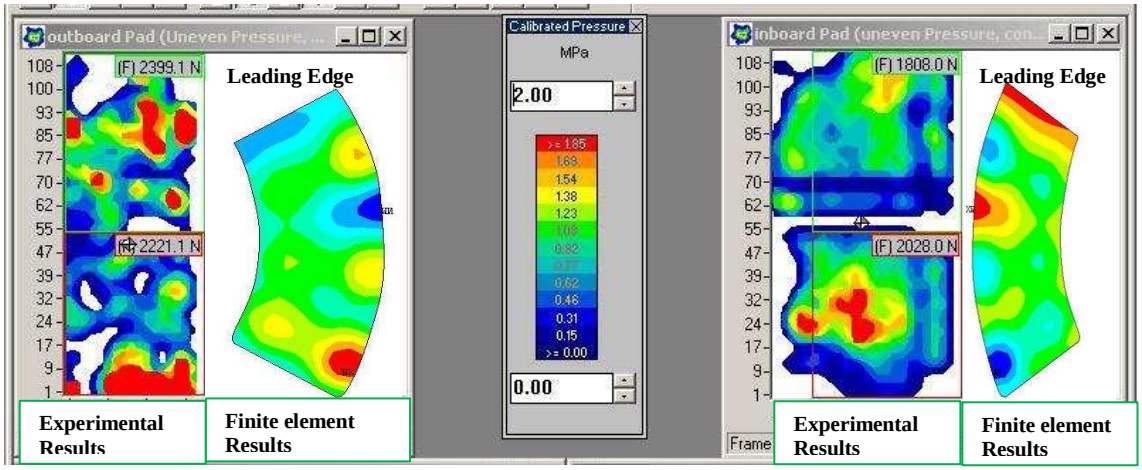

Stage 5

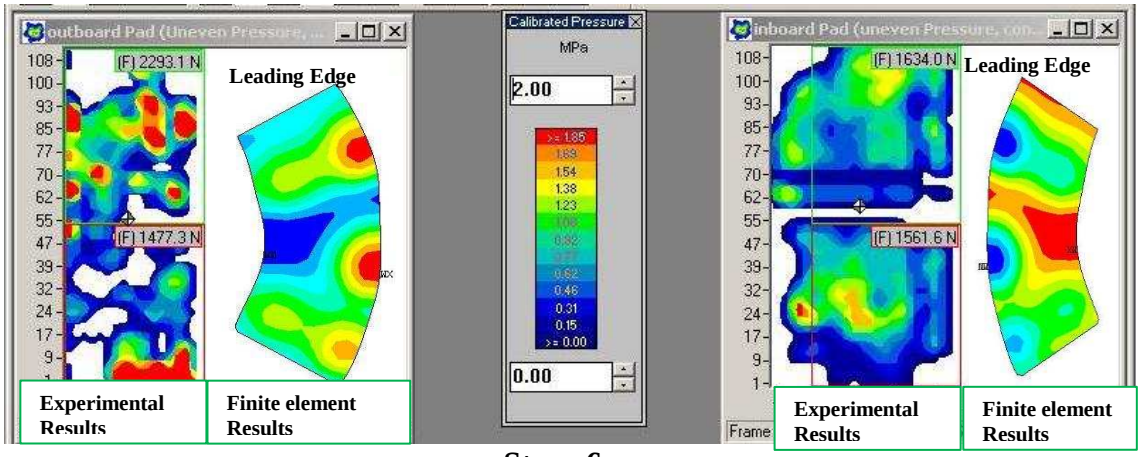

Stage 6

Outboard Pad **Inboard Pad**

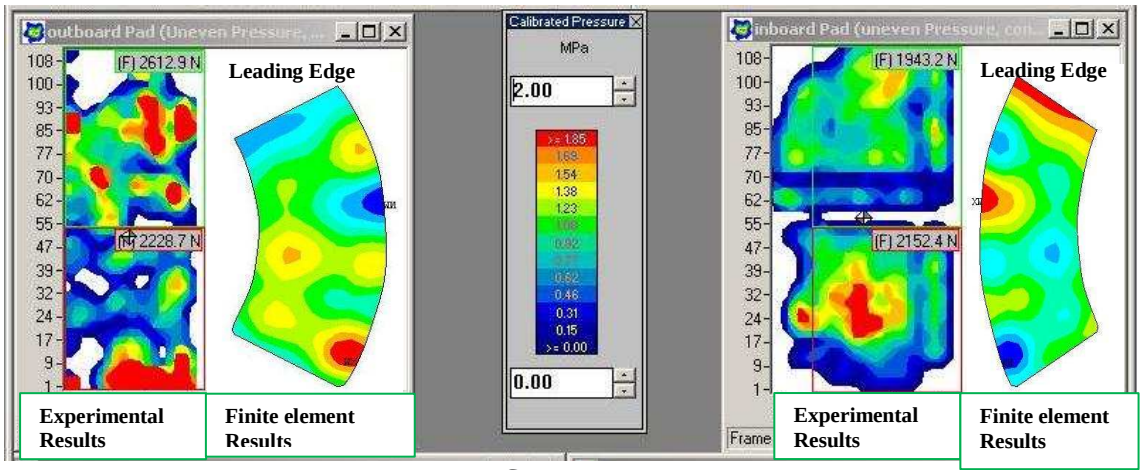

Stage 7

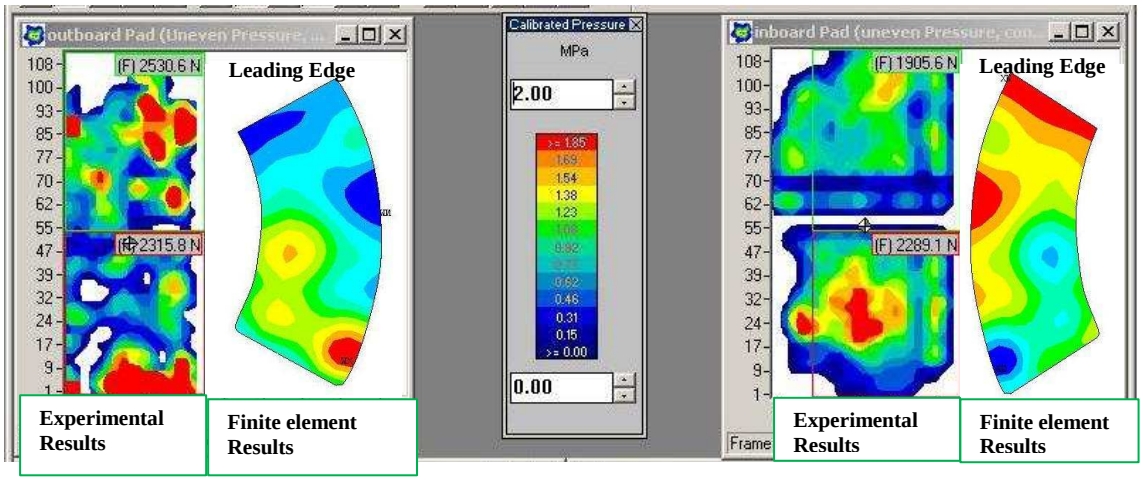

Stage 8

Appendix L

FE images of Pressure Distribution of Both Inboard and Outboard Pads under Various Frictional Conditions

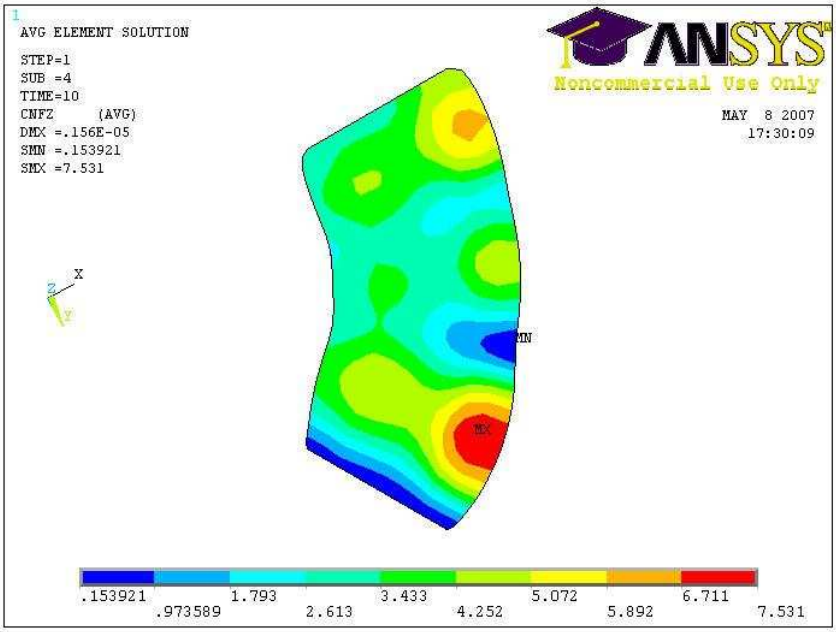

Figure L.1 Pressure distribution of outboard pad under frictionless conditions (μ=0)

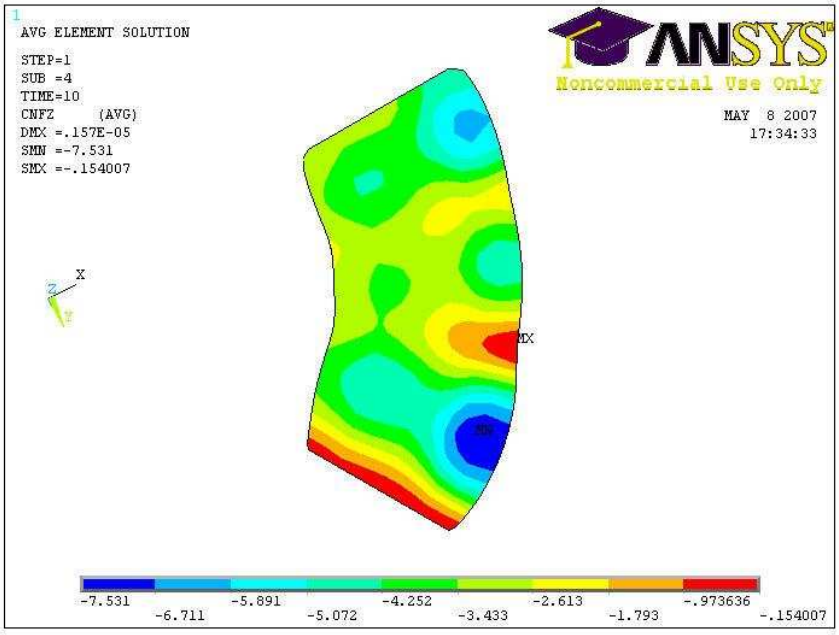

Figure L.2 Pressure distribution of inboard pad under frictionless conditions (μ=0)

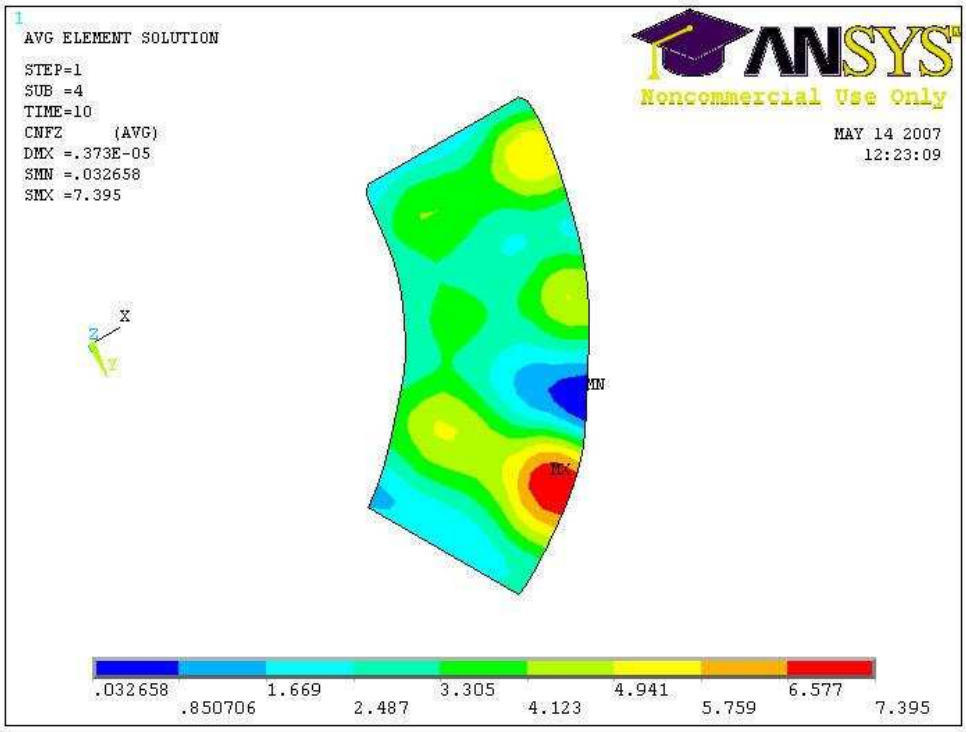

Figure L.3 Pressure distribution of outboard pad under frictional conditions (μ=0.4)

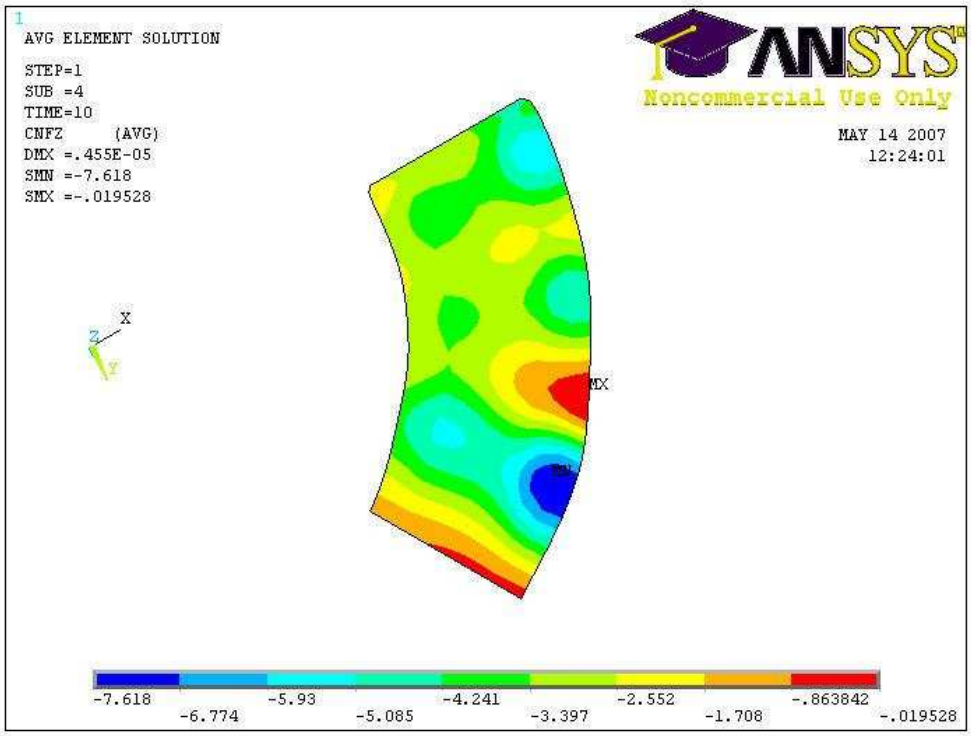

Figure L.4 Pressure distribution of inboard pad under frictional conditions (μ=0.4)

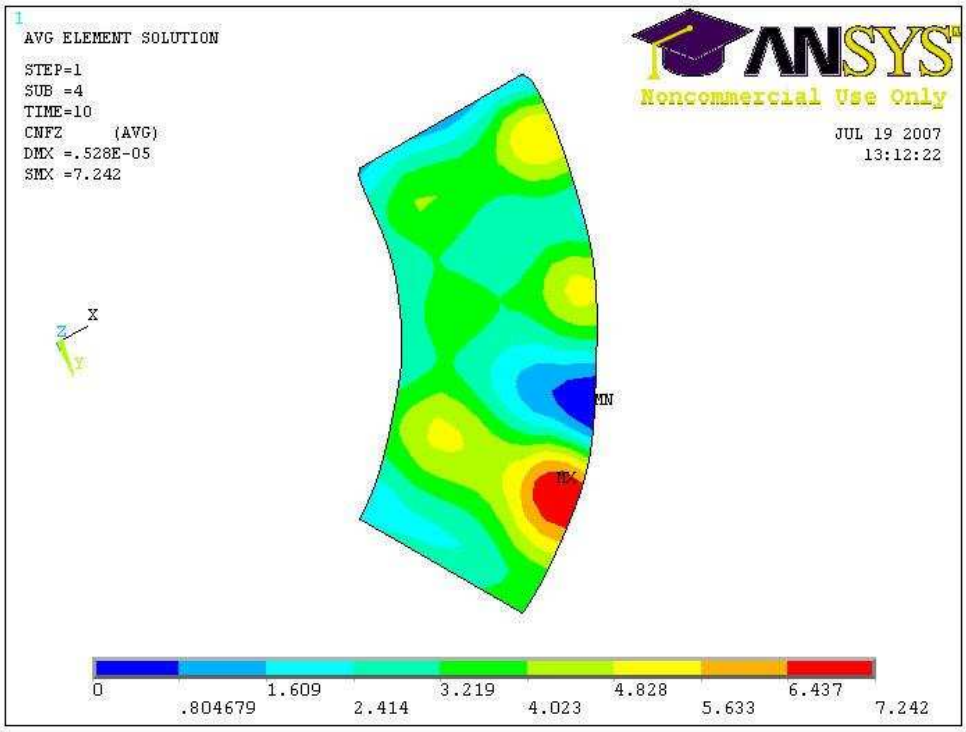

Figure L.5 Pressure distribution of outboard pad under frictional conditions (μ=0.6)

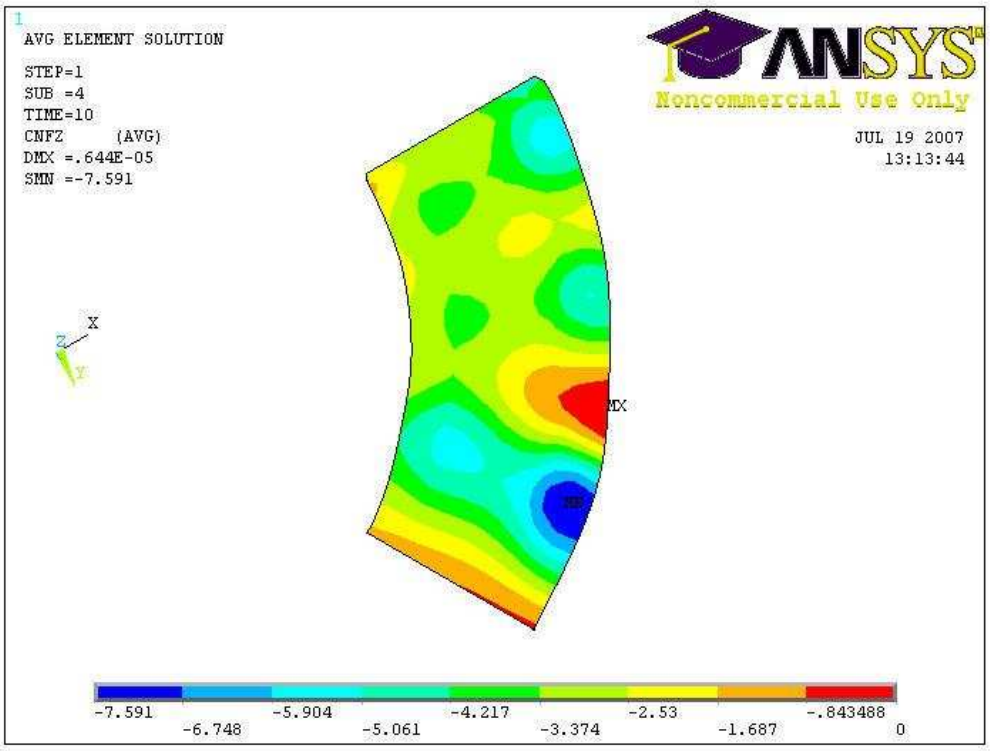

Figure L.6 Pressure distribution of inboard pad under frictional conditions (μ=0.6)

Appendix M

FE Images of the Contact Pressure Distribution for various Pad Modulus of Elasticity

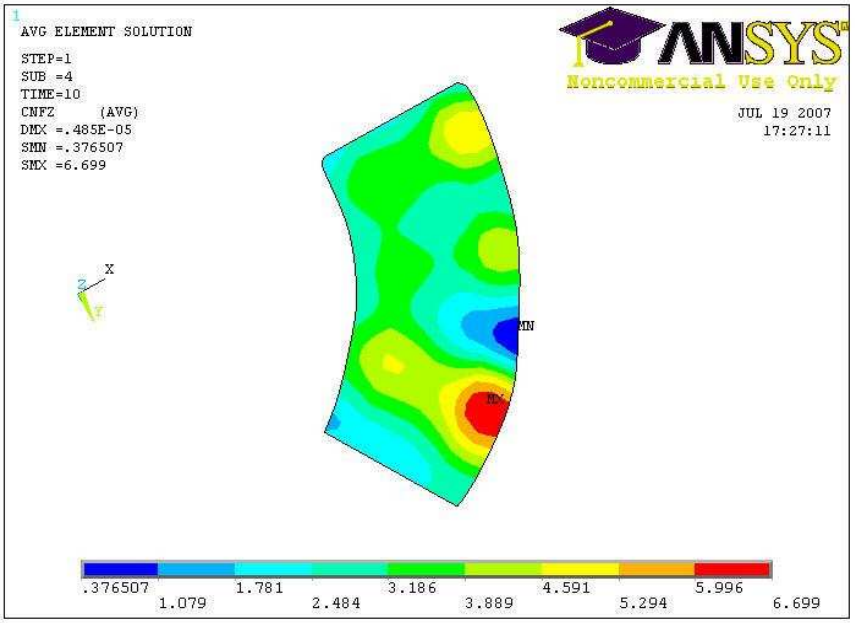

Figure M.1 Pressure distribution of outboard pad for various pad modulus of elasticity (E= 1.0 GPa)

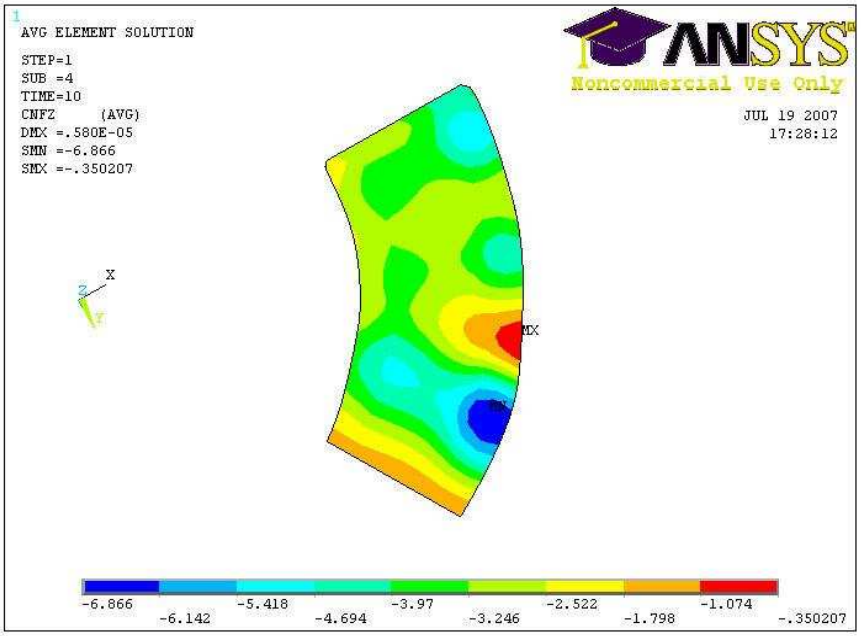

Figure M.2 Pressure distribution of inboard pad for different pad modulus of elasticity (E=1.0 GPa)

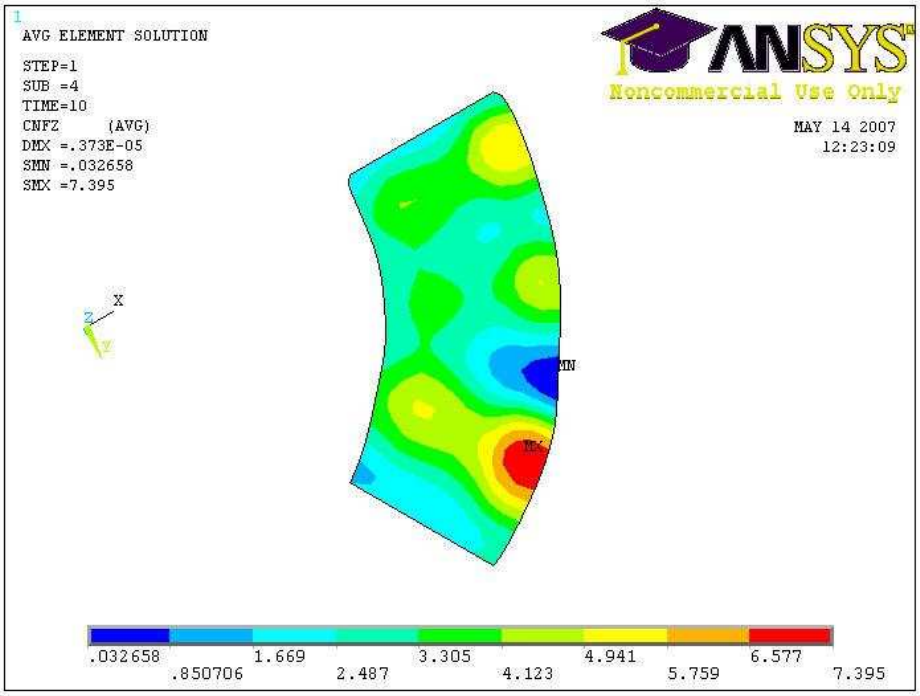

Figure M.3 Pressure distribution of outboard pad for different pad modulus of elasticity (E=1.5 GPa)

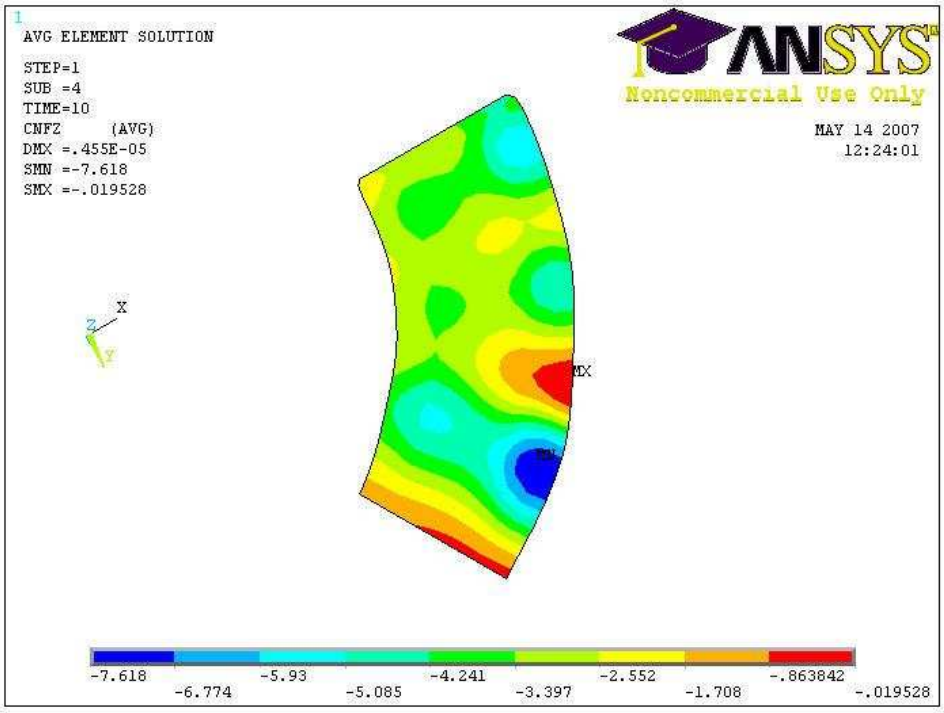

Figure M.4 Pressure distribution of inboard pad for different pad modulus of elasticity (E=1.5 GPa)

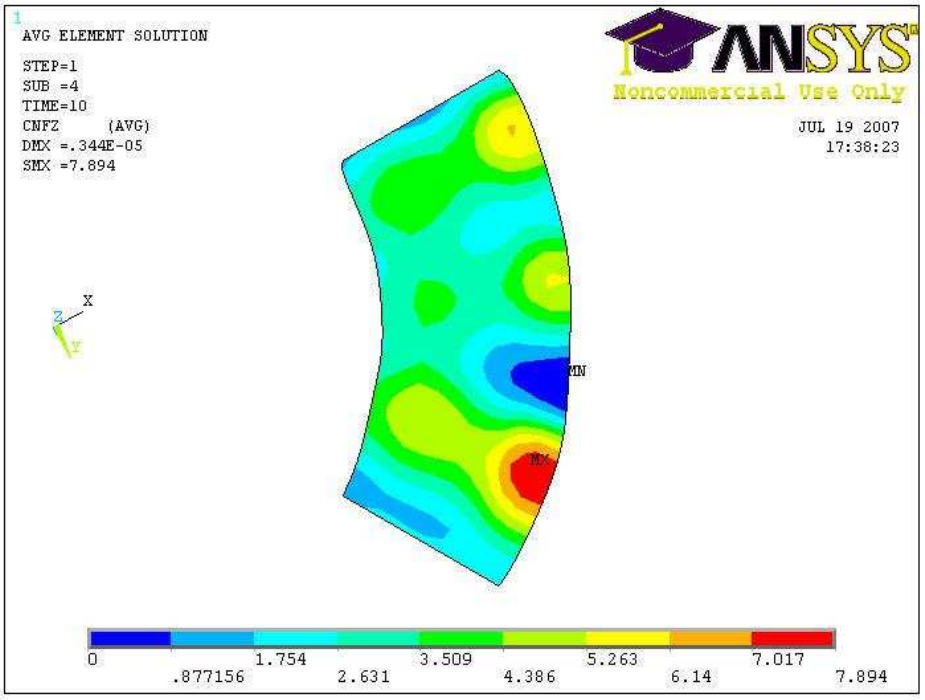

Figure M.5 Pressure distribution of outboard pad for different pad modulus of elasticity (E=2.0 GPa)

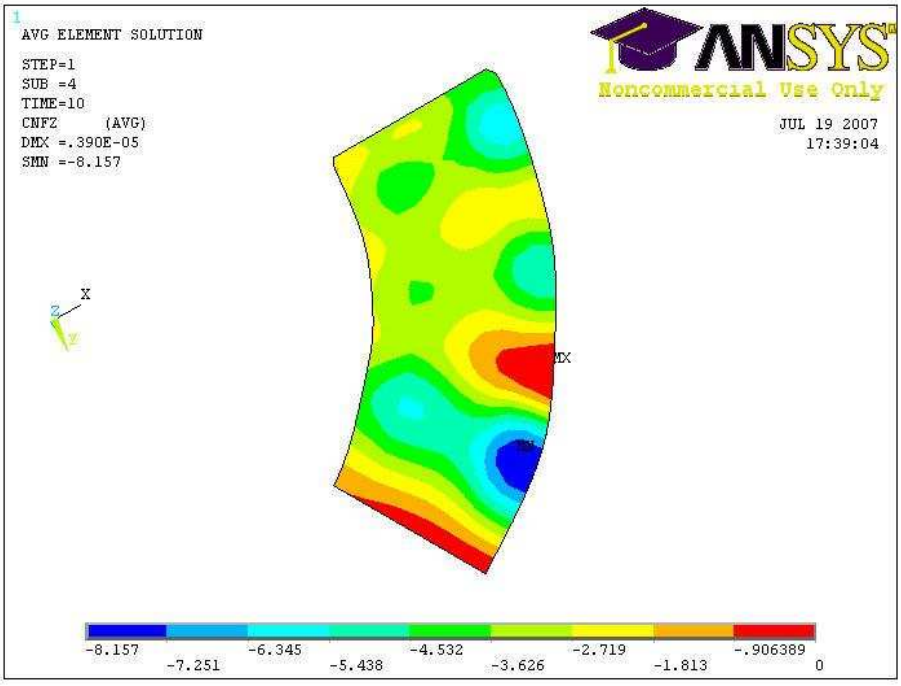

Figure M.6 Pressure distribution of inboard pad for different pad modulus of elasticity (E=2.0 GPa)

Appendix N

Graphical Images of the Contact Pressure Distribution for various Backplate Materials

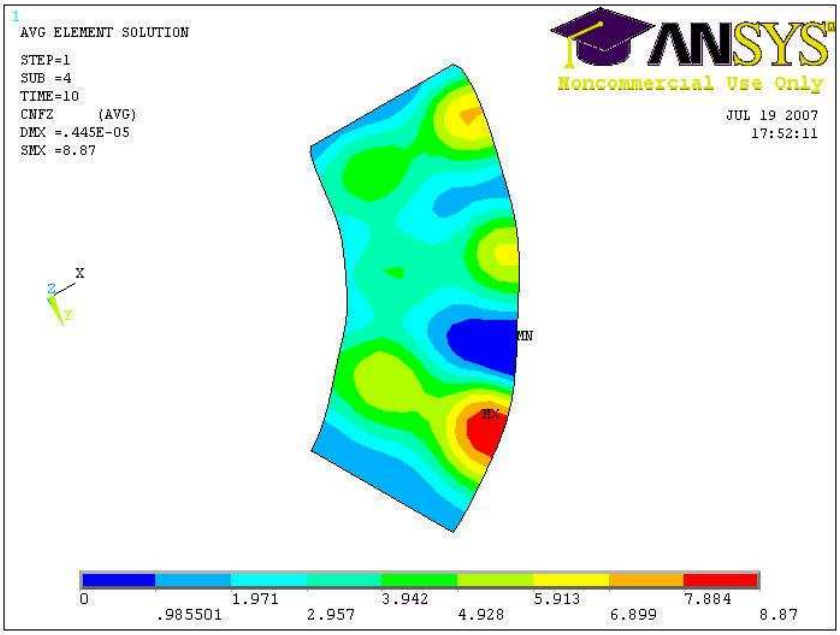

Figure N.1 Pressure distribution of outboard pad for different backplate materials (Grey cast iron, E=96 GPa)

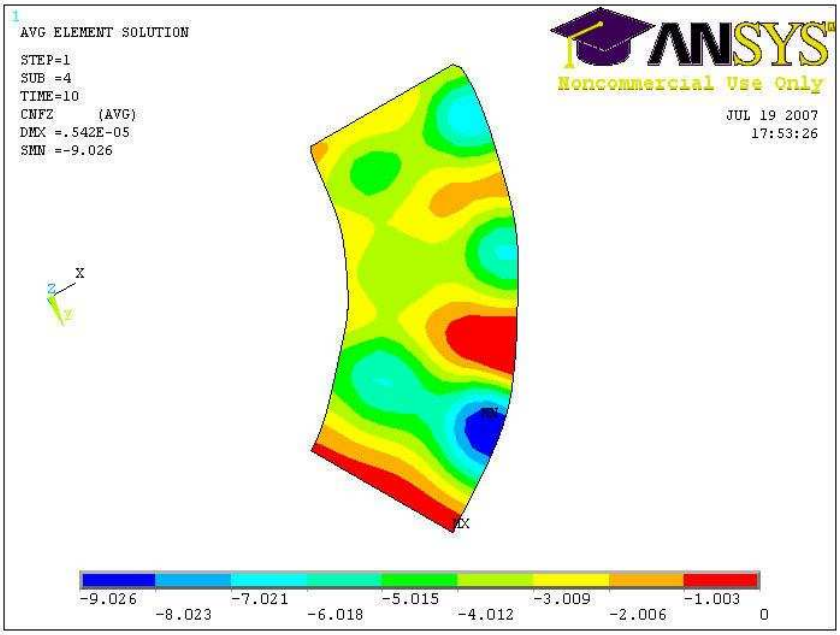

Figure N.2 Pressure distribution of inboard pad for different backplate materials (Grey cast iron, E=96 GPa)

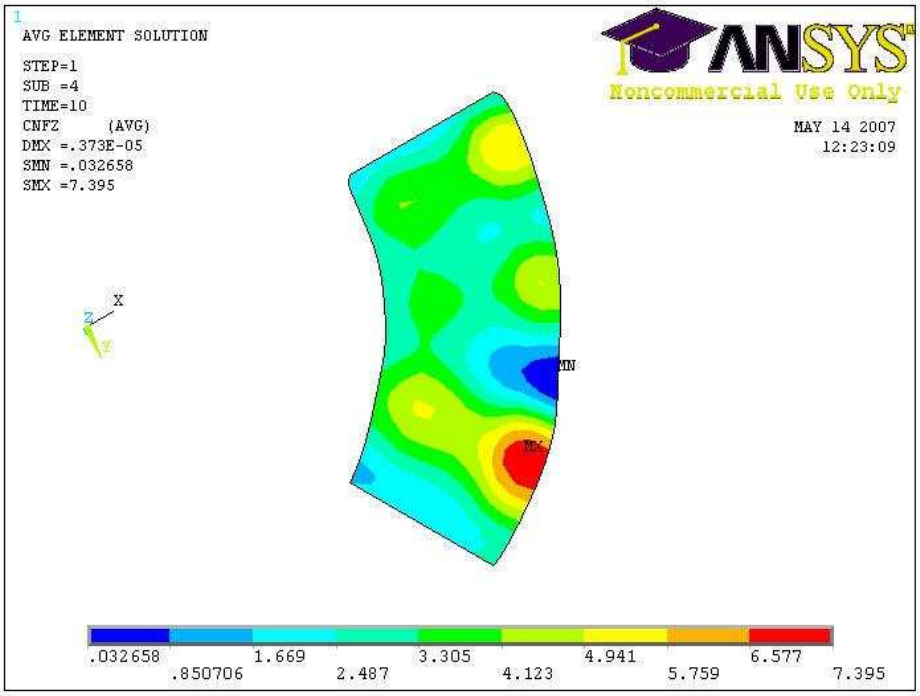

Figure N.3 Pressure distribution of outboard pad for different backplate materials (Steel, E=200 GPa)

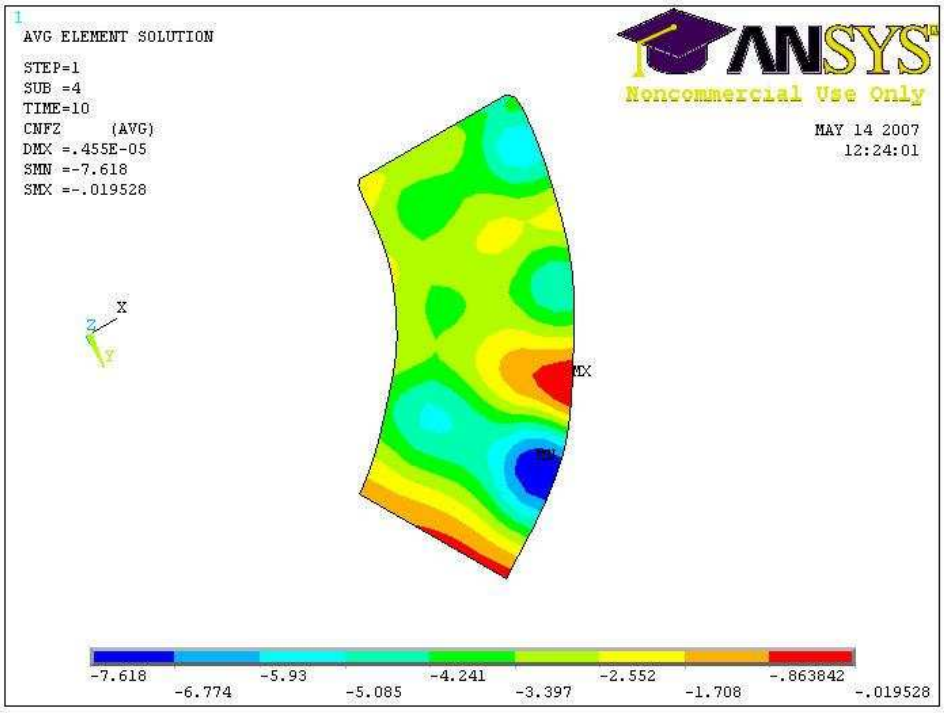

Figure N.4 Pressure distribution of inboard pad for different backplate materials (Steel, E=200 GPa)

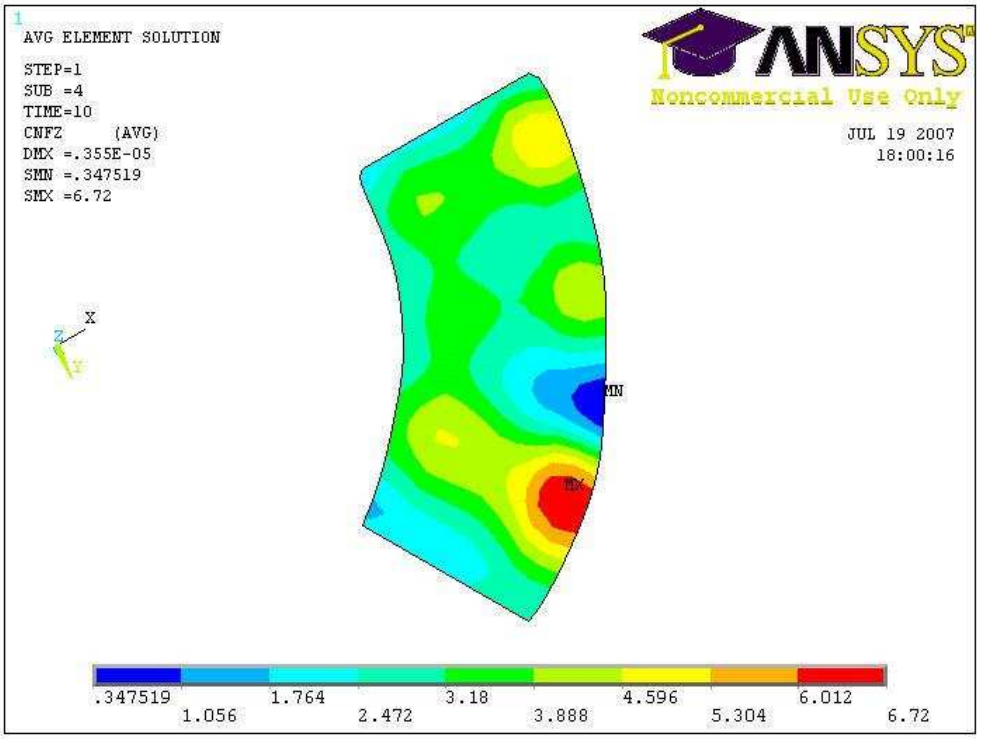

Figure N.5 Pressure distribution of outboard pad for different backplate materials (Steel alloy, E=300 GPa)

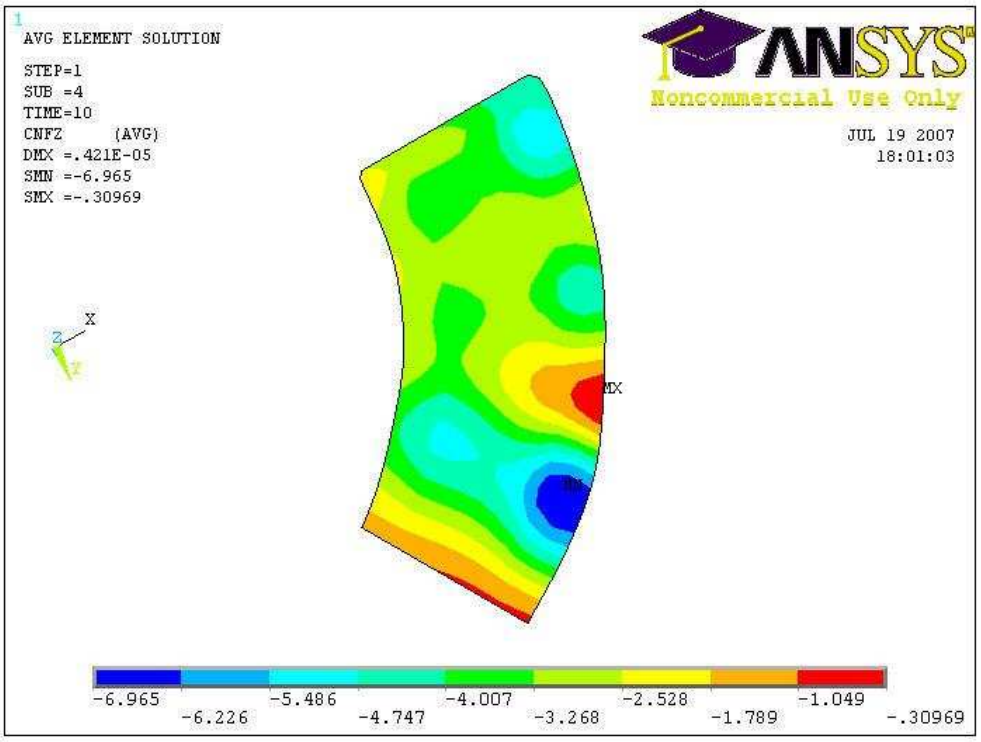

Figure N.6 Pressure distribution of inboard pad for different backplate materials (Steel alloy, E=300 GPa)

Appendix O

Graphical Images of the Contact Pressure Distribution for Various Disc Materials

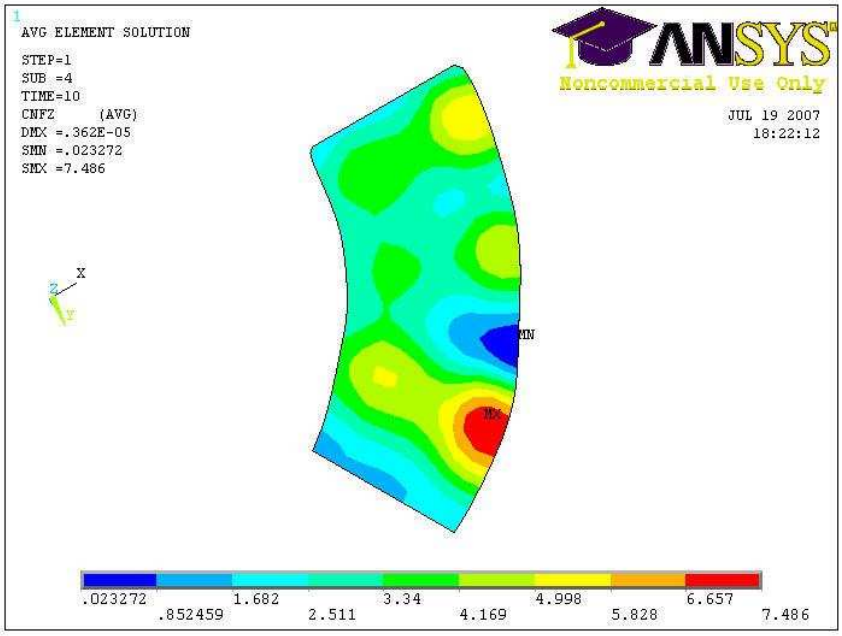

Figure O.1 Pressure distribution of outboard pad for different disc materials (Steel, E=200 GPa)

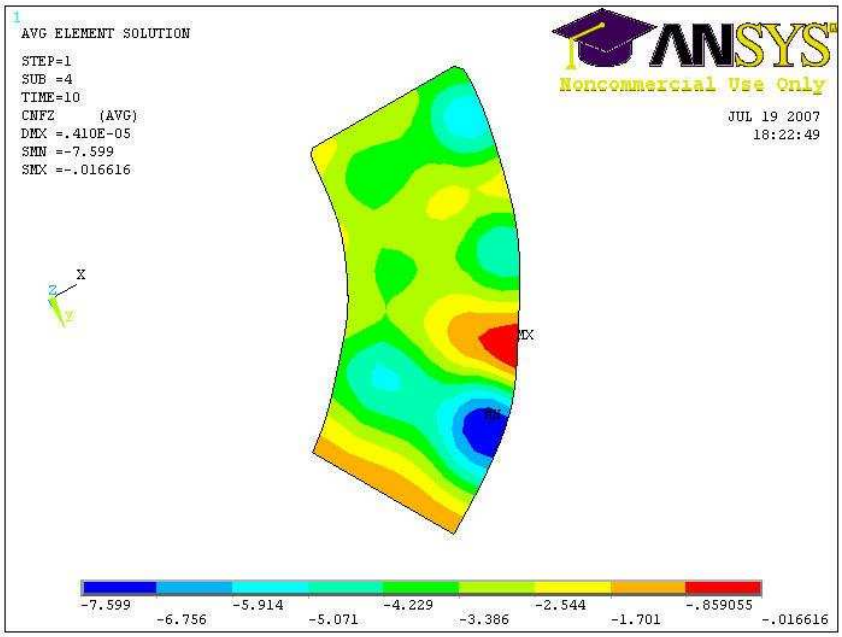

Figure O.2 Pressure distribution of inboard pad for different disc materials (Steel, E=200 GPa)

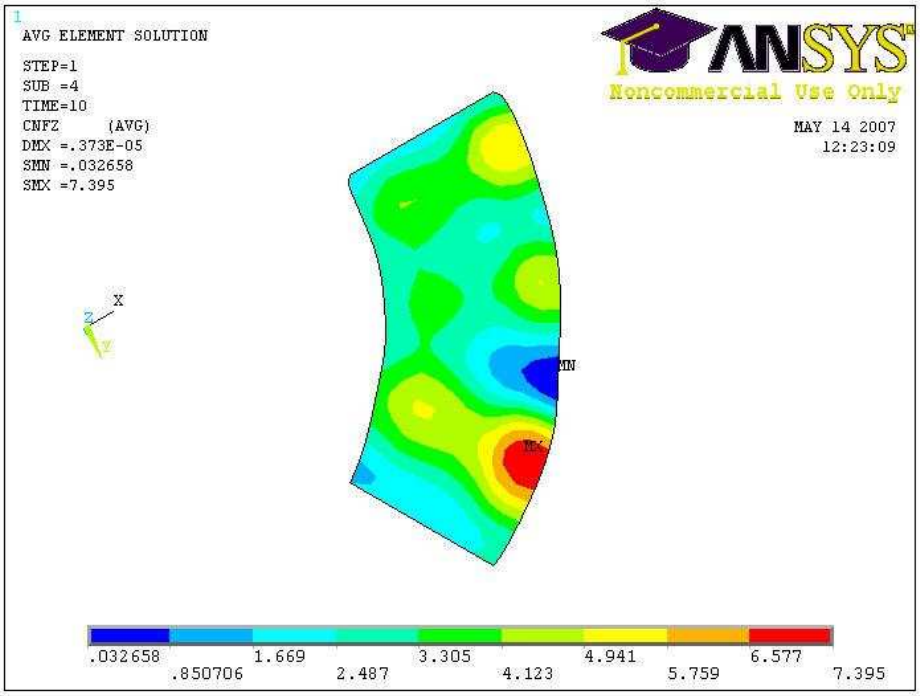

Figure O.3 Pressure distribution of outboard pad for different disc materials (Grey cast iron, E=96GPa)

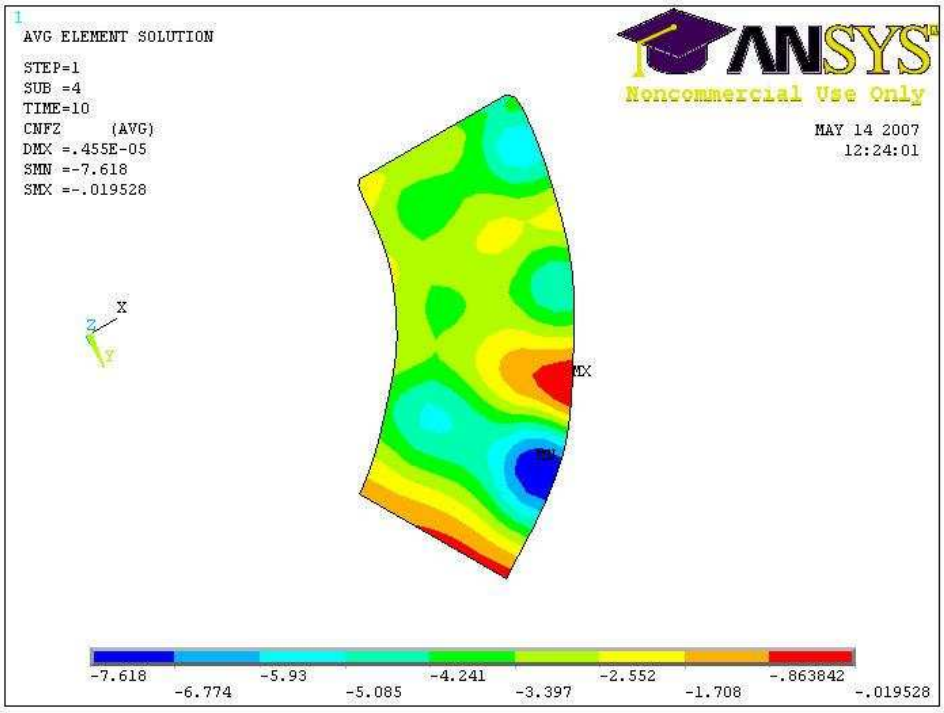

Figure O.4 Pressure distribution of inboard pad for different disc materials (Grey cast iron, E=96 GPa)

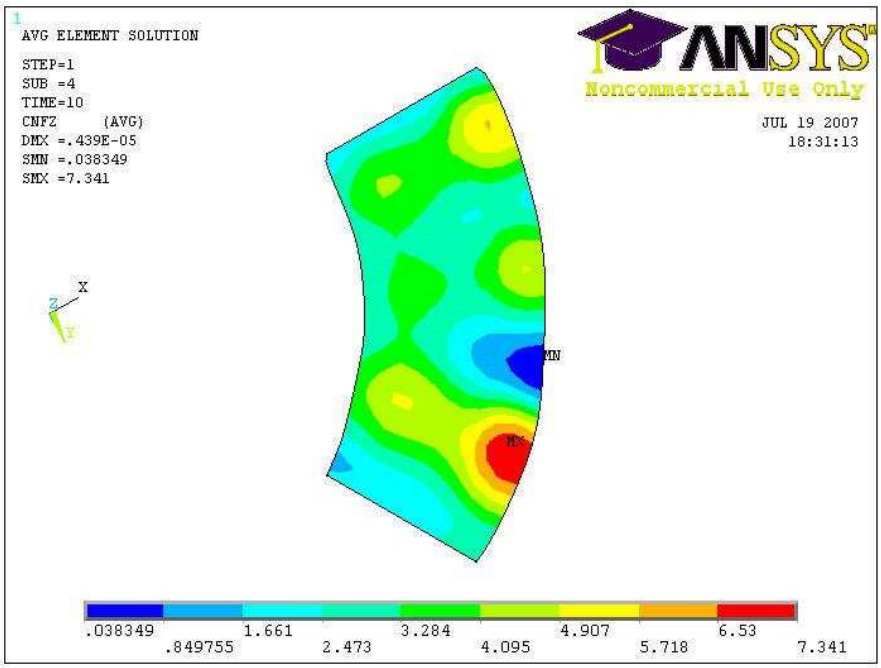

Figure O.5 Pressure distribution of outboard pad for different disc materials (Aluminium alloy, E=73 GPa)

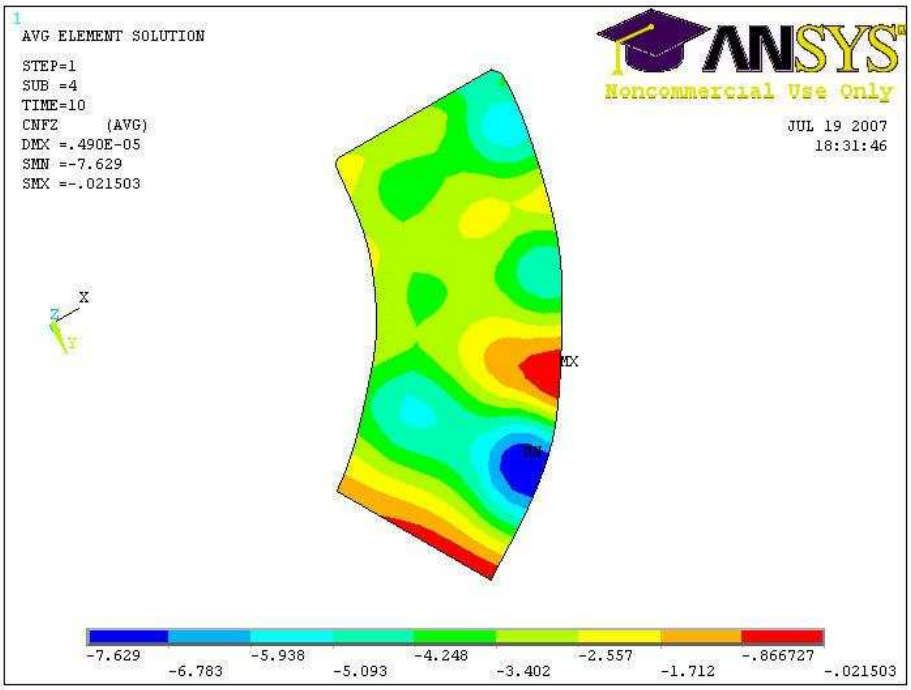

Figure O.6 Pressure distribution of inboard pad for different disc materials (Aluminium alloy, E=73GPa)

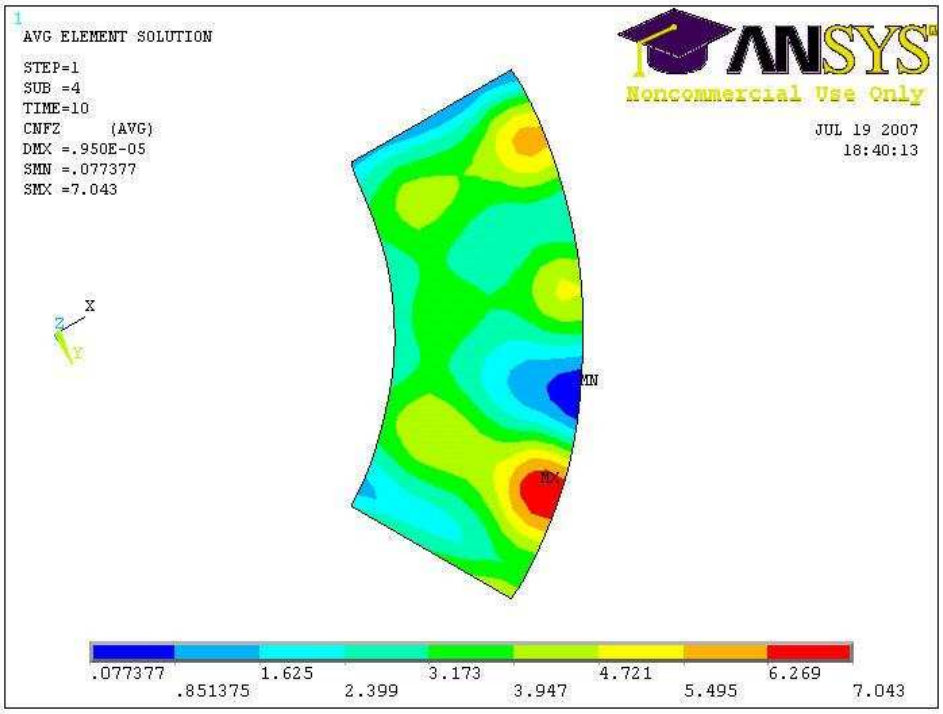

Figure O.7 Pressure distribution of outboard pad for different disc materials (Carbon ceramic, E=29 GPa)

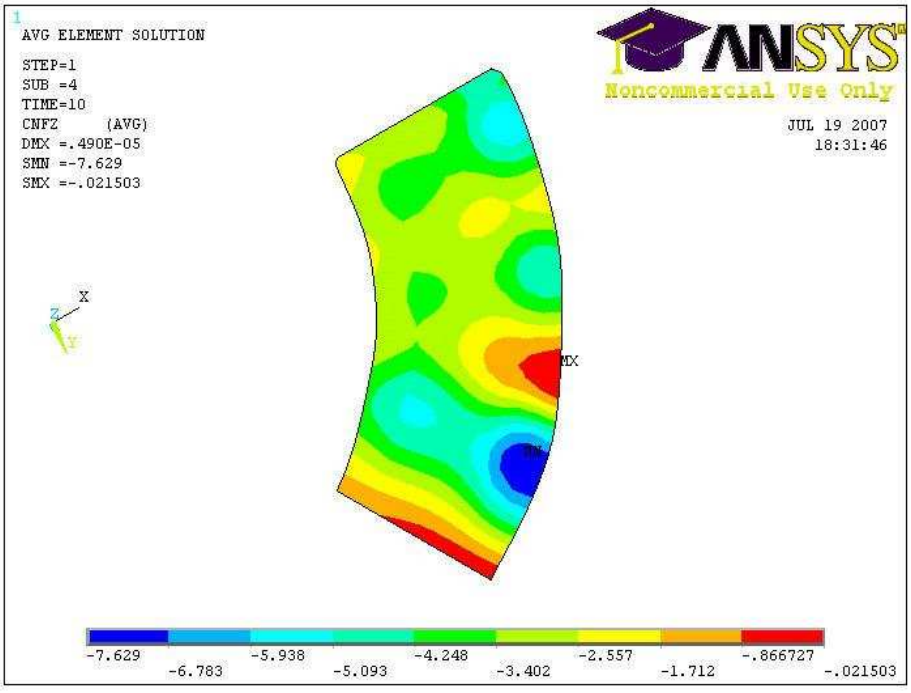

Figure O.8 Pressure distribution of inboard pad for different disc materials (Carbon ceramic, E=29 GPa)

References

1. Kinkaid, N.M., O'Reilly, O.M. and Papadopoulos, P., "Automotive disc brake squeal: a review", Journal of Sound and Vibration, Vol. 267, No. 1, pp.105–166, 2003.

2. Fieldhouse, J., "A proposal to predict the noise frequency of a disc brake based on the friction pair interface geometry", SAE Technical Paper 1999-01-3403, 1999.

3. Fieldhouse, J. D. and Newcomb, T. P., "An experimental investigation into disc brake noise", IMechE International Conference on The Braking of Road Vehicles, paper C444-036, pp. 145–159, London, 1993.

4. Fieldhouse, J. D. and Newcomb, P., "The application of holographic interferometry to the study of disc brake noise", S.A.E. Technical Paper 930805, 1993.

5. Norbert P. Hoffmann & Lothar Gaul, "Friction Induced Vibrations of Brakes: Research Fields and Activities", SAE Brake Colloquium, Paper 08BC-0033, 2008.

6. Spurr, R.T. "Brake squeal", Symposium on Vibration and Noise in Motor Vehicles, I.Mech.E, Paper No. C95/71, pp 13 - 16, 1971.

7. Jarvis, R.T. and Mills, B., "Vibrations induced by dry friction", Proceedings of I.Mech.E, Vol. 178 (32), pp 846 - 866, 1963.

8. Earles, S.W.E. and Soar, G.B., "Squeal noise in disc brakes", Symposium on Vibration and Noise in Motor Vehicles, I.Mech.E, Paper No. C101/71, pp 62 - 69, 1971.

9. Earles, S.W.E. and Lee, C.K., "Instability arising from the frictional interaction of a Pin-Disk system resulting in noise generation", Tran. ASME Journal of engineering industry, Paper No.75-DET- 25, pp 81 -86, 1976

10. Earles, S.W.E., "A mechanism of disc brake squeal", SAE Paper No. 770181, Detroit, 1977.

11. Earles, S.W.E. and Badi, M.N.M., "On the interaction of a Two-Pin-Disc System with reference to disc Brake Squeal", SAE Paper No.780331, Detroit, 1978.

12. Earles, S.W.E. and Chambers, P.W., "Disc brake squeal noise generation: predicting its dependency on system parameters including damping", International Journal of vehicle Design, vol 8(4/5/6), pp 538 - 552, 1987.

13. Fieldhouse, J., Ashraf, N. and Talbot, C., “Measurement of the dynamic centre of pressure of the disc/pad interface during a braking operation”, International Journal of Vehicle Design, 51 (1/2), pp. 73-104, ISSN 0143-3369, Inderscience publishers, 2009.

14. Dubensky R. C., Experimental techniques for rotor performance measurements. SAE paper 850078, 1985.

15. Tumbrink, H. J., “Measurement of load distribution on disc brake pads and optimization of disc brakes using the ball pressure methods”, S.A.E. Technical Paper 890863, 1989.

16. Samie, F. and Sheridan, D. C., “Contact analysis for a passenger car disc brake”, S.A.E. Technical Paper 900005, 1990.

17. Tirovic, M., Day, A. J., “Disc brake interface pressure distributions”, Proceedings of I.Mech.E, vol. 205, p.137-146, 1991.

18. Fieldhouse, J. D., “A study of the interface pressure distribution between pad and rotor, the coefficient of friction and caliper mounting geometry with regard to brake noise”, Proc. of IMechE International Conference on Automotive Braking, Professional Engineering Publishing Ltd, pp. 3-18, 2000.

19. Limpert, R., “Brake design and safety”, 2nd Edition, Society of Automotive Engineers, Inc, Warrendale, 1999.

20. Fieldhouse, J., Ashraf, N., Talbot, C., Pasquet, T., Franck, P. and Gabriel, R. (2006) ‘Measurement of the dynamic centre of pressure of a brake pad during a braking operation’ SAE Technical Paper 2006-01-3208, 2006.

21. M. Eriksson, “Friction and contact phenomena of disc brakes related to squeal”, Comprehensive summaries of Uppsala dissertations from the faculty of science and technology, Acta University Upsaliensis, Uppsala, 2000.

22. Mills, H. R., “Brake squeak”, Institution of. Automobile Engineers, Technical Report 9000B, 1938.

23. Tuchinda, A., “Development of validated models for brake squeal predictions”, PhD thesis, Imperial College London, September 2003.

24. Spurr, R. T., “A Theory of Brake Squeal”, Proc. of the Automotive Division, Institution of Mechanical Engineers, Vol. 1, pp. 33-40, 1961.

25. North, M.R., "Disc brake squeal - A theoretical model." Motor Industry Research Association (MIRA) Research Report, Report No. 1972/75, 1972.

26. North, M. R., “Disc brake squeal”, IMechE, paper C38/76, pp. 169-176, 1976.

27. Yang, S. and Gibson, R.F., “Brake vibration and noise: review, comments and proposals”, Int. J. Mater. Product Tech., Vol. 12, Nos.4–6, pp.496–513, 1997.

28. Felske, A. and Hoppe, G. and Matthai, H., "Oscillations in squealing disc brakes - An analysis of vibration modes by holographic interferometry." SAE Paper No. 780333, 1978.

29. Felske, A. and Hoppe, G. and Matthai, H. "A study on drum brake noise by holographic vibration analysis." SAE Paper No. 800221, 1980

30. Nishiwaki, M., Harada, H., Okamura, H. and Ikeuchi, T. "Study on disc brake squeal." SAE Paper No. 890864, 1989.

31. Lang, A.M. and Newcomb, T.P., "An experimental investigation into drum brake squeal", EAEC Conference on New Developments in Powertrain and Chassis Engineering, I.Mech.E, Strasbourg, Paper No. C382/051, pp 431 - 444, 1989.

32. Lang, A.M., Schafer. D.R., Newcomb, T.P. and Brooks, P.C., "Brake squeal - The influence of rotor geometry", Braking of Road Vehicles, I.Mech.E, London, Paper No. C444/016/93, pp 161 - 171, 1993.

33. Fieldhouse JD & Beveridge C, “A Visual Noise Investigation of a Twin Caliper Disc Brake”, 18th SAE Brake Colloquium and Engineering Display San Diego, Paper No 2000-01-2771, pp 111-122, ISBN 0 7680 0645 7, 2000.

34. Steel, W.P., Fieldhouse, J.D., Talbot, C.J., Crampton, “A modelling of 3D displacement in disc brake rotor generating noise”, FISITA World Automotive Congress, Barcelona, 2004.

35. Ichiba, I. and Nagasawa, Y., "Experimental Study on disc brake squeal", SAE Paper No. 930802, Detroit, 1993.

36. Ishihara, N., Nishiwaki, M. and Shimizu, H., “Experimental analysis of low frequency brake squeal noise”, S.A.E. Technical Paper 962128, 1996.

37. James, S., “An experimental study of disc brake squeal”, PhD Thesis, Department of Engineering, University of Liverpool, May 2003.

38. Kumamoto, F., Kawai, K. and Baba, H., “A study on relationship between pad restraint condition and brake squeal generation”, S.A.E. Paper No 2004-01 2801, 2004.

39. Fieldhouse, J., Ashraf, N. and Talbot, C., “The Measurement and Analysis of the Disc/Pad Interface Dynamic Centre of Pressure and its Influence on Brake Noise”, Brake Technology 2008, SAE International, ISBN 9780768020304, 2008.

40. Wang Z., Ettemeyer A., “Pulsed ESPI to solve dynamic problems” Report No 04-97, Dr. ETTEMEYER GmbH & Co, 1997.

41. Reeves, M., Taylor, N., Edwards, C., Williams, D. and Buckberry, C. H., “A study of brake disc modal behaviour during squeal generation using high-speed electronic speckle pattern interferometry and near-field sound pressure measurements”, Proceedings of I.Mech.E, Part D, Vol. 214, pp. 285-295, 2000.

42. Fieldhouse, J., Steel, W P., “A study of brake noise and the influence of the centre of pressure at the disc/pad interface, the coefficient of friction and caliper mounting geometry”, Proceedings of the Institution of Mechanical Engineers, Part D: Journal of Automobile Engineering, pp 957-973, 2003.

43. Liles, G., "An analysis of disc brake squeal using finite element methods." SAE Paper No. 891150, 1989.

44. P loannidis, P C Brooks and D C Barton, “Brake system noise and vibration- a review”, Braking 2002: From the Driver to the Road, pp 53-73, 2002.

45. Lee, Y.S., Brooks, P.C., Barton, D.C., Crolla, D.A., “A predictive tool to evaluate disc brake squeal propensity. Part 2: System linearisation and modal analysis”, International Journal of Vehicle Design, vol. 31, pp.309-329. 2003.

46. Lee, Y.S., Brooks, P.C., Barton, D.C., Crolla, D.A., “A predictive tool to evaluate disc brake squeal propensity Part 1: The model philosophy and the contact problem”, International Journal of Vehicle Design, vol. 31, pp.289-308. 2003.

47. Nack, W., “Brake squeal analysis by finite elements”, S.A.E Paper No 1999-01-1736, 1999.

48. AbuBakar, A.R., “Modelling and Simulation of Disc Brake Contact Analysis and Squeal”, PhD Thesis, Department of Engineering, University of Liverpool, 2005.

49. Tekscan I-Scan User Manual, Tactile force and pressure measurements system, v. 5.8x, published by Tekscan Inc, South Boston, MA, 2001.

50. Rose, J. and Stith, J., “Tekscan Sensors – Rail/Tie Interface Pressure Measurement in Railway Trackbeds, Proceedings of Railway Engineering”, 7th International Conference and Exhibition, London, United Kingdom, June 2004.

51. Evgeny Barkanov, “Introduction to the Finite Element Method”, Institute of Materials and Structures, Faculty of Civil Engineering, Riga Technical University, Riga, 2001.

52. Crolla, D.A. and Lang, A.M. "Brake noise and vibration - The state of the art." Proceedings of 17th Leeds-Lyon Symposium on Tribology, University of Leeds, pp 165 – 174, 1990.

53. ANSYS, Basic Analysis Guide, ANSYS release 10.0, August 2005.

54. Ripin, Z.B.M. "Analysis of Disc Brake Squeal Using the Finite Element Methods" Ph.D. thesis, University of Leeds, Leeds, UK, 1995.

55. Lee, YS; Brooks, PC; Barton, DC; Crolla, DA, "A predictive tool to evaluate disc brake squeal propensity Part 3: Parametric design studies" International Journal of Vehicle Design, vol. 31, pp.330-353. 2003.

56. Ashraf, N., "Brake squeal analysis using surface to surface elements", Master thesis, University of Leeds, Leeds, UK, 2003.

57. P. Ioannidis, P. C. Brooks, D. C. Barton, "Drum Brake Contact Analysis and its influence on squeal noise prediction", SAE Paper, 2003-01-3348, 2003.